Stable and Highly Accurate Pointing Earth-imager

Design of a CubeSat Attitude Determination and Control System for Very Low Earth Orbit Earth Observation

T. de Boer	4007352	B. Kizavul	4210298
J. E. C. Brederveld	4140346	S. H. Rosanka	4210107
R. E. Diaz Chicaiza	4180755	B. J. J. Stijnen	4191242
R. Drost	1310747	L. Wheeler	4174836
D. Gerritzen	1364278		

Design Synthesis Exercise 2015

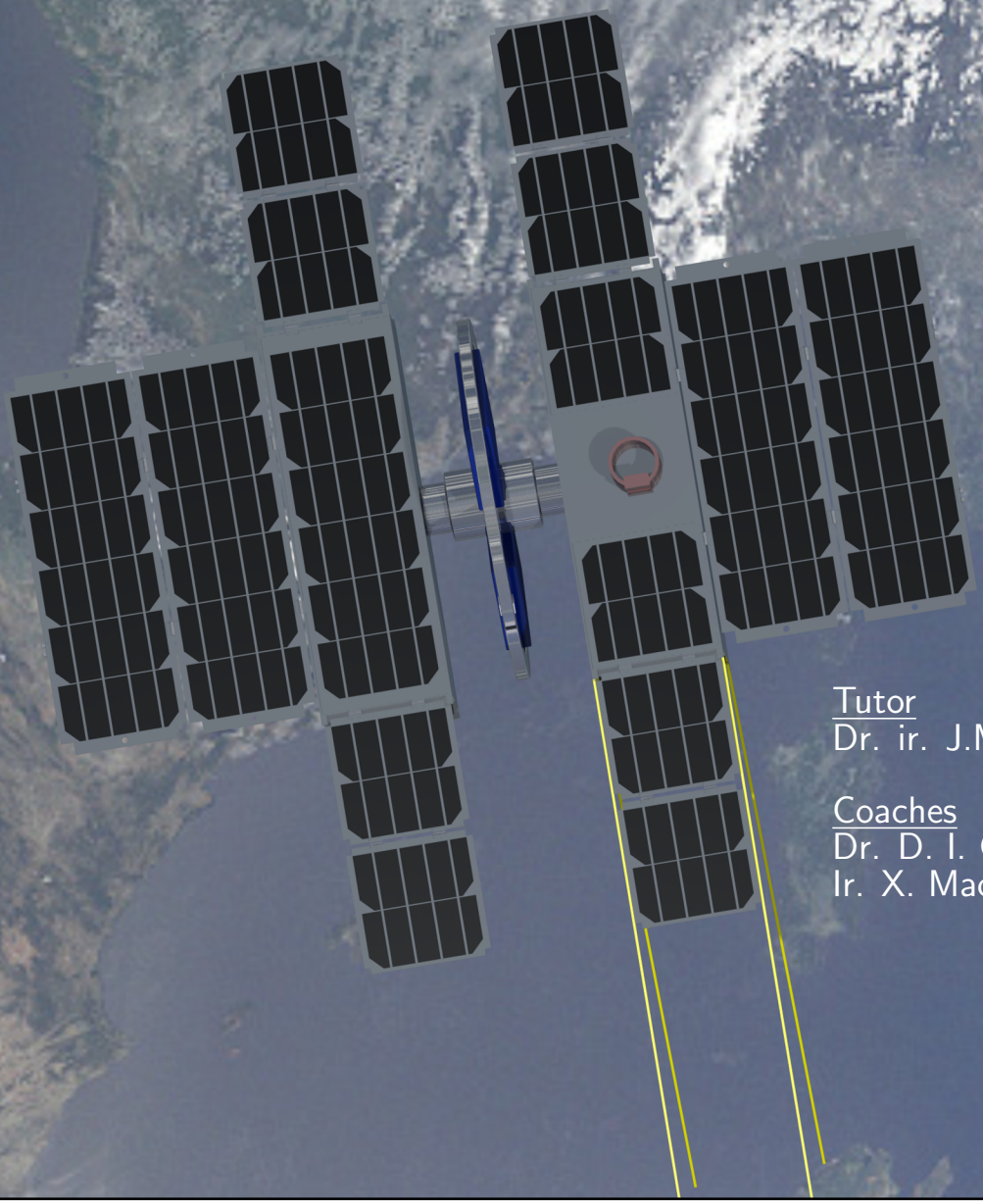

Tutor
Dr. ir. J.M. Kuiper

Coaches
Dr. D. I. Gransden
Ir. X. Mao

TU Delft Delft University of Technology

Aerospace Engineering

June 30, 2015

Preface

The present report is the final documentation of group S08 in the Design Synthesis Exercise, DSE, at the Technical University of Delft, TU Delft, in the year 2014-2015. For ten weeks, the group has been working to tackle a design problem presented by the project's supervisor, Dr. ir. J.M. Kuiper. The exercise consisted of designing a cube satellite which shall operate in a very low Earth orbit. The mission goal is to be able to provide a stable platform, from which accurate Earth images can be taken. This final report describes the process and the steps that were undertaken throughout the DSE to come to the final design.

The final concept consists of two conventional 3-unit CubeSats connected by a momentum wheel in the centre. All design choices and justifications will be described throughout this report.

Group S08 is very grateful to Dr. ir. J.M. Kuiper, our tutor, for suggesting the assignment and for his enthusiasm shown throughout the whole project. We are in addition greatly indebted to Dr. D. I. Gransden and Ir. X. Mao, our coaches, for their technical suggestions, time and dynamism. Also, the group wants to thank D. Dolkens in particular for his contribution towards the satellite's payload design.

A final thanks goes out to the remaining few who enthusiastically provided information and advice to the group. Namely, these are Dr.ir. E. Mooij, Ir. J. Bouwmeester, Dr. A Cervone, Dr.ir. E.N. Doornbos, J.A.P. Leijtens, P. Rumler, Dr. M. Pilinski, T. van den Dool, S. Kuiper, and ir. B.T.C. Zandbergen.

Summary

SHAPE is a very stable satellite at a Very Low Earth Orbit which provides a high accuracy for high-resolution Earth imagery. In order to achieve a high level of stability, SHAPE makes use of the principle of momentum conservation by integrating a substantial momentum wheel into its design of two conventional 3-unit CubeSats. The speed of this wheel is increased to a high velocity to ensure that the momentum counters the torque of the external disturbances. Momentum and reaction wheels are commonly used in satellites, but, as far as research shows, this is the first application of a substantial momentum wheel in a nano-satellite at Very Low Earth Orbit for the purposes of stabilising high-resolution Earth imagery.

Research shows that the market for CubeSats offers a significant potential for an Earth observation satellite with a high re-visit time. SHAPE provides an innovative, out of the box, and simple solution, by tackling the problems of instability on Earth imagery from a Very Low Earth Orbit. Costs are very competitive: just €$450,000$ for the platform, including an improved camera design. However, a variety of cameras can be used, inexpensively and efficiently, with this platform through a standard plug & play interface.

In conclusion, SHAPE, Stable & Highly Accurate Pointing Earth-imager is a platform optimally designed to withstand the disturbances commonly experienced by other satellites at Very Low Earth Orbits, with a view to improving the effectiveness of the satellite for high-resolution Earth imagery. A momentum wheel at the centre of the design plays the main role in stabilising the platform, using a simple, trusted, reliable and efficient method.

List of Symbols

Greek symbols

α	Absorption coefficient	$[m/s]$
α	Accommodation coefficient	$[-]$
α	Angular acceleration	$[rad/s^2]$
$\alpha_{pointing}$	Pointing accuracy	$[^\circ]$
$\triangle r$	Displacement	$[m]$
ΔV	Delta V budget	$[m/s]$
ϵ	Emissivity	$[-]$
η	Efficiency	$[-]$
γ	Specific heat ratio	$[-]$
λ	Eigenvalue	$[-]$
λ	Failure rate	$[Failures/year]$
λ	Inclination Factor of the Orbit	$[-]$
λ	Wavelength	$[m]$
μ	Earth's gravity constant	$[m^3/s^2]$
μ	Magnetic field of magnetorquers	$[Am^2]$
ω	Angular velocity	$[rad/s]$
ω_0	Spin rate of the momentum wheel	$[m]$
ω_d	Damped natural frequency	$[Hz]$
ω_n	Undamped natural frequency	$[Hz]$
ρ	Air density	$[kg/m^3]$
ρ_d	Diffusive reflection coefficient	$[-]$
ρ_s	Specular reflection coefficient	$[-]$
σ	Stefan-Boltzman constant	$[W/m^2K^4]$
τ	Torque	$[Nm]$
θ	Force angle	$[^\circ]$
θ	Maximum deviation of the vertical axis	$[^\circ]$
θ_a	Allowable motion	$[m]$
ζ	Damped natural frequency	$[-]$

Roman symbols

$\alpha_{y_{maxx}}$	Maximal rotation around the y-axis	$[rad]$
$\dot{e}_n$	Energy flux	$[J/m^2s]$
$\dot{m}$	Mass flow rate	$[kg/s]$
$\vec{n}$	Normal plane vector	$[m]$
$\vec{u}_n$	Unit incident vector	$[m]$
A	Cross-sectional area	$[m^2]$
a	Radius of the tube containing the damping liquid	$[m]$
A^*	Throat area	$[m^2]$
A_r	Frontal area	$[m^2]$
a_R	Acceleration due to the solar pressure	$[m/s^2]$
Ae	Nozzle area	$[m^2]$
B	Magnetic field strength	$[kg/As^2]$
b	Radius of the endpot	$[m]$
C	Consequence	$[-]$
C	Damping matrix	$[Ns/m]$
C	Heat capacity	$[J/kgK]$
C	In-plane damping	$[Ns/m]$
c	Rotordynamic Damping	$[Ns/m]$
c	Speed of light	$[m/s]$

c_c	Cross-coupling Damping	$[Ns/m]$
C_d	Drag coefficient	$[-]$
C_p	Specific heat capacity at constant pressure	$[J/kgK]$
C_{mp}	Thermal velocity	$[m/s]$
C_{r_n}	Radiant force coefficient	$[-]$
c_{r_n}	Local contributions to the radiant force coefficient	$[-]$
cg	Centre of gravity	$[m]$
cp_a	Centre of aerodynamic pressure	$[m]$
d	Distance	$[m]$
d_g	Ground shift	$[m]$
E	Young's modulus	$[Pa]$
F	Force	$[N]$
F_d	Damping force	$[N]$
F_r	Solar radiation pressure	$[N/m^2]$
G_{acc}	Ground accuracy	$[m]$
G_{AR}	Antenna loss gain	$[dB]$
G_{AT}	Cable loss gain	$[dB]$
H	Angular Momentum	$[Nms]$
h	Enthalpy	$[J/kg]$
I	Area moment of inertia	$[m^4]$
I	Mass Moment of Inertia	$[kgm^2]$
I	Solar radiation	$[W/m^2]$
K	In-plane stiffness	$[N/m]$
K	Stiffness matrix	$[N/m]$
k	Boltzmann constant	$[J/K]$
k	Rotordynamic stiffness	$[N/m]$
k	Spring stiffness	$[N/m]$
k_c	Cross-coupling stiffness	$[N/m]$
L	Distance between the endpots	$[m]$
L	Inductance	$[\Omega s]$
L	Length	$[m]$
M	Brake torque	$[Nm]$
M	Mass matrix	$[kg]$
M	Moment	$[Nm]$
m	Mass	$[kg]$
n_a	Number of assembled units	$[-]$
n_{cell}	Amount of solar cells	$[-]$
P	Orbital time	$[s]$
P	Power	$[W]$
P	Probability	$[-]$
p	Pressure	$[N/m^2]$
P_{Rx}	Received signal power	$[dBm]$
P_{Tx}	Transmitted signal power	$[dBm]$
Q	Heat energy	$[W]$
q	Incidence angle	$[^\circ]$
q	State Space variable	$[m]$
R	General Gas Constant	$[J/kgK]$
R	Resistance	$[\Omega]$
R	Risk	$[-]$
r	Reflection coefficient	$[-]$
R_e	Radius of the Earth	$[m]$
R_i	Imaginary radius	$[m]$
R_i	Inner radius	$[m]$
R_o	Distance from the centre of the momentum wheel to the damper	$[m]$
R_o	Orbit radius	$[m]$
R_o	Outer radius	$[m]$
S	Molecular speed ratio	$[-]$
T	Temperature	$[K]$
T	Total disturbance torques	$[Nm]$
t	Thickness	$[m]$

t	Time	$[s]$
T_a	Disturbance torque due to aerodynamic drag	$[Nm]$
t_a	Average time needed for assembly	$[s]$
t_f	Time needed to assemble the first unit	$[s]$
T_g	Disturbance torque due to gravity	$[Nm]$
V	Orbital speed	$[m/s]$
V_{exit}	Exit velocity	$[m/s]$
x	Learning factor	$[-]$

List of Abbreviations

ADCS	Attitude Determination and Control System
ADN	Ammoniumdinitramide
AMB	Active Magnetic Bearing
CFD	Computational Fluid Dynamics
CPU	Central Processing Unit
CTP	Cross-Track Pixel
C&DH	Command and Data Handling
DSE	Design Synthesis Exercise
EB	Electrodynamic Bearing
EO	Earth Observation
EoM	Equations of Motion
FBS	Functional Breakdown Structure
FEM	Finite Element Method
FFD	Functional Flow Diagram
FRAM	Ferroelastic Random Access Memory
GEO	Geostationary Orbit
GENSO	Global Educational Network for Satellite Operations
GPS	Global Positioning System
IARU	International Amateur Radio Union
IR	Infrared Radiation
I2C	Inter-Integrated Circuit
ISEB	International Space Education Board
ISIS	Innovative Solution in Space
LCC	Life-Cycle Cost
LEO	Low Earth Orbit
MAD	Multiple Analogue Digital
MEO	Medium Earth Orbit
MEMS	Micro Electrical Mechanic System
MLI	Multi Layer Insulation blankets
MMOI	Mass Moment of Inertia
MTF	Modulation Transfer Function
NASA	National Aeronautics and Space Administration
OBC	On Board Computer
PMB	Passive Magnetic Bearing
RAAN	Right Ascension of the Ascending Node
RAM	Random Access Memory
RAMS	Reliability, Availability, Maintainability and Safety
RBF	Remove Before Flight
RF	Radio Frequency
ROI	Return on Investment
RPM	Revolutions Per Minute
SD	Secure Digital
SHAPE	Stable and Highly Accurate Pointing Earth-Imager
SNR	Signal-to-Noise ratio
SPI	Serial Peripheral Interface
SSBV	Satellite Services BV
SSD	Solid Stage Drive
SSO	Sun-Synchronous Orbit

SST	Satellite to Satellite tracking
S08-GTC-M-	Mass requirement
S08-GTC-P-	Power requirement
S08-GTC-S-	Structure requirement
S08-GTC-V-	Volume requirement
S08-MC-ADC-	Attitude Determination and Control requirement
S08-MC-C-	Cost requirement
S08-MC-DU-	Down-/Up-Link requirement of the Mission Communication
S08-MC-GC-	Ground Control Mission Communication requirement
S08-MC-L-	Lifetime requirement
S08-MC-PC-	Power Control requirement
S08-MC-RD-	Redundancy requirement
S08-MC-RG-	Regulations requirement
S08-MC-S-	Spacecraft Mission Communication requirement
S08-MC-TC-	Thermal Control requirement
S08-MDH-CP-	Computational Power requirement
S08-MDH-DS-	Data Storage requirement
S08-ME-FL-	Flight Loads requirement of the Mission Environment
S08-ME-R-	Radiation requirement of the Mission Environment
S08-ME-T-	Temperature requirement of the Mission Environment
S08-MP-	Mission Payload requirement
S08-MT-S-	Sustainability requirement
TNO	Nederlandse Organisatie voor Toegepast Natuurwetenschappelijk Onderzoek
TT&C	Telemetry, Tracking and Command
TU Delft	Technical University of Delft
UHF	Ultra High Frequency
USB	Univeral Serial Bus
VHF	Very High Frequency
VLEO	Very Low Earth Orbit

Contents

Introduction

The Design Synthesis Exercise, DSE, is the name of the project that captivated the attention of nine students during the last ten weeks of the academic year 2014-2015. During the project the students use knowledge acquired throughout the Aerospace Engineering Bachelor. The DSE forces the students to apply the design and analytical tools learnt in a work-like environment and to collaborate and tackle a design challenge as a group.

The challenge, or mission objective, of group S08 is to design a CubeSat for Very Low Earth Orbit (between 230 and 380 km), VLEO. The design's main goal is to achieve a pointing accuracy of 5°. Given this requirement, the goal of the DSE is to provide a stable platform to which a camera can be mounted, and ensure that the pointing accuracy is met. However, an orbit in Very Low Earth Orbit provides many difficulties due to the nature of the atmosphere at this altitude. The thermosphere is affected by solar flux and magnetic indices which ensures that the temperature and density fluctuates significantly. This is in combination with the flow, a free molecular flow, which requires a complex model to predict any disturbances that will be faced.

The first steps towards the final design were already taken by the project plan, baseline report and the mid term report. Therefore, this report, the final one, will provide all the information needed to replicate the design process that was undertaken by group S08 during the DSE 2014-2015.

The layout of the report is as follows. Chapter 1 introduces the mission objective, requirements and thereafter, the final design. Chapter 2 describes the general process. In this chapter, the market analysis, sustainable engineering strategies, production plan, operations and logistics involved, and lastly a risk assessment is shown. Chapter 3 describes the environment, by mentioning the aerodynamics, astrodynamics and the disturbances caused. Also, the payload and its stability is considered in here. Chapter 4 includes a section for individual subsystems and explains the final design for each one. Information about the bearing and the dampers can be found in the last sections of this chapter. The budgets, compliance matrices and methods are described at the end of the subsystems sections. Finally, Chapter 5 gives final suggestions on final considerations for future students involved in the project.

Chapter 1

Mission Analysis and Final Design

The main purpose of this report is to present the final design and the design process undergone to conclude this design. Therefore this Chapter is mainly dedicated to analyse the mission and the final design. Firstly, the mission objective will be presented in Section 1.1. In a second step the final design will be presented in Section 1.2. This is mainly intended to give an overview and therefore enable the reader to understand each justification easily.

1.1 Mission Objective

In this section the mission objective is analysed and presented. The main focus will be on the project objective, the general requirements and the functional flow diagram of the mission.

1.1.1 Project Objective

The project objective is the following:

> *"Design a Very Low Earth Orbit (VLEO) CubeSat to enable Earth Observation for a spatial resolution* < 4 *m with* $5°$ *pointing accuracy (goal) at a maximum price of* 500 *k€ (goal)."* [1]

1.1.2 General Requirements

In order to perform the mission as described in the introduction, the following general requirements have been proposed.

- **S08-ME-R-01** *The satellite shall resist solar radiation levels lower than* 1408.5 W/m^2 *[2]*
- **S08-ME-T-01** *The satellite shall withstand the in-orbit temperature differences between* 1000 *and* 1500 K
- **S08-ME-FL-01** *All subsystems shall be able to withstand thrust loads introduced by the propulsion system*
- **S08-ME-FL-02** *All subsystems shall be able to withstand loads introduced by the flight conditions*
- **S08-GTC-V-01** *The whole unit shall have a size smaller than* 30 *cm x* 30 *cm x* 34 *cm*
- **S08-GTC-M-01** *The mass of one CubeSat unit shall be lower than* 1.33 *kg [3]*
- **S08-GTC-S-01** *The satellite shall not be pressurised except for the propulsion unit*
- **S08-GTC-S-02** *All subsystems shall be able to withstand acceleration loads during launch*
- **S08-GTC-S-03** *All subsystems shall be able to withstand vibrations during launch*
- **S08-MT-S-01** *The satellite shall be able to de-orbit after its maximum lifetime*
- **S08-MC-C-01** *Total unit cost shall be lower than* €500000
- **S08-MC-RG-01** *The satellite shall be able to be carried as a piggy-back option in a launcher*
- **S08-MC-L-01** *The design shall have a reliability of* 99 % *over its whole lifetime [4]*
- **S08-MC-L-02** *The satellite shall have no single point of failure*
- **S08-MC-L-03** *The lifetime of the satellite shall be at least* 90 *days*

1.1.3 Functional Flow Diagram

In this subsection, a flow diagram of the mission is given. It is difficult to represent the mission by using a simple diagram since this does not give any information about the time between each action

that is performed. Also, each phase can be explained into more detail, which is done in this section.

Firstly, a pre-operation check is performed. This part of the process is there to ensure that all subsystems are ready for launch and is a way to make sure everything is in order. The mechanical structure is checked first, thereafter the electrical power, then the communications and finally the payload. These subsystems represent the most important subsystems for the success of the mission, excluding the Attitude Determination and Control System, ADCS, however this cannot be tested without having the satellite inside the space environment. They are tested in this order because this will also be the order in which they will be activated during the mission. If a problem is encountered, reparations are made, and the whole process is started over to ensure that the sequence of operations will not fail during the actual mission. Finally, the fuel is loaded to the momentum wheel after being pre-filtered to avoid pollution.

Secondly, the launch phase begins. This phase is straightforward and similar to any regular launch phase. After launch, the different stages separate, the rocket is injected into orbit and the satellite is deployed from the launch platform.

Once the satellite is in space, several operations need to be performed before the mission can begin. Firstly, the battery is checked to determine whether there is enough power to start the mission. If not, the fail-safe mode is activated until the battery is charged. If the battery has enough power, the antennae are deployed, then the ADCS is switched on to allow detumbling and providing rough nadir pointing. Thereafter, the solar panels are deployed to instigate the drag mode. The drag mode consists of increasing the drag by a great degree to slow down the satellite and allow the satellite to drop to the required orbit. At the same time, the pointing accuracy should be increased and the momentum wheel is unlocked to start the spinning. Just before reaching the 355 km orbit, the momentum wheel has reached the necessary angular velocity and the CubeSat is stabilised. When the momentum wheel spins, the attitude of the bus needs to be controlled such that the desired observation path is obtained. Finally the camera is switched on.

Once the satellite is stable, the actual mission can then begin. The satellite takes continuous pictures during its orbit, given that there is enough light for the payload. For every picture taken, the picture is momentarily saved before being compressed and then permanently saved. The altitude is then computed and depending on the altitude, the mission is continued or moved to end-of-life mission. A minimum operational altitude is set to be 230 km. If the satellite reaches this altitude, it is considered too low, and the mission cannot continue anymore. The mission then moves to its last phase which is the End-of-Life mission.

If the altitude is below 230 km, the mission is finished and the end-of-life mission can begin. The data storage is checked to make sure there is no more data. If there is, the remaining data is sent to the ground. Finally, as an End-of-Life mission, the satellite is tested in terms of temperature, to test the temperature during disintegration.

In Figure 1.1, the Functional Flow Diagram, FFD, is shown.

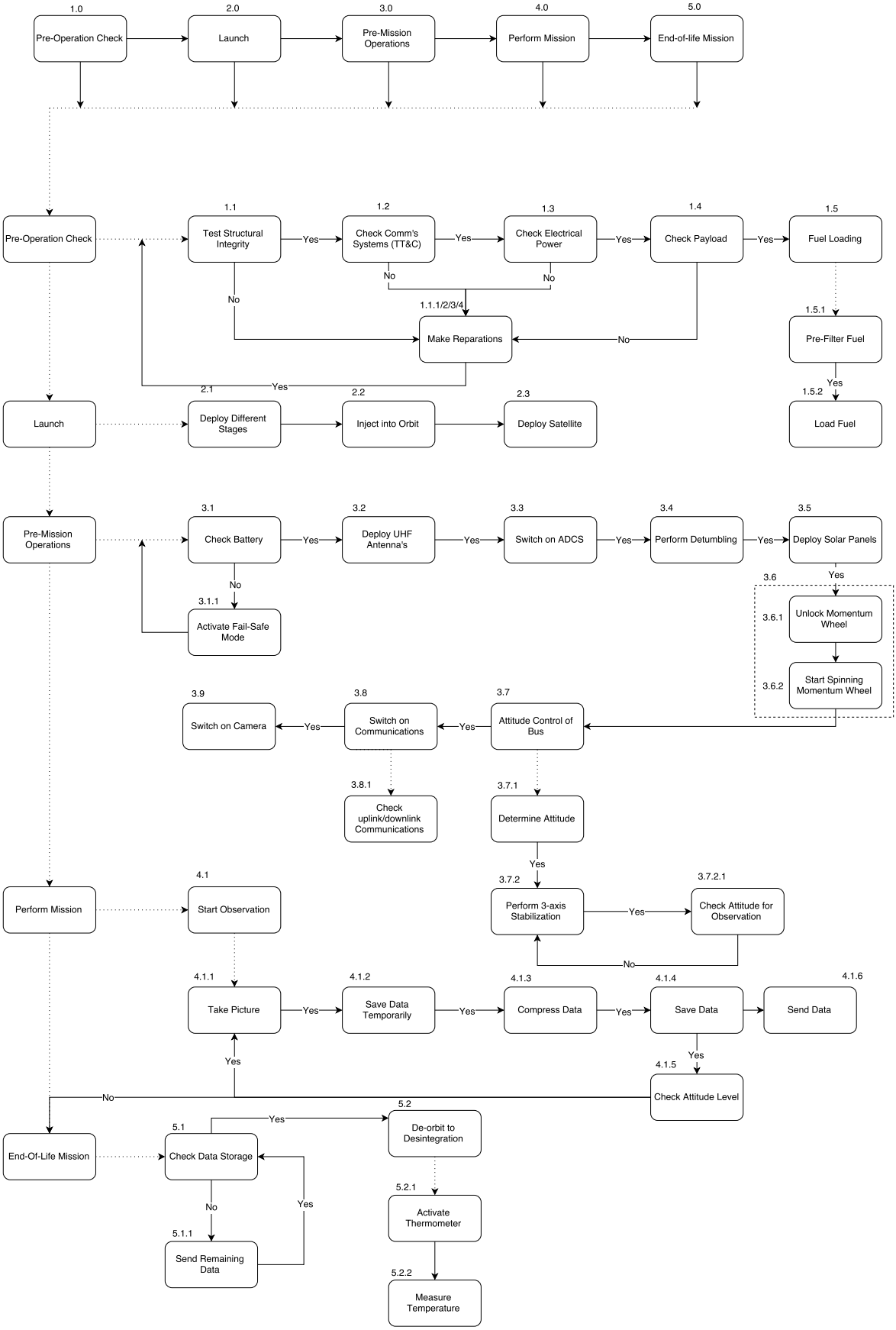

Figure 1.1: Functional Flow Diagram of the Earth Observation Mission

Similar to the Functional Flow Diagram, the Functional Breakdown Structure, FBS, is shown in Figure 1.2. The only difference between both diagrams is the absence of sequence in the FBD and some additional comments about actual hardware which is performing a certain function inside the

FBD

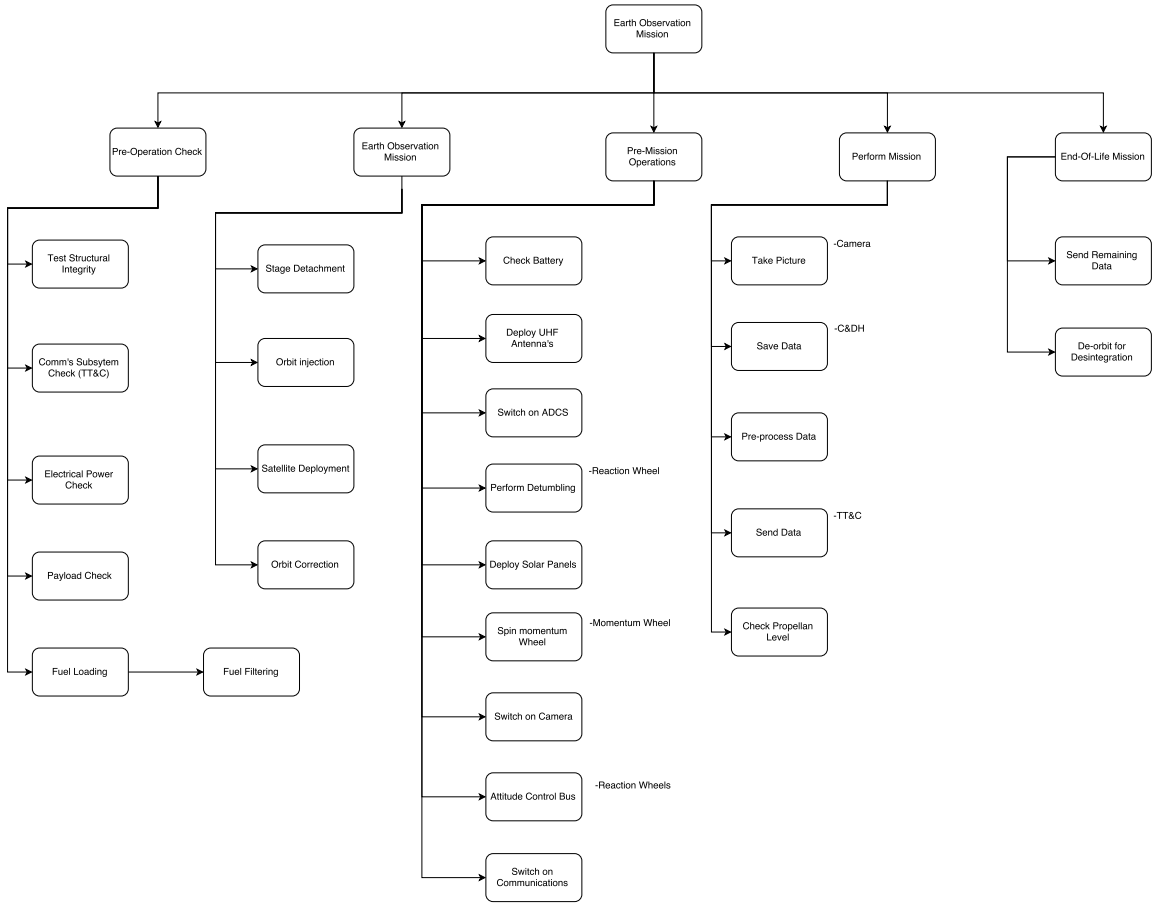

Figure 1.2: Functional Breakdown Diagram of the Earth Observation Mission

1.1.4 Compliance Matrix

In order to have a quick overview whether the requirements are all met, a compliance matrix was created which is shown by Table 1.1.

Table 1.1: General Requirements Compliance Matrix

Requirements	**Compliance**
S08-ME-R-01	✓
S08-ME-T-01	✓
S08-ME-FL-01	✓
S08-ME-FL-02	✓
S08-GTC-V-01	✓
S08-GTC-M-01	✓
S08-GTC-S-01	✓
S08-GTC-S-02	✓
S08-GTC-S-03	✓
S08-MT-S-01	✓
S08-MC-C-01	✓
S08-MC-RG-01	X
S08-MC-L-01	✓
S08-MC-L-02	✓
S08-MC-L-03	✓

As shown with Table 1.1, all the requirements that were set, that are general for the whole satellite, are met. This ensures that the final design choice is suitable for this mission. Firstly, the thermal subsystem provides enough protection to ensure that requirements S08-ME-R-01 and S08-ME-T-01

are met. The design for the structures subsystem ensures that requirements S08-GTC-S-01, S08-GTC-S-02, S08-GTC-S-03 and the general requirements, which apply to all subsystems, are able to sustain themselves during the launch and operation mission phases. Only the requirement S08-MC-RG-01 cannot be met since the size of this satellite varies significantly from other CubeSat missions and will therefore not fit into a piggy-back. For the remaining few requirements, all the design choices that are presented, in further sections, will describe how the satellite remain in its requirements.

1.2 Final Design

SHAPE, Stable and Highly Accurate Earth-Imager, is an exceptionally stable satellite for Very Low Earth Orbit optimised for an orbital altitude between $350 - 230\ km$. In order to achieve a high level of stability, SHAPE. makes use of the principle of momentum conservation by integrating a substantial momentum wheel into its centre. Around this high spinning momentum wheel two main conventional 3-Unit CubeSats are placed to accommodate the main payload to perform its imaging mission and the other important subsystems. The final design layout can be seen in Figure 1.3.

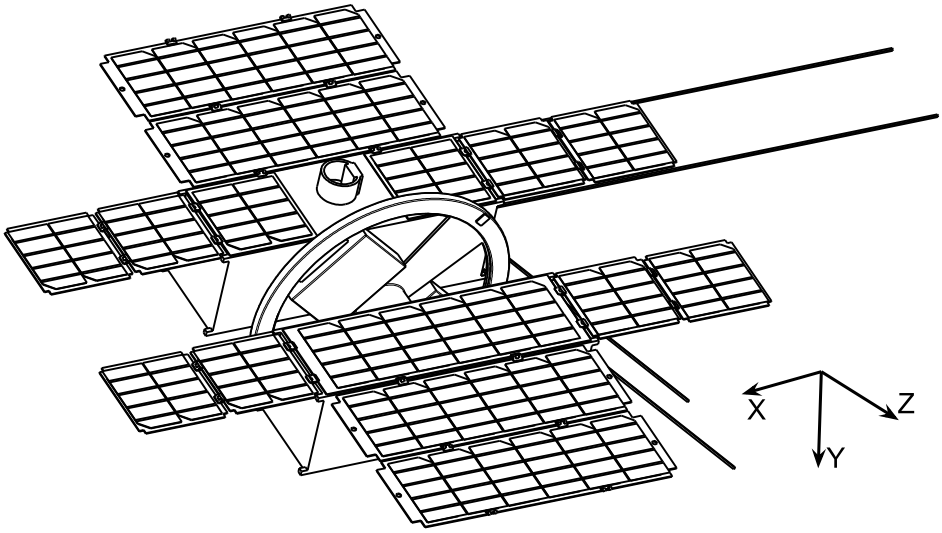

Figure 1.3: Final Design Layout

The payload uses an Off-Axis Modified Ritchey-Chretien Telescope in combination with two corrective lenses. This enables a compact design and, in a combination with a 4000-pixel line sensor, a spatial resolution of 4 m at an orbital altitude of 350 km. As the altitude is lowered to 230 km, a spatial resolution of up to 2.63 m can be obtained. By using this optimally designed momentum wheel, the stability requirement for the imaging can be obtained by the Attitude Determination and Control System. Therefore, this ADCS can be considered to be an innovative design which will enable future missions, which require a high accuracy in a Very Low Earth Orbit, to be feasible. To gain the high accuracy and stability that the momentum wheel is designed for, it will need to spin up to a rotational speed of $7,000\ rpm$. This can not be gained by a elective motor for this small sized satellite and therefore a high, efficient propulsion system is installed in the momentum wheel to fulfil this task. Due to the rotation, a bearing that provides low friction and vibrations is required. Therefore, a newly developed magnetic bearing will be used to guarantee a successful mission.

Furthermore, the imaging mode generates a significant amount of data which needs to be sent to the ground station using an X-band antenna. The X-band antenna requires a significant amount of power. To be able to provide this power, 25 solar cells distributed over multiple deployable solar panels are used, including two separate battery designs. The solar panels are positioned in a way in which the overall aerodynamics performance is optimised to reduce the total drag of the satellite as well as stabilising the satellite.

Since the cost budget was rather limited, the design needed to be cheap but efficient at the same time. However, the total cost of this design is estimated to be around € $450,000$ at this design stage, if a constellation of 100 satellites is considered to be used. It is also important to design this satellite with keeping sustainability in mind and therefore a special end-of-life mode was considered. The end-of-life mission goal is to increase the drag of the whole design, enabling the satellite to de-orbit from an

orbital altitude of 230 km in a single day. The general overview of the final design will be given in Table 1.2.

Table 1.2: Summary of the SHAPE solution

	Value	**Contingencies** [%]
Dimensions $[cm]$	28.3 $\times$ 30 $\times$ 31	$\pm$ 5
Dry Mass $[kg]$	7.85	$\pm$ 5
Total Mass $[kg]$	8.1	$\pm$ 5
Pointing Accuracy $[^\circ]$	1.3	$\pm$ 10
Orbital Altitude $[km]$	350 - 230	–
Mission Time $[days]$	$\approx$ 200	$\pm$ 20
Launch Date $[-]$	1st half 2016	–
Ground resolution $[m/pixel]$	2.63 - 4	–
Cost [€]	450,000	$\pm$ 10
Idle Power Usage $[W]$	7.4	$\pm$ 5
Peak Power Usage $[W]$	21	$\pm$ 5

Chapter 2

Design Process

The process of designing a satellite or any other product most of the times starts with doing a market analysis and see if the market is big enough to commercialise your product. For SHAPE the market analysis is done in Section 2.1. After the market analysis the budget allocation of a space mission is on of the first and important task to keep track off, a description for the SHAPE mission is given in Section 2.2. In Section 2.3 it is shown how the mission can be made more sustainable. Now that the satellite is designed the production plan has to be made and is given in Section 2.4. The operations and logistics are given in Section 2.5 and lastly a risk assessment has been made for the entire design process in Section 2.6.

2.1 Market Analysis

The space-industry is a costly market where large investments are paid up front. Not only do these companies compete with each other but also compete with governmental funded programs. This makes a market analysis a crucial part of a successful expenditure for a company. A closer look will be taken at the market trends, needs and demographics.

Market Trends
The market for small Earth observation satellites has increased over the last four years and it is expected to continue to grow in the near future. According to a study done by Spaceworks [5], the number of nano/micro satellite launches is expected to increase in the following years. This is represented by Figure 2.1. The number of small satellite Earth observation missions has increased from 10%, before 2013, to 60% in 2014. This is due to a general acceptance of the advantages of small satellites. For example, comparable performance, lower cost, lower risk and faster deployment all favour the use of small satellites.

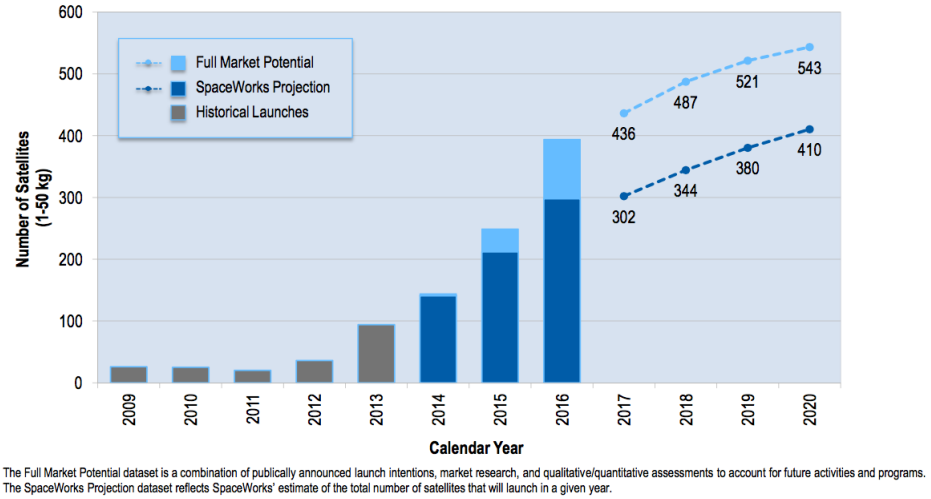

Figure 2.1: Prospected Market Growth [5]

The total market worth also started growing around 2015 as can be seen in Figure 2.2. With the

launch planned in 2016 or 2017, the total market capital is around € 2,750,000,000.

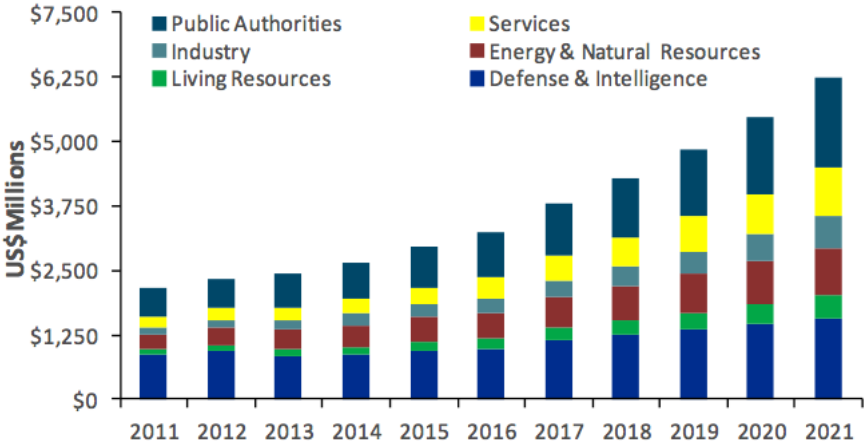

Figure 2.2: Market Growth per Sector [6]

Market Needs

The main characteristics for multispectral Earth observation missions are the spatial resolution and the revisit time. Plotting these in a graph for existing missions shows that there is a market for resolutions lower than 1.25 m, see Figure 2.3. It is not yet possible to compete with this resolution using Cubesats. However, there is much research being done in miniature cameras so it is to be expected that in a short period, CubeSats can be able to compete with traditional satellites. Having a swarm of Cubesats can be used to achieve a higher revisit time.

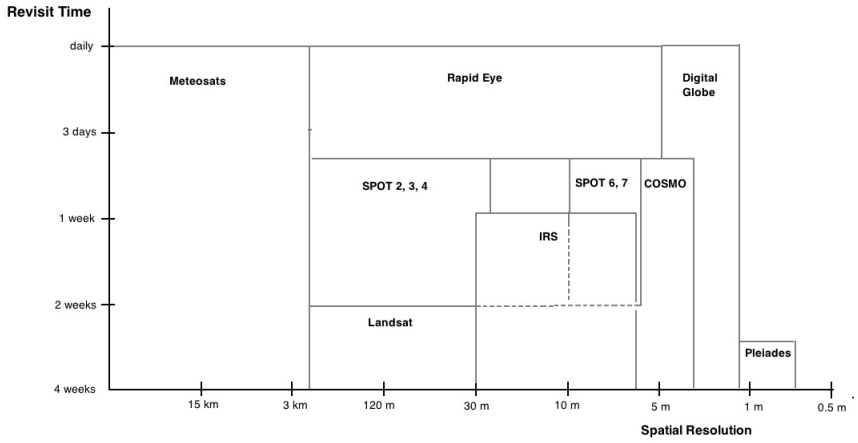

Figure 2.3: Existing Multispectral Earth Observation Missions

Market Demographics

In the 20th century, almost all of the Earth observation services were used by North-American and European businesses and institutions. In the past decade, other countries are also seeing the benefits for spaceborne Earth observations, and especially an increase in the Asian market is to be expected in the coming years according to Northern Sky Research [6]. Which can be seen in Figure 2.4.

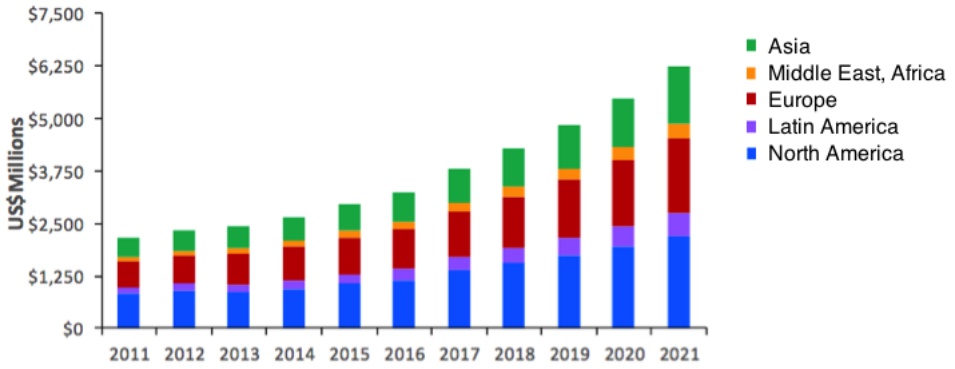

Figure 2.4: Prospected Market Growth per Continent [6]

2.1.1 Return on Investment

To find investors to invest into the mission use, is made of performance indicators. One of the most important indicators is the Return On Investment, ROI.

Market Price
For traditional satellites, the cost for Earth Observation, EO, data with a resolution lower than 5 m is around 1.5 €/km^2. According to studies conducted on performance based cost modelling for small observation satellites, it is expected to have lower mission cost with a factor between 2 to 10 compared to traditional satellites [7]. Assuming the average discount factor of 6 would give a price of 0.25 €/km^2 which will be a big advantage compared with the competition of traditional satellites.

Market Share The total number of existing and projected EO satellites from 2009 to 2020 can be seen in Figure 2.1. Adding the historical launches and spaceworks projection until 2016 comes to a total number of 850 EO satellites. Dividing the total market capital in 2016 by the number of earth observation satellites will give a market share of around € 3,250,000 per satellite.

Cost One of the requirements for the mission is a maximal development and production cost of € 500,000. As it will be explained in Section 5.2, the total unit cost for a single satellite when assuming a constellation of 100 CubeSats is € 445,000. The direct operational cost will mainly consist of the launch cost, which will be around € 100,000. The overhead cost is also estimated around € 100,000 [1]. These cost will give a total cost of € 645,000.

Return on Investment
The return on investment is a performance measure used to evaluate the efficiency of an investment and is given in Equation 2.1.

$$ROI = \frac{Gain\,from\,Investment - Cost\,of\,Investment}{Cost\,of\,Investment} = \frac{3,250,000 - 645,000}{645,000} = 4.04 \qquad (2.1)$$

2.2 Budget Allocation

During the design phase, it is important to keep track on every driving resource allocated for each subsystem. Especially for a space mission, the resources are rather limited. As a result of this, all main resources are allocated at the beginning of the project to each subsystem. For this satellite, mass, volume, cost and power were considered to be the main driving resources which influence each subsystem. Computational power was also considered, however, since mainly every subsystem has its own computation unit, these resources were neglected.

2.2.1 Budget Analysis

To be able to efficiently distribute the different budgets to each subsystem, different steps needed to be performed. Firstly, an extensive literature research was performed. While performing this task

[1] http://www.lr.tudelft.nl/en/organisation/departments/space-engineering/space-systems-engineering/expertise-areas/mission-concept-exploration/small-satellite-projects/ [cited 19 June 2015]

it became clear that there is not enough historical data for nano-satellites available to conclude a solid budget allocation since most of the statistical approaches rely on data which deal with heavier and larger satellites above 100 kg [3]. Therefore, this method was discarded as a base of this budget allocation. Secondly, similar missions were identified and their budget allocation were analysed. Here, the Delfi-n3Xt mission was the main point of analysis since it represents a nano satellite mission and its budget was available [8][9][10]. However, since the mission purpose of the Delfi-n3Xt totally differs from this mission, it was decided to also base the budgets on a first estimate method for each subsystem. Based on these methods the budget allocation given in Table 2.1 was applied for this satellite design.

Table 2.1: Final Budget Allocation

	Mass [%]	**Volume [%]**	**Cost [%]**	**Max. Power [W]**
Payload	24	50	25	2
ADCS	10	16	22	12
Structures	18	1	8	0
TT&C	9	9	7.5	12
C&DH	3	8	3	2
Propulsion	10	5	15	3
Power	20	10	18	1
Thermal	2	1	1	1
Other	4	-	0.5	0

In this budget allocation, it is important to notice that in the structures section, also the bearing part is included. The section "Other" mainly consists out of cabling. Also, it should be noticed that in the volume budget, only the volume inside the bus is taken into account. Any other parts which are attached to the satellite, like solar cells, are not taken into account here. Since the thermal control mainly consists out of thin layers of paint, no specific volume budget was allocated here. The same holds for the structures section since the sizing of the momentum wheel was not able to be estimated in the first analysis. During the mission, the power consumption by each subsystem varies significantly and therefore, it was decided to limit each subsystem to a maximum power consumption instead of allocating a percentage to each system. In this budget allocation, it can easily be seen that most of the budget is allocated to the payload and then followed by the ADCS and the power subsystem. In a first estimation, the resources assumed for the satellite were as followed. For the mass budget, a total mass of the satellite was assumed to be 8645 g based on the fact that 6 CubeSat units were assumed for the main bus and half to one CubeSat unit for the momentum wheel. This mass estimation of the momentum wheel was based on a first order estimate. For a single CubeSat unit, a mass of 1330 g was assumed as used for most CubeSats [3]. In the cost analysis, it was assumed that the total cost of the components of the different subsystem is lower than € 400,000. The other € 100,000 would be allocated to production, assembly, tooling, development and research. This allocation will be further analysed in Section 5.2.

To ensure that the final design will meet all the budgets a contingency method was used which will be further elaborated in Section 5.1.

2.3 Sustainable Engineering

In this section, different approaches to improve the sustainability of a space mission will be analysed. To begin, a definition of sustainability, based on the Brundtland Comission report of 1987 [11] and the context of an engineering field, is given.

"Engineering design for human development that meets the needs of the present without compromising the ability of future generations to meet their own needs"

Space missions are inherently polluting. The most critical stage is the launching; it not only about the polluting nature of the exhaust gases liberated to the atmosphere but also about the non-reusable nature of the rockets and other components. This overall contamination is harshly criticised by external parties to the space industry and the general outcry among the sustainably conscious population compromises the acceptance and support of these missions in the future. Therefore, it is clear for the space scientists and engineers that various approaches to tackle this problem should be proposed, as suggested by Kilston [12] and hereby presented.

2.3.1 Green Propellants

In the past, hydrazine mono-propellants were extensively used as a main fuel option. These were cost efficient and commonly deemed as a dangerous solution in terms of safety and toxicity. This has changed in recent times with the advancements in the rocketry field and the utilisation of green propellants for small satellites is gradually turning into a common practice.

The benefits of using green propellants are associated with the following aspects:

- Low toxicity and low carcinogenic risks
- Hardly explosive
- Environmentally beneficial

A type of green propellant that is being presently developed is the ammoniumdinitramide, ADN, propellant. ADN is a solid oxidizer salt initially developed for high performance solid rocket propellants.

Another type is the use of nitrous oxide monopropellant thruster. For this type of propellant, a barrier of 1000 °C needs to be attained. Although the performance of this propellant is not as high as the hydrazine propellant, it is much more cost effective [13][14].

2.3.2 Sustainable Manufacturing

Another approach is to consider stages prior to the launching in where the space mission can be made sustainable. The manufacturing of the spacecraft shows enormous potential.

A greener production process could be achieved in several ways. Firstly, manufacturing processes result in a lot of waste and if this waste stream can be efficiently quantified, many materials could be recycled, reprocessed and possibly reused down the line.

Secondly, an approach towards the selection and utilisation of off-the-shelf components for the spacecraft can reduce the impact of the manufacturing process. This also reduces the costs involved. However, it is important to consider that these components sometimes need to be transported from across the world. In addition, the manufacturing environmental standards of the suppliers is difficult to trace back.

2.3.3 3D Technology

Continuing on the manufacturing line, the utilisation of 3D technology in space could result in an enormous reduction of the weight that must be carried by the launcher, thereby reducing the amount of fuel needed for lift off. Nevertheless, this technology is still at its early phases, and there is still a long way to go.

The concept introduced by the National Aeronautics and Space Administration, NASA, is to build satellites components inside the International Space Station, then bring the satellite together, and ultimately insert the space produced and assembled satellite into orbit from the space station itself. As stated, this would reduce the launch budget greatly and increase the sustainability of the overall mission [15].

2.3.4 Sustainability of Mission

Another way of assessing the sustainability of a space mission is by considering that the purpose of the space missions will result in applications that will increase sustainability on Earth. There is much ongoing debate on the use of space technologies due to its cost, the related contamination of the environment, and the actual benefits of the mission. Most space engineers stand behind the profitability of such missions on the long term, however, people from other disciplines do not immediately identify them. A top goal for the space sector is therefore to prove that with the right space technology, very valuable and unique results of Earth can be obtained.

One special application of space technology is the use of high-resolution imagery. Namely, high-resolution images from the Earth that can provide data on natural phenomena occurring across the

globe. For instance, organisations and agencies in the field of water management and forest control could utilise this input to monitor changes and predict threatening situations.

The present CubeSat mission aims to serve this Earth observation purpose. In particular, this type of satellite is equipped with a high resolution camera and is located at a low Earth orbit. Due to the type of orbit and selected altitude, the satellite will pass over the same area several times in the course of a day. This being ideal for monitoring missions and representing a competitive advantage over aircraft which serve the same purpose, namely as airplane bases missions will require a higher fuel quote [12].

2.4 Production Plan

Now that a final design is chosen, it is important to consider how the final concept will be manufactured, assembled and integrated into a working satellite. This can be described by the production plan, which is described in this section.

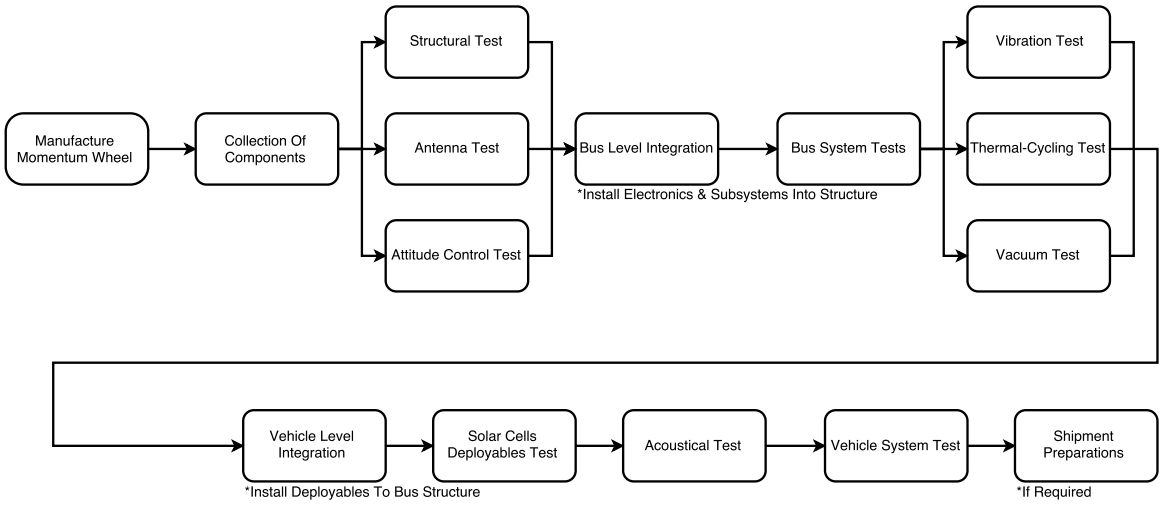

Figure 2.5: Flow Diagram of the Production Plan

In general, the production plan considers the manufacturing of all basic parts, however, since this project focuses primarily on the design of the ADCS, all other parts needed will be bought, if possible, from companies such as Innovative Solutions In Space, ISIS. Therefore, the manufacturing steps have been skipped for the subsystems, which can be seen in Figure 2.5. The only manufacturing left in the figure is for the momentum wheel, since wheels this large are not as common as the parts for other subsystems. Once the momentum wheel has been manufactured and all the parts have been collected from the various companies, the reliability of each electronic circuit board and subsystem will need to be tested, even if it is guaranteed to work. The initial testing phase is split into Structural, Antenna and Attitude Control tests. Thereafter, if all tests are positive, the systems will be integrated into the bus structure, including the momentum wheel. Again, this structure will be tested accordingly. A vibration, thermal-cycling and vacuum test will be performed on the bus.

If all test outcomes are positive, it will be of crucial importance to test the deployable solar panels. Therefore, the bus structure will have the deployables installed and tested. An acoustic test will then be performed.

Lastly, the final test of the whole vehicle will be performed, shown by the Vehicle System Test bubble. If the final test is positive, the satellite will be prepared for shipment and eventually, shipped to the launch site.

2.5 Operations and Logistic concept description

In this section various operational components related to mission stages will be presented. The terms operations and logistics are sometimes used interchangeably with a slight distinction between them.

In here, operations will be referred to as a stage within the whole mission cycle and logistics as the organisational consequence of that particular mission stage. As defined in SMAD [3], Mission Operations is the collection of activities, plans, procedures, policies, and tasks necessary to complete the original mission objectives of a spacecraft. Particularly for the CubeSat mission, the following stages can be identified:

- Design & Development
- Production and Testing
- Pre-Launch
- Final Preparation and Delivery
- Integration and Testing
- Launch
- Spacecraft (Payload) Operations
- End-of-Mission

All these stages differ from each other in resource allocation and complexity. Design & Development is considerably larger in terms of workforce involved and scheduling time than Pre-Launch, for instance.

From the outset of the project, technical divisions start collaborating on possible design concepts at the same time that the administrative segment provides input on possible modification of mission guidelines, especially if external parties, including possible customers, market trends, or governmental organisations demand it. However, the extension of these activities for a CubeSat project is narrowed when compared to industrial projects. The CubeSat, a typical university project, is characterised not only by a tight financial budget and a smaller size of the working group, but also by the simplified nature of the mission to be performed. The inexperience of the student working group is balanced by the lack of communication difficulties that sometimes burden large organisations. In a small university technical group, various divisions readily collaborate and project decisions are more straightforwardly taken.

As the project gains maturity, the collaboration continues to utilise financial, human and physical resources. This latter in particular when the satellite components need to be manufactured and tested. Though, for the case of the present CubeSat off-the-shelf components will be used. This approach decreases the complexity of manufacturing single components but a possible incompatibility and wrong integration of components can compromise the whole mission. More information on this mission stage is presented in the Production Plan in Section 2.4.

The following operational stage requires external coordination and also consumes communication resources from the beginning of the project. CubeSats are commonly launched as secondary payloads. The responsible launch provider needs to agree first on carrying along other secondary payloads as they could possibly jeopardise the success of the primary mission. For this coordination between CubeSat developers and launch providers, there are intermediate integration organisation that make arrangements on behalf of both parties. Firstly, the CubeSat developer will agree on a date for the intermediary to receive the satellite. This is the last time the university team has contact with the satellite until it is first inserted into orbit. From this point onward, the intermediary has the responsibility for the testing and integration to the launcher.

The following stage is seen as the crux of the mission – the time when the satellite is in orbit and can finally perform its intended mission. The working divisions that collaborate at this stage are: mission control, data transfer, spacecraft and payload operations, data processing and archiving, and navigation and orbit control. The CubeSat is commanded from a CubeSat Earth station. This is commonly a low cost station and the communication and commanding is usually based on amateur radio technology. Primarily with UHF/VHF, Ultra High Frequency and Very High Frequency, stations; S-band stations are considerably larger. At an earlier stage of the project, namely at the development stage, administrative resources have already been used to coordinate with the international Amateur Radio Union, IARU, for a communication frequency allocation. This process can be simplified with the assistance of the Global Educational Network for Satellite Operations, GENSO, which is a project initiated and supported by the International Space Education Board, ISEB. Additionally, in the case of the CubeSat which carries a sensing device, such as a camera, a licence for Earth remote sensing must be acquired [3].

At the end of operations, it is commonly required for the launch providers to obtain a certification of the de-orbit time for the CubeSat to be 25 years or less. This is not a major problem as CubeSats

commonly have a mission life spanning from a couple of months to maximum a couple of years. Moreover, they are located at low orbits so they are more easily de-orbited. Finally, mission management, which has been carrying out administrative activities from the outset should formally terminate the mission by reviewing internally and externally the outcome of the whole project.

From the summary just presented, it can be seen that the CubeSat process involves a high degree of resource allocation. The fact of maintaining an engineering and administrative division, communicating with external parties for permission and arrangements, renting testing facilities and transportation is commonly known as the logistics involved in an operational stage. The collection of resource-consuming activities, either financial, time, human or physical is part of all operational stages. The objective of operations engineering is therefore to streamline the process, and as a consequence of this to reduce the life-cycle costs, LCC, and increase the system's reliability.

2.6 Risk Assessment

In this section, a risk analysis and a risk map are given. These components are essential for the resource allocation since they will determine the amount of consideration that needs to be brought to each part of the project.

2.6.1 Risk Analysis

It is hardly feasible to design an entire spacecraft system that is 100% reliable. The risk analysis is useful in these kind of situations where levels of priority among subsystems should be determined. It becomes a question of time and budget allocation. The risk of a certain subsystem failing influences this decision.

Risk is dependent on consequence and probability of failure with Equation 2.2 [16].

$$R = C \times P \tag{2.2}$$

Where C represents consequence and P the probability. Two types of risks exist: implementation risk and mission risk. Mission risk is usually defined as the risk resulting from the mission, which looks at the consequence that would result from failure in terms of the mission.

In order to determine risk, a risk management plan is setup. To setup this plan, all the mission phases are analysed and potential risks are taken into account for each phase. The mission plan was determined inside the FFD. Inside this plan, only the risks that are likely to affect the mission and that are relevant to the mission purpose are analysed. Those risks are determined out of previous similar missions where failure occurred.

Inside the whole mission process, the first phase is the design phase. Here, by design phase, it is defined as the period starting from the initial setting up of the project plan until the launch, including the manufacturing phase. Inside this design phase, several potential risks are listed :

- **1. Going over budget**: At the start of a project, the budget that is available is usually fixed. Since it is difficult to foresee parts that will not go according to plan from the start, some flexibility is generally possible. However, since infinite money does not exist, at one point, the integrity of the mission can be compromised if the resources are not used wisely.
- **2. Failure to meet deadlines**: Similarly to budgeting, a deadline for each phase is set. However, these deadlines can sometimes be difficult to meet. Different from budgeting, intermediate delays always occur, however they do not create large issues such as going over budget. The final deadline however has to be met. There is no possibility of postponing the final deadline, since the project can be considered a failure.
- **3. Structural failure due to manufacturing defects**: During the manufacturing of the CubeSat, care needs to be taken in order to produce a structure that is defect-free. If there are cracks present, these can grow during mission lifetime and result in catastrophic failures.

Once the satellite is designed, it needs to be launched. During this launch phase, the satellite is put into orbit, a checkout is performed and the attitude correction phase can begin. This phase is really important since it will determined the extent of the camera's precision into taking pictures of the Earth. Similarly to the design phase, several potential risks are evaluated :

- **4. Structural failure due to vibrations during launch phase**: An important consideration during the launch phase is the presence of vibrations. These vibrations can sometimes lead to catastrophic consequences if the structure is not properly designed.

- **5. Failure to determine the attitude**: In order to stabilise the satellite, the attitude needs to be determined. This plays a significant role inside the mission since it is complicated to achieve.

- **6. Failure to stabilise the CubeSat in orbit**: A really important action before the start of the mission is the stabilisation of the satellite in its orbit. This has a huge impact on the mission because it is complicated to realise in such low orbits and reduces the chances of success of the mission. During the Mid-term phase of this project, this part was critical during the process. However, as the design process progressed, new methods were investigated which allowed the stabilisation of the satellite to take place without much likelihood of failure.

Once all operational checkouts are performed, the actual mission can begin. During this phase several critical risks can occur:

- **7. Payload failure**: Probably one of the most critical aspects of the mission will be the payload failure. Indeed, if the payload fails, the mission will not take place. This will therefore have a very high importance.
- **8. Failure to transmit data to ground station**: Similarly, once the picture is taken, if the on-board computer is not able to transmit the images, the mission's purpose is irrelevant.

- **9. Structural failure due to space debris**: This aspect can also be considered during check out. The occurrence of space debris at VLEO is rare but will have high consequences if it were to happen.

2.6.2 Risk Map

Once all the relevant risks have been determined, a risk map can be built. However, before that can be done, the severity of each risk needs to be determined. In Table 2.2, a risk map is presented. Below the map, the reasons for the different positions are explained.

Table 2.2: Risk Map for the CubeSat

5 Near Certainty					Red
4 Highly Likely					
3 Likely		Yellow		2	
2 Low Likelihood				1,3,4,8	7
1 Not Likely	Green				9 ,6
Probability/ Consequence	1 No Consequence	2 Negligible	3 Marginal	4 Critical	5 Catastrophic

Inside the Risk Map in Table 2.2, the red zone represents parts that need special attention during the risk mitigation process. The yellow zone is an area where some risk mitigation still needs to be applied but not in a extensive way. The green zone is a safe zone where risk mitigation is not really necessary. Since the purpose of this risk map is to have a reliable tool that will be helpful inside the design process, only risks that are considered important are stated here.

1. **Going over budget**: Comparing with the Delfi missions which cost around € 200000 compared to the actual budget of € 500000. Both satellites can be compared although this mission has an imaging payload and therefore more focus is given in the current project on the ADCS system. However the budget is a factor of 2.5 higher than the Delfi-N3xt budget. It can be concluded that there is a low likelihood of going over the budget. In case that would happen however, the consequences could be critical since the cost limit is a hard requirement.

2. **Failure to meet deadline**: The end of this project is concluded by a symposium day where all the work done is presented during a presentation. It is critical to meet this deadline since there will be no chance for a deadline extension. Therefore, the consequence is very big. Though this project is designed in such a way that the time to finish usually is adequate, it can be that specific deadlines are not met. Therefore there is a medium likelihood of this happening.

3. **Structural failure due to manufacturing defects**: This risk is related to the occurrence of manufacturing defects. Structurally speaking, the CubeSat in itself follows from other subsystems and the process has been implemented number of times. The manufacturing process under its production is therefore not very complicated and the chances of having defects is low. However if these defects would create some failure mode, the whole structure would collapse catastrophically. Therefore it is necessary to be careful during the production phase.

4. **Structural failure due to vibrations during launch phase**: One important phase inside the mission is the launch phase. It is during this phase that the spacecraft is subjected to its highest vibration loads. It is therefore critical that the spacecraft is able to sustain those loads. A consequence from this would be critical.

5. **Failure to determine attitude**: Before the actual mission can begin the attitude must be determined. In order to do that, a feasible concept needs to be implemented. It is important to have a good read of the attitude in order to stabilise it. In the space environment where the satellite is travelling, the satellite is relatively close to the Earth, between 230 and 350 km. This makes the attitude determination more straightforward. Therefore it is not likely that a problem presents itself. However, the consequence is important. The attitude determination will help for the attitude control since the attitude needs to be known before it can be corrected.

6. **Failure to stabilise the CubeSat in orbit**: Probably the most important part of the mission. The stabilisation of the CubeSat is determinant for the success of the mission. If the satellite is not properly stabilised, the camera cannot perform the mission. In the drag environment where the satellite is located, it is very difficult to stabilise the satellite. Therefore it is likely that this might not succeed. Moreover, a failure in this would be catastrophic.

7. **Payload Failure**: The failure of the payload would be disastrous since it is the main element inside the success of the mission. However, the likelihood of the camera failing is rather low since the technology can be tested on Earth and has been used for many years.

8. **Failure to transmit data to ground station**: Once the data is collected, it needs to be transmitted to the station. The data transmission is often tricky since there is a need for direct transmission between the ground station and the CubeSat. Since data exchange is important for an observation satellite, this will have a large consequence if failure occurs.

9. **Structural failure due to space debris**: Debris is a very dangerous part of the space environment. An impact from a space debris is disastrous. However considering the space environment, the likelihood of a debris hitting the satellite is very low

Chapter 3

Environmental Analysis

In this chapter the Space Environment is analysed. Every aspect of the region in space where the mission is conducted will be elaborated on in this chapter. Firstly, the payload is analysed. In the second section the disturbances are presented. All the details about the orbit are in the third section about Astrodynamics. Fourthly, the Aerodynamics are elaborated on and the last section is devoted to the Stability.

During the design process the axis system is defined as in Figure 3.1. The x-axis is pointing in the flight direction the y-axis is nadir pointing and the z-axis is perpendicular to both following the right hand rule.

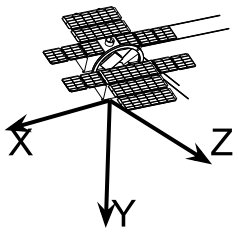

Figure 3.1: Defined Axis System

3.1 Payload

For a successful design, it is important to analyse the required stability of the satellite platform. The stability in this case is mainly driven by the payload. As a result, the payload needs to be analysed first. This section is therefore dedicated to analyse the target payload. Firstly, the given requirements for the payload will be analysed and afterwards the design solution will be presented. From the given design, the maximal orbital altitude can be concluded which is important for the completeness of the environment analysis. The stability of the payload will be further elaborated in Section 3.5.

3.1.1 Payload requirement

The main driving requirements could be derived from the mission statement for the payload. The main requirement can be seen in the following list:

- **S08-MP-01** *The spatial resolution shall be lower than* 4 m
- **S08-MP-02** *The maximum spatial resolution shall be provided at a pointing accuracy of* 5°
- **S08-MP-03** *The payload subsystem shall be able to operate in the visible spectrum of light (*400 nm - 700 nm*)*
- **S08-GTC-V-05** *The payload subsystem shall have a volume smaller than* 10 cm x 10 cm x 30 cm
- **S08-GTC-M-05** *The payload mass shall be lower than* 2.0 kg
- **S08-GTC-P-02** *The total power used by the payload shall be lower than* 2 W
- **S08-MC-C-09** *The payload shall cost less than* € 100.000

3.1.2 Payload Design

The payload design is the main driving system of the whole satellite design. Therefore, it is important to find the an efficient design for the payload. To achieve that a market analysis was performed to find possible designs which was than used as a base to develop the payload.

Possible Payloads
As already described earlier, a market analysis was performed to analyse the possible payloads to meet the given requirements. From this market analysis, two main designs could be concluded that were able to meet those requirements. On the one hand it is the 600-75-16-VIS [17] and on the other hand it is the ANT-2A [18] designed by the Technical University of Delft. The technical drawings of both possible payloads can be seen in Figure 3.2.

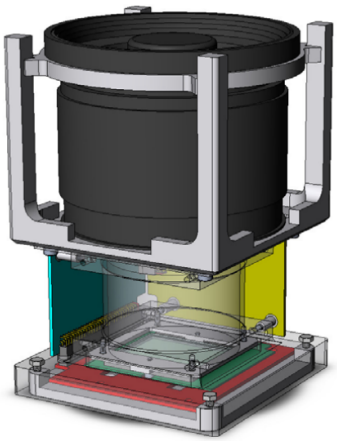

(a) 600-75-16-VIS[17]

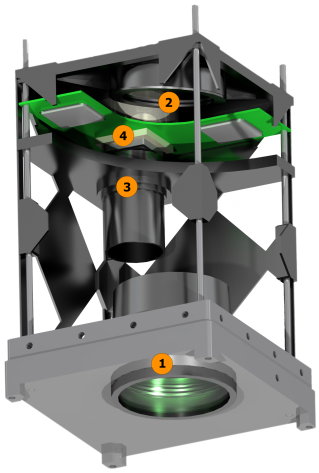

(b) ANT-2A; first lens(1), two flat mirrors(2), final lens(3), sensor(4)[18]

Figure 3.2: Possible Payloads

By analysing both possible payloads, it can be concluded that both provide a spatial resolution of 7.05 m at 540 km orbital altitude. This results in a spatial resolution of 4 m at an orbital altitude of around 288 km for both designs. A summary of the main features can be seen in Table 3.1. Due to a lag of information a comparison for the Modulation Transfer Function, MTF and the Signal-to-Noise ration, SNR could not be performed for this two designs.

Table 3.1: Possible Payloads

	600-75-16-VIS [17]	**ANT-2A [18]**
Spatial Resolution	7.5 m @ 540 km	7.5 m @540 km
Size [cm]	10x10x20	10x10x15
Active Pixel	4872 x 3248	2048 x 2048

As can be seen from Table 3.1, the ANT-2A has a smaller size. Based on this fact and that way more data was accessible for this payload design, the ANT-2A was chosen the better solution for this satellite platform. However as already concluded the target altitude of the satellite will be 288 km which leads to a mission life of slightly higher than one month. Since this design is intended to have a mission life longer than 90 $days$, this design solution would require a significant amount of propellant to counteract the orbital drag. Based on this fact, it was decided to use this design as a base to generate an improved design to increase the orbital altitude and therefore increase the mission life.

Improved Payload Design
The final design is an off-axis modified Ritchey-Chretien Telescope in combination with two corrective lenses. A layout of the new payload design can be seen in Figure 3.3.

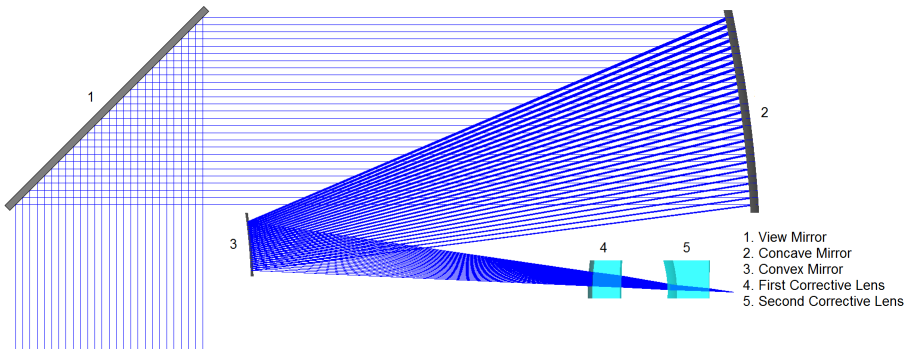

Figure 3.3: Improved Payload Design Layout[19]

By using this off-set design, it is ensured that the improved design is a rather compact design solution in comparison to other possible solutions. It also enables the design to have a nadir viewing angle perpendicular to the optical axis of the telescope. Moreover, the satellite bus is designed, to ensure that a smaller frontal area is pointed into the flight direction which, at the same time, reduces the drag coefficient and therefore the total aerodynamic drag encountered by the satellite. By reducing the aerodynamic drag, the mission life will be considerably increased. To maximise the incoming light, it was decided to use a rectangular aperture size of 80×60 mm. This higher aperture size leads to a better Signal-to-Noise ratio which is favourable for a higher image quality. The design uses aspherical mirrors which are more complex and therefore increase the production cost and time but at the same time enables a nearly diffraction limited performance over a wide Field-of-View [19].

In this design, a line sensor is going to be used to convert the incoming light into a usable image. The main difference between a line sensor and a conventional image sensor is the fact that the sensor size has a height of only one pixel. Therefore, it needs to image constantly and will generate a single image instead of multiple images which needs to be merged together. The main disadvantage of this sensor type is the fact that the stability around the nadir pointing axis needs to be better in comparison to conventional sensors. This will be further elaborated in Section 3.5. This payload design uses a AWAIBA Dragster DR-4k-7 detector with a pixel number of 4000×1 pixels and a pixel pitch of $7\mu m$. This high pixel pitch is favourable in terms of image quality and digital noise as well as dynamic range during imaging [20]. A short summary of all payload data is given in Table 3.2.

Table 3.2: Final payload summary[19][20]

Parameter	**Value**
Size	$10 \times 10 \times 30$ cm
Mass	2 kg
Power	2 W
Focal Length	612.5 mm
Aperture Shape/Dimensions	$Rectangular$ / 80×60 mm
Spatial Resolution	4 m @ 350 km
Field of View	2.6 deg
Swath Width	16 km @ 350 km
Number of Cross-Track-Pixel	4000
Pixel Pitch	7 μm
Sensor Optimised Bandwidth	$400 - 700$ nm
Optical Optimised Bandwidth	$450 - 700$ nm
SNR	88.6
MTF @ Nyquist	> 52 %

By using this payload design the satellite will be operated in an imaging mode in an orbital altitude between 350 km and 230 km.

3.1.3 Compliance Matrix

As a final step, the improved payload design needs to be checked if all its requirements can be met. Therefore, a compliance matrix is created and can be seen in Table 3.3.

Table 3.3: Payload Compliance Matrix

Requirements	Compliance
S08-MP-01	✓
S08-MP-02	X / ✓
S08-MP-03	✓
S08-GTC-V-05	✓
S08-GTC-M-05	✓
S08-GTC-P-02	✓
S08-MC-C-09	✓

It can be concluded that all requirements are met by this improved design. However, it is important that requirement S08-MP-02 can not be checked at the moment since it is highly related to the ADCS design. Therefore, it will be further elaborated in Section 4.1. Also, it is important to take into account that requirement S08-MP-03 can be met by both the sensor design and the optical design. It is important to notice that the optical design is augmented for a bandwidth of $450 - 700\ nm$ as it can be seen in Table 3.2. However, the optical design is still able to represent the bandwidth between $400 - 450\ nm$ in an acceptable manner. Finally, it can be concluded for this section that the improved design will be used for this satellite platform.

3.2 Disturbances

The space environment is a harsh environment. Every little disturbance can have a large effect on the attitude. In order for the ADCS system to work properly, all external disturbances need to be taken into account in the design of the ADCS. In the altitude range from 230 km to 380 km, the biggest disturbance will be the gravity, which is discussed in Section 3.2.1, followed by the atmospheric drag which is introduced in Section 3.2.2. Below 700 km, the solar radiation is the third strongest disturbances, and is explained in Section 3.2.3. Lastly, the magnetic disturbances are discussed in Section 3.2.4. Throughout this section, the misalignment between the centre of gravity and the centroid of the satellite is assumed to be 1 mm. The value calculated from Section 4.8.1 is smaller than 1 μm, however, inaccurate placing is taken into account in this section. For the disturbances, the lowest altitude is taken into account because the disturbances are the biggest at lower altitudes, especially the aerodynamic disturbances. Note that for the calculations, the solar activity is assumed to be medium, because models show that the expected solar activity in 2016 is medium [3].

3.2.1 Gravity Gradient

The gravity gradient is a torque resulting from the difference between the centre of mass and the centre of gravity. On Earth, due to negligible gravity variations, the centre of mass is mostly considered the centre of gravity. However inside the micro gravity environment of space, the centre of gravity changes become more important compared to the centre of mass shift. This creates an internal torque due to the difference in location. Also, differences in the mass moment of inertia, MMOI, heavily influence this torque. The gravity gradient torque is given by Equation 3.1 [3]

$$T_g = \frac{3\mu}{2R_o}|I_z - I_x|\sin(2\theta) \tag{3.1}$$

In order to lower this disturbance, the centre of mass should be kept as close as possible to the geometrical centre of the satellite. By doing this, the gravity torque resulting from the satellite becomes very low and this disturbance can usually be neglected. In this prospect, the centre of mass is usually defined within a fixed range before launch, and failure to comply with this could result in gravitational torques that can not be overcome by ADCS control.

For the CubeSat, the magnitude of the gravity disturbances at 230 km altitude are in the order of $10^{-9}\ Nm$, because the satellite is small and therefore the moment of inertia can be balanced very well [3]. These disturbances are rather small in comparison the the aerodynamic disturbances, and are therefore neglected in the sizing of the ADCS in Section 4.1.

3.2.2 Atmospheric Drag

The atmospheric drag can be calculated by means of the NRLMSISE-00 model. In Section 5.7 the model is validated and verified with the built in function of MATLAB. The input variables are the altitude, day of the year, solar flux average, the solar flux daily, latitude, longitude and the magnetic index.

The first estimation however, was done using Equation 3.2 from SMAD [3].

$$T_a = \frac{1}{2}\rho C_d A_r V^2 \left(cp_a - cg\right) \tag{3.2}$$

The magnitude of this aerodynamic drag is in the order of 10^{-6} Nm. This value is highly dependent on the solar activity, since the properties of the atmosphere, such as temperature, pressure and density, are highly influenced by the amount of solar radiation. The lower the solar activity, the lower the density, so the longer the lifetime, as can be seen in Section 3.3 about the astrodynamics.

3.2.3 Solar Radiation

Radiation pressure is caused by the momentum of photons colliding with the spacecraft and is strongest for light satellite with a large surface area. The solar pressure is the second largest disturbance for satellites above a altitude of $500-800$ km depending on the atmospheric model. The radiation pressure can be divided into 4 sources; sun pressure, albedo pressure, IR earth radiation and IR radiation of the spacecraft itself. From which the direct sun radiation is the dominant factor. Incoming light can either be absorbed or reflected. Which can be diffusive or specularly reflected. This is denoted by ρ_d and ρ_s respectively. The absorbed fraction is denoted by α. Summing these values gives Equation 3.3 [21] which for non-transparent materials is equal to 1 and is known as Lamberts distribution.

$$\rho_d + \rho_s + \alpha = 1 \tag{3.3}$$

The solar radiation pressure can be calculated according to Klinkrad and Fritsche [21], using Equation 3.4 where the summation sign is used to include all radiation pressure sources. $\dot{e}_n$ is the energy flux, c the speed of light and A_{ref} is a reference satellite cross section. $\vec{C}_{r_n}$ is the radiant force coefficient which is given by Equation 3.5 [21]. The radiant coefficients consist of an integration of all the local contributions $\vec{c}_{r_n}(\vec{r})$.

$$\vec{F}_r = \sum_{n=1}^{4} \frac{\dot{e}_n}{c} A_r \vec{C}_{r_n} \tag{3.4}$$

$$\vec{C}_{r_n} = \frac{1}{A_r} \int_{(A_n)} \vec{c}_{r_n}(\vec{r}) dA \tag{3.5}$$

The local contributions can be calculated using Equation 3.6 [21], which is dependent on the unit incident vector $\vec{u}_n$, the normal plane vector $\vec{n}$, the material properties such as the deflections, emissivity ϵ and temperature. It is further dependent on the the Stefan-Boltzmann σ constant and the speed of light.

$$\vec{c}_{r_n}(\vec{r}) = (\vec{u}_n\vec{n})(1-\rho_{s_n})\vec{u}_n + \frac{2}{3}\frac{\sigma}{c}\epsilon_n T_w^4 \vec{n} + (\vec{u}_n\vec{n})\left(2\rho_{s_n}\vec{u}_n\vec{n} - \frac{2}{3}\rho_{d_n}\right)\vec{n} \tag{3.6}$$

When the design is not yet determined Larson gives a good approximation for the solar pressure acceleration according to Equation 3.7 [22]. The accelerations is the solar pressure force divided by the mass of the satellite. In Equation 3.7, A is the cross section exposed to direct sunlight, M is the mass of the spacecraft and r is a reflection factor. Where r is a value between 0 and 1 in where an r of approximately 0.4 corresponds to a complete diffusive reflection, which is a good first approximation.

$$a_R \approx -4.5 \times 10^{-6}(1+r)\frac{A_r}{M} \tag{3.7}$$

The magnitude of the solar pressure disturbances are in the order of 10^{-7} Nm. Therefore, they are also negligible with respect to the aerodynamic disturbances and are therefore disregarded in the sizing of the ADCS in Section 4.1.

3.2.4 Magnetic Field

Magnetosphere components and the iron core dynamo form the Earth's magnetic field. The magnetosphere components consists of the ring current, the cross-tail current and the magneto pause surface current. The calculation of the magnitude of the Earth's magnetic field follows from a combination of the Maxwell's equations, Ohm's Law and the Equation of Continuity. The final equation is given by Equation 3.8.

$$B(R,\lambda) = \left(1+\sin(\lambda)^2\right)^{\frac{1}{2}} \frac{B_0}{R^3} \tag{3.8}$$

In where B is the local magnetic field intensity, λ is the magnetic latitude, R is the measured Earth's radius (R_E), and B_0.

Electrical Charging
The magnetic field itself does not have much influence on the spacecraft. The real problem occurs when the magnetic field interacts with solar winds. This interaction causes the magnetic field which is on the night side of the Earth to become a long, stretched magnetic field called the magneto-tail. This results in the creation of magnetic storms. Inside this magnetic storm area, an energised plasma is produced. The interaction of this plasma in low-earth altitudes results, occasionally, in serious problems for the attitude sensors of the CubeSat. This phenomenon is called electrical charging.

This charging produces an accumulation of charges on the surface of the satellite. This, in turn, generates an electric field that accelerates oppositely charged particles. At the end of this process, the surface attains its maximum charging potential and no more charges can be accumulated. Another charging effect results form solar radiation but this will not be discussed here. This interaction of the plasma with the surface of the satellites results in negative effects.

Arc-charging is one phenomenon that results from excessive interaction. Arc-charging results when the generated electric fields go over a maximum threshold of surface charging. These arcs generate a electromagnetic pulse that interacts with the electrical subsystems of the spacecraft. These interactions greatly affect the attitude sensors of the satellite resulting in wrong measurements. Moreover, physical damages also occur from this charging effect.

A wrong reading from the sensors will of course compromise the whole mission purpose. It is therefore important to come up with measures to avoid this. One important consideration is the choice of adequate materials. In order to reduce the effects of this charging, conductive coatings can be applied to increase the potential electric field. If this does not provide to be useful, some changes can be implemented in the electrical subsystem itself.

Magnetic Torque
While the electrical charging mostly affects the sensoring part of the ADCS, this section analyses the disturbances inside the active stabilisation of the satellite.

As stated above, the Earth possesses a magnetic field resulting from the Earth's liquid core. However, satellites also possess a certain level of residual magnetic field. This field's magnitude is usually very low , however when it is not aligned with the direction of the Earth's magnetic field, this results in a differential torque called the magnetic torque. Although the Earth's magnetic field is constantly varying, an assumption is made to consider the field as constant dipole. From there, the magnetic torque can be calculated using Equation 3.9.

$$T_m = DB = D\left(\frac{M}{R^3}\lambda\right) \tag{3.9}$$

In this equation, D is the spacecraft residual dipole moment. M is the magnetic moment of the Earth multiplied by the magnetic constant, which gives a value of $7.8 \times 10^{15} T \cdot m^3$ [3]. R is the radius of the Earth plus the altitude of the satellite and λ is a term that is influenced by the orbit. For a polar orbit, it is 2, and for an equatorial orbit, it is 1. The magnitude of the magnetic disturbances are in the order of $10^{-8}\ Nm$.

3.2.5 Third Body

Third body disturbances are an example of another disturbance that may occur during the orbit. However, from Figure 3.4, it can be concluded that they are negligible in comparison to the gravity gradient disturbance of the earth, especially for low orbits.

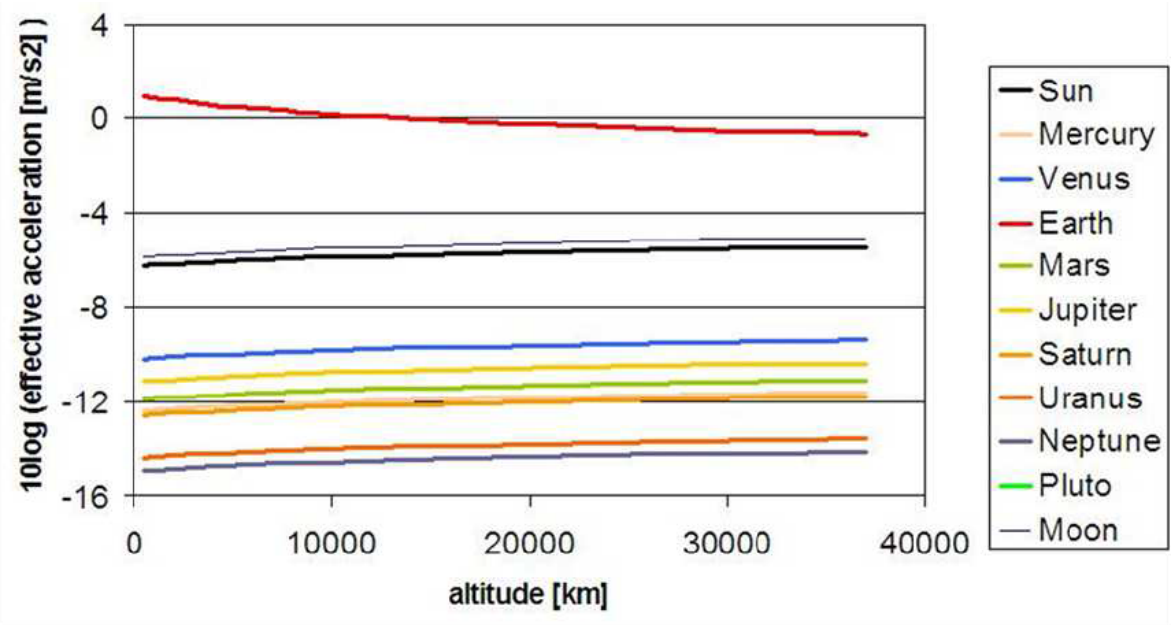

Figure 3.4: Third Body Disturbances as a function of the Altitude [23]

The conclusion of this section is that the aerodynamic disturbances play the most important role in the chosen orbit, so the ADCS system should mainly be designed to be able to counteract this kind of disturbances. Therefore, in the rest of the report, T will be the magnitude of the aerodynamic disturbances, since the sum of all disturbances is basically equal to this value, independent on the altitude.

3.3 Astrodynamics

In this section, the evaluation whether the requirements on astrodynamics are met is presented, describing the requirements and presenting the compliance matrix afterwards in Table 3.4. The requirements for the astrodynamics are the following:

- **S08-MC-ADC-01** *The satellite shall operate in a VLEO Orbit between* 230-350 *km*
- **S08-MC-ADC-02** *The satellite shall be able to maintain the same orbit with an accuracy of* ± 10 *km*
- **S08-MC-ADC-03** *The satellite shall be able to change its orbital altitude with a rate of* 500 m/day

3.3.1 Orbit

Based on Requirement **S08-MP-01** and the properties of the camera as described in Section 3.1, the maximum altitude of the orbit should be 350 km. Based on this value and the value for the minimum altitude according to Requirement **S08-MC-ADC-01**, the mission will take place between 350 km and 230 km altitude. According to Kepler[23], the orbital times are 91.5 and 89.1 minutes respectively.

Based on another property of the Payload; the amount of light it needs in order to be able to operate, the orbit was chosen to be sun-synchronous, SSO, with a Right Ascension of the Ascending Node, RAAN, such that the satellite will always fly over at midnight and at noon. The inclination for such an orbit is 96.85° [23]. An important property of the orbit is the eclipse time. Based on basic calculations, the eclipse time at 350 km altitude is calculated to be 36.3 minutes. The eclipse time at 230 km is 37 minutes. However, due to various effects, this value is not accurate up to seconds.

The real value can deviate around half a minute because of the flattening of the Earth (max 22 s), refraction of light in the atmosphere (max 8 s) and the difference between umbra and penumbra (max 8 s) [23].

In order to have the same quality and properties for every picture taken, Requirement **S08-MC-ADC-02** should be met. In order to do this, the satellite is launched with an initial eccentricity of 0. However, there can be imperfections during the launch and deployment, and due to the equatorial bulge, the gravity acting on the satellite is not equal everywhere. Therefore, the eccentricity has a value in the order of 10^{-5}. This value however induces a variation in the altitude of $\pm$ 7.5 km.

3.3.2 Launch

In order to launch the satellite, a suitable launcher is needed. Since the ceiling for the QB50 project is 350 km altitude[1], and they have ordered a customised launch, it might be possible to enroll on this launch and get in orbit slightly above 350 km altitude in 2016. However, if this is not possible, an already scheduled launch should be chosen in order to minimise the launch costs. A promising launch for a Sun-synchronous orbit takes place in 2017, launching the payloads in SSO at 500 km altitude[2]. However, since a SSO at 500 km has a different inclination than a SSO at 350 km, the inclination of the CubeSat should be half a degree different than the inclination of the launcher. In order to change the inclination of the satellite, a ΔV budget of 0.07 km/s is needed. In order to decrease the altitude from 500 km to 350 km using a Hohmann transfer orbit, another 0.14 km/s is needed [23]. This implies thrusters are needed.

However, there are other solutions that do not need a ΔV budget. In order to decrease the ΔV budget needed for the inclination change, the satellite should be launched in a slightly other direction than the satellites that will be launched in SSO at 500 km altitude. Furthermore, satellites in general tend to decrease their altitude. This decrease is dependent on the frontal area as can be seen from Equation 3.2. Therefore, the satellite can be rotated in order to decrease the time it naturally needs to decrease the altitude from 500 km to 350 km. However, this would only be necessary of the launch for the QB50 project is not suitable.

3.3.3 Orbital Decay

The time the satellite needs to decrease its altitude is calculated using a program from the Australian Government Bureau of Meteorology [24]. The time it takes to lower the altitude from 500 km to 350 km is 680 days in drag mode, using a drag coefficient of 3, so there is plenty of time to spin up the momentum wheel during this phase as can be seen in Figure 1.1, Function 3.6. The time it takes the satellite to decay from 370 km to 230 km in drag mode is 12 days. This time can be used to detumble and to spin up the reaction wheel.

The time it takes the satellite to decay from 350 km to 230 km in normal mode, the mission time, is 200 days [24], assuming a drag coefficient of 2. In this calculations, a solar flux of 80 SFU is assumed, which would be the average predicted F10.7 in 2016 according to NASA[3].

Requirement **S08-MT-S-01** says that the satellite should be able to de-orbit after its maximum life-time. Again, the drag mode can be used, by turning the satellite 90° using the ADCS. At 230 km altitude, in drag mode, independent of the solar flux, the satellite will re-enter the atmosphere within one day.

3.3.4 Justification

All values calculated in this section are based on analytical expressions. Therefore it is a simple task to see whether the equations were performed correctly. For instance in the back cover of SMAD [3]. Since the equated values are all in the range of the values given in SMAD, it is assumed that the calculations are performed correctly, and the only difference in the value is induced by rounding errors.

[1] `https://www.qb50.eu/index.php/project-description-obj/mission-objectives` [cited 18 June 2015]
[2] `http://www.spaceflightindustries.com/schedule-pricing/` [cited 18 June 2015]
[3] `http://www.swpc.noaa.gov/products/predicted-sunspot-number-and-radio-flux` [cited 18 June 2015]

3.3.5 Compliance Matrix

In Table 3.4 the compliance matrix is presented. As can be read in the section above, all requirements on astrodynamic properties are met.

Table 3.4: Astrodynamics Compliance Matrix

Requirements	Compliance
S08-MC-ADC-01	✓
S08-MC-ADC-02	✓
S08-MC-ADC-03	✓

3.4 Aerodynamics

Throughout this mission, the satellite will orbit the earth in the thermosphere. Although general aerodynamics does not occur at this altitude, there is still some effect from the atmosphere, namely the free molecular flow. Here, the atmosphere is so dense that molecules are spread out by large distances. Therefore, the characteristics of the atmosphere due to this flow depends largely on the random chances of molecules hitting the satellite. This section gives details of what can be expected.

3.4.1 Temperature, Pressure and Density

As mentioned before, the thermosphere contains a low density of molecules, which affects the satellite in many ways. Firstly, the ambient temperature at the thermosphere is relatively high, with a value of 900 K to 1600 K. This is the temperature of the molecules, however, since the molecule density is so low, the temperature affecting the satellite is much lower than sea level temperature. Also, the density changes throughout the thermosphere are significant, sometimes a factor of 10 variations. This is mainly due to solar flux and the magnetic indices. Lastly, pressure is related to temperature and density, meaning any changes in density also affects the pressure in the same manner.

3.4.2 Thermospheric Model

For this project, a simulation has been made in order to approximate the drag and lift that the CubeSat will experience at the VLEO, where free molecular flow dominates. This flow is hard to predict, therefore a complex model was used. The Atmospheric lift and drag was calculated by means of the NRLMSISE-00 model. In Section 5.7, the model is validated and verified with built in functions of MATLAB and also compared with the thesis from Dr. ir. E.N. Doornbos [25]. The input variables of the model are the altitude, day of the year, solar flux average, the solar flux daily, latitude, longitude and the magnetic index.

3.5 Stability

The main goal of the CubeSat design is to provide a stable platform to be able to generate sharp and correctly pointed images. The sharpness of the image is mainly influenced by two satellite characteristics. On the one hand it is influenced by the ground shift of satellite position while taking the image and on the other hand, the angular stability of the CubeSat. Both of these characteristics are related to the integration time of the payload. Which in turn is mainly influenced by the exposure time. Therefore, the required exposure time is going to be derived first. Since the payload will be operating between 350 and 230 km altitude, a stability analysis will be done for both altitudes. A summary of all calculated values can be seen in Table 3.5.

3.5.1 Exposure Time

For this analysis, it is assume that a shift of half a pixel width is the maximal boundary to generate a sharp image. This means that the maximum exposure time allowed is equal to the time the satellite

needs to travel 2 m on its ground path. The image shift resulting from the movement of the satellite can be calculated by using Equation 3.10.

$$d_g = \frac{R_e}{\sqrt{\frac{R_o^3}{\mu}}} \cdot t_i \tag{3.10}$$

In this equation, the ground distance is given by d_g, R_e represents the Earth radius, R_o is the orbital radius, μ is the gravity parameter and t_i is the integration time of the payload. The integration time can be calculated by using Equation 3.11.

$$t_i = \frac{d_g}{R_e} \cdot \sqrt{\frac{R_o^3}{\mu}} \tag{3.11}$$

From this equation an exposure time of 0.274 ms and 0.175 ms is required for a sharp image at an orbital altitude of 350 km and 230 km respectively. However, as described in Section 3.1 the exposure time of the payload should be 0.548 ms and 0.351 ms for 350 km and 230 km orbital altitude respectively, these exposure times are going to be used in the further analysis. This higher exposure time is required for an improved signal to noise ratio. From this longer exposure time the image needs to be kept more stable than for a smaller exposure time. Therefore, the ADCS will need to provide a lower angular change during integration time to improve the stability of the CubeSat and therefore the payload.

3.5.2 CubeSat Stability

As already described earlier, the CubeSat platform needs to be able to provide a certain stability around all axis to generate stable and sharp images. Therefore, an analysis of the required angular velocities will be done. Here, the angular velocity is of high importance since a change in the attitude during exposure will also cause a shift in the ground image. Since it is not possible to keep the CubeSat completely stable, it is important to analyse the angular velocity around all axes. In this analysis it was assumed that only the stability of the payload bus itself is analysed and not the rotating momentum wheel.

Angular Velocity Analysis around the x- and z-axis
An attitude change around the x- and z-axis of the payload results in a image shift on the ground. The concept of these shift around the x- and z-axis can be seen in Figure 3.5.

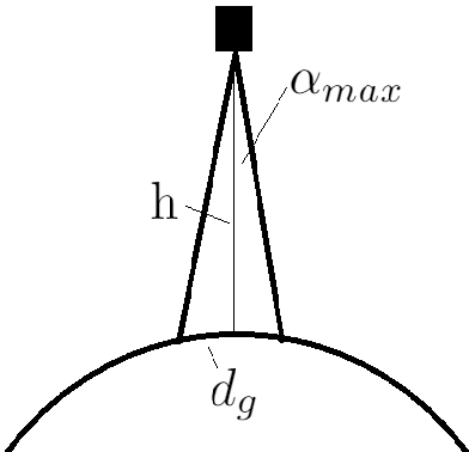

Figure 3.5: Image stability around the x- and z-axis

As a result, the maximal allowed angle for a sharp image can be calculated with Equation 3.12 by using simple geometry.

$$\alpha_{x\&z_{max}} = \arctan\left(\frac{d_g}{R_o - R_e}\right) \tag{3.12}$$

Here, the same assumption as for the exposure time was used and therefore a maximal shift of half a pixel is assumed to generate a stable and sharp image. The next step is to calculate the

resulting angular velocity. This can be done by dividing the result from Equation 3.12 by the maximal integration time for the image as given in Section 3.5.1.

$$\omega_{x_{max}} = \omega_{z_{max}} = \frac{\alpha_{x\&z_{max}}}{t_i} \tag{3.13}$$

Resulting from this, it can be concluded that the maximal angular velocity during imaging around the x- and z-axis is 1.536 deg/s.

Angular Velocity Analysis around the y-axis

The analysis around the y-axis differs from the other axis in the sense that here, the rotation around the nadir axis is analysed and therefore a rotation of the image itself. As described in Section 3.1, the sensor of the payload has a resolution of 4000×1 pixel. From the spatial resolution of 4 m at 350 km and a spatial resolution of 2.63 m at 230 km a imaginary image radius of 16000 m and 10520 m can be calculated respectively. If now again a maximal allowed change in the image is assumed to be half a pixel, the maximal allowed angle can be calculated by using Equation 3.14. The corresponding concept can be seen in Figure 3.6.

$$\alpha_{y_{max}} = \frac{d_g}{2\pi R_i} \tag{3.14}$$

In this equation $\alpha_{y_{max}}$ is the maximal allowed rotation around the y-axis and R_i is the imaginary radius. This can be converted to the maximal allowed angular velocity around the y-axis by using Equation 3.15.

$$\omega_{y_{max}} = \frac{\alpha_{y_{max}}}{t_i} \tag{3.15}$$

As a result the maximal allowed angular velocity around the y-axis is 5.746 deg/s and 5.903 deg/s for an orbital altitude of 350 km and 230 km respectively.

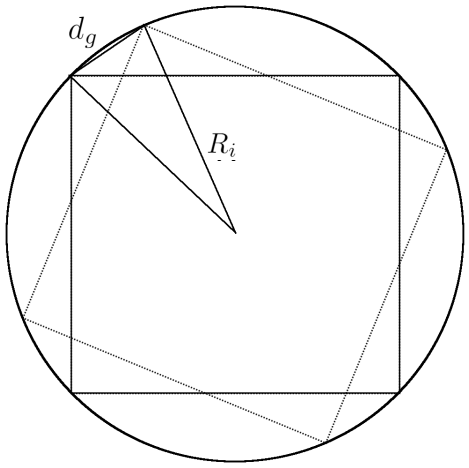

Figure 3.6: Image Shift due to a Rotation about the y-axis

Resulting from both analyses, the angular velocities can be concluded as seen in Table 3.5. Here, it is important to notice that this analysis only takes into account that a single rotation around one axis occurs. However, in reality, this is not true and due to disturbances, the satellite will tend to rotate around multiple axis. Therefore, an analysis of multiple rotations needs to be done.

Table 3.5: Image Stability Summary

		Angular Velocity $[deg/s]$		
Orbital Altitude $[km]$	**Exposure time** $[ms]$	**x-axis**	**y-axis**	**z-axis**
350	0.548	0.598	5.746	0.598
230	0.351	0.934	5.903	0.934

Rotation around Multiple Axes
As already described earlier, it is necessary to analyse rotations around multiple axis instead of assuming that the satellite bus will only rotate around a single axis each time. For this analysis all allowed rotation combinations were calculated to still ensure a maximal pixel shift of half a pixel on its ground path. This was done by calculating the length of the resulting vector from all rotations. All possible combinations can be seen in Figure 3.7.

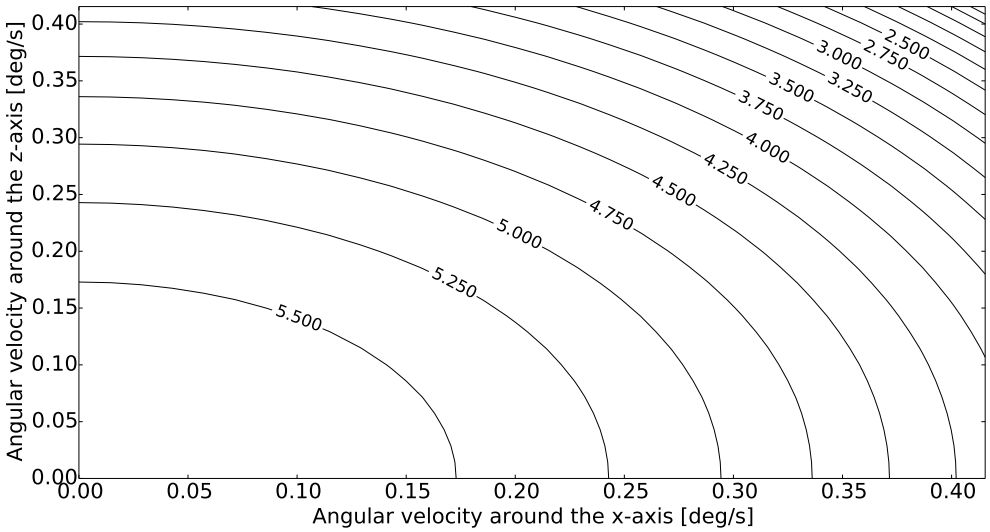

Figure 3.7: Image Stability Analysis; contoured line represent the angular velocity around the y-axis in deg/s

In this figure the x- and z-axis represent the angular velocity around the same axis. The contoured lines represent the corresponding maximal allowed angular velocity around the y-axis in deg/s. Therefore it is possible to derive all possible combinations of angular velocities around the different axis to still generate a stable and sharp image. However there should be a balance between all three allowed angular velocities since a high freedom around one axis would result in a strong restriction in angular velocity around the other axes. As it can be seen in Figure 3.7 and in Table 3.5, the rotation around the y-axis are not as important as the rotations around the x- and z-axis are. Therefore it was decide, that the combination of a maximal angular velocity around the x- and y-axis of 0.29 deg/s and a maximal angular velocity around the y-axis of 4.25 deg/s will provide a good balance between all rotations to guarantee a sharp image.

3.5.3 Ground Accuracy

One of the main driving requirements, namely S08-MP-02, is the 5° pointing accuracy during imaging. Therefore it is important to analyse the ground accuracy for this requirement. To calculate the ground location accuracy, simple geometry can be used. This calculation can be seen in Equation 3.16.

$$G_{acc} = (R_o - R_e) \cdot \tan(5.0^\circ) \tag{3.16}$$

In this equation G_{acc} is the the ground accuracy. If Equation 3.16 is used, a ground accuracy of 30620 m and 20120 m can be calculated for the orbital altitude of 350 km and 230 km respectively. If it is now taken into account that every image can cover an area of 16000 $m \times 4$ m and 10520 $m \times 2.63$ m can be covered, it can be concluded that with a pointing accuracy of 5°, the image taken could represent an area which was not intended to be imaged. Therefore, it would be wise to reduce the pointing accuracy to increase the image quality. The required pointing accuracy can be calculated by using Equation 3.17.

$$\alpha_{pointing} = \arctan\left(\frac{G_{acc}}{R_o - R_e}\right) \tag{3.17}$$

If it is now assumed that the image should point with the middle of the sensor on the target, half of the sensor can be used for the ground accuracy. Therefore, the ground accuracy for 350 km and

230 km is 8000 m and 5260 m respectively. By using Equation 3.17 a pointing accuracy of 1.3° for both orbital altitudes can be concluded. Based on this analysis it was decided that in the requirement S08-MP-02, the pointing accuracy will change from 5.0° to 1.3° to represent the minimum deviation of the target.

Chapter 4

Subsystem Design

This chapter is devoted to the design and design process of all the subsystems. Firstly, the ADCS system will be explained. Secondly, the Telemetry, Tracking and Command will be elaborated on. In the third section the Command and Data Handling is described. The Propulsion system will be presented in section four. Fifthly, the Power subsection will be presented. In the sixth section the Thermal Control subsystem can be read. The last two sections are devoted to Materials and the Structural design.

4.1 ADCS

The Attitude Determination and Control System is the main focus of this CubeSat platform since stability plays an important role in the taking of accurate pictures.

4.1.1 ADCS Requirements

Before the designing phase could be started, it was important to consult the requirements that were specifically created for the stability of the spacecraft. The requirements that were taken into account are shown below:

- **S08-MC-ADC-04** *The Nadir Pointing accuracy shall be <1.3°*
- **S08-MC-ADC-05** *The ADCS shall use an Earth Centred, Earth Fixed coordinate system*
- **S08-MC-ADC-06** *The ADCS shall provide an attitude status with a frequency of* 5 Hz
- **S08-MC-ADC-07** *The ADCS shall provide a position status with a frequency of* 1 Hz
- **S08-MC-ADC-08** *The ADCS shall be able to operate in a safe mode*
- **S08-MC-ADC-09** *The ADCS shall be able to provide control ability around all axis at any time*
- **S08-GTC-M-02** *The total mass of the ADCS shall be lower than* 10% *of the total mass*
- **S08-GTC-P-01** *The total power used by the ADCS shall be lower than* 12 W *max*
- **S08-MC-C-02** *The ADCS shall cost less than* 22% *of the total cost*
- **S08-MC-RD-01** *The ADCS shall provide redundancy*
- **S08-GTC-V-02** *The ADCS shall have a volume smaller than* 10 *cm x* 10 *cm x* 10.2 *cm*

Each of these were used as a driving factor in choosing the right options for the ADCS, which will now be described in this section.

Based on studies in the previous reports, it is concluded that a dual-spin ADCS subsystem is the most suitable option in order to provide the necessary pointing accuracy. This is done using a big momentum wheel as will be explained later in this section. However, in order to have a dual-spin ADCS, the MMOI around the spinning axis, the Z-axis, should be larger than the MMOI around the other axes. This is not the case for this satellite, so an active solution is needed. This is one of the reasons the ADCS also has an active control part as described in this section. Example of satellites that started rotating around another axis than initially meant to, because there was no active system to compensate for this, are for instance the Pioneer and the Explorer mission.

4.1.2 Possible choices

Excluding the computer, the ADCS consists of two main sections, namely the sensors and actuators. For a CubeSat, it is important to note that most conventional sensors and actuators will not fit, therefore, the options considered in this section will only compromise of the instruments that do fit.

Sensors
Sensors are needed to determine the attitude of the CubeSat. They send the information they acquire to the Attitude Determination and Control computer. Five different options for sensors are considered.

- **Star trackers**
  A star tracker is a sensor that uses the stars in the milky way to determine the position of the satellite. It is accurate, with a pointing accuracy of 6 arcsecs[1]. However, it does require a large amount of space, practically one unit cube and has a mass of 350 grams. There are also some other possibilities, mainly a lighter weight, cheaper sensor, however, these will be less accurate. Basically, the cheaper solution has an accuracy of 30 arcsecs [2].

- **Sun sensors**
  Sun sensors use the sun as a reference point, which for VLEO is effective. However, if the satellite were to be in an eclipse period, these sensors become useless. Considering this, they still are a good source for redundancy due to its light weight and cheap characteristics. Nonetheless, the accuracy that these can provide is high. For example, one sun sensor can yield an accuracy smaller than 0.5° for a field of view of 120° [3].

- **Horizon sensors**
  These sensors use the Earth's atmosphere as a reference, mainly using thermal or infrared sensors to determine the position of the satellite. Therefore, the accuracy that these can provide is substantial, with an accuracy of 0.5°, whilst only having a weight of 85 g, excluding electronics. Also, it uses small amount of power, namely 350 mW [4].

- **Inertial measurement units**
  The Inertial measurement unit is not a single sensor, but a system for sensors combined. This composition of sensors, involving accelerometers and gyros, can provide accurate velocity and rotational values. Mostly, this is combined with sensors to increase accuracy and redundancy.

- **GPS**
  The GPS sensor uses the Global Positioning System that is already in place in Medium Earth orbit. This allows a simple sensor to be used, which is light weight, less than 30 grams, and cheap. The GPS is used in order to determine the position, the orbital velocity and the acceleration. The technique of using one satellite to determine the position of the other is called Satellite to Satellite tracking, SST. The accuracy however, is low, with a value of approximately 10 m and a velocity accuracy of 25 cm/s. The frequency of the sensor is 1.5 GHz, which must be taken into account.

Actuators
Actuators are the controlling part of the ADCS, using the information from the sensors via the computer to correct the orientation. To do this, three main types of actuators can be chosen for a CubeSat, which are shown below.

- **Thrusters**
  Thrusters provide a simple yet effective method to control the altitude. However, this does require a propulsion system and propellant. Some illustrations of this can be found from CubeSat suppliers, for example the CubeSatShop web store. Here, an ADCS propulsion system weighing

[1] `http://bluecanyontech.com/` [cited 9 June 2015]
[2] `http://www.berlin-space-tech.com/index.php_id=42.html` [cited 9 June 2015]
[3] `http://www.cubesatshop.com/index.php?page=shop.product_details&flypage=flypage.tpl&product_id=104&category_id=7&keyword=sun+sensor&option=com_virtuemart&Itemid=69` [cited 9 June 2015]
[4] `http://www.cubesatshop.com/index.php?page=shop.product_details&flypage=flypage.tpl&product_id=103&category_id=7&option=com_virtuemart&Itemid=69` [cited 9 June 2015]

300 g can be found, providing a pointing resolution of 0.1 $arcs$[5]. Also, the maximum power usage is two watts, meaning, this system can be effective for VLEO.

- **Reaction Wheels**
  Reaction wheels are actuators that use the conservation of angular momentum to provide small torques to the spacecraft. These have the benefit of using no propellant, however, tend to be more space consuming compared to thrusters. Nevertheless, combinations of wheels can be used to create a 3-axis stabilisation. An example of the 3-axis system can be seen on CubeSatShop, where it, apparently, can provide 0.625 mN of torque per wheel. However, this system does weigh 640 g, which will impact the design drastically[6].

- **Magnetic torquers**
  Magnetic torquers offer an alternative way of controlling the altitude. The advantage of these is that they consume little power, no propellant and are highly reliable.[26] However, it must be used in conjunction with reaction wheels for complete stabilisation and they are more complex to design. Also, in VLEO, the orbit speed is very high. Therefore, the experienced magnetic field of the earth is rapidly changing and magnetic torquers might become unusable. Nevertheless, they are also lightweight and thus valuable for CubeSat applications[7].

- **Momentum Wheel**
  Momentum wheels are similar to reaction wheels, except for the fact that they have an initial rotation in order to provide stability. Usually they are used for heavier satellites, but when customised, these provide a possibility.

Other choices
In most cases, engineers design the ADCS system from scratch using sensors and actuators available on the market. However, it is also possible to include some ADCS boards that already include a few stability control. For example, the Cube ADCS offered by CubeSatShop which offers a full coverage in sensoring and control for a CubeSat [27]. Nonetheless, this option is not accurate enough for this mission.

4.1.3 Final ADCS design

After considering the requirements for the ADCS and the types of sensors and actuators, an engineer must finally make a choice on the layout of the ADCS. For this mission, this can be seen in Figure 4.1.

[5] `http://www.cubesatshop.com/index.php?page=shop.product_details&flypage=flypage.tpl&product_id=74` [cited 10 June 2015]

[6] `http://www.cubesatshop.com/index.php?page=shop.product_details&category_id=7&flypage=flypage.tpl&product_id=55&option=com_virtuemart&Itemid=69` [cited 10 June 2015]

[7] `http://www.cubesatshop.com/index.php?page=shop.product_details&flypage=flypage.tpl&product_id=75&category_id=7&option=com_virtuemart&Itemid=69` [cited 10 June 2015]

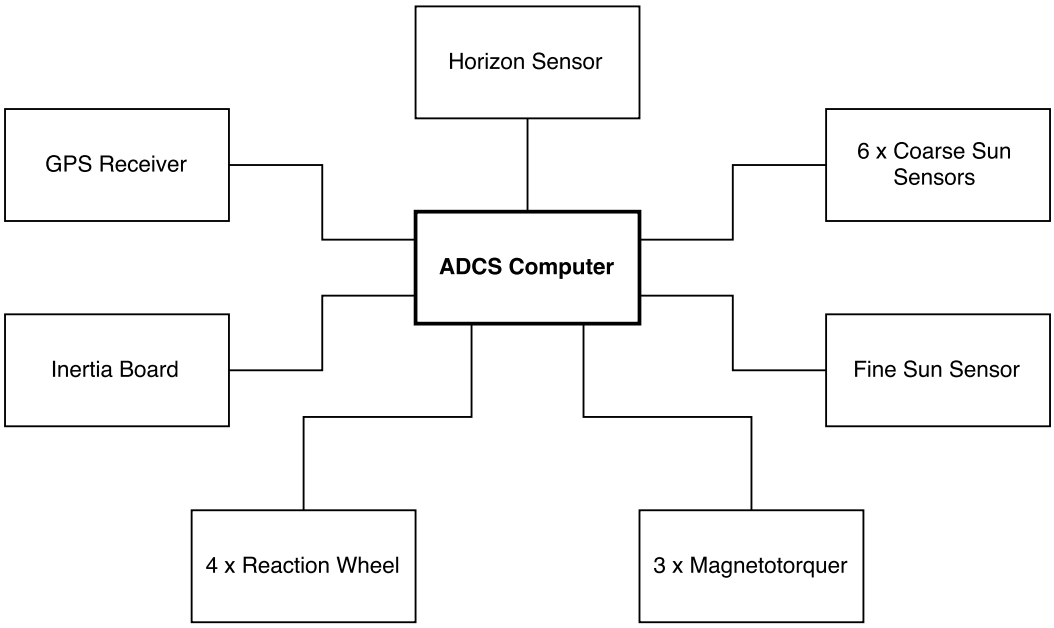

Figure 4.1: Final ADCS Design

It is important to design the ADCS to be able to determine and control the satellite's position during the detumbling phase, which can be seen as the worst case scenario. However, the layout of the ADCS was chosen due to nature of the orbit. It is obvious that the two main points of interest, at that altitude, will be the Sun and the Earth horizon's position. Hence, it is a logical choice to use a combination of both sun and horizon sensors. However, it is expected that the CubeSat will have an initial rotation of maximum 1.5 rad/s around the axis with the largest MMOI, it is therefore necessary to ensure that the spacecraft is stable on each axis. Hence, one coarse sun sensor will be placed on each side of the CubeSat. These coarse sun sensors will act as an initial measurement of the position, which plays an important role during the detumbling.

Additionally, a Fine sun sensor and an Earth horizon sensor are chosen since these will provide accurate measurements when a stable orbit has been achieved. Only one of each will be used, since the orbit is sun synchronous and that the bottom part of the satellite always points in the nadir axis. Due to the disturbances inside the atmosphere at the orbit altitude, inertia sensors will be attached to the board to be able detect the slight changes caused by these disturbances. Lastly, to ensure not only the attitude determination, but also the orbital position, a GPS receiver board will be used.

After the sensor layout were designed, the actuators needed to be chosen. As mentioned before, there are three main types of actuators that can be used on a CubeSat, meaning the choices are limited. Thrusters are the best option since they can be used for dual purposes, which would be as propulsion and actuators [3], however, the large consumption of propellant, meaning a higher weight, makes it an inadequate choice. For this CubeSat, a combination of the remaining two options was chosen. As seen in Figure 4.1, four reaction wheels were chosen, one for each axis and one for redundancy. The magnetorquers were then needed as a means to dissipated the momentum that was created by the reaction wheels.

4.1.4 Momentum Wheel

The momentum wheel was sized based on the magnitude of the disturbances, determined in Section 3.2. The aerodynamic disturbances appeared to be the largest, so those are the dominating factor in determining the magnitude of the momentum wheel. According to SMAD [3], the equation that can be used in order to size momentum wheels is the following

$$H = \left(\frac{T}{\theta_a}\right)\left(\frac{P}{4}\right) \tag{4.1}$$

In this equation, θ is the allowable motion, T is the disturbance torque and P is the orbital time.

The reader by Ir. B.T.C Zandbergen can be used to determine the mass of momentum wheels just like the mass of reaction wheels can be determined[8] [28].

$$M_{rw} = 1.7881 \cdot H_{rw}^{0.422} \tag{4.2}$$

Using the value for H from Equation 4.1, the mass according to Equation 4.2,the rotational speed of 7000 rpm based on the bearing design in Section 4.9.2 and aluminium as material, the MMOI can be determined. The final results are given in Table 4.1

H	0.014 Nms
m	0.469 kg
$\mathbf{R}_o$	0.15 m
$\mathbf{R}_i$	0.13 m
t	0.01 m

Table 4.1: Sizing momentum wheel

A figure of this wheel can be found in Figure A.1.
In order to provide the required stability, different vibrations have to be damped out. This can be effectively done using fluid dampers. The properties of the fluid in these dampers are a very low surface tension and viscosity.

4.1.5 Chosen Sensors

In the section above, 4.1.3, it was described what type of sensors are needed for this mission. However, sensors can vary from supplier to supplier. Therefore, research had to be done in order to find specific details. This research and its findings will be shown in this section.

Firstly, coarse sun sensors are common, meaning many choices are possible. Nonetheless, coarse sun sensors with quality are limited to a few. Namely, sensors from SSBV [29] and CubeSatShop [9] offer promising specifications. After comparison, it can be seen that these two seem to be equal in each aspect, therefore the cheapest is chosen. This is the coarse sun sensor offered by CubeSatShop at a price of €2,500. The coarse sun sensor itself, provides an accuracy of less than 0.5° for a minimal mass of five grams.

Secondly, the fine sun sensor is similar to the coarse sensor. There are many options, mainly from SSBV and the CubeSatShop again. Using the same approach, the fine sun sensors were compared. From this it can be seen that the SSBV sensor offers better accuracy. Namely, a value of 0.1 ° compared to the 0.5 ° of CubeSatShop [10] [30]. Hence, the SSBV options was chosen this time, resulting in a cost of € 10,000.

For the Earth horizon sensor, there are three main options. These are provided by Maryland Aerospace, CubeSatShop and SSBV. After reviewing these options, it becomes clear that the SSBV earth horizon sensor falls out due to its heavy mass of 500 g [31]. The remaining two options are then compared, resulting in CubeSatShop providing the heavier but more accurate sensor with a price of € 13,000 [32][11].

An accurate GPS receiver board can be provided by SSBV, Surrey Satellite Technology or perhaps the non-space related company Novatel. To choose a potentially successful GPS was a challenge, however, when comparing the space companies, SSBV and Surrey, it is found that the two options weight approximately the same but SSBV provides a slightly lower accuracy for the receiver. With an accuracy of less than 10 m and a velocity accuracy of less than 25 cm/s. Nonetheless, due to the tight cost budget, the SSBV option is also better choice in this case due to a lower cost[12][33]. It is

[8] Personal conversation, 20-06-2015, 11:00-12:00, Room 8.10, Faculty of Aerospace Engineering, TU Delft

[9] http://www.cubesatshop.com/index.php?page=shop.product_details&flypage=flypage.tpl&product_id=104&category_id=7&keyword=sun+sensor&option=com_virtuemart&Itemid=69 [cited 10 June 2015]

[10] http://www.cubesatshop.com/index.php?page=shop.product_details&flypage=flypage.tpl&product_id=99&category_id=7&keyword=sun+sensor&option=com_virtuemart&Itemid=69 [cited 10 June 2015]

[11] http://www.cubesatshop.com/index.php?page=shop.product_details&flypage=flypage.tpl&product_id=103&category_id=7&keyword=horizon+sensor&option=com_virtuemart&Itemid=69 [cited 10 June 2015]

[12] http://www.sst-us.com/shop/satellite-subsystems/gps/sgr-05u-space-gps-receiver [cited 11 june 2015]

preferred to use a GPS designed for space, to ensure reliability, which is why Novatel was disregarded.

Micro Electrical Mechanic System Gyros, MEMS-Gyros, are used to provide inertial reference attitude determination. For this satellite, the ADXRS649 is chosen[13]. The good things about MEMS-gyros is that they are cheap[14] ($ 68.35), small, light and accurate [34]. Six of them are used in order to provide attitude determination in all three axes, and for the required redundancy.

4.1.6 Chosen Actuators

In Section 4.1.3, it was described that four reaction wheels and three magneto-torquers were chosen for the ADCS. This in conjunction with the momentum wheel will provide full attitude control during the mission. However, the tumbling phase was also considered during the design and the actuators chosen accordingly.

Firstly, there are many options for the reaction wheels. Some main suppliers include SSBV, Blue Canyon Tech, Clyde Space, Maryland Aerospace and CubeSatShop. The reaction wheels need to provide enough torque, at a low price and mass due to the ADCS constraints. To do this, there are two types of systems that may provide useful. Namely a 3-axis reaction wheel assembly or single reaction wheels bought separately. Looking at the actuators offered by SSBV, Blue Canyon and Clyde space, it is obvious these would be too heavy for this mission[15][16] [35]. The final decision is to choose from CubeSatShop or Maryland Aerospace. When comparing these two, it is seen that they both offer the same reaction wheel assembly, MAI-101, and both offer single wheels. An initial look at the reaction wheel presented by CubeSatShop shows that these would not be sufficient, therefore the choice is between the MAI-101 and the MAI-400, a single reaction wheel offered by Maryland [36][37]. Due to the high mass of the MAI-101, four MAI-400 wheels were chosen as the actuators.

Secondly, the same story applies for the magnetotorquers, where choices had to be made between SSBV, Zarm-technik and CubeSatShop. It is hard to choose the best option for the magnetotorquers since they need to be able to comply with the momentum created by the reaction wheels. Zarm-technik provides plenty of choices [26], however, the price and size does not fit the budget. Therefore, two choices are left. When comparing SSBV and CubeSatShop, it can clearly be seen that they both offer the same product, where the one from SSBV is cheaper. Therefore, the magnetotorquer chosen are worth € 1,400 each [17][38].

4.1.7 Detumbling

The detumbling will be done using the reaction wheels. Because the reaction wheels can not reach a high enough velocity to compensate for the angular momentum, there must be some way to dump momentum. This is done using the magnetotorquers mentioned before. Since the magnetotorquers cannot deliver such a high torque in comparison to the momentum wheels, they are the limiting factor for the detumbling time. The reaction wheels can provide an angular moment of 9.351 $mNms$ @ 10000 rpm[37] and a torque of 0.635 mNm. This means that the reaction wheels need 15 *seconds* to spin up. The magnetic moment for the magnetorquers is between 1 and 100 Am^2[38]. However, since the magnetic torquers used by us will be the smallest ones, the magnetic moment is assumed to be 1 Am^2. The torque that can be delivered can be calculated using the following equation,

$$\bar{\tau} = \mu \times \bar{B} \tag{4.3}$$

, where τ is the torque, μ is the magnetic field of the magnetorquers and B the magnetic field of the Earth. The value for the torque is around 0.03 mNm, assuming a value of 30 μT for the strength of the Earth's magnetic field. This gives a value of 312 seconds to dump the momentum. In total, the time needed to detumble is around 2 h and 16 min, which is less than two orbits. However, for redundancy, the battery is capable of detumbling for three orbits, as described in section

[13] `http://www.analog.com/parametricsearch/en/10136#10136/p4510=Gyroscope` [cited 10 June 2015]

[14] `http://www.analog.com/en/products/mems/mems-gyroscopes/adxrs649.html#product-samplebuy` [cited 10 June 2015]

[15] `http://www.clyde-space.com/products/reaction_wheels` [cited 11 June 2015]

[16] `http://bluecanyontech.com/portfolio-posts/reaction-wheels/` [cited 11 June 2015]

[17] `http://www.cubesatshop.com/index.php?page=shop.product_details&flypage=flypage.tpl&product_id=75&category_id=7&option=com_virtuemart&Itemid=69` [cited 11 June 2015]

4.1.8 Budgeting

Since all the sensors and actuators have been chosen, it is possible to determine to mass, power and cost budget for the ADCS. This section dedicates itself to that.
In Table 4.2, the finalised budgets for mass, cost and power are shown.

Table 4.2: ADCS Budgets

Mass	$[g]$	660
Peak De-tumbling Power	$[W]$	11.1
Peak/Nominal Imaging Power	$[W]$	5.7/4.4
Cost	[€]	85000

The peak de-tumbling power occurs during the initial phase of the mission, where the satellite needs to gain its orientation after being ejected from the launch pad. The peak imaging power occurs once the satellite is orbiting as planned, meaning when it is in a stable orbit taking pictures. The final design was chosen after two iterations of the ADCS. The first design seemed to be an accurate system, however there was no redundancy and the momentum storage of the reaction wheels was not taken into account. Meaning, the first design is similar to the final one, however magnetotorquers were not present, and only three reaction wheels were chosen. Once the errors were recognised, the iterative process is undergone, to improve the initial design to a second one, which is the final design since the magnetotorquers and an extra reaction wheel were added. The reasoning behind the small amount of iteration steps comes from the fact that ADCS are widely implemented. Also due to the information received from the Delfi CubeSats team. Furthermore, a presentation from PlanetLabs, about their CubeSats, was followed and the layout of their ADCS, was mentioned

4.1.9 ADCS Compliance Matrix

In order to have a quick overview whether the requirements are all met, a compliance matrix was created which is shown by Table 4.3

Table 4.3: Attitude Control and Determination Subsystem Compliance Matrix

Requirements	Compliance
S08-MC-ADC-04	✓
S08-MC-ADC-05	✓
S08-MC-ADC-06	✓
S08-MC-ADC-07	✓
S08-MC-ADC-08	✓
S08-MC-ADC-09	✓
S08-GTC-M-02	✓
S08-GTC-P-01	✓
S08-MC-C-02	✓
S08-MC-RD-01	✓
S08-GTC-V-02	✓

As seen in Table 4.3, the chosen layout for the ADCS seems to meet all the requirements. The cost, mass and volume budgets are all within the given thresholds. The ADCS computer provides the frequency required to update the attitude determination. However, in order to be sure that the pointing accuracy indeed is met, testing can be done afterwards. This can be done by the means of giving the satellite a command to take for instance a picture when the Eiffeltower is expected to be in the middle of the image, and determine the ofset from the middle afterwards.

4.2 Telemetry, Tracking & Command

In the following section the telemetry, tracking and command, TT&C subsystem design options will be investigated. The TT&C subsystem of a satellite is responsible for the connection between the facilities on the ground and the satellite itself. This subsystem has three major tasks to ensure the successful operation of an application satellite:

- Monitoring of the health and status of the satellite through the collection, processing and transmission of the data from other subsystems
- Determination of the satellite's exact location through the reception, processing and transmitting of ranging signals (for example GPS)
- Control of satellite through the reception, processing and implementation of commands transmitted by the Command and Control stations on the ground segment.

In the following sections the design choices and specifications of the telemetry, tracking and command subsystem are determined. First the requirements are stated, afterwards the design options to meet the requirements are discussed.

4.2.1 Telemetry Subsystem requirement

- **S08-MC-S-01** *The antenna cabling shall provide a noise rating lower than 20 dB*
- **S08-MC-GC-01** *The telemetry subsystem shall provide at least a rx sensitivity of -140 dBm for the ground station*
- **S08-MC-DU-01** *The telemetry subsystem shall have a data uplink of 0 Kbit/s*
- **S08-MC-DU-02** *The telemetry subsystem shall have a data downlink of 1 Mbit/s*
- **S08-MC-DU-03** *The telemetry subsystem shall have a command uplink of 1200 bit/s*
- **S08-MC-DU-04** *The telemetry subsystem shall have a command downlink of 1200 bit/s*
- **S08-GTC-V-08** *The telemetry subsystem shall have a volume smaller than 10 cm × 10 cm × 6 cm*
- **S08-MC-RD-04** *The telemetry subsystem shall provide redundancy*
- **S08-GTC-M-08** *The telemetry subsystem shall have a maximum mass of 9 % of the total mass*
- **S08-MC-C-07** *The telemetry subsystem shall cost less than 7.5 % of the total cost*
- **S08-GTC-P-06** *The telemetry subsystem shall have a power lower than 12 W*

4.2.2 Downlink

In a single orbit of a Earth observation mission, a significant amount of data can be generated. Especially when using a high resolution camera as a payload. This data would be useless if it is not possible to download it to the ground. The data volume that can be downloaded is limited mainly by the telemetry data rate.

The payload that will be used in the CubeSat is described in Section 3.1. In a 91 *minutes* orbit the payload will generate 33.8 GiB of data, taken into account that no data is generated during the eclipse, which is 36 *minutes* for this particularly orbit. To download this amount of data to a single ground station, with a contact time of 9.4 *minutes*, a data rate of about 490 $Mbps$ is required. With current technology, this is not possible for CubeSat size transmitters. To overcome this problem there are two main options to consider, the image data can be compressed by a certain factor and/or adding more ground stations.

There are two types of compression, lossy and lossless. Lossy compression can be as much as needed, but one has to consider that the higher the compression ratio, the higher the decrease in quality. Lossless compression can be up to a compression factor of two, there will be no loss in quality for this type of compression [18].

Compression is one method to decrease the required data rate, another way is to add more ground stations. Adding a ground station will lead to an increase in contact time and therefore there is more time to download the same amount of data. However, the best option for decreasing the data rate is a combination of compression and increasing the number of ground stations.

There are several types of transmitters available for CubeSats. The main frequency bands they use are the ultra high frequency, UHF, band, the S band and the X band. In Table 4.4 the frequency ranges and possible data rates are given.

Table 4.4: Frequency Band Specifications

	UHF	**S**	**X**
Range:	300-3000 MHz	2-4 GHz	8-12 GHz
Wave Length:	3-1 m	15-7.5 cm	3.75-2.5 cm
Data Rate:	$\leq$10 $kbps$	$\leq$2 $Mbps$	$\leq$50 $Mbps$

The UHF band is clearly not sufficient for the mission, in one pass of 9.4 *minutes* only 0.7 MiB can be transmitted, which will result in a compression ratio of 50000 for a single ground station. A compression ratio of this magnitude is far from desirable, considering the loss in quality that goes with it. Adding more ground stations may decrease the compression ratio, however it will require a lot of ground stations to decrease it to a feasible amount.

The S band has data rates up to 2 $Mbps$[18], in one pass 141 MiB can be transmitted using the maximal data rate. To transmit all data in a single pass to one ground station, hence a compression ratio of about 245 is required. Using multiple ground stations per orbit, for example six, a compression ratio of about 40 will be sufficient. Using the S band will still result in a significant decrease in quality, only a large number of ground stations can reduce the needed compression ratio.

The third frequency band suitable for CubeSats is the X band, which offers data rates up to 50 $Mbps$[19] [39]. In a single pass 3.5 GiB can be transmitted, a compression ratio of about 10 will be sufficient. The ratio can be a lot smaller if more ground station are used per orbit. The X band is therefor the most promising frequency band for the mission purpose.

Considering all possible options, the X band is the frequency band that will be used. In Table 4.5 the possible compression ratios in combination with the number of ground stations is shown.

Compression Ratio	**Compressed Data** [GiB]	**Download Time** [min]	**Ground Stations**
1	33.8	92.3	10
2	16.9	46.1	5
4	8.45	23.0	3
6	5.63	15.4	2
8	4.23	11.5	2
10	3.38	9.23	1

Table 4.5: Compression Ratio Versus Ground Station

As can be seen from Table 4.5, a compression ratio of 10 is needed to send the data to one ground station. Adding a ground station will result in a required compression ratio of 6, which is a lot less lossy, so better for the quality of the images. Therefore, the spacecraft should have contact to at least two ground stations per orbit and use a compression ratio of 6. The contact time per ground station should be at least 7.7 *minutes*.

4.2.3 Uplink

Communication from the ground to the spacecraft is a crucial part of the mission. To accomplish this, a suitable frequency band for uplink is chosen. For downlink, massive amounts of data have to be downloaded to the ground, for uplink this is not the case. The data uploaded to the spacecraft mainly consists out of commands and occasionally some software updates, the size of this data is in the order of several KiB.

An uplink data rate of 1200 *bps*, in one pass of 9.4 *minutes*, results in 82.6 KiB of data that can be received by the spacecraft, which is sufficient for the needs of the mission. To accomplish a data rate of 1200 *bps* for uplink, the UHF band will fit the needs.

[18] `http://www.clyde-space.com/cubesat_shop/communication_systems/301_cubesat-s-band-transmitter` [cited 12 June 2015]

[19] Presentation by: C. Boshuizen, *The Planet Labs Earth-Imaging Constellation*, 8th International Workshop on Satellite Constellations and Formation Flying, 8 June 2015

4.2.4 Transmitter & Receiver

The two assigned frequency bands, UHF and X band, both will have their own transmitter and receiver. For the X band, a transmitter is sufficient. For the UHF band, a transmitter and receiver, or transceiver, will be used. The UHF transmitter can be used for transmitting status updates and housekeeping data.

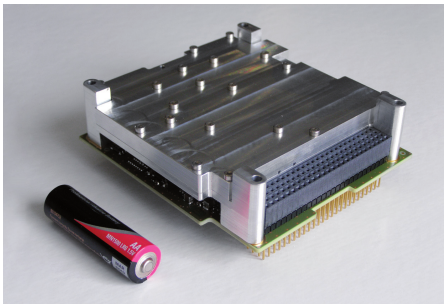

Figure 4.2: EWC 27 HDR-TM X Band Transmitter[20].

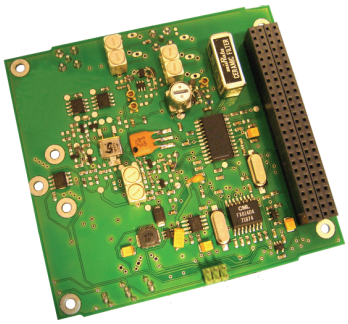

Figure 4.3: ISIS VHF downlink/UHF uplink Full Duplex Transceiver[21].

The X Band transmitter that fits the requirements is the EWC 27 HDR-TM X Band Transmitter[20] (Figure 4.2), which was developed by Syrlinks. For the UHF transceiver, the ISIS VHF downlink / UHF uplink Full Duplex Transceiver [40] (Figure 4.3) fits the requirements. In Table 4.6 the technical specifications are given:

Table 4.6: Transmitter and Transceiver Specifications

	X Band Transmitter [39]	**VHF/UHF Transceiver** [40]
Transmit Frequency	8025 to 8400 MHz by 1 MHz step	130 to 160 MHz
Receive Frequency	-	400 to 450 MHz
RF Output Power	30 to 33 dBm, programmable in flight	22 dBm average
Downlink Data Rate	2.8 to 50 $Mbps$, programmable in flight	1200, 2400, 4800 or 9600 bps
Uplink Data Rate	-	300 or 1200 bps
Supply Voltage	8 to 20 V with no galvanic isolation	6.5 to 12.5 V
Power Consumption	< 10 W	< 1.7 W (Tx on), < 0.2 W (Rx only)
Size	24 mm + cubesat compliant	$96 \times 90 \times 15$ mm
Mass	< 0.4 kg	85 g
Life Time	2 $years$	-
Operating Temperature	-40 °C/ $+50$ °C	-20 °C/ $+50$ °C
Costs (per unit)	€ 12000 *	€ 7250

* Estimation based on the cost budget, costs were not available at the time

4.2.5 Antennae

There are two types of antennae necessary for transmitting and receiving, one for the X band and one for the UHF band. For both there all multiple options available.

Isoflux omnidirectional or steerable antennae are the usual antennae for X band telemetry links [39]. However, isoflux antennae are not suitable for CubeSat, cause of size and structural limitations. Although there is another omnidirectional antenna that is suitable for CubeSat, a patch antenna (Figure 4.4). Which will only take one earth facing panel and is therefore simple to mount on the structure

[20] http://www.syrlinks.com/en/products/cubesats/hdr-x-band-transmitter.html [cited 16 June 2015]

[21] http://cubesatshop.com/index.php?page=shop.product_details&flypage=flypage.tpl&product_id=73&category_id=5&option=com_virtuemart&Itemid=67 [cited 16 June 2015]

of the CubeSat. However, these kind of antennae are not widely available for X band. Therefore the best solution is to develop one which fits the requirements. The requirements for the antenna are given in Table 4.7.

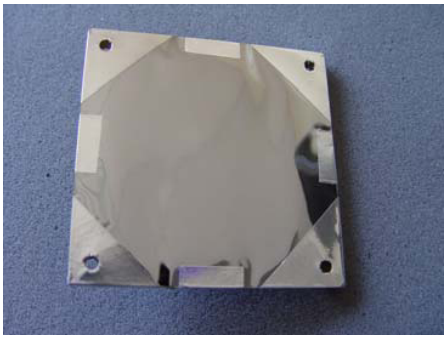

Figure 4.4: Example X Band Patch Antenna [41].

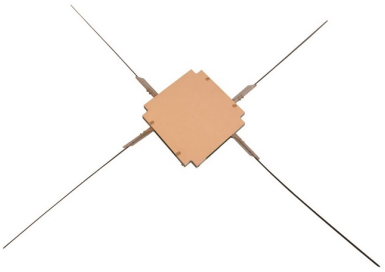

Figure 4.5: The Deployable Antenna System for CubeSats [42].

UHF band telemetry mainly uses monopole antennae for CubeSat purposes. These antennae need a certain deployment mechanism, there are different ways to accomplish this. For example, the Delfi-N3xt uses multiple tapeline as antennae which are coiled inside the bus at first and were uncoiled after the deployment. The type of deployment depends on several things, like the amount of space within the spacecraft, the length of the antennae and the number of antennae.

A suitable option for the monopole antennae is the deployable antenna system for CubeSats [42], developed by ISIS (Figure 4.5). The specifications of the antennae are given in Table 4.7. The antenna system has four antennae, for redundancy two of them can be used for downlink and two for uplink. The antennae can be placed at the back of the space craft.

Table 4.7: Patch Antenna Requirements and Monopole Antenna Specifications

	X Band Patch Antenna [39]	**VHF/UHF Monopole Antenna [42]**
Frequency	8025 to 8400 MHz	130 to 160 MHz
Bandwidth	50 MHz	10 MHz
Gain	> 0 $dBic$	0 dBi
Return Loss	< -21 dB	< -10 dB
RF Power	2 W	max. 2 W
Size	7×7 cm	$9.8 \times 9.8 \times 0.7$ cm
Mass	< 100 g	< 100 g
Cost	€ 6000 *	€ 4500

* Estimation based on the cost budget, costs were not available at the time

Mass, Size, Power and Cost

Now that all components are determined and chosen, it is important to make sure everything fits within the budget requirements, like mass, size, power and costs. In Table 4.8 the budgeted values are given and the current estimate of the real value.

Table 4.8: Current Values vs. Budget Values

	Budget Value	**Current Estimate**
Mass [g]	700	< 685
Size [mm]	50	46
Power [W]	12	< 11.7
Cost [€]	30000	29750

4.2.6 Ground Stations

In Section 4.2.2, it was determined that the CubeSat needs at least two ground stations per orbit to be able to download all the image data from one orbit. In this section, the number and location of the ground stations will be discussed further.

In Figure 4.6 the ground track of the CubeSat is shown. A best location for a ground station would at the location which is covered the most by the spacecraft, since a polar orbit is used for the mission, the polar areas are covered every orbit, which is also clearly visible in the ground track figure. The ideal location for the two required ground stations will therefore be one at the North Pole and one at Antarctica.

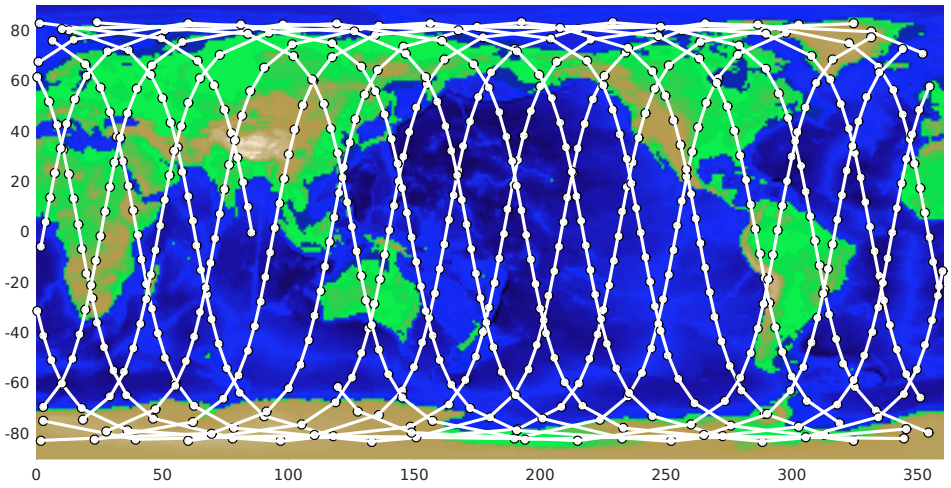

Figure 4.6: Ground Track of the Spacecraft in Polar Orbit at an altitude of 350 km

At the North Pole, the North Pole Satellite Station can be used, which has X band downlink capabilities [22]. At Antarctica the Troll Satellite station is a suitable option, this station is also capable to receive X band signals[23].

Free Space Loss Calculation
According to requirement **S08-MC-GC-01**, the received signal should be at least $-140\ dBm$. This value can be verified using the following equation:

$$P_{Rx} = P_{Tx} \cdot G_{AT} \left(\frac{\lambda}{4\pi d} \right)^2 \cdot G_{AR} \tag{4.4}$$

Where P_{Rx} is the received signal power in dBm, P_{Tx} is the transmitted signal power in dBm, G_{AT} and G_{AR} is the cable and antenna loss Gain respectively, d the distance in m and λ the wave-length in m.

As given by the specifications of the transmitter the signal power is 2 $Watts$. Assuming the cable and antenna loss of 10% and an maximum distance of 350 km, the Free Space Loss is given by $-129\ dBm$, which will fit the requirement.

4.2.7 Telemetry, Tracking and Command Compliance Matrix

In order to have a quick overview whether the requirements are all met, a compliance matrix was created which is shown by Table 4.9. As can be seen, all the requirements are met at this stage, however requirements like loss and sensitivity, S08-MC-S-01 and S08-MC-GC-01, are not verified with any form of testing. During the next steps in the development these numbers should be verified. According to the requirements the data downlink should be at least 1 $Mbit/s$, as was determined in Section 4.2.2 this is not sufficient for the needs of the mission. A data rate that is sufficient is about 50 $Mbit/s$, however, this is not a usual data rate for CubeSat. Extensive testing in the next stage of the development will be a necessity.

[22] `http://www.sscspace.com/north-pole-satellite-station-4` [18 June 2015]
[23] `http://ksat.no/node/79` [cited 18 June 2015]

Table 4.9: TT&C Subsystem Compliance Matrix

Requirements	Compliance
S08-MC-S-01	✓
S08-MC-GC-01	✓
S08-MC-DU-01	✓
S08-MC-DU-02	✓
S08-MC-DU-03	✓
S08-MC-DU-04	✓
S08-GTC-V-08	✓
S08-MC-RD-04	✓
S08-GTC-P-06	✓

4.3 Command & Data Handling

Receiving, validating, decoding and distributing commands to the other subsystems and gathering, processing and formatting spacecraft housekeeping and mission data for downlink or use by the on board computer are the major tasks of the command and data handling system, C&DH. It is also used for security interfaces, health monitoring and time keeping [22]. In the following sections, the requirements are stated and the design options to meet the requirements are discussed.

4.3.1 Command and Data Handling requirements

The requirements for the C&DH subsystem are the following:

- **S08-MDH-CP-01** *The C&DH subsystem should be able provide* 3.2 $GFLOPS$ *of computational power*
- **S08-MDH-CP-02** *The C&DH subsystem should allow for a maximum failure of* 10^{-5} *BER*
- **S08-MDH-DS-01** *The C&DH subsystem shall provide a temporary data storing*
- **S08-MDH-DS-02** *The C&DH subsystem shall provide a UDP data format*
- **S08-GTC-V-07** *The C&DH subsystem shall have a volume smaller than* 10 $cm \times 10$ $cm \times 4.8$ cm
- **S08-GTC-M-07** *The C&DH subsystem shall have a mass lower than 3 % of the total mass*
- **S08-GTC-P-04** *The C&DH subsystem shall use less than* 2 W
- **S08-MC-C-06** *The C&DH subsystem system should cost less than 3 % of the total costs*
- **S08-MC-RD-03** *The C&DH subsystem shall provide redundancy*

4.3.2 Hardware Block Diagram

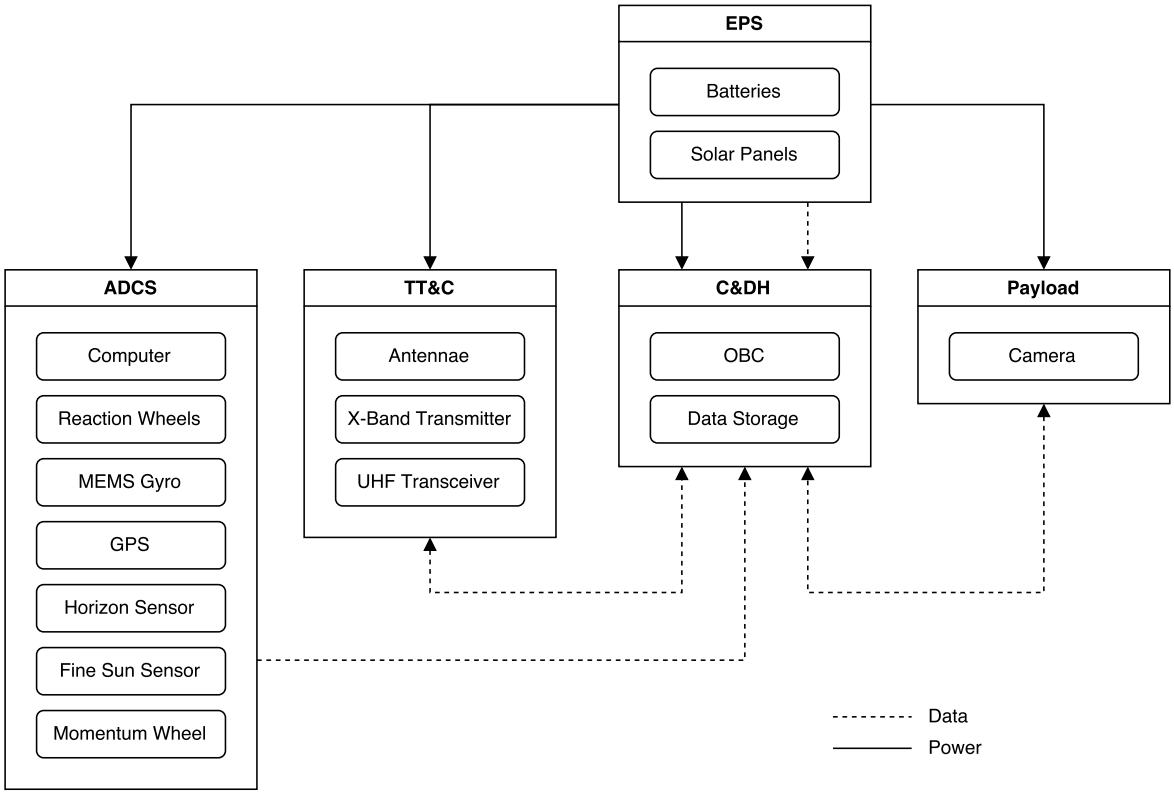

Figure 4.7: Hardware Block Diagram

Figure 4.7 shows the hardware block diagram of the spacecraft. It shows the data flows between the different subsystems and the power flow. For some subsystems the flows goes both ways, for example the TT&C and the C&DH, commands from the ground station go from TT&C and C&DH, and from there they are distributed further. The system status and the image data go from C&DH to TT&C.

4.3.3 Software Block Diagram

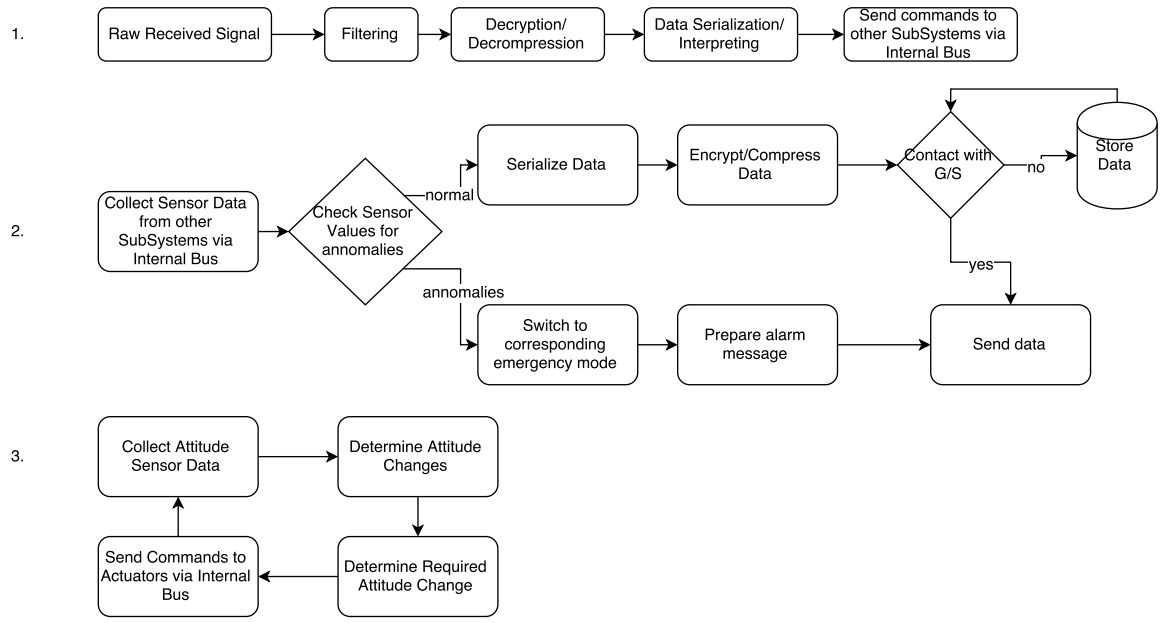

Figure 4.8: Software Block Diagram

In Figure 4.8, the software block diagram is shown. It consists of three main parts, the first part is the data received by the telemetry subsystem, which has to be filtered, decrypted, interpreted and processed. The second part is the data generated by the subsystems and the payload. For the subsystems this is mainly system status information, like temperatures. For the payload it is the image data. If everything works fine, the data can be prepared for downlink or storage. If anomalies occur, the system has to switch to a safe mode and an alarm message needs to be sent. The third part is the ADCS software, which is a loop of checks and actions which can be seen from the figure.

4.3.4 Design Solution

The design of the command and data handling subsystem consists of three parts, the first part is the on board computer, the second part is the data storage and the third part is the data transport or connections. All parts have to fit the requirements stated in Section 4.3.1.

On-Board Computer

To be able to process all the image data generated by the payload, a capable on board computer, OBC, has to be implemented in the spacecraft. The processing power required for the image processing depends on the compression algorithm and the compression ratio. The compression ratio is mainly determined by the telemetry subsystem and the contact time with one or more ground stations per orbit. A compression ratio of six, which is determined in Section 4.2.2, is used during the mission. The chosen OBC has an 400 MHz 32-bit ARM9 processor which is capable to do real-time data compression at high data rates. The advantage of ARM-processors is the way how the, Central Processing Unit, CPU uses the RAM very efficiently due to the separated memory controller. This provides the advantage that in case of high processing load the CPU could queue the tasks relatively easily[24].

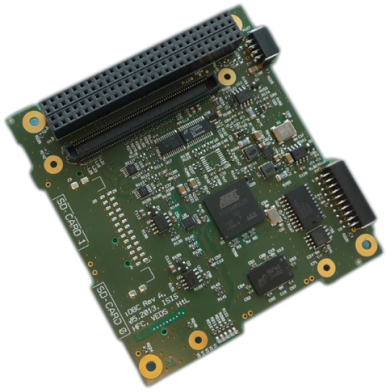

Figure 4.9: ISIS On Board Computer [43].

A suitable OBC for the mission is the ISIS On Board Computer [43] (Figure 4.9). The specifications of the OBC are given in Table 4.10.

[24] `http://www.atmel.com/Images/ARM_926EJS_TRM.pdf` [cited 19 June 2015]

Table 4.10: ISIS On Board Computer Specifications [43]

Specification:	
Processor	400 MHz 32-bit ARM9 processor (AT91SAM9G20)
Volatile Memory	64 MB SDRAM
Data Storage	2× 8 GB High Reliability SD cards 2× any size standard SD cards
Code Storage	1 MB NOR Flash
FRAM	256 kb
Operating Temperature	−25 °C to +65 °C
Power Consumption	400 mW typical, 550 mW max 3.3 V supply
Size	$96 \times 90 \times 12.4$ mm (Including FM daughter board)
Mass	94 g (Including FM daughter board)
Cost	€ 4300, –

For redundancy, two OBC can be placed in the spacecraft, if one fails the other can take over or if there is more computing power needed the second OBC can be added.

Storage
In one orbit 33.8 GiB of data is generated by the payload only, after compression, with a compression ratio of 6, 5.63 GiB of data is ready for downlink. However, there will not be contact with the ground station during the whole orbit, therefore the data needs to be stored until it can be fully sent to a ground station.

At least 5.63 GiB of data storage capacity will be sufficient to store the data for one complete orbit. However, if for some reason it is not possible to contact the satellite for multiple orbits, a larger storage capacity has to be considered. The orbital time is 90 $minutes$, so every day the spacecraft makes 16 orbits, which results in about 100 GiB of image data. To store a day of image data, the storage capacity should therefore be around 100 GiB.

The radiation in the target orbit of 350 km is small in comparison with higher altitudes. Astronauts in the International Space Station are able to use consumer electronics, like iPads and iPods, inside the station. Using consumer electronics inside spacecraft at low altitudes is therefore a good option[25]. Nowadays, solid state drives, SSD, are available up to 1 TiB and probably even more, for this mission a SSD of 100 GiB is enough. They are available for low prices, are light weight and can fit easily into a CubeSat.

Data Transport
A main task of the C&DH subsystem is transporting all commands and data to the different subsystems. There are several types of transportation methods needed in the spacecraft. The thrusters in the momentum wheel will be given commands with a Radio Frequency, RF, connection. The payload, which generates the highest amount of data, is on the other side of the wheel, therefor a data connection within the shaft of the wheel is needed. The other subsystems are all in the same bus.

As was discussed before, the payload produces 33.8 GiB of data per orbit, an orbit takes 91 $minutes$. To transfer all data from the payload to the OBC, an internal data rate of around 50 $Mbps$ is required. The processor of the OBC, which was selected earlier this section, is capable of supplying this data rate[26]. The motherboard however, is not suited for this type of connection, the remaining options available are Serial Peripheral Interface, SPI, and Inter-Integrated Circuit, I2C, which deliver speeds up to 10 $Mbps$ and 500 $kbps$, respectively. Therefore the OBC needs to be adjusted to handle the high speeds needed for the payload.

The RF connection which is needed for communicating to the thrusters in the wheel can be accomplished by adding a RF module to the OBC. This module is used once to command the thrusters to start, after the thrusters are burned out they are not used anymore.

[25]Presentation by: C. Boshuizen, *The Planet Labs Earth-Imaging Constellation*, 8th International Workshop on Satellite Constellations and Formation Flying, 8 June 2015
[26]`http://www.atmel.com/Images/ARM_926EJS_TRM.pdf` [cited 19 June 2015]

Finally, the other subsystems, e.g. ADCS and Power, will not generate massive amounts of data and therefore the I2C connection will be sufficient. The I2C bus is a widely used data bus for CubeSats, for example in the Delfi-N3xt [44].

The mass of all cabling and other data transport parts is estimated to be $< 120\ g$. This is based on the budget of other CubeSats, like the Delfi-N3xt, which has a cabling mass of around 40 g. The SHAPE. is a 6U CubeSat, therefore more cabling is probably required. The costs are estimated to be less than € 1000.

Mass, Size, Power and Cost
Now that all components are determined and chosen, it is important to make sure every thing fits within the budget requirements, like mass, size, power and costs. In Table 4.11 the budgeted values are given and the current estimate of the real value.

Table 4.11: Current Values vs. Budget Values

		Budget Value	Current Estimate
Mass	$[g]$	260	< 250
Size	$[mm]$	48	< 30
Power	$[W]$	1	< 0.55
Cost	[€]	10000	< 9600

4.3.5 Data Handling Block Diagram

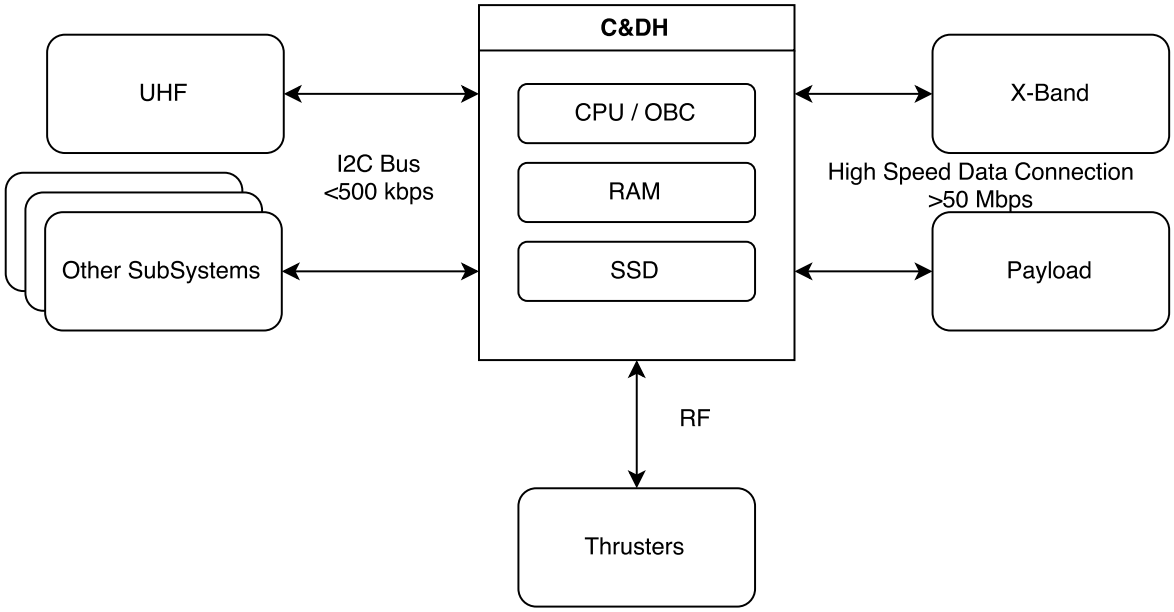

Figure 4.10: Data Handling Block Diagram

Figure 4.10 shows the data handling block diagram. It can be seen that there are three main types of connection, I2C, a high speed data connection and a RF connection. All connections are duplex, which means it can communicate both ways.

4.3.6 Command and Data Handling Compliance Matrix

In order to have a quick overview whether the requirements are all met, a compliance matrix was created which is shown by Table 4.12. From the table it can be seen that all requirements are met, however two of the requirements S08-MDH-CP-01 and S08-MDH-CP-02 are open for discussion. The OBC looks capable to meet this requirements, however there will be some testing needed in the next stages of the development to verify if the OBC is really capable of meeting all necessary requirements. Another requirement which was not discussed earlier is S08-MDH-DS-02, which was about the data format. Meeting this requirement depends on which software is used and what format is

supported by the ground stations, this also has to be verified in the further development of the project.

Table 4.12: Command and Data Handling Subsystem Compliance Matrix

Requirements	Compliance
S08-MDH-CP-01	✓
S08-MDH-CP-02	✓
S08-MDH-DS-01	✓
S08-MDH-DS-02	✓
S08-GTC-V-07	✓
S08-GTC-M-07	✓
S08-GTC-P-04	✓
S08-MC-C-06	✓
S08-MC-RD-03	✓

4.4 Propulsion

The propulsion system can be used for a vast variation of applications like orbit maintenance change, in inclination, attitude control and end of life sequence. In this design, it will be used for non of them, but it will be used for spinning up the main momentum wheel. Where these design choices originate can be read in the first section. Further sizing will be explained in the second and in the third section the compliance matrix will be elaborated on.

- **S08-MC-ADC-10** *The propulsion subsystem shall have a response time lower than 200 s*
- **S08-MC-ADC-11** *The propulsion subsystem shall provide a delta V of* $20m/s$
- **S08-MC-ADC-12** *The propulsion subsystem shall counteract a drag of* $0.0143\ N$
- **S08-GTC-V-03** *The propulsion subsystem shall have a volume smaller than* $10cm \times 10cm \times 3cm$
- **S08-GTC-M-03** *Total mass of the propulsion subsystem shall be lower than 10 % of the total mass*
- **S08-GTC-M-13** *The propulsion subsystem shall have a propellant mass lower than 8 % of the total mass*
- **S08-GTC-P-05** *The propulsion subsystem shall have a power budget lower than 3 W*
- **S08-GTC-S-06** *The propulsion subsystem shall withstand all the loads induced by the launch*
- **S08-MC-C-03** *The propulsion subsystem shall have a cost lower than 15 % of the total cost*
- **S08-MC-RD-02** *The propulsion subsystem shall provide redundancy*

4.4.1 Design Process

While making the first orbital altitude estimations and decay of the satellite, it was discovered that the satellite starting at an altitude of 288 *km* would only survive for fourteen days. Therefore, an option to increase life time would be to use thrusters. During the performance of the trade off three different thruster types are investigated. It turned out that the MEMS ion spray is the most feasible for orbit maintenance, however, the technology readiness level of this thruster system is not yet of the right value. Therefore, an extensive study into possibly increasing the orbital height was done and succeeded. The altitude was increased to 350 km which severely increased the life time, this can be read in Section 3.3. Due to this, propulsion is not needed for orbital maintenance.

This design explores new areas in CubeSat stabilisation, one of the new features are the magnetic bearings on the main reaction wheel. These are placed here to reduce the friction and vibration. The reason this is mentioned in this section is that the wheel will spun up by the use of thrusters. The driving choices for using thrusters and not an electric motor is the decoupling of the wheel and the cubes. This way the friction is reduced and the effect of the magnetic bearings is maximised.

In this section, the thruster design will be further detailed and a trade off on the propellant will be performed, considering mass, power and tank volume.

4.4.2 Propulsion Sizing

The Layout of the the propulsion system can be seen in Figure 4.11. The figure contains a tank to store the propellant at five bar, a pressure regulator to reduce the pressure, a solenoid valve and the

heater plus nozzle which can be seen from left to right. The exact dimensions of the heater and nozzle can be found in [45]. In the layout, there is no filter in the feed system meaning the filter will be placed in the tank and can be seen in Figure 4.13. A cross section of the combustion camber and nozzle can be seen in Figure 4.12. Here, the throat radius R_t is equal to 12.5 μm, $\theta_1 = 15°$, $\theta_2 = 20°$ The nozzle to throat was chosen to be 20 according to [46]. In Table 4.13, all the input constants can be found that were used to calculate the propellant mass, volume and consumed power.

Table 4.13: Table of Propellant Constants

	Water	**Ethanol**	**Butane**
Molar Mass [M] (mol)	18	46	58
Specific Heat Capacity[c](j/K)	4180	1880	1675
Gas Constant [R] (j/kgK)	461.5	220	143
Specific Heat Ratio [γ]	1.33	1.13	1.096
Mass Density[ρ] (kg/m^3)	1000	789	601

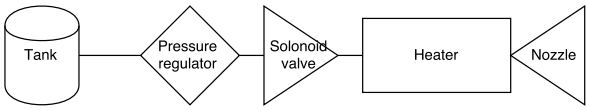

Figure 4.11: Layout of the feed system [46][47]

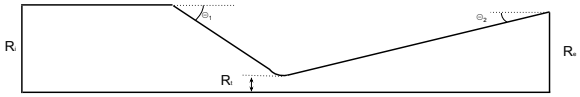

Figure 4.12: Cross section of the nozzle and chamber [45]

Now that the layout of the thruster system is determined, the sizing of the tanks can be performed. For fuel, three substances are considered, which are: water, ethane and butane. To start the design, the nozzle exit velocity is determined by Equation 4.5, where T is the propellant temperature in the chamber which is taken to be $550°C$[46], R is the general gas constant in $j/molK$. M is the molar mass and γ is the specific heat ratio. The only unknown left is the ratio $\frac{p_e}{p}$ which depends mainly on the expansion ratio and is related through Equation 4.6. Table 4.14 displays the results for an expansion ratio of 20. Equations 4.5, 4.6, 4.7 and 4.8 are taken form reference [48]

$$V_{exit} = \sqrt{\frac{T \cdot R}{M} \cdot \frac{2 \cdot \gamma}{\gamma - 1} \left[1 - \left(\frac{p_e}{p}\right)^{\frac{\gamma-1}{\gamma}}\right]} \tag{4.5}$$

$$\frac{A_e}{A^*} = \frac{\Gamma(\gamma)}{\sqrt{\frac{2 \cdot \gamma}{\gamma - 1} \cdot \left(\frac{p_e}{p_c}\right)^{\frac{2}{\gamma}} \left[1 - \left(\frac{p_e}{p}\right)^{\frac{\gamma-1}{\gamma}}\right]}} \tag{4.6}$$

The pressure ratios can be used to solve the exit velocity expressed in Equation 4.5.

Table 4.14: Pressure Ratios for Water, Ethane and Butane at a Constant Expansion Ratio of 20

	Water	**Ethanol**	**Butane**
$\frac{p_e}{p_c}$	0.0033	0.0064	0.0072

An other important feature to determine the tank volume is the mass flow rate, which can be calculated using Equation 4.7. In this equation, A^* is the throat area, P_t is the tank pressure, T_t is the temperature in the chamber and γ is the specific heat ratio. These mass flows are in the order of mg/s, which corresponds to values found in tests done according to [46].

$$\dot{m} = \frac{A^* \cdot P_t}{\sqrt{T_t}} \cdot \sqrt{\frac{\gamma}{R}} \cdot \left(\frac{\gamma + 1}{2}\right)^{-\frac{\gamma+1}{2 \cdot (\gamma-1)}} \tag{4.7}$$

After the mass flow rate is known, the thrust can be computed by using Equation 4.8.

$$T = \dot{m} \cdot V_{exit} + (p_e - p_a) \cdot A_e \tag{4.8}$$

The next step is to calculate the time it will take two thrusters to spin up the wheel to 7000 rpm. To calculate this, a relation between the force on the wheel, the mass moment of inertia and the rotational speed is needed. This will be derived starting with Equation 4.9. Where M is the moment exerted on the wheel, I the mass moment of inertia and α the rotational acceleration.

$$M = I * \alpha \tag{4.9}$$

Since the propellant is stored inside the wheel, the mass moment of inertia is a function of time. Assuming that the wheel can be modelled as a disk with symmetric properties and the two thrusters are expelling the same amount of propellant in time. The equation for the mass moment of inertia can be expressed as in Equation 4.10.

$$I = \frac{m - \dot{m} \cdot t}{2} \cdot r^2 \tag{4.10}$$

Where α is equal to the time multiplied by the rotational speed ω and is expressed in Equation 4.11.

$$\alpha = \omega \cdot t \tag{4.11}$$

The moment on the wheel due to the two thrusters can be computed by multiplying the thrust with the arm (which is taken to be the radius of the momentum wheel) and, of course, by two. This results in Equation 4.12.

$$M = 2r \cdot T \tag{4.12}$$

Substituting Equations 4.10, 4.11 and 4.12 in equation 4.9 and rewriting for the time, results in Equation 4.13.

$$t = \frac{m}{\frac{4 \cdot T}{r \cdot \omega} + \dot{m}} \tag{4.13}$$

The propellant mass needed for spinning up the wheel is then the time multiplied by the mass flow. Once the mass is known the propellant can be multiplied by the mass density to get the volume required to store the propellant.

$$m_p = \dot{m} \cdot t \tag{4.14}$$

A second important parameter is the power needed to operate up the thrusters. The steps presented in Equations 4.15 and 4.16 are an indication of the power that is needed to power the heater during burn. Firstly, the enthalpy change is calculated using Equation 4.15. Once this is known, the power can be computed by making use of a relation that relates the mass flow, the molar mass an the enthalpy change displayed in Equation 4.16. Equation 4.16 is taken from [49] and is the power required to heat the propellant.

$$\Delta h = c_p \cdot (T_2 - T_1) \tag{4.15}$$

$$P = \frac{\dot{m} \cdot \Delta h}{M_i \cdot \eta} \tag{4.16}$$

The results of the analysis shown in this section can be seen in Table 4.15. From these outcomes, it can be concluded that water is the worst choice of the three due to the mass and the power required. Ethanol is therefore chosen as the most fitting propellant for this application

Table 4.15: Results of the Analysis of Different Propellants

	Water	**Ethanol**	**Butane**
Mass $[kg]$	0.3262	0.2540	0.2739
Power $[W]$	0.2609	0.0627	0.0544
Volume $[cm^3]$	326.2	321.9	455.8
Time $[h]$	69.2	39.4	34.7
Thrust$[mN]$	0.5	1	1.1

In Figure 4.13, a sketch of the integration of the propulsion system in the wheel is shown. The different parts, as mentioned before, are indicated in the figure. Apart from the valve and the pressure regulator, everything will be custom made for this application. The resistojet itself is made by TU Delft. The tanks need to be made so that they can store the precise amount of fuel needed. The dimensions of the tank are $10 \times 8.2 \times 2cm$. This equals a total volume of $164cm^3$ per tank. The tanks are interconnected meaning if one thruster fails, the other one will still have enough fuel to spin the wheel. The thrusters will be powered by two separate battery's which need to deliver $0.0627W$ for $39.4h$. This, however, is the power needed for the heater (including an efficiency of only 70%). The solenoid valve chosen is ASCO RB-series two way normally closed solenoid valve [50]. This valve is normally closed as is stated in the name so if open it will require a continues power of $0.5\ W$. This sums up to a total of $40Wh$ (taken into account small line losses and efficiency of the solenoid) which can be delivered by a simple laptop battery. Laptop batteries are large compared to the wheel but this battery does not have to be reachable and can consist of simple cells in parallel or series. The system will be connected to the on-board computer by means of Radio Frequency, RF.

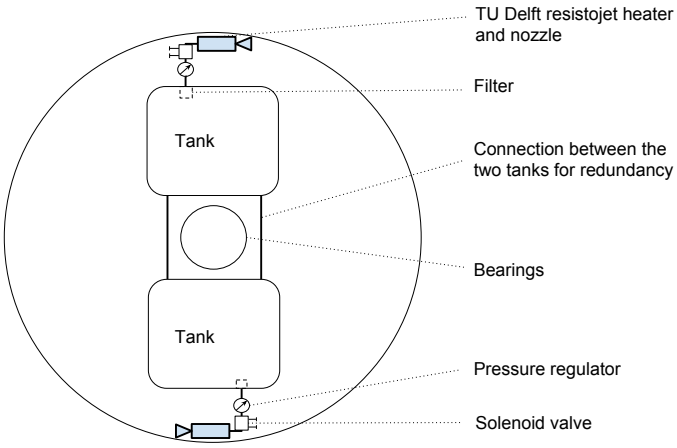

Figure 4.13: Integrated Propulsion System

4.4.3 Propulsion Compliance Matrix

In order to have a quick overview whether the requirements are all met, a compliance matrix was created which is shown by Table 4.16. For the propulsion system, all requirements are met except for S08-MCADC-11 and S08-MCADC-12. This is because these are not applicable anymore. Since the payload has been updated the satellite can fly at a higher altitude and differential drag control is used to guide the satellite in the desired orbit.

Table 4.16: Propulsion Subsystem Compliance Matrix

Requirements	**Compliance**
S08-MC-ADC-10	✓
S08-MC-ADC-11	X
S08-MC-ADC-12	X
S08-GTC-V-03	✓
S08-GTC-M-03	✓
S08-GTC-M-13	✓
S08-GTC-P-05	✓
S08-GTC-S-06	✓
S08-MC-C-03	✓
S08-MC-RD-02	✓

For further recommendations, the solenoid valves could be changed to more complex ones that save power [51]. Also a system of fast acting valves could be used instead of a combination of pressure regulator and a solenoid valve, however that would have large influence on the limited power budget in the wheel. A third point to improve on could be the propellant now only three well known substances

are used, one could investigate a more complex chemical mixture that improves the performance of the thruster and reduces the propellant volume/mass.

4.5 Power

The power subsystem is one of the key subsystems since a malfunction of the power system leads to an immediate failure of the mission. The power subsystem consists mainly of three components. A primary and a secondary energy source and a power control unit. To be able to design the power subsystem properly, the driving requirements for this subsystem need to be analysed. This is the first step and will be elaborated in Section 4.5.1. During the design process different design solution were taken into account and thus a trade-off was performed, which is summarised in Section 4.5.2. In Section 4.5.3, the power required and the power generated will be analysed to be able to size the selected design solution. Finally, the design solution will be presented and a requirement compliance analysis will be performed.

4.5.1 Power Subsystem requirement

From the design option tree given in earlier reports, it is possible to derive the following driving requirements for the power subsystem.

- **S08-MC-PC-01** *The power subsystem shall have a power output of at least* 19 W
- **S08-MC-PC-02** *The power subsystem shall be able to sustain satellite during fail-safe mode*
- **S08-MC-PC-03** *The voltage output of the power subsystem shall be in the range of* 3.3 *to* 5.0 V
- **S08-MC-PC-04** *The power decay of the power subsystem shall be lower than* 3.0 $W/month$
- **S08-GTC-V-09** *The power subsystem shall have a volume smaller than* $10cmx10cmx6cm$
- **S08-GTC-M-09** *The power subsystem shall have a maximum mass of 20 % of the total mass*
- **S08-MC-C-08** *The power subsystem shall cost less than* 18% *of the total cost*
- **S08-MC-RD-05** *The power subsystem shall provide redundancy*

4.5.2 Trade-Off

For the power subsystem, multiple design solutions are possible, therefore, a trade-off was performed to select the most feasible one for this mission design. As already described, the power subsystem can be split up in three main parts, a primary energy source, a secondary energy source and the distribution board. Based on this it was decided to split up the trade-off procedure into three parts as well.

Primary Energy Source
For the primary energy source, three main option were taken into account. Namely thermal, photovoltaic and nuclear. The main output of the primary energy source trade-off was that a photovoltaic design solution will be used. This is mainly based on the fact that the size can be rather small and this energy source provides a high specific power when compared to other solutions [22]. This leads to a lower total mass. The reliability is high since the sun provides a constant and reliable energy source with a energy variation between 1322 W/m^2 to 1414 W/m^2 between winter and summer time respectively [2]. At the same time, it is regularly used as a primary energy source in other small satellites. Nuclear energy was discarded as a solution since it provides a low specific power and could harm the Earth environment during re-entry [22]. A thermal energy source was discarded based on the fact that propulsion is only used to spin up the momentum wheel and therefore could only provide power for a very short time [3].

Secondary Energy Source
For the secondary energy source only chemical solutions were considered. This means that only fuel cells and batteries were taken into account. Fuel cells provide a high specific power but since fuel cells need to store fuel and the storage is limited, fuel cells are not a feasible option. Therefore, a battery design was chosen since it cancels out the main disadvantages of a fuel cell solution and can provide good recharging performance. However, the lifetime of one charging process is low, based on a lower specific power [3].

Distribution Board
Based on the fact that the distribution board is a very standardised part of the power subsystem and does not really change for different satellite platforms, no trade-off was performed for this part of the power subsystem.

4.5.3 Power Analysis

In order to size the power subsystem properly, it is important to fully analyse the power needed for the whole satellite during every mission phase. Therefore, all different mission phases are analysed to derive the power to be provided by the power subsystem. There are four different mission phases which need to be analysed: the imaging mode, the eclipse time, the drag mode to reduce the orbital altitude, and the pre-mission/detumbling mode.

The imaging mode describes the mode where the primary mission is executed. This means that the payload is fully operating and taking continues images as it was described in Section 3.1. During the eclipse time, it is not possible to generate images and also a power generation using solar cells is not possible. Therefore, most of the subsystems will be operated in idle mode or even going to be shutdown to reduce the power consumption during the eclipse time. The drag mode is going to be used during the mission to reduce the orbital altitude in a pre-mission phase to the target altitude of 350 km as well as for de-orbiting at the end of the main mission as a end of life solution. Here only the important system are going to be operated like the ADCS and the TT&C to receive commands from the ground station. The last considered mission phase is the pre-mission/detumbling phase where the subsystems are booted up and the satellite is going to be detumbled after it left the launch fairing. A summary of which subsystem operate during each mission phase and there corresponding power consumption can be seen in Table 4.17. Here the "x" describes that the subsystem is going to be operated in an active mode and an "-" describes that the subsystem does not use this operation mode during this mission phase.

Table 4.17: Power Consumption and Operation Mode for all Subsystems

			Operation Mode							
			Imaging		**Eclipse**		**Drag Mode**		**Pre-mission/Detumbling**	
	Peak Power [W]	**Idle Power** [W]	**Peak**	**Idle**	**Peak**	**Idle**	**Peak**	**Idle**	**Peak**	**Idle**
Payload	2	0	x	-	-	x	-	x	-	x
ADCS	5.7/11.1	4.4	x/-	-	-/-	x	-/-	x	-/x	-
TT&C	12	1.7	x	x	x	x	-	x	-	x
C&DH	0.6	-	x	-	x	-	x	-	x	-
Power	0.1	-	x	-	x	-	x	-	x	-
Propulsion	2.2	-	-	-	-	-	-	-	x	-

It can be seen that both modes can be used in one mission phase, since the subsystem power consumption changes over time in this mission phase. As described in Section 4.2.2, the transmitting time for sending all generated data down to the ground station is 462 s by using two ground stations. Based on this fact, it was assumed that the images are transmitted one time during the eclipse phase as well as one time during the imaging mode. The next step is to analyse all possible modes to analyse the necessary power consumption as well as the number of solar panels necessary to generate enough power. For this analysis, it is going to be assumed that the solar panels have an efficiency of 28.0% and an effective area of 60.00 cm^2. These values represent a good average of the solar panels available for small satellites at the moment [52]. Also, it is going to be assumed that the solar radiation is equal to 1322 W/m^2 which represents the solar radiation during winter times [2].

Analysis method

For this analysis, two main steps are necessary. Firstly, the power necessary to operate all systems in the specific mode needs to be calculated and in a second step the number of solar cells necessary to generate the power for one orbit will be calculated. In a later stage of the design phase, a battery analysis will be done. This part will be covered in Section 4.5.4.

The first step is to calculate the power required by all systems. This can be simply calculated by taking the sum of all powers required by each subsystem for the specific mode. The power consumption for each mode can be taken from Table 4.17. The total power required can be then calculated by using Equation 4.17.

$$P_{total} = \sum P_i \cdot t_i \tag{4.17}$$

In this equation, P_{total} is the total power, P_i is the power used by the specific subsystem and t_i is the time the subsystem is used.

The second step is to calculate the number of solar cells necessary to generate enough power to operate the satellite for one orbit. The power generated by a singular solar cell mainly depends on two factors: the solar radiation which is assumed to be 1322 W/m^2 for a worst case analysis and the incident angle of solar radiation on the solar cell.

Since the satellite will operate in a sun-synchronous orbit, the z-axis will always be perpendicular to the incoming solar radiation. Therefore, the rotation of the satellite around the z-axis will influence the power generation of the solar cells. The relation between the incident angle, the incoming solar radiation and the resulting effective solar radiation for the solar cell can be calculated by using Equation 4.18.

$$I_{eff} = I_{in} \cdot \cos(q_i) \tag{4.18}$$

In this equation, I_{eff} represents the effective solar radiation for the solar cell, I_{in} represents the incoming solar radiation and q_i is the relative angle between the solar cell and the incoming solar radiation.

In a second step, the total number off solar cells can be analysed. This can be done by using Equation 4.19.

$$n_{cell} = \frac{P_{total}}{I_{eff} \cdot \eta_{cell} \cdot \eta_{add}} \tag{4.19}$$

Here, in this equation, the n_{cell} represents the number of solar cells necessary, η_{cell} represents the cell efficiency and η_{add} represents the sum of additional efficiencies. These additional efficiencies are listed in the following list. Here the assumed efficiency is given in parentheses and are based on a good average provided by other small satellites at the moment.

- Yearly solar cell degradation (3 %/year) [53]
- Power conversion efficiency (90 %) [54]
- Charging efficiency (85 %) [55]
- Discharge efficiency (90 %) [55]
- Cable losses (10 %) [56]

During these calculations it is important to notice that the relative angle q_i changes at every orbital position which leads to an iterative process. In this analysis it is assumed that all solar cells are placed on top of the satellite.

Continuing with the analyses, it is important to notice that in all graphs shown in this section, the $0'$ s of orbital time represents the orbital instance when the satellite leaves the eclipse phase of the orbit. Therefore it is important to notice that in all figures the eclipse phase of the orbit begins at a orbital time of 3302 s. Also, it should be noticed that all analysis were done for different orbits since the orbital time and therefore the time spent imaging and in the eclipse phase will differ. However, the number of solar cells did not differ and were even less for a lower orbital altitude and therefore, the analysis of an orbital altitude of 350 km will be presented here to represent the worst case possible.

Imaging Mode
During the imaging mode, most systems function at their highest power consumption as it can be concluded from Table 4.17. This does make sense since during the imaging mode the payload, is operated and the ADCS, which has the highest constant power consumption, needs to provide a high accuracy and stability to provide stable and sharp images. If now Equation 4.17 is used for the imaging mode and afterwards divided by the time spent during imaging mode, an average power consumption of 11.64 W can be concluded. This leads to a total power needed for the imaging mode of 10.68 Wh since the orbit time is 55.05 min in the imaging mode. The power consumption for the imaging mode can be seen in Figure 4.14.

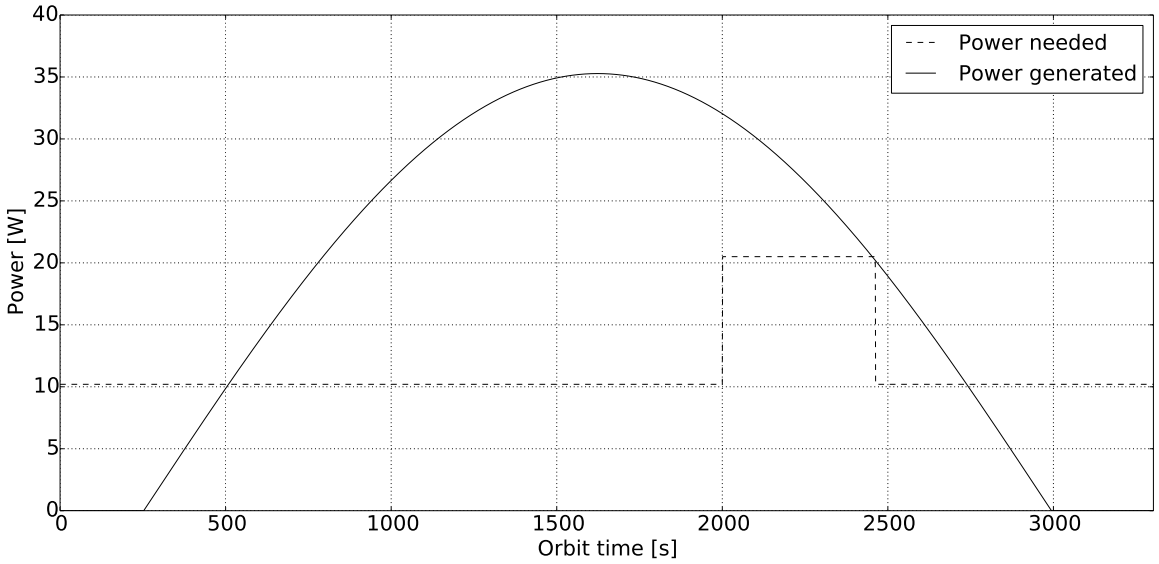

Figure 4.14: Required Power for Imaging Mode

In this graph, the peak in the power needed represents the transmitting time of the data to the ground station. Here, the power generated represents the power generated by the solar cells calculated for the power needed to operate in imaging mode and eclipse mode will be later calculated. The same holds for Figure 4.15. To be able to analyse the number of solar cells necessary to generate this power, the eclipse phase needs to be analysed first since during eclipse time, the solar cells will not be able to generate any power. Therefore, the solar cells need to generate the amount of power for the eclipse phase during the imaging mode.

Eclipse Mode
During eclipse mode, all systems which are not needed, like the payload which is not capable to take images during eclipse, are turned either off or into idle to reduce power consumption. This can be concluded from Table 4.17. However, the TT&C still needs to transfer data once during eclipse. Based on this and a shorter eclipse time of only 36.3 min, the average power consumption is still high with 9.08 W. Due to a shorter operation time the power needed is only 5.50 Wh. In Figure 4.15, the power consumption for the eclipse mode can be seen.

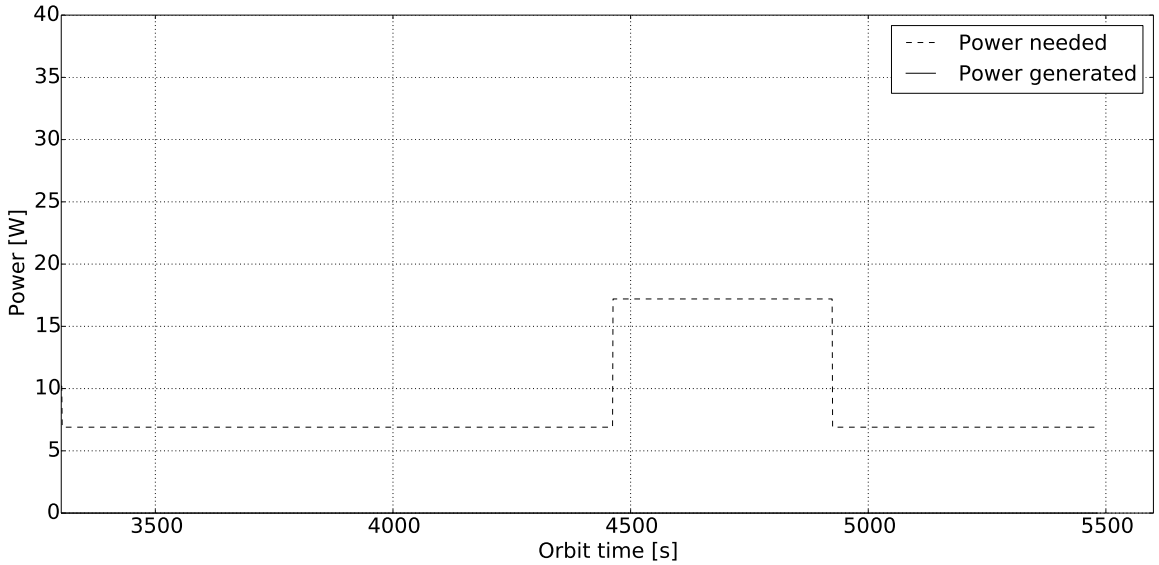

Figure 4.15: Required Power for Eclipse Mode

Here the peak again represents the transmitting of the data to the ground station. In Figure 4.15 it can be immediately seen that there is no power generation during eclipse time. If now both, the imaging mode and the eclipse mode, are combined to calculate the number of solar cells necessary, it

can be concluded that the total power required to be generated by the solar cells needs to be 17.10 Wh for each orbit. If Equation 4.19 is used, a total number of 24 solar cells can be calculated. The power generated by the solar cells can be seen in Figure 4.14.

Drag mode
During the drag mode only the ADCS (idle mode), the TT&C (idle mode) and the C&DH (peak mode) needs to be operated as seen in Table 4.17. If the same method is used as before it can be concluded that the average power consumption is 7.22 W and the total amount of power needed is equal to 10.51 Wh. In Figure 4.16 the power consumption for one orbit in drag mode can be seen.

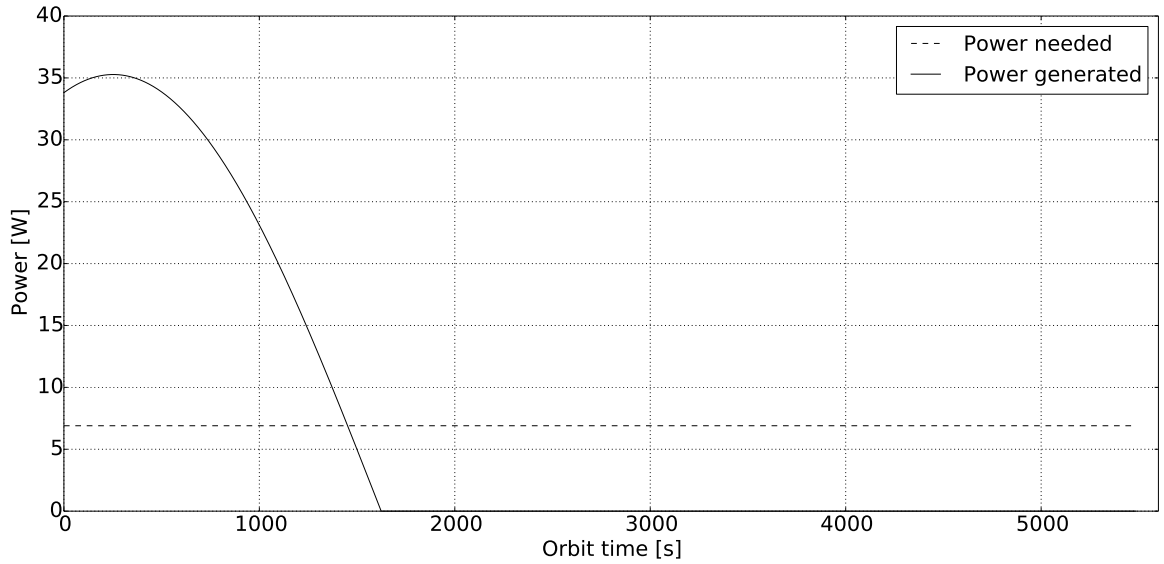

Figure 4.16: Required Power for Drag Mode

Since during the drag mode, the nadir axis is pointing into the flight direction, the possible power generated by the solar cells is lower than for the other two cases. The total power needed for one orbit is 10.51 Wh smaller than for the imaging and eclipse mode but by using the same method also 24 solar cells are necessary to generate enough power to operate the satellite. This power generation can be as well seen in Figure 4.16.

Pre-mission/Detumbling Mode
The pre-mission phase can be divided into a pre-detumbling, a detumbling, and a propulsion mode. During detumbling, only the ADCS in peak mode of 11.1 W, the TT&C is operated in idle mode and the C&DH in peak mode. This leads to an average power consumption of 13.4 W and a total power needed for one orbit of 20.41 Wh. Based on the fact that the total time of the detumbling is considered to be two hours, a total power needed for this mission phase is going to be 26.8 Wh. However, it was assumed that the power needed for detumbling is going to be 40.2 Wh to provide some margin if the detumbling takes longer than calculated. Therefore, a detumbling time of three orbits was chosen. Since not all solar cells are yet deployed in this stage and the angular velocities around all axis are rather high, the solar cells cannot be used for a reliable power generation. Therefore this phase needs to be mainly powered by the battery. In the required battery capacity additional power should be reserved for the pre-detumbling phase where most systems are powered up. Here not all power can be generated by the solar cells since not all panels are deployed. An addition of 10 Wh was assumed for this phase.

In the propulsion mode, the momentum wheel is spin up to a rotation speed of 7000 rpm as already described in Section 4.4. From this, it can be concluded that this phase needs a total power of 31 Wh. This power also needs to be taken into account during the battery design since this power can not be generated by solar cells in that mission phase. The battery will be charged before the launch and will than provide the power for the pre-mission phase up to the point were all solar cells are deployed. From there on the battery will be recharged every orbit to provide the power for the eclipse time.

4.5.4 Design solution

After the power required in every mission phase was analysed, all sub-parts of the power subsystem can now be designed. First, the power generation is going to be analysed followed by the power storage design and concluded with the power distribution. In a final step a small budget analysis will be done.

Solar cell design
The power generation sub-part of the power subsystem is the main part since it generates the power needed for the most time of the mission. Only at the beginning of the mission, in the pre-mission phase, the power for the whole satellite will be provided by the battery. Therefore, it is of high importance that the solar cells generate enough power for every part of the mission since a negative power budget during the mission would lead to a lower quality of the mission output or even a total failure of the mission. During the power analysis, a solar cell with an efficiency of 28% with an effective area of 60.00 cm^2 was assumed. From this, it could be concluded that the minimum number for all mission phases is 24 solar cells. To determine the final number of solar cells, it is necessary to first decide which solar cell is going to be used. By analysing the actual market, it was decided that the NanoPower P110 designed by GomSpace is providing the best balance between performance, mass ad cost. A summary of the performance data for the NanoPower P110 can be seen in Table 4.18.

Table 4.18: The NanoPower P110 main data sheet [57]

	Value
Efficiency	30 %
Effective area	60.36 cm^2
Voltage	4.6 V
Current	500 mA
Mass	26-29 g
Cost	2000 €
Material	GaAs

It can be seen that the efficiency is 2% higher and the effective area is 0.36 cm^2 larger than the one assumed during the power analysis. Based on this fact, and the fact that the worst case was analysed, namely an operation only during winter time, it was decided that 25 solar cells will provide enough power to operate the whole satellite in each mission phase. This number will provide a buffer large enough to provide redundancy if some solar cells do not provide enough power output [57].

The satellite design consist of two main buses which provide a top area of $10 \times 10 \times 60$ cm. Therefore, 6 solar cells could be mounted directly on the satellite. However, it is important to notice that one cube area of $10 \times 10 \times 10$ cm needs to be solar cell free to be able to mount the fine sensor of the ADCS which needs to point in the negative y-axis. Therefore only five solar cells can be mounted directly on the satellite. To be able to mount 20 more solar cells on the satellite, additional solar panel need to be mounted which will deployed after launch and will therefore increase the top area of the satellite. Here it is important to keep symmetry to not negatively influence the moment of inertia and the mass moment of inertia. The final mounting of all 25 solar cells on the satellite can be seen in Figure 4.17.

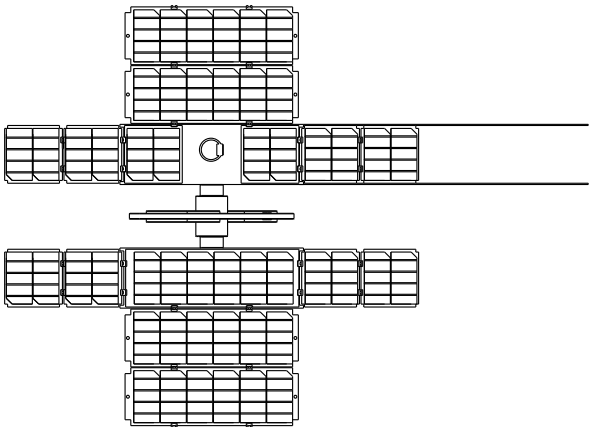

Figure 4.17: The solar cell position on the satellite

These deployed solar panels also have a positive effect on the aerodynamic properties and therefore will improve the stability of the satellite.

Battery design
It was decided to use two different batteries for the battery design. The second battery will be used to power the propulsion subsystem. The reasoning for this design solution will be evaluated in a later stage. Therefore, first the main battery design followed by the separate battery design for the propulsion will be presented.

The main battery design mainly needs to be able to provide enough power to operate the satellite in all modes. The total power needed is summarised in Table 4.19 which can be concluded from Section 4.5.3.

Table 4.19: Power consumption summary

	Power needed $[Wh]$
Imaging	10.68
Eclipse	5.50
Drag mode	10.51
Pre-mission / Detumbling	50.20

Resulting from this it can be concluded that the maximal power to be stored in the battery is 50.20 Wh. If actual batteries are compared which are available on the market at the moment, the battery NanoPower BPX 2S-3P using 2600 mA cells design by GumSpace was selected. These batteries provide the best performance required for this mission [58]. A summary of the performance data can be seen in Table 4.20.

Table 4.20: NanoPower BPX 2S-3P Data Sheet [58]

	Value
Capacity	58.5 Wh
Voltage	6-8.4 V
Current	7800 mA
Size	$40.0 \times 85.73 \times 85.90$ mm
Mass	370 g
Cost	5500 €

This battery design already provides a heater for thermal control. All power modes can be stored at least once in the battery solution. The imaging and eclipse mode can be stored 3.62 times, the drag mode can be stored 5.67 times and the pre-mission can be stored 1.17 times in the battery. This provides enough redundancy to operate the satellite in a good manner and even be used to compensate multiple orbits if the power generation will be lower in a single orbit due to high disturbances or other circumstances. During the battery design it is important to take into account that battery capacity will degrade with each cycle. This is not important for the pre-mission phase since it is the first

charge cycle, however for the other mission modes it can be crucial and will therefore be analysed. For modern batteries it can be assumed that after 5000 charging cycles an average depth-of-discharge of $15 - 25\%$ [22]. Since it is assumed that the total number of charging cycles is around 4800 cycles, this can be used as a good estimate. Resulting from this at the end of the mission the satellite will be able to store 2.71 times the imaging and eclipse time and 4.17 times the drag mode if a degradation of 25% is assumed. This is still enough to operate the satellite in a good manner and can therefore be considered to be a good design solution. Therefore, the satellite is still able to provide enough power to operate all systems even in a safe mode.

As already described earlier, the propulsion needs to be provided with power to be operated. Since the propulsion system is located in the momentum wheel, distributing the power to the propulsion system is complicated and would require an additional slip-ring which would drastically increase the risk of failure since operating a slip-ring at this high rotational speeds introduces a to high risk for space application. Therefore, it was decided to provide the propulsion system with a separate power system which is stored in the momentum wheel as well. There will be a power connection between the battery and the propulsion system which will be activated by using a RF module. To be able to operate the propulsion system, 31 Wh are required at a voltage between $5 - 12$ V. By taking this into account, it is possible to select a proper battery for the propulsion system. After some market analysis it was decided to use the NanoPower QuadBat BP4 from GomSpace since it provides the best performance at rather low cost and weight. A summary of the main data sheet is given in Table 4.21.

Table 4.21: NanoPower BP4 Data Sheet [59]

	Value
Capacity	38.5 Wh
Voltage	6-8.4 V
Current	5200 mA
Size	$19.0 \times 87.44 \times 93.39$ mm
Mass	240 g
Cost	€ 2450

This battery also includes a battery heater and therefore can be used for this purpose but therefore a higher capacity is needed since the power for the heater needs to be provided by the battery itself. Therefore, a higher capacity of 38.5 Wh was selected [59]. A block diagram of the chosen battery circuit including the propulsion can be seen in Section 4.5.5.

Distribution Board

The distribution board mainly has to convert the power and has to distribute the power to the different subsystems. Also, it has to charge and discharge the battery. In general most of the distribution boards provide three parallel solar panel power converter. Therefore, it is necessary to split up all 25 solar cells in 3 main circuits. To fit all 25 solar cells into three solar cell circuits it was decided to create two circuits with two solar cells in series and four solar cells parallel. This will than create two circuit which provides a voltage of 9.2 V and a current of 2000 mA each. The third circuit was decided to have three solar cells in series and three solar cells in parallel. This will provide a single circuit with a voltage of 13.8 V and a current of 1500 mA. The distribution board also needs to be able to convert the power into two different voltages of 5.0 V and 3.3 V required for all other subsystems. From these requirements, it was decided to use the NanoPower P31us power distribution board from GomSpace as a distribution board. This is also in favour since a high compatibility exist between all other power subsystem parts since they are all produced by the same company, GomSpace [60]. A summary of the power distribution board can be seen in Table 4.22 and a functional block diagram of the distribution board is given in Section 4.5.5.

Table 4.22: NanoPower P31us Data Sheet [60]

	Value
Conversion efficiency	93 %
Solar power converter	3
Power output:	5 V @ 3 A
	3.3 V @ 3 A
Max power output	30 W
Size	$25.6 \times 89.1 \times 92.8$ mm
Mass	270 g
Cost	5550 €

Budget analysis / Conclusion
After the final design of the power subsystem is done, it is possible to analyse the total performance data of the system. Therefore a summary of the total system can be seen in Table 4.23.

Table 4.23: Summary of the Complete Power Subsystem

	Main Power subsystem	**Propulsion Power subsystem**
Mass	1327.5 g	240 g
Size	$10 \times 10 \times 60$ mm	$10 \times 10 \times 20$ mm
Power consumption	< 0.1 W	< 0.1 W
Cost	61050 €	2450 €

It is also important to notice that the power subsystem provides redundancy in the power generation. Therefore, the solar cells provide more power than it is required by the satellite. This is in favour since many moving solar panels are used which introduce a risk of failure. If one of the mechanisms would fail the power subsystem will still be able to perform the main mission. It only maybe requires to reduce the power consumption slightly which would reduce the total imaging time slightly for each orbit. Also a solution could be used where only every second orbit images are going to be taken and the other orbit will be used to generate enough power for the imaging phase. It also ensures that no negative power budget is possible during the mission which enables a successful mission.

4.5.5 Electrical Block Diagram

The power subsystem needs to provide the power to all other subsystems. Therefore, the power subsystem needs to convert and distribute the power generated over the whole satellite. To get an idea how this process will look like, an Electrical Block Diagram was created. Since two different power systems are used, one general main power subsystem and a separate power subsystem for the propulsion subsystem, two different Electrical Block Diagrams were created. The Electrical Block Diagram for the main power subsystem can be seen in Figure 4.18 and the Electrical Block Diagram for the separate power subsystem for the propulsion subsystem can be seen in Figure 4.19.

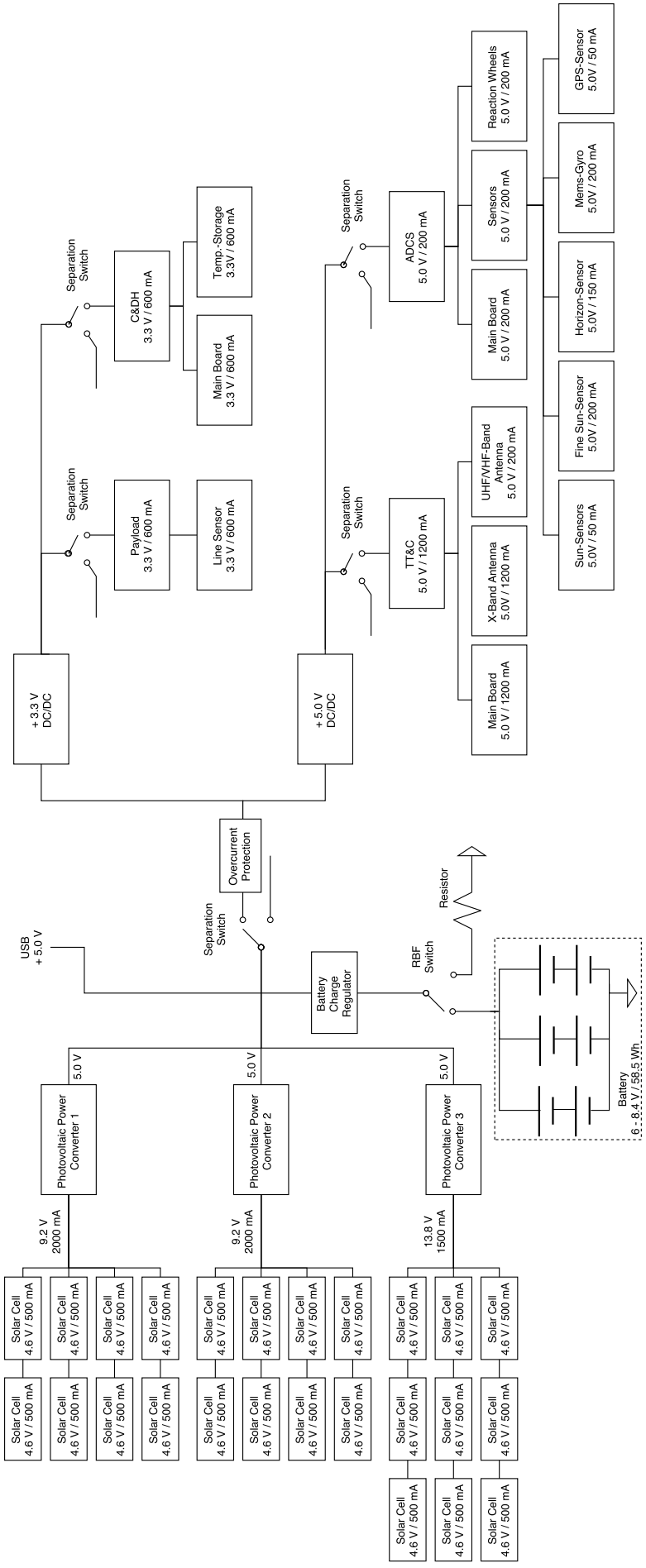

Figure 4.18: Electrical Block Diagram

As it can be seen in this Figure 4.18, the whole process of power generation starts in the top left corner. Here, all solar cells are split up in three main circuits as described before. From this, the generated power will be converted by three different power converter to a voltage of 5.0 V, one for each solar cell circuit. This is necessary since the different circuits generate different power condition but the distribution board is improved for one specific power condition. After the power is converted, the power load will be levered and the power will be either distributed to the battery or will be passed to the to the power converter. If the power is distributed to the battery, it first passes a battery charge regulator to change the voltage to an efficient charging voltage of $6.0 - 8.4$ V. Afterwards, the power will be used to charge the battery or ,during eclipse phase, the battery will provide power to the main circuit. If the power will be distributed to the power converter it first passes an over-current protection to ensure that the power subsystem is not damaged. Thereafter, the power will be converted to either 3.3 V or 5.0 V. This is necessary since different subsystems require different voltages to be operated. Finally, the power will be distributed to the variety of subsystem which will then distribute it further to their specific parts. To be able to charge the battery and test the subsystem before launch, a Univeral Serial Bus, USB, charging capability is given with a voltage of 5.0 V. This USB-port is implemented immediately after photo voltaic power converters, in the circuit, to be able to charge the battery efficiently. It is important to notice that two different switches are implemented. There are Separation Switches which are implemented to protect the power subsystem during launch and to be able to fully shutdown the system as it is required by most launchers. Also, there are RBF ("Remove Before Flight") switches which are implemented to separate the battery before launch. Also, to ensure that, during testing, the best battery performance is seen at the beginning of the mission as well as to reduce the discharge before the launch. Before the launch, the RBF switch is connected to a resistor to ensure that the power subsystem will is not harmed whilst the solar cells and the subsystem itself are tested.

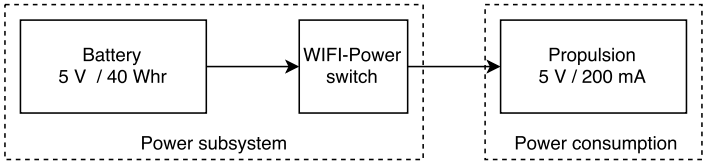

Figure 4.19: Electrical Block Diagram for the Propulsion Subsystem

The Electrical Block Diagram shows how the separate power is used in the propulsion subsystem. It can be seen in Figure 4.19 that this block diagram is significantly simpler than the ones used for the general power subsystem. Here, the only power source is the battery and this one will be fully charge before the launch. After the power connection is opened by the RF module, the propulsion subsystem will be powered up. Once the momentum wheel has reached its maximum velocity or when the propellant tanks are empty, the RF module will close the power connection.

4.5.6 Power Subsystem Compliance Matrix

In order to have a quick overview whether the requirements are all met, a compliance matrix was created which is shown by Table 4.24

Table 4.24: Power Subsystem Compliance Matrix

Requirements	**Compliance**
S08-MC-PC-01	✓
S08-MC-PC-02	✓
S08-MC-PC-03	✓
S08-MC-PC-04	✓
S08-GTC-V-09	✓
S08-GTC-M-09	✓
S08-MC-C-08	✓
S08-MC-RD-05	✓

It can be concluded that all requirements can be met with this design and therefore it can be considered that a good design solution has a been presented. However, it is still possible to improve the design even further. For example, the power consumption for the different subsystems may be reduced, which

will improve the overall power consumption needed to operate the satellite. Also, more efficient solar cells could be chosen. However, this comes with the disadvantage that the cost will increase as well.

4.6 Thermal Control

The thermal control subsystem of the CubeSat guarantees that the temperature range, in which the electronic and mechanical equipment efficiently and reliably operates, is maintained. Moreover, the thermal balance ensures that no material, irrespective of its function, is distorted by the temperature fluctuations. Based on a short literature study of the initial mass and cost estimations for previous nano satellite missions, which share similar technical requirements with ours, the following mission requirements were proposed:

Thermal Control Subsystem Requirements

- **S08-MC-TC-01** *The thermal subsystem shall keep all subsystems in a temperature range of* $-10°C$ *to* $30°C$
- **S08-GTC-V-06** *The thermal subsystem shall have a volume smaller than 10 cm x 10 cm x 0.5 cm*
- **S08-GTC-M-06** *The thermal subsystem shall have a mass lower than 2 % of the total mass*
- **S08-GTC-P-03** *The total power used by the thermal subsystem shall be lower than 1 W*
- **S08-MC-C-05** *The thermal subsystem shall cost less than 1 % of the total unit cost*

The first step towards a thermal analysis is the identification of the heating sources that will influence the satellite's temperature changes. The space environment, including type of orbit and altitude are the main points of consideration. The main factors influencing the temperature changes are:

- Direct Solar radiation
- Solar radiation reflected on Earth (Albedo)
- Earth's Infrared Radiation
- Aero-thermal Flux (Free Molecular Heating)
- Internal Components Heating

The spacecraft temperature is ultimately determined by the heat gained and lost due to the interactions of these factors during the various mission phases. Let us now look closely at each of these factors.

Solar Radiation
The Sun's radiation is the most important source of incident heating on the CubeSat. Although it only presents variations of 1% over its 11 year solar cycle, given the elliptical nature of the Earth's orbit the intensity of the impinging sunlight varies with ±3.5%. These values vary between 1322 W/m^2 during the Summer solstice and 1414 W/m^2 during the Winter solstice [2].The present analysis considers the solar rays as parallel beams emanating from a point source.

Albedo
The fraction of incident sunlight that hits the Earth's surface and is then reflected back to space is called albedo; it varies around the globe. Over continental regions albedo values vary depending on the nature of the landscape. For example, forest areas have smaller albedo values than desert areas. Oceans, on the contrary, do not reflect back and absorb most of the radiation. Also, with increasing latitude the albedo values tend to increase due to snow and ice coverage. Atmospheric conditions over a particular region also play a role, as it is with cloudy areas which reflect most of the incident radiation. Albedo values range from 25% in equatorial orbits to 50% in polar orbits [3].

Earth's Infrared Radiation
The Earth is not at a non-zero temperature and it radiates heat. The infrared radiation, IR, around the globe varies as the temperatures on Earth do; local time, geography and atmospheric conditions determine the intensity. However, for practical reasons it can be assumed that the Earth radiates uniformly along its whole cross-sectional area with an intensity of 237 W/m^2 [61]. This intensity drops as the spacecraft increases its altitude. The relation is given by Equation 4.20.

$$J_p = 237 \cdot \left(\frac{R_{Earth}}{R_{orbit}} \right)^2 \tag{4.20}$$

Free Molecular Heating
Due to the residual atmosphere at the relatively low Earth orbit, the spacecraft experiences an aerodynamic heating. The heat rate at which this occurs can be calculated with Equation 4.21. When analysing the inputs for this computation, it can be seen that, although the satellite's velocity, V is of a high value, 7.701 km/s at an altitude of 350 km, the average air density, ρ, has a very low value of $1.5113 \cdot 10^{-}11$ kg/m^3. Therefore, it is safe to consider this contribution as negligible for the present analysis. More information on the density variations on orbit is presented in Section 5.7.

$$Q_{FMH} = \frac{1}{2}\rho V^3 \tag{4.21}$$

Internal Components Heating
Subsystems do not have an efficiency of 100% and a part of their energy consumption is lost as heat. The total contribution of the heat generated by each subsystem is known as the internal heat dissipation. The heat losses vary from component to component and depend on the mission phase. For simplicity two main phases are considered: the hot phase and the cold phase. During the daylight part of the orbit the power consumption increases as the camera payload is constantly functioning. During the cold, or eclipse phase, the satellite generates less heat. The following heat dissipation values have been obtained by assuming an efficiency of between $70 - 90\%$ and relating to the peak and idle power values presented in Table 4.17. Nominal values are presented in Table 4.25.

Table 4.25: Internal Heat Dissipation for Hot and Cold Cases

Subsystem	**Hot Case (W)**	**Cold Case (W)**
Structure	0	0
Power	0.02	0.02
ADCS	1.1	0.44
Payload	0.2	0
Propulsion	0.66	0.03
TT&C	1.2	0.02
C&DH	0.09	0.12
Total	3.27	0.63

4.6.1 Thermal Analysis

One Node Approach
Now that the main heating factors have been identified the next step towards a thermal analysis is the consideration of the worst-case conditions, namely the hottest and coldest operating scenarios in which the CubeSat will operate. Rough upper and lower bound values can be obtained by first proposing a steady-state model. However, this approach is not very accurate as it does not consider the cyclical heating and cooling rates of the spacecraft in orbit. A solution, which is not considerably more complicated, is to propose a transient approach which takes average values of incident heating factors and does consider internal temperature fluctuations over time. The calculation can be started by defining the following transient equation.

$$Q_{in} - Q_{emitted} = m_i C_i \frac{\mathrm{d}T_i}{\mathrm{d}t} \tag{4.22}$$

In Equation 4.22 the term Q_{in} contains the direct incident sunlight, the planetary albedo, the Earth's IR, and the heat dissipated by the internal components. The term $Q_{emitted}$ refers to the heat rejected from the spacecraft to the environment. On the right side of the equation the transient condition is determined with m_i and C_i being the mass and heat capacity of the node, respectively. For simplicity the CubeSat is first modelled as one node only. It is made entirely of aluminium $7075 - T1$ with a heat capacity 0.91 kJ/kgK and weighing 8.2 kg .

$$\alpha_{abs} J_s A_{solar} + \alpha_{abs} J_a A_{albedo} + \epsilon_{abs} J_E A_{Earth} + Q_{internal} - \sigma \epsilon_{emi} T^4 A_{surface} = m_i C_i \frac{dT_i}{dt} \tag{4.23}$$

Equation 4.23 expands each of the individual heating contributions: J_s is solar radiation; J_a is the intensity of the solar radiation after being reflected on our planet ($J_s \times a$), where a is the albedo factor; J_E is the Earth's IR intensity. A_{solar}, A_{albedo} and A_{Earth} are the exposed areas of the spacecraft. The α_{abs} coefficients for the first two terms are the absorptivity constants for the exposed surfaces.

The ϵ_{abs} on the third term is also used as an absorptivity constant but particular of the infrared wavelength. In the fifth term the σ is the Stefan-Boltzmann constant and the ϵ is the emissivity constant of the specified surfaces. T is temperature in degrees Kelvin.

The approach is to evaluate Equation 4.23 with the values for the hot and cold cases as presented in Table 4.26. In the hot case, peak values for solar radiation, albedo, Earth's IR, and internal heat dissipation are used. During the eclipse, or cold case, only the values for Earth's IR and internal heat dissipation are used. For the modelling the orbit is considered to be a perfect sphere with the starting point for the angle of 0° defined as the upper most part of the circumference. Given the orbit type, as further described in Section 5.7, the exposed surfaces of the CubeSat are perpendicularly oriented with respect to the sun rays. For a simplified analysis, upper, bottom, front, back, and side faces of the CubeSat are identified. Due to the satellite's orientation, the bottom face always points towards the Earth. Lastly, the number of exposed faces to the sunlight varies, from 2 to 8. The present modelling does consider gradual angle variations of incident sunlight impinging on the spacecraft's surfaces.

Table 4.26: Inputs for Hot and Cold Case Modelling

Variable	**Hot Case**	**Cold Case**	**Units**
J_s	1414	0	W/m^2
a	0.42	0	-
J_a	593.88	0	W/m^2
J_E	237	237	W/m^2
$\alpha_{abs_{solar}}$	0.88	0.88	-
$\alpha_{abs_{aluminium}}$	0.13	0.13	-
ϵ_{emi}	0.065	0.065	-
σ	$5.6704 \cdot 10^{-8}$	$5.6704 \cdot 10^{-8}$	W/m^2K^4
A_{solar}	$0.02 - 0.08$	0	m^2
A_{albedo}	0.06	0	m^2
A_{Earth}	0.06	0.06	m^2
$A_{surface}$	0.28	0.28	m^2
Q_{in}	3	2	W

Table 4.27 gives the recommended operation ranges for each subsystem. The results of this initial computation, as presented in Figure 4.20, give an upper bound value for the hot case of $45.8°C$ and for the cold case of $33.8°C$. These temperatures are above the recommended operating temperature for various subsystems, in particular for the battery and the payload. This problem presents the need for thermal control methods. Passive methods are frequently used as they translate into low volume, mass and cost budget. Moreover, they do not need a power input to be activated and as they are not mechanically based, it is less likely that they fail once in orbit. Nevertheless, active methods are also utilised as they can be more effective in maintaining and rejecting heat, especially for critical areas within the CubeSat that operate in a narrower temperature range [3].

Table 4.27: Nominal Temperature Requirement for each Subsystem

Subsystem	Component	Minimum (°C)	Maximum (°C)
Power	Battery	-20	20
	Solar Panels	-40	125
Structure	Structure	-30	50
C&DH	Computer	-20	60
TT&C	Antenna	-30	70
	Transmitter	-20	50
Propulsion	Engine	-10	50
	Feed System	-10	60
Payload	Electronics	-30	70
	Structures	-50	40
	Optics	-60	70
ADCS	Computer	-40	80
	Sensor	-40	80
	Actuator	-40	70
Bearings	Bearings	-180	20

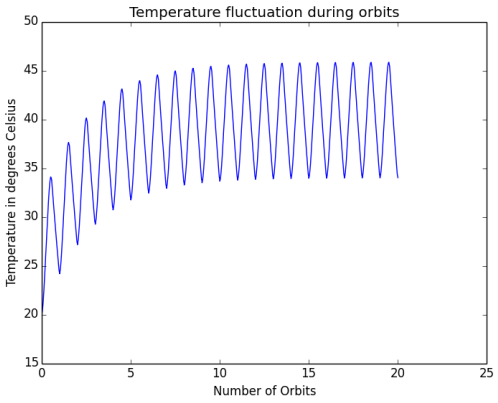

Figure 4.20: Temperatures without Coatings

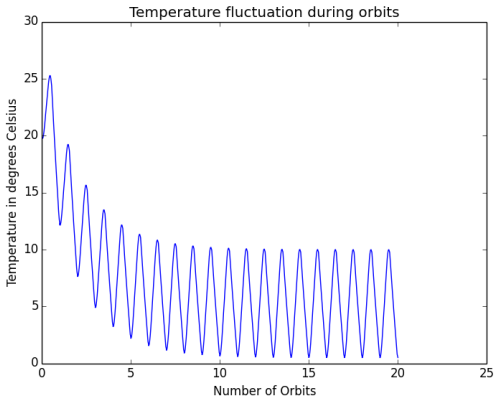

Figure 4.21: Temperatures with One-Node Coatings

The present CubeSat mission is tightly constrained in its budgets. Moreover, in engineering practice the simplest solution is oftentimes the best solution. Therefore, following this design philosophy, the first step towards determining what thermal control design complies best with the requirements is to start by modelling the satellite with the simplest passive control methods — paints and coatings. The design considers three main areas over which the control coatings can be applied: the front and back faces together with the areas surrounding the solar cells as the cells themselves only cover 64% of the upper faces, the bottom sides, and the lateral sides. This distinction follows from the fact that each area is exposed to different heating sources. The front and back faces together with the areas surrounding the solar cells are exposed to direct sunlight; the bottom face is constantly exposed to the Earth's infrared radiation and during the daytime to the albedo; and the sides are simply exposed to deep space. They are all affected by the internal heat dissipation.

Various combinations of coatings on these three surfaces are possible; each of them may help complying with the temperature range requirement but certain designs may give a wider or narrower operating range. In addition, some of them might not be good design options as they make use of more expensive, less available and harder to apply coatings. Table 4.28 gives an overview of frequently used thermal control paints and coatings. Considering the above-mentioned environmental conditions, and using as inputs for Equation 4.23 the values presented in Tables 4.26 and 4.28, a first design option that matches the temperature requirement is presented. The front and back faces and the areas surrounding the solar cells are painted with white paint, the bottom side coated with a thin-film of aluminised Teflon, and the sides left as simply polished aluminium faces. Figure 4.21 shows the temperature fluctuations for this coatings-combination. The peak value for the hot case is now of approximately $26°C$ and lower bound value for the eclipse phase plunged to $1°C$.

Table 4.28: Passive Control Paints and Coatings

Type	Coating	Producer	α	ϵ	Mils	Density
Black Paint	$Z307$	Aeroglaze	0.97	0.89	4	$3g/cm^3$
	$MLS85SB$	AZ Technology	0.98	0.91	2/4	$1.8g/cm^3$
	$RM550IB$	AZ Technology	0.97	0.91	2/4	$2.5g/cm^3$
White Paint	$SG121FD$	MAP	0.20	0.88	4/5	$1.87g/cm^3$
	$AZ93$	AZ Technology	0.15	0.91	5/6	$2.2g/cm^3$
	$AZWLAII$	AZ Technology	0.09	0.91	10	$1.66g/cm^3$
Various	Aluminium Tape	$3M$	0.21	0.04	3	$1.5g/cm^2$
	Polished Aluminium	-	0.24	0.08	-	-
	Aluminised FEP	DuPont	0.16	0.47	1	$1.88g/cm^3$
	Al. Kapton/Al. Outside	Dunmore	0.14	0.05	5	$1.38g/cm^3$
	Al. Kapton/Kapt. Outside	Dunmore	0.40	0.63	5	$1.38g/cm^3$
	Al. Mylar	Dunmore	0.27	0.81	0.5	$1.33g/cm^3$
	Al. Teflon	Dunmore	0.14	0.75	5	$2.13g/cm^3$
	Dacron	Apex Mills	-	-	6	$0.039g/cm^3$

With this basic coating selection the temperature requirement is achieved, let us now look whether the mass, volume, power and cost requirements are also satisfied. First of all, let us state some technicalities. An imperial pint of paint is the minimum amount of product commonly sold by suppliers; This is 0.57 l and it suffices for covering approximately 9300 cm^2. The thickness of each coatings is commonly measured in mils; A mil is 1/1000 of an inch or simply 25.4 μm. Now, quickly estimating that there are 4 full faces in addition to the 6 partly painted faces around the solar cells from which only 36% is covered with a 5-mil layer of AZ Technology $AZ93$ white paint, and considering the given paint's density as listed in Table 4.28, the added weight is 17.2 g and the total volume of these layers is 7.82 cm^3. In addition, bearing in mind that each of the CubeSat's face has an area of 100 cm^2, and the painting is performed over the 4 full faces and the other partly painted 6 faces in paint layers of exactly 1 mil per pass, the total area to be covered is of approximately 3080 cm^2. Therefore, one pint is enough for the coating of the full faces and the areas around the solar cells. This, according to first values provided by the supplier, at a relatively low cost of under 400 € per pint.

Let us perform a similar analysis for the coatings on the bottom and lateral sides of the CubeSat. The bottom side consists of 6 faces, these being 600 cm^2. Considering the Teflon density and the fact that they are applied in layers of exactly 5 $mils$ the added weight of these panels is of a maximum of 16.46 g. The added volume is 7.62 cm^3. With respect to the financial terms, the cost for the aluminised Teflon by Dunmore varies depending on the tape's grade, length and width, though in average € 250 for the required amount can be considered in the budget. Regarding the side faces, these do not have any particular coating and in this way the polished aluminium walls do not affect the weight, nor the financial budget. The polishing of the surfaces can be ordered as an extra feature to the structure supplier, or even polished in-house. Strictly speaking, it may be that the fact of ordering polished surfaces entail an extra cost to the structure budget but it is not considered as determinant for the thermal subsystem budget. In summary, this first design concept complies with the requirement of maintaining a safe temperature range of between 1 and $26°C$; in terms of weight it fulfils the requirement by weighting less that $35g$; with respect to the volume it is less than $16cm^3$; it needs no power input as all control methods are passive; and financially speaking, it borders a maximum of € 700, including products only.

Multi-Node Approach

The one-node analysis just presented is used as a preliminary method to determine general upper and lower temperature values. It also gives a technical appreciation of the possible passive control coatings that can be used. The approach, however, is not very accurate as the internal components in reality do not dissipate heat uniformly in all directions and the heat is not equally distributed over the whole structure. An improved analysis is the multi-node approach in where the temperature fluctuation for each of the CubeSat's faces is calculated. The first step towards a multi-node analysis is the identification of the various nodes. The selection of the nodes can be as complicated as the thermal control engineers decides to. This decision is based on the geometry, material and thermal properties of internal components, and the internal heat distribution on-board.

For the present analysis 29 nodes have been identified: the momentum wheel is node 0; nodes 1 to 14 are the faces of the CubeSat on body A where the most of the subsystems are located; and nodes 15 to 28 are the faces of body B where the payload has been placed. Figure 4.22 shows the numbering of the faces. More specifically, faces 1 and 15 are the front faces of the CubeSat in the flight direction 3.1; faces $2-4$ and $16-18$ are the upper side faces; $6-8$ and $20-22$ are the bottom side faces pointing towards Earth; $9-11$ and $26-28$ are side faces closely located to the wheel surface; $12-14$ and $23-25$ are the side faces directed only towards space.

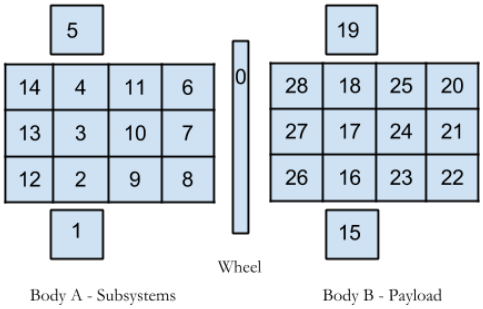

Figure 4.22: Multi-node analysis - Numbering of faces

In the present multi-node modelling the incident heating variations, exactly as for the one-node model, have been assumed. Namely, the values for incident sunlight, Earth's IR and albedo are the same as the ones from Table 4.26. The orbit is once more considered to be a perfect sphere where the starting point of 0° is defined as the upper most part of the circumference. The exposed surfaces of the CubeSat are perpendicularly oriented with respect to the sun rays and the bottom face containing the camera always points towards Earth. The present modelling too considers the angle variations of the incident sunlight impinging on the spacecraft's surfaces. The main new incorporation to the model is the internal heat dissipation. This has been modelled per section and is based on the subsystem internal distribution as presented in Figure 4.32. For simplicity however, the distribution follows the number of CubeSat units per body, these have been taken as exactly three sections per body: $1-3$ belong to body A and $4-6$ to body B. The momentum wheel is referred to as body 0. The internal heat dissipation values for each body are presented in Table 4.29. These values are, similarly as from Table 4.25, based on the peak and idle power consumption values presented in Table 4.17.

Table 4.29: Internal Heat Dissipation per Body

Body	**Faces**	**Subsystem**	**Hot (W)**	**Cold (W)**
0	0	Propulsion	0.66	0.03
1	$1, 2, 8, 9, 12$	Power	0.02	0.02
2	$3, 7, 10, 13$	ADCS	1.5	0.44
3	$4, 5, 6, 11, 14$	C&DH/TT&C	1.29	0.14
$4-5$	$15-17, 21-24, 26, 27$	Optics	0	0
6	$18-20, 25, 28$	Power Unit Payload	0.2	0

The first endeavour with the multi-node modelling uses the same coatings as for the one-node only: white paint for front and back faces in addition to the areas surrounding the solar cells, aluminised Teflon thin film for the bottom sides, and polished aluminium for the sides. The results for this modelling are presented in Figures 4.23, 4.24, and 4.25. The results show that certain panels, in particular panels $1, 4, 5, 12, 15$ do not stay within the allowed temperature range. More critically, panels $3, 14, 26$ and 28 soar to undesired high temperatures. This calls for a reselection of the coatings to be used on each panel. Before proceeding, however, let us state that the analysis continues to a certain extent to be inaccurate. For simplicity of the present multi-node analysis the thermal interactions between adjacent panels are not taken into account. This simplifies the modelling to the degree that each panel is isolated and analysed on a one-to-one basis. If that specific panel does not meet the temperature requirements, the coatings on that specific panel are modified until it does.The design objective is to tailor each panel with the most suitable coatings from Table 4.28 and thus maintain all panels within the desired temperature range.

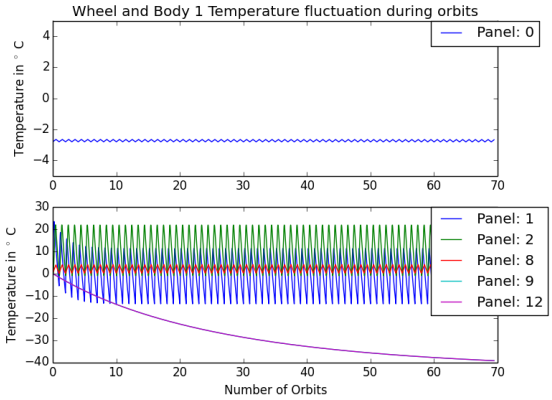

Figure 4.23: Body 0-1 One-Node Coatings

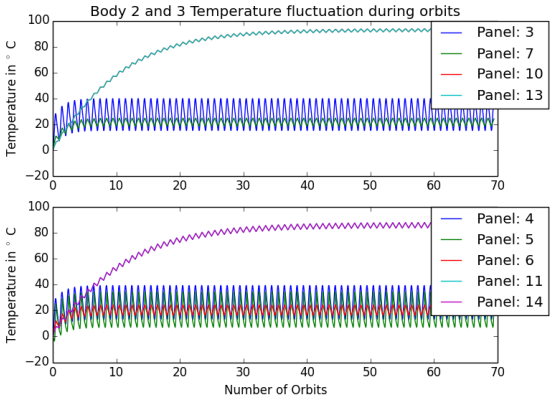

Figure 4.24: Body 2-3 One-Node Coatings

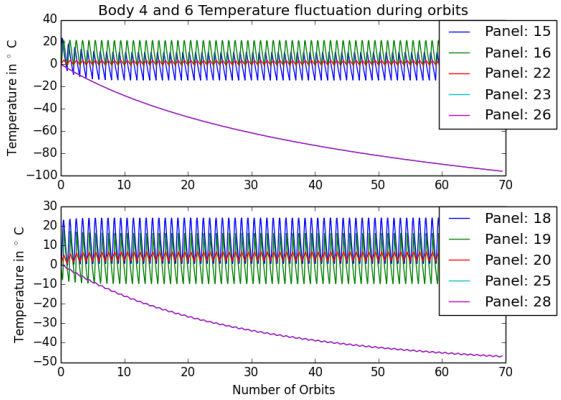

Figure 4.25: Body 4-5 and 6 One-Node Coatings

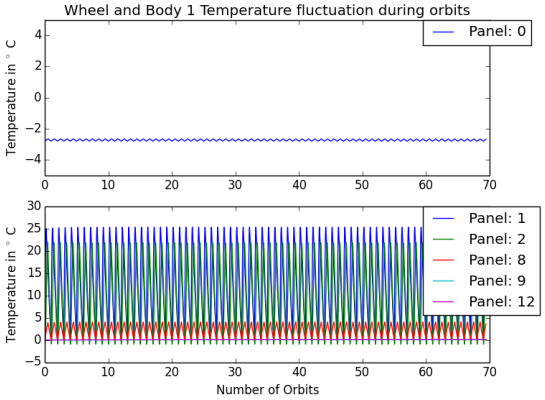

Figure 4.26: Body 0-1 Multi-Node Coatings

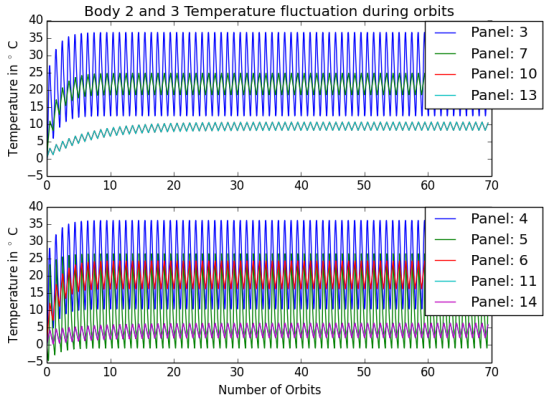

Figure 4.27: Body 2-3 Multi-Node Coatings

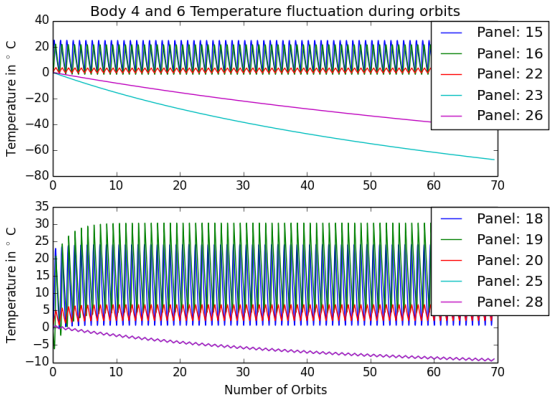

Figure 4.28: Body 4-5-6 Multi-Node Coatings

Figures 4.26, 4.27 and 4.28 show the results of the new temperature fluctuations. Each panel was analysed individually and coated specifically to stay within the allowable range. Table 4.30 presents the selected coatings for each face.

Table 4.30: Thermal Control Coatings for Faces 0 to 28

Body	**Face**	α	ϵ	**Coating**
0	0	0.24	0.08	Polished Aluminium
$A1$	1	0.4	0.63	Al. Kapton/Kapton Outside
$A1$	2	0.19	0.86	White Paint
$A1$	8	0.15	0.77	Al. Teflon
$A1$	9	0.21	0.04	Al. Tape
$A1$	12	0.21	0.04	Al. Tape
$A2$	3	0.15	0.91	White Paint
$A2$	7	0.15	0.77	Al. Teflon
$A2$	10	0.3	$0.15 - 0.3$	MLI
$A2$	13	0.3	$0.15 - 0.3$	MLI
$A3$	4	0.19	0.86	White Paint
$A3$	5	0.19	0.86	White Paint
$A3$	6	0.15	0.77	Al. Teflon
$A3$	11	0.3	$0.15 - 0.3$	MLI
$A3$	14	0.3	$0.15 - 0.3$	MLI
$B4$	15	0.4	0.63	Al. Kapton/Kapton Outside
$B4$	16	0.19	0.86	White Paint
$B4$	22	0.15	0.77	Al. Teflon
$B4$	23	0.25	$0.02 - 0.04$	Al.Tape/Al. Kapton
$B4$	26	0.25	$0.02 - 0.04$	Al.Tape/Al. Kapton
$B5$	17	0.19	0.86	White Paint
$B5$	21	0.15	0.77	Al. Teflon
$B5$	24	0.25	$0.02 - 0.04$	Al.Tape/Al. Kapton
$B5$	27	0.25	$0.02 - 0.04$	Al.Tape/Al. Kapton
$B6$	18	0.19	0.86	White Paint
$B6$	19	0.4	0.63	Al. Kapton/Kapton Outside
$B6$	20	0.15	0.77	Al. Teflon
$B6$	25	0.25	$0.02 - 0.05$	Al.Tape/Al. Kapton
$B6$	28	0.25	$0.02 - 0.05$	Al.Tape/Al. Kapton/MLI

From the graph interpretation, it can be seen that most of the panels have been coated strictly to comply with the temperature requirement. There are, however, a number of panels that either barely comply with the requirement, or do not manage to do it at all. Temperatures for panels 3 and 4 rise beyond the limit and reach approximately $35°C$. These panels do not meet the requirement and a further redesign of the thermal coating should be proposed. Specifically one that helps rejecting the undesired heat. A possible solution is the utilisation of a coating with a lower emissivity coefficient. In the present analysis no coating that shares such good absorption and emissivities properties was found. However, take a look at the specific location enclosed by these panels as presented in Figure 4.32. Below panel 3 the ADCS system is located, and below panel 4 the C&DH and TT&C can be found. Moreover, looking again at the recommended temperature ranges presented in Table 4.27, it can be concluded that extra measurements should be taken in order to bring all panels below the originally proposed maximum temperature requirement. Nevertheless, there is some flexibility at the time of designing given that the subsystems around these panels are not strictly compromised, for they have an allowable operating temperature higher than $50°C$. As stated, no thermal interaction between panels is considered and this allows for such a straightforward conclusion.

There are, in addition, panels on body B that do not meet the temperature requirement. Panels 23, 24 26 and 27 plummet down to freezing temperatures. Temperatures around this area are far below the lower desired boundary, however, a similar approach as with panel 3 and 4 can be taken. Specifically around these panels on body B the camera optics are located. Referring, once more, to Table 4.27 the operating temperatures for the optics give some leeway at the time of designing, for they can also operate below the temperature requirement at around $-50°C$. The sensitivity of the coating design can be nicely appreciated in Figure 4.28. Panel 24 which has been coated with aluminised Kapton of an $\epsilon = 0.04$ drops to a temperature of $-60°C$. Panel 23 sharply falls to $-40°C$, only because it has been coated with a different type of Kapton with an $\epsilon = 0.02$. The difference on these emissivity stems from the exact film thickness and outer cover material composition, aluminised v. goldised. Being this latter superior in performance but significantly less convenient in availability and financial

terms.

There is one more critical panel on body B. Panel 28 barely makes it and reaches a constant temperature of $-10°C$ after 70 orbits. Around this panel the camera's sensors and electronics are located. These can operate at lower temperatures, so a redesign is not urgently consider. However, a commonly simple solution for this critical area could be the utilisation of a Multi-Layer Insulation blanket, MLI. This approach is also recommended for panels $10, 11, 13, 14$ on body A as they are side panels and for optimum performance require a coating with ϵ between 0.15 and 0.3. MLIs are extensively applied around critical components as batteries, payloads and propulsion systems and their primary function is to retain the heat inside the spacecraft. MLI commonly consists of 15 to 30 thin layers of aluminised Mylar or Kapton, separated by inner layers of Dacron, and closed on the sides by 1 or 2 Kapton or Teflon covers [2].

Regarding the mass, volume, cost and power budget for this new design let us perform a simplified analysis based on Table 4.28 as done with the coatings for the One-Node approach. Aluminised Kapton with a specified thickness of 5 mils is applied over 11 faces; this results in 19.28 g and a volume of 14 cm^3. Teflon is applied over 7 panels, similarly with a specified thickness of 5 mils; this results in 18.93 g and a volume of 8.89 cm^3 . White paint is applied over 6 surfaces surrounding the solar cells and one full face; this results in 8.82 g and 4.01 cm^3. Lastly, MLIs with an average $\epsilon = 0.3$ are needed over 5 surfaces. The design selected considers 25 interior layers of aluminised Mylar, with a thickness of 0.5 mil separated by 26 inner layers of Dacron, and closed by 2 outer covers of Kapton of 2 mils; this results in 36.76 g and a volume of 229.35 cm^3. The total mass of these coatings is 83.79 g and the volume is 256.22 cm^3 .

Concerning financial terms, one pint of AZ Technology $AZ93$ white paint covers, as stated, 9300 cm^2, given that the required surface is of 1580 cm^2, one pint valued in €370 suffices. In addition, one aluminised Teflon 5-mil tape by Dunmore is necessary to cover the 700 cm^2 of required satellite's surface and it has a market price of around €250. The Dunmore supplier contacted for the present project pointed out that MLIs are not sold as pre-fabricated blankets by their company, but instead as assembly kits for a starting price of €500. Based on the technical specification of this initial set requested to Dunmore, the kit satisfies to cover 9290.30 cm^2 of aluminised outer cover 2-mil Kapton, and a surface of 23225.76 cm^2 of aluminised 0.25-mil Mylar. The 11 faces of aluminised 5-mil Kapton translate to approximately 2750 cm^2, and the MLIs require 2000 cm^2 for the required 5 faces in addition to the 10000 cm^2 of interior aluminised 0.25-mil Mylar. Hence, the material included in the kit provides the passive control coating for the present design. As a final note, no power consumption is required for the thermal control as the satellite's temperature has been shown to be controlled by means of passive methods only.

4.6.2 Thermal Control Subsystem Compliance Matrix

The preliminary set of requirements presented in Table 4.31 are only partly fulfilled. The most important Requirement **S08-MC-TC-01** is, strictly speaking, not satisfied as in more than one occasion it was found that certain panels surpass the originally proposed temperature limits. Nonetheless, no specific subsystem is seriously compromised by this requirement's infringement. As suggested at the end of the one-node approach, the satellite's thermal design requires one step further into a more advanced analysis. The present multi-node modelling allowed for a more accurate prediction of the in-orbit temperatures but it disregarded important thermal considerations as the thermal conduction and radiation within the spacecraft. Moreover, little attention was paid to the material and thermal properties of the various internal components. It might be that the temperature range of $-10°C$ to $30°C$ was proposed on too strict grounds. In fact, when looking at the recommended temperature ranges for each subsytem as presented in Table 4.27 the lower temperature value is mainly driven by the engine's integrity and the upper bound by the battery and the bearings. The engine and the battery are known to be of major consideration for the thermal control, and it is a reality that they operate in a narrower range, but a tailored, more specific coating for these subsystems can be devised. The present analysis has considered the utilisation of MLIs exclusively for protection of the satellite's walls. Though these type of blankets are also commonly located around the critical areas, thereby engulfing and protecting the more sensitive components. Similarly, the bearings operate only up to the rather low upper bound temperature of $20°C$. A more detailed investigation of the thermal conduction between the bodies and the wheel should be performed. In the previous analysis, the wheel was modelled as a uniformly composed aluminium body, no attention was paid to the interaction

between the localised heating of the bearings and the wheel. By and large, initial predictions for the temperature ranges and good first estimations for mass, volume and cost budget have been given, but the design calls for a more thorough investigation of the criticality of each subsystem, accompanied by a more accurate software thermal modelling.

Table 4.31: Thermal Subsystem Compliance Matrix

Requirements	Compliance
S08-MC-TC-01	X
S08-GTC-V-06	✓
S08-GTC-M-06	✓
S08-GTC-P-03	✓
S08-MC-C-05	✓

4.7 Materials

Inside the space environment, a trade-off needs to be implemented with criterias different than in space. In space, the environment is harsh which means that the materials needs to be selected carefully, implementing all elements that could affect the structure into one compatible structure. In this section, the process that was used to come up with suitable materials is explained.

4.7.1 Material type

The number of different types of materials that can be used inside space applications is limited. From reference [61] and [3], a main list of materials suited for space applications are given.

- **Aluminium**: Aluminium is by far considered the most used material in space. Its high strength versus weight characteristics makes it a primary candidate. Moreover, it is easily available and simple to manufacture. Its main drawback include the high coefficient of thermal expansion and its low toughness against impacts.
- **Hard Metals**: Steel and Titanium are mostly used in space missions where a high strength against impacts are needed at the expense of heaviness. However, it is significantly difficult to machine and usually comes with defects.
- **Composites**: Composites are a new emerging type of material in the spacecraft industry. At the moment only a few CubeSats are using composites for experimentation. However the main disadvantage of composites is the fact that their properties only hold in a certain direction.

In the following section a trade-off will be made. However, instead of taking a long list of criteria only the most important criteria for the space environment will be considered. [61]

4.7.2 Trade-off with respect to the environment

In the first part, a trade-off taken into account the environment is made. The space environment is very different from the atmosphere environment on Earth. In order to comply with the requirements, the satellite should be able to survive the space environment

Temperature
Moreover, a second parameter needs to be taken into account which is the thermal expansion of the material. Inside CubeSat designs, a slight shift of the centre of mass with respect to the geometric centre can have undesirable torques and result in added difficulties when trying to stabilise the entire satellite. With regard to the temperature that the satellite is subjected to, the thermal expansion can then be computed and a new centre of mass can be calculated. This calculated centre of mass should stay within a small margin from the existing centre of mass shift which was determined in Section 4.8.1. This property is more extensively discussed as a material property. [3]

Debris
Another important environmental parameter is the presence of debris resulting from previous satellite mission which have either collided with other satellites or have been abandoned. These debris pose a serious threat for any space mission since they can easily compromise an entire mission. For this reason, most satellites usually have important shielding for debris up to a certain size. In the scope of

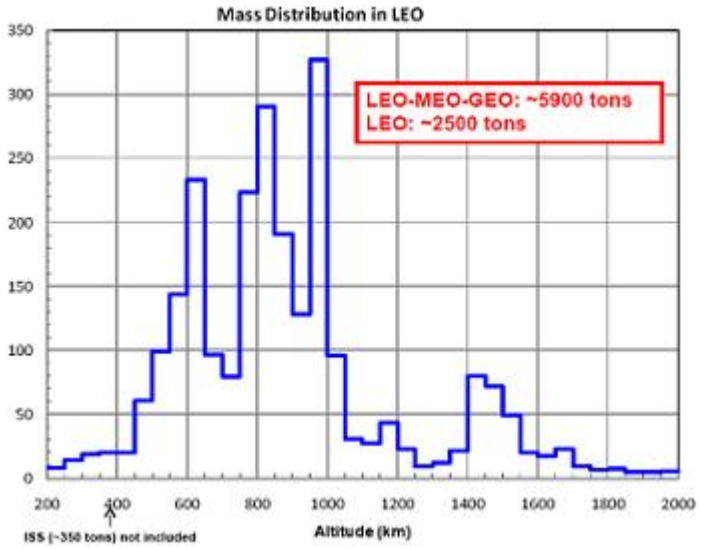

Figure 4.29: Spatial density of debris with altitude[27]

the VLEO mission, debris are not taken into account. Due to the small size of the satellite combined with the rarity of debris at 350 km altitude, it is very unlikely that a debris will strike the satellite. Figure 4.29 shows the occurrence of debris with respect to altitude. A risk assessment was done in Section 2.6. [3]

4.7.3 Trade-off with respect to material properties

Properties closely related to the material type also need to be taken into account. For

Specific Stiffness
In space, most of the time, the satellite is subjected to minor loads. However during launch, the satellite is subjected to important vibrations that need to be measured. In order to determine if the structure might fail because of these dynamic loads, a stiffness coefficient is determined with respect to the structure type and the material type. This stiffness coefficient is highly dependent on the Young's modulus of the material which must be high enough in order to sustain the loads. However, at the same time, the material should be light enough. For this, the specific properties of materials are analysed, especially in this case the E/ρ ratio. Figure 4.30 illustrates the best materials suited for the specific stiffness. [3]

[27] `http://www.nasaspaceflight.com/2011/01/project-adr-removal-large-orbital-debris-nasa-study` [cited 24 June 2015]

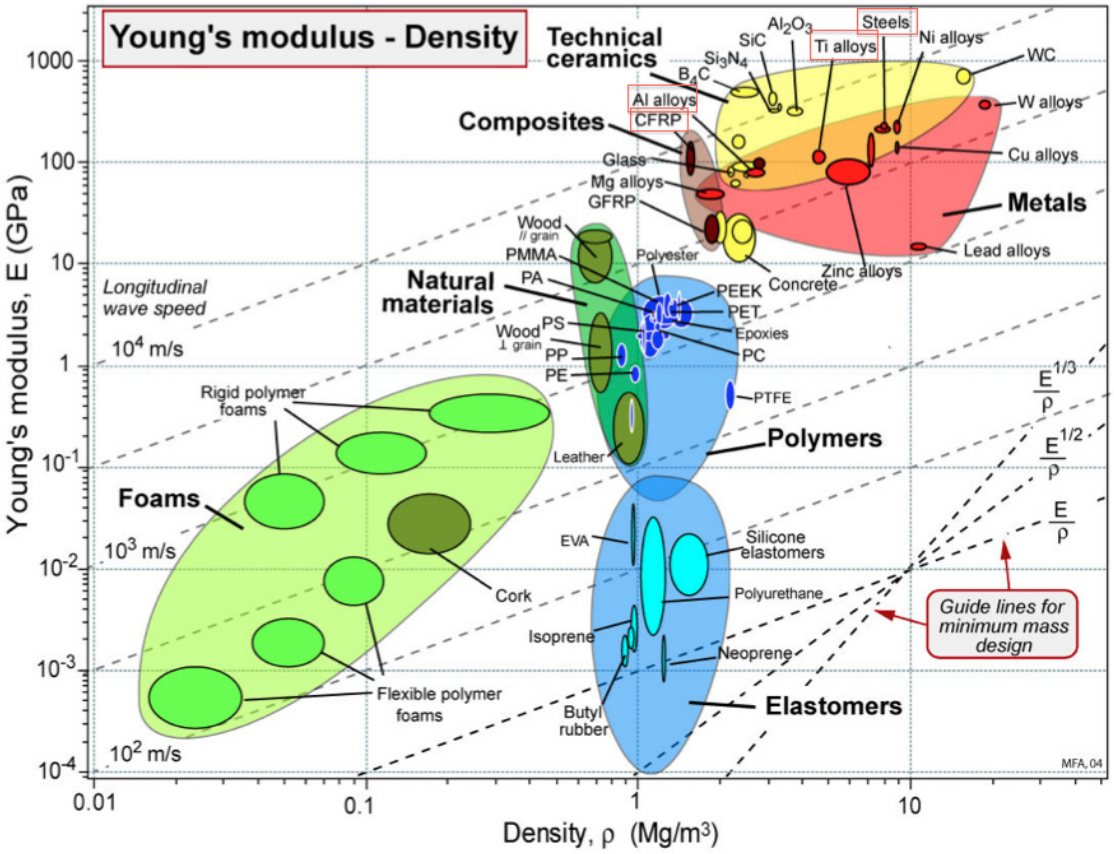

Figure 4.30: Specific stiffness properties of materials[28]

From Figure 4.30, the best properties are found to be in technical ceramics. However, ceramics are too brittle to sustain loads during launch and would quickly break.

Thermal Expansion

As mentioned before in Section 4.7.2, the thermal expansion of the metal is an important property in space. When high precision features need to be used, the material is usually not allowed to expand much. A similar figure is found for the thermal expansion in Figure 4.31.

[28] `http://www.mie.uth.gr/ekp_yliko/2_Materials-Charts-2009.pdf` [cited 17 June 2015]

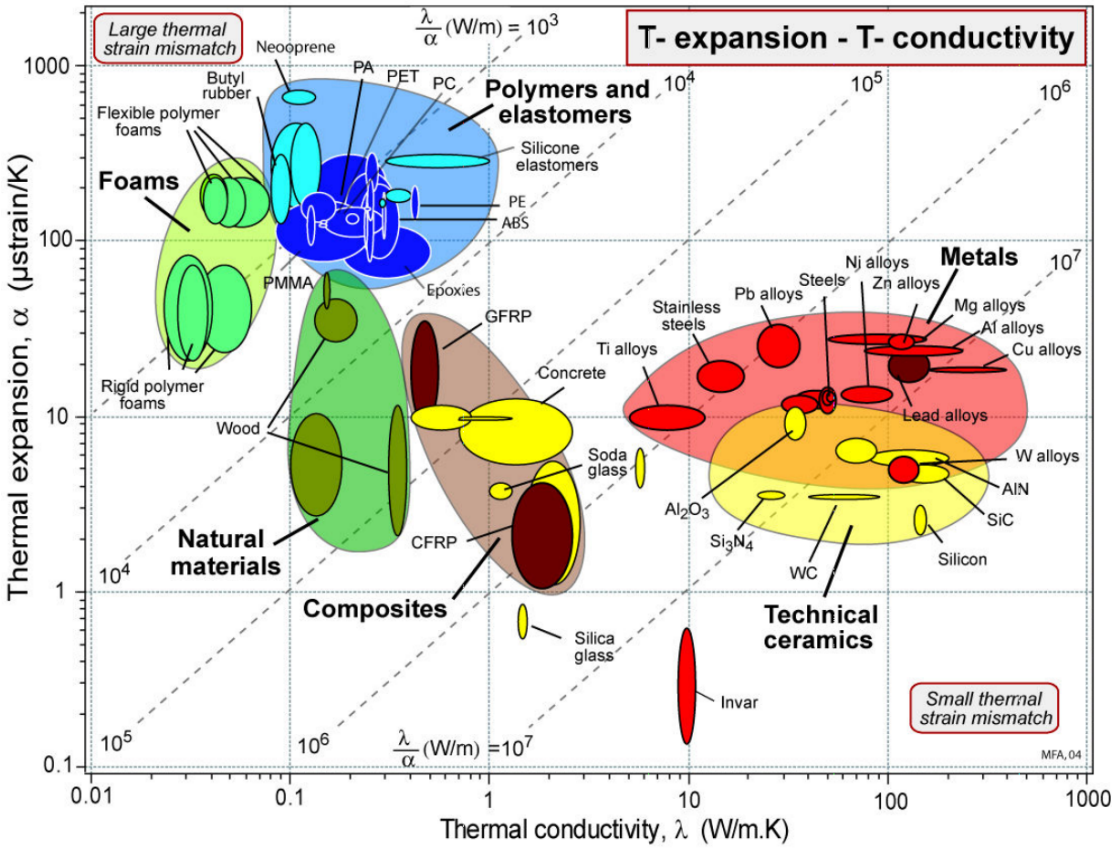

Figure 4.31: Thermal Expansion vs. Thermal Conductivity of Materials[29]

In here the thermal expansion is plotted versus conductivity. The desired material needs to have good conductivity while having low thermal expansion.

Conclusion
From each trade-off a conclusion can be made:

Temperature and Thermal Expansion: taking only temperature properties, the best material is the use of INVAR. As a second choice, Aluminium can be chosen to have good thermal properties if compared to other metals.
Stiffness: In terms of stiffness from Figure 4.30, the best material to use is technical ceramics. However these are not suitable material for a space environment. As a second choice, the best option would be to use metallic alloys. In this category, the aluminium alloys tend to have the best properties in terms of specific stiffness.
Debris: Even though debris are a requirement inside the project, from statistics, the chance of hitting a debris at this altitude is very low. Moreover, in order to protect the satellite, a whipple shield needs to be used. In a small scale satellite, the implementation of such a shield is very complicated as there is not enough space to put all layers to protect the structure. Taking this into account, the protection from debris was deemed unnecessary, as the likelihood of occurrence is really low and not enough protection could be implemented to protect the satellite.
Conclusion: Overall, two materials, INVAR and aluminium come out as favourite candidates. The INVAR however is nowhere what the aluminium can offer in terms of stiffness. The INVAR material is actually a special material used for very special applications where only thermal expansion is the main driver. Also in terms of thermal expansion, the aluminium possesses good properties compared to other materials except the INVAR. Therefore aluminium alloys were opted as the best option.

Types of Aluminium
For the Aerospace industry, two main types of aluminium are used. These consists in the 7075 and the 6061 aluminium alloys. For space applications, the 7075 alloy is preferred in this case since the

[29] `http://www.mie.uth.gr/ekp_yliko/2_Materials-Charts-2009.pdf` [cited 17 June 2015]

satellite is sized in terms of vibrations. The 7075 alloy is proven to be much more stronger in terms of dynamic load.

4.8 Structural Design

- **S08-GTC-V-04** *The structure shall have a volume smaller than* 10 $cmx10$ $cmx60cm$
- **S08-GTC-M-04** *The mass of the structure shall be lower than* 18 % *of the total mass*
- **S08-GTC-S-04** *All components shall stay attached to the satellite*
- **S08-GTC-S-05** *The satellite shall be easily accessible during manufacturing*
- **S08-GTC-S-07** *The structure shall be able to carry all loads introduced by the propulsion system*
- **S08-GTC-S-08** *The lateral mode frequency shall be higher than* 15 Hz
- **S08-GTC-S-09** *The longitudinal mode frequency shall be between* 31 *and* $45Hz$
- **S08-GTC-S-10** *The materials used shall have a thermal expansion coefficient lower than* $22.2 \cdot 10^{-6} m/mK$
- **S08-GTC-S-11** *The structure shall be able to accommodate all subsystems*
- **S08-MC-C-04** *The structure cost shall be lower than* 8 % *of the total cost*

Even though the space environment is harsh in general, the spacecraft is not subjected to many loads. In the scope of our mission, the aerodynamic disturbances are taken into account in Section 3.4. Since this loads are modelled to be mostly uniform, this section will deal with more structural loads occurring during launch. But first, the internal and external layout are described.

4.8.1 Internal/External Layout

Internal Layout
For the internal layout, it is of utmost importance that the centres of gravity are aligned with the geometric centre. Since the form of the satellite is symmetric, the weight of the camera should be equal to the weight of the subsystems in the other cube in order to stabilise the CubeSat in around every axis. Since this was initially not the case, some additional mass needed to be added to the camera, equally distributed over the 3 cubes containing the camera. However, this is not the only requirement on the stability. Another requirement is that the MMOI of the camera cube is equal to the MMOI of the other cube. This is because different MMOI give different rotational reactions to torques, and that should not be the case. The location of the subsystems is determined such that the MMOI for the payload cubes is the same as for the cubes containing the other subsystems. The actual layout is presented in Figure 4.32.

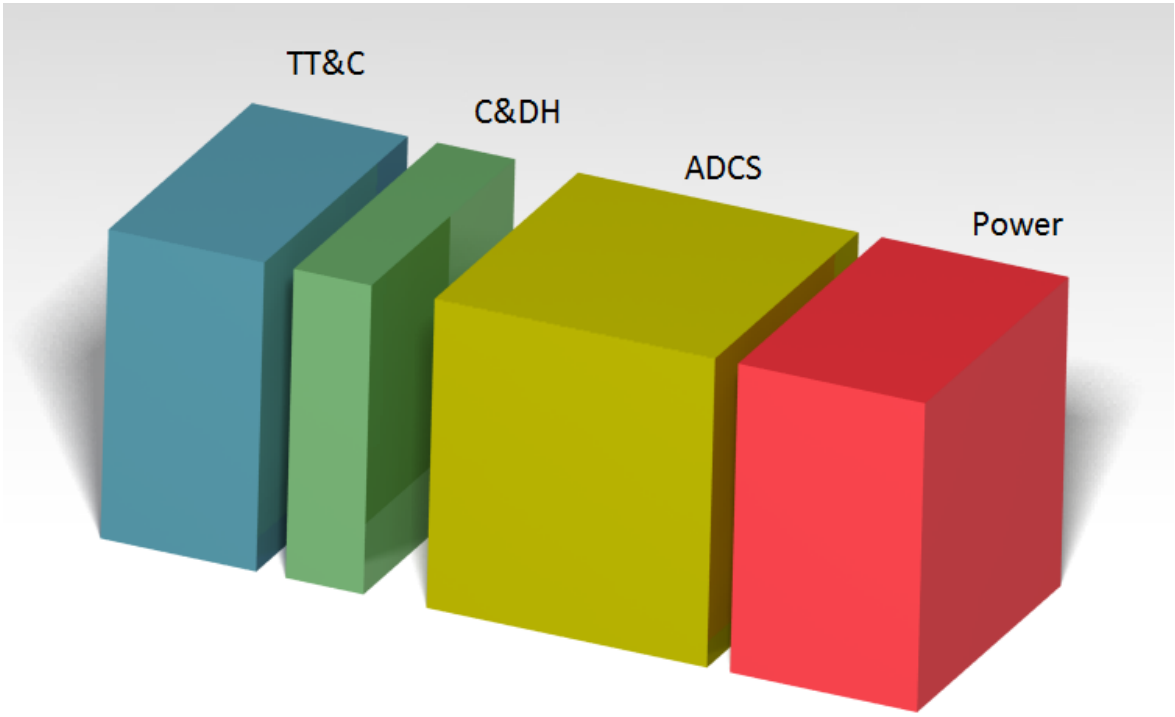

Figure 4.32: Location of the C&DH, TT&C, ADCS and Power subsystem

The location of the subsystems should be up to a tenth of a millimetre accurate in order to provide the least difference in distance between the centroid and the centre of gravity. With the placement as can be seen in Figure 4.33, the offset between the centre of gravity and the centroid is smaller than $1\mu m$. However, a value of 1mm is assumed in the disturbance section, Section 3.2, because of possible inaccuracies in the placing of subsystems. The MMOI of the camera cube is 0.02150 kgm^2, as for the other cube it is 0.02151 kgm^2. Although the difference seems minimal, the ADCS has to counter for it as well.

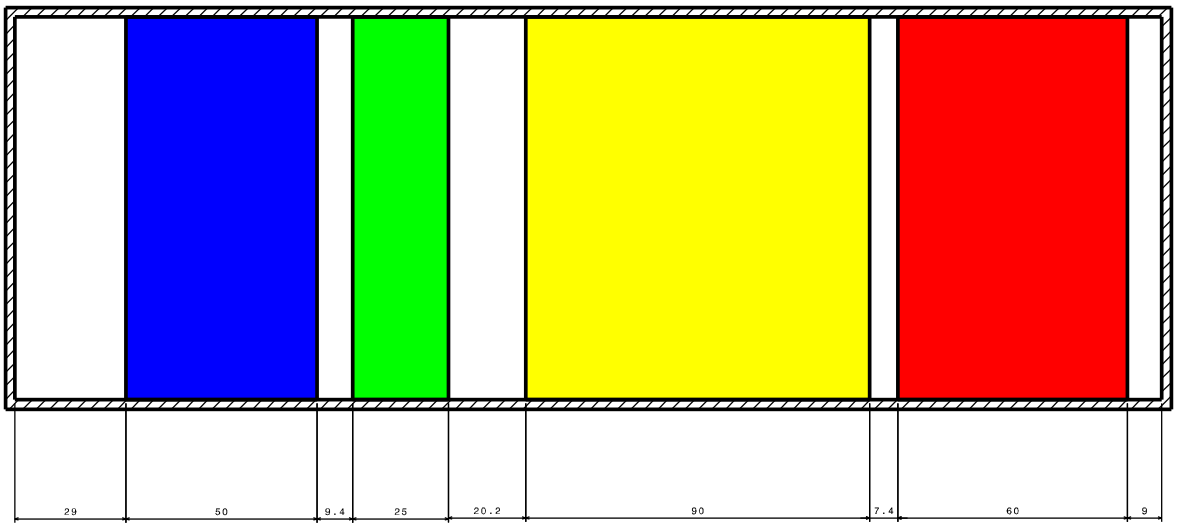

Figure 4.33: Subsystem Placements with Values

Figure 4.33 gives a detailed view of the layout of the cube with the subsystems. The flight direction is to the left.

External Layout
The external layout deals mostly with the implementation of solar panels. In order to provide enough power to the satellite, both body mounted and deployable solar panels are used. These usually requires the implementation of special hinges that will be able to deploy the solar panels. In order to have

the solar panels deployed without any problems, the solar panels need to be folded accordingly. The folded solar panels are represented in 4.34.

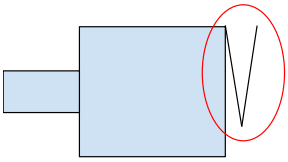

Figure 4.34: Retracted Solar Panels

The mechanism implemented for the solar cell deployment needs to be reliable since a failure would lead to a failure of the whole mission since not sufficient power could be generated. Also, the mechanism needs to withstand all loads during launch since a separation of the solar cell would cause space debris. This deployment system was already usefully used in other CubeSat mission and can therefore considered to be sufficient. Moreover, the orientation of the antennae are also important. Overall, the main consideration to have is to avoid the antennae to be in the way of the wheel when these are spinning.

4.8.2 Preliminary analysis

Before the launch loads are determined, the way the CubeSat is fixed inside the launcher is important. Depending on the way the satellite is present inside the launch will result in more or less vibrations. The idea is to find the optimal way to have the satellite fixed inside the launch fairing to reduce the vibration level. For this the optimal boundary conditions have to be considered. In Figure 4.35, different types of launch options are presented. For the design of the CubeSat, a large structure with space is necessary in order to accommodate the large size of the satellite during launch. Moreover, the structure needs not to be too rigid in order to be able to absorb the energy resulting from vibrations. Another consideration is the fact that too many fixed parts inside the launch fairing could result in unnecessary loads that could be avoided by choosing a simply fixed structure, fixed on one end. In Figure 4.35, different options for launch are examined. In the scope of the project, the best option was circled. This option was chosen since it would give enough space to accommodate the design. It is important to emphasise that these are existing launch fairings that are not specifically adapted to the SHAPE. For that reason, the launch fairing will probably need adjustment in order to accommodate the satellite, but this can already give an overall idea of the launch fairing. The other launch fairing, if adapted could also proved to be good options, but the truss structure offered by the circled option allows designers to constantly have a look during launch on the satellite. Moreover, this also saves weight compared to other structures.

Table 4.32: Launch Quasi-Static Loads for Ariane 5

	Acceleration $[g]$			
	Longitudinal		**Lateral**	**Additional line load** $[N/mm]$
Critical Flight Event	**Static**	**Dynamic**	**Static+Dynamic**	
Lift off	-1.8	+/- 1.5	+/- 2	10
Maximum dynamic pressure	-2.7	+/- 0.5	+/- 2	14
SRB end of flight	-4.55	+/- 1.45	+/- 1	20
Main core thrust tail off	-0.2	+/- 1.4	+/- 0.25	0
Max. tension case: SRB jettisoning		+2.5	+/- 0.9	0

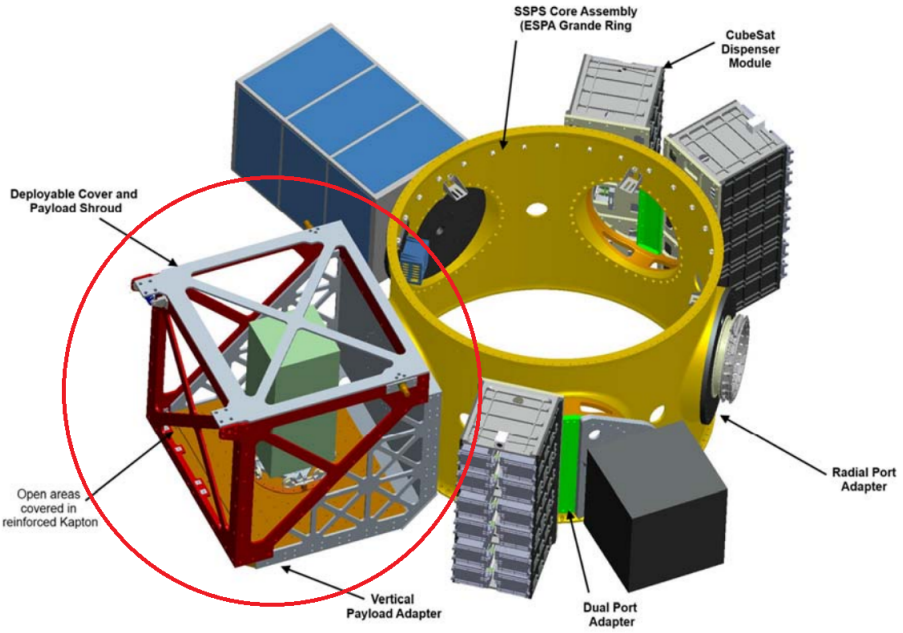

Figure 4.35: Launch options[30]

The launch phase usually represents the most important phase of a space mission since it is subjected to the most important accelerations. Accelerations that occur during the launch of the Ariane 5 launcher are listed in Table 4.32. These show an overview of accelerations that could be subjected during launch. The Ariane 5 represents a very general rocket that is used for space mission, and therefore the accelerations are accelerations that could be expected during the launch of SHAPE. [61]

4.8.3 Modelling

Before the structural analysis can begin, the satellite needs to be modelled into a simpler structure. As a first step, an analytical solution is computed. It is important to not simplify the actual design too much in order to still have a good approximation. In this section, the different types of boundary conditions are investigated in order to have the optimal combination with reduced vibrations and still a feasible solution. In Figure 4.36, different combinations of boundary conditions are presented. For each combination, the natural frequency is shown. The options are of course very broad in terms of boundary conditions. In here, a preliminary trade-off was made to decide on feasible options in the launch fairing that was chosen.

[30] `http://www.spaceflightindustries.com/wp-content/uploads/2015/05/SPUG-RevF.pdf` [cited 16 june 2015]

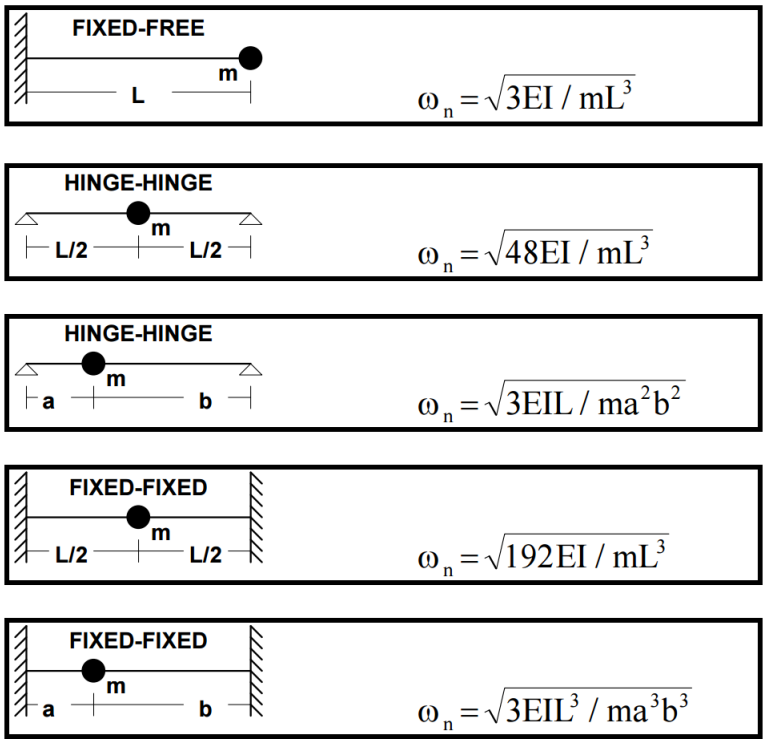

Figure 4.36: Massless Beams with Concentrated Masses

From Figure 4.36, the best option proves to have both ends clamped at both edges. This represents the option with the highest natural frequency. Also it should be noted that these represent the vibrations in the lateral condition, when the beam is subjected to bending. However, this proves to be risky due to the fact that there are two points of failure during the launch of the satellite, on top and the bottom. If one of the fixed points fails to detach, the mission is compromised. Also a clamped edge is usually difficult to manufacture due to the fact that all degrees of freedom need to be constrained. Usually in order to achieve the purpose, a rail system is designed. It is therefore much more reliable to have one edge fixed with another edge free. For this, the best option is therefore to have a clamped edge with a free edge. Even though this will not result in the best stability option, it will still meet the requirement. This will also cancel the risk to have buckling loads during loads which could cause catastrophic consequences. A simple model of the satellite without the wheel can be seen in Figure 4.37.[31]

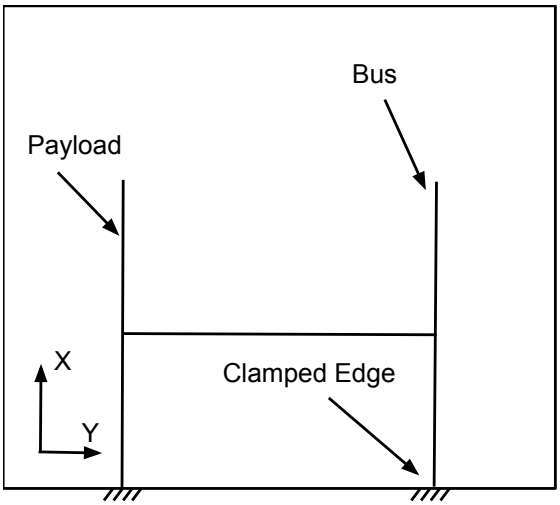

Figure 4.37: Simplified Model of the Satellite during Launch

This model represents the satellite with the bus and the payload on each side with the shaft attaching

[31] http://faculty.uml.edu/pavitabile/22.403/web_downloads/Frequencies_of_Common_Systems.PDF [cited 17 june 2015]

them. Moreover, the two main bodies are both clamped to the launch fairing base. This will be the model that will be used for the analytical solution. The model may seem very simple, however, since the purpose of this project is to complete a first iteration, the obtained result is a very good basis for a more advanced approach. Small note is that in this idealisation, the wheel is assumed to be included in the mass of the shaft and acts in the middle.

4.8.4 Static Loads

First, the structure is sized for strength. The structure needs to be strong enough and to withstand the static loads during launch. With static loads, an assumption of the random loads that occur during launch, is meant. The loads during launch are hardly static and vary in time. For that reason it is difficult to have an accurate assessment of the exact static loads that occur during launch. However, the loads can be assumed static during the launch. In order to assess the static loads Equation 4.24 is used. [28]

$$\sigma_{tot} = \frac{g_y M L c}{I} + \frac{g_x M}{A} \tag{4.24}$$

From Table 4.32, the worst lateral and longitudinal accelerations are considered. These are 2 and 4.55 g's in absolute values respectively. The mass is mainly distributed so the total mass is assumed to be acting in the middle. Filling in the following properties :

Table 4.33: Parameters for Strength Calculations

Parameters	**Values**
Mass (M)	2.6 kg
Moment arm (L)	0.15 m
Extreme fiber distance (c)	0.05 m
Second moment of area (I)	13.25 cm^4
Cross-sectional area (A)	0.01 m^2

$$\sigma_{tot} = 121\, MPa \tag{4.25}$$

From [32], the ultimate yield strength of the aluminium 7076 is 503 MPa. The maximum load is therefore well below the maximum allowed load.

4.8.5 Dynamic Loads

Although it is important to size for strength, usually, during launch of space missions, the most important parameter to consider are the self-induced vibrations as well as the forced vibrations. For this a vibrational analysis is required to fulfil the requirements.

Every structure has a natural frequency during vibrations. This natural frequency is really important for dynamic loads. If a forced load with a vibration ω is subjected to a structure, the frequency should always stay far from the natural frequency of the structure. If not a phenomenon known as resonance occurs which means that the amplitude of the vibrations increases gradually and the structure fails. In order to calculate the natural frequency of the satellite, the satellite needs to be modelled as a mass-spring system. This idealised mass-spring system is shown in Figure 4.38

[32] `http://asm.matweb.com/search/SpecificMaterial.asp?bassnum=MA7075T6` [cited 17 June 2015]

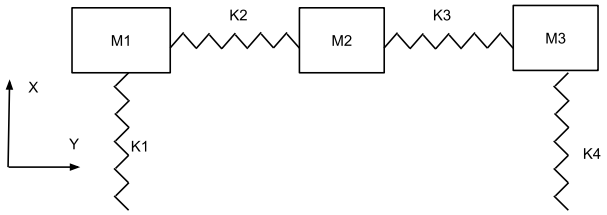

Figure 4.38: Idealised mass-spring System of the CubeSat at Launch

With the different values listed in Table 4.34

Table 4.34: Parameters for Dynamic Analysis

Parameters	**Values**
Young's Modulus (E)	69.9 $[MPa]$
Moment of inertia - Rectangular Beam	$\frac{0.1^4}{12}$ $[m^4]$
Moment of inertia - Circular Shaft	$\frac{\frac{0.0075^4\pi}{4}}{}$ $[m^4]$
Cross-sectional Area - Rectangular Beam	0.1^2 $[m^2]$
Cross-sectional Area - Circular Shaft	$pi * 0.0015^2/4$ $[m^2]$
Length - Half Rectangular Beam	0.15 $[m]$
Length - Half Circular Shaft	0.055 $[m]$
Mass of Subsystem Bus	3.137 $[kg]$
Mass of Payload Bus	3.137 $[kg]$
Mass of Wheel + Shaft	$1,79$ $[kg]$

One important assumption that was made inside the structure is that the second half of each beam representing the payload or the bus subsystem is no present. The mass is assumed to act in the middle of a block, and the springs are assumed to be weightless. The set-up can be seen in Figure 4.38. However, this approach can create a discrepancy for the calculation of the natural frequency. If the discrepancy is too large compared to statistical values, a second iteration might be necessary. However, in general the natural frequencies are in the order of a few thousands Hertz. After computing them, they will be compared to the numerical values computed from a FEM analysis discussed in Section 5.7.

In order to solve the idealisation mentioned above, first the undamped natural frequencies of the system must be computed in two directions. This is done using Equation 4.26.

$$[M]\ddot{x} + [k]x = 0 \tag{4.26}$$

Depending on analysis direction, the springs are loaded axially or lateral. First the lateral loading in the direction of the Y-axis is considered. For this case, the k_1 and k_4 springs are loaded in bending while the k_2 and k_3 springs are loaded axially. Therefore, as represented in Equation 4.28

$$k_1 = k_4 = \frac{3EI}{L^3} \tag{4.27}$$

$$k_2 = k_3 = \frac{EA}{L} \tag{4.28}$$

If the system is described into a detailed matrix form, Equation 4.29 is obtained for the analysis of the y-axis.

$$\begin{bmatrix} M1 & 0 & 0 \\ 0 & M2 & 0 \\ 0 & 0 & M3 \end{bmatrix} \begin{bmatrix} \ddot{x}_1 \\ \ddot{x}_2 \\ \ddot{x}_3 \end{bmatrix} + \begin{bmatrix} k_2 + k_1 & -k_2 & 0 \\ -k_2 & k_2 + k_3 & -k_3 \\ 0 & -k_3 & k_3 + k_4 \end{bmatrix} \begin{bmatrix} x_1 \\ x_2 \\ x_3 \end{bmatrix} = 0 \tag{4.29}$$

The displacement x is a harmonic displacement which is described by Equation 4.30

$$x = \sin(\omega t) \tag{4.30}$$

Replacing Equation 4.26 by Equation 4.30, the equation becomes Equation 4.31 to solve :

$$[k] = \omega^2[M] \tag{4.31}$$

where $\omega^2 = \lambda$. Solving this equation will then give the natural frequencies of the system since the λ values represent the eigenvalues. Solving this equation gives the eigenvalues in Table 4.35 [33]

Table 4.35: Eigenvalues for Lateral Vibrational Motion

Modes	**Lateral Natural Frequency** $[Hz]$
1	1651.8
2	2423.2
3	3068.8

It is stated in the reference list that the natural frequency should be higher than a reference frequency of 15 Hz. This objective is largely met but care should be taken to avoid resonance at higher frequencies. Taking as a reference the vibration frequency of 15, in order to avoid resonance, the natural frequency obtained should not be a multiple of the launch frequency of the rocket. In Equation 4.32, the occurrence of resonance is investigated.

$$K = \frac{\omega_n}{\omega_0} = \frac{1651.8}{15} = 110.12 \tag{4.32}$$

From this result, it can established that the resonance factor will not occur since the launch frequency is not a factor of the natural frequency, even though care should be taken since it is still close to become a factor.

Secondly the longitudinal condition is considered. The longitudinal condition is essentially the same as Equation 4.29 with the difference that the springs that were loaded axially initially are now loaded in bending and vice-versa.

The process then becomes the same as for the longitudinal case. After solving for the natural frequencies, they are listed in Table 4.36

Table 4.36: Eigenvalues for Lateral Vibrational Motion

Modes	**Longitudinal Natural Frequency** $[Hz]$
1	2957
2	6073.1
3	6073.1

For the longitudinal analysis, the frequency should be between 31 and 45 Hz. This requirement needs to be modified since it is actually impossible to be met. The natural frequencies will always be way too high due to the fact that the Young's Modulus is to high. In Section 5.7, the analytical values are verified

4.8.6 Structures Subsystem Compliance Matrix

In order to have a quick overview whether the requirements are all met, a compliance matrix was created which is shown by Table 4.37

[33] `http://www.brown.edu/Departments/Engineering/Courses/En4/Notes/vibrations_mdof/vibrations_mdof.htm` [22 June 2015]

Table 4.37: Structures Compliance Matrix

Requirements	Compliance
S08-GTC-V-04	✓
S08-GTC-M-04	✓
S08-GTC-S-04	✓
S08-GTC-S-05	✓
S08-GTC-S-07	✓
S08-GTC-S-08	✓
S08-GTC-S-09	✓
S08-GTC-S-10	✓
S08-GTC-S-11	✓
S08-MC-C-04	✓

All requirements are met. The structure volume comprises two buses with sizes of $10x10x30$ cm. The requirements in terms of dynamic load and vibrations are met. Since even the smallest debris will have a huge amount of energy when incoming from the opposite direction, the structure is not able at this point to sustain the impact of debris. It was not possible to combine the weight requirement with the debris requirement, which seemed to be a killer requirement at the end. The structure is able to accommodate all subsystems. The requirements in terms of cost and weight are met.

4.8.7 Structural Considerations for Payload Design

Now that it was proven that the satellite was design to operate in space, a few additional remarks need to be made in terms of payload design. Inside the whole structure, the payload is the most fragile object. When dealing with very high resolution, a few change in camera orientation can have big consequence. It is therefore important to make sure that the whole structure will not be impacted by the surroundings.

Supports
The payload is constructed as a system of interconnected mirrors need to be fixed to the outside frame. It is very important that these attachment need to be extremely solid as they should not be allowed any movement. The first mirror is made of aluminium and a "mushroom attachment" as shown in Figure 4.39. This is a very conventional fixing method that can be used in such a structure due to the flatness of the structure and has very high reliability.

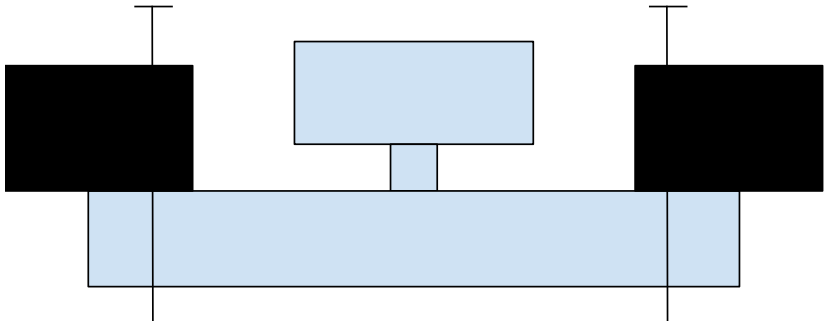

Figure 4.39: Mushroom fixed to external structure

The second mirror is more difficult to fix due to its concave shape. For that a GERB support is used that is then fixed to an upper attachment travelling with length across the structure. This GERB support has the advantage to be able to accommodate circular objects. Finally the glass lenses need to be taken into account. These represent the most important part due to their brittleness. A damped system is therefore needed since a rigid structure would immediately brake the mirrors.

Taking all that in consideration, an optical mount design for harsh environments is chosen. This support has the advantage to use springs as connectors therefore reducing the risk of damage. [62] Combining all supports and attaching all supports to a support skeleton, the payload is mostly assured to have no damage during launch and during its mission lifetime.

Reflectivity
Some considerations can also be made in terms of optics. The optic rays are very sensible to their surrounding environment. For that it is important to have any structural components far away as possible from the rays. This means that the outer shell is usually built in as far as possible from the optic rays. Moreover, in order to minimise reflectivity, all elements excluding the mirrors are covered with black coatings to reduce the capacity of a surface to absorb light.

4.9 Bearing

To increase the stability of the CubeSat moving components should be avoided. As this is not always possible bearings are used to connect moving components. A bearing is used simultaneously to provide support and reduce friction. In Subsection 4.9.1 different types of bearings will be presented. Afterwards the best solution will be presented and a more elaborated description of the chosen bearing will be given in Section 4.9.2. The bearing has to be integrated in the CubeSat, which is done in Section 4.9.3. The bearing section is concluded in Section 4.9.3 with recommendations for further design options.

4.9.1 Type of Bearings

Although traditional bearing technologies have been widely utilised in spacecraft design, they still come with friction, wear, lubrication and vibrational problems. Especially the vibrations can be a serious problem. This is why more research is done on contact-less bearings than air and magnetic bearings.

Traditional Bearings
Traditional roller bearings come in many different types designed for specific loads and functions. They consist of an inner and outer housing with the bearing balls in between, this is to reduce the friction. One thing they have in common is that vibrations are generated which will distort the image taken by the camera. There is also friction which is inefficient for energy efficiency. Wear of the bearing is off influence on the life time and reliability. Most roller bearings need lubrication but in a space environment this will cause additional problems like degassing. The advantages are that they are cheap, small and have a high stiffness.

Air Bearing
An air bearing is a contact-less bearing which has the advantages of less friction, no wear and no lubrication is needed. However, using an air bearing in space is complicated and not very efficient, since compressed air has to be taken on board, the size and mass of the CubeSat will increase drastically. If the air should be re-used the design will become complex.

Magnetic Bearing
A magnetic bearing is also a contact-less bearing with the same advantages as the air bearing like no wear, which will increase the lifetime. No lubricants are needed and the bearing is almost vibration free. Using a magnetic bearing in space does not introduce extra problems except that it becomes harder to use magnetometers to determine the satellites attitude. Because magnetic bearings seem a promising concept a further look will be taken into different kind of magnetic bearings like, passive magnetic bearing, PMB, active magnetic bearing, AMB, superconducting magnetic bearing and electrodynamic bearing, EB.

A PMB is a bearing which only uses permanent magnets to levitate the axis. The additional advantage is that the bearing design is simple because no power or control is needed. The main disadvantage when using a PMB is that according to Earnshaw's theorem it is only possible to achieve stability in two directions (most commonly the in-plane and radial directions of the bearing), which will give the need for a additional axial bearing to achieve axial stability. Also, the achieved stiffness and damping coefficient are low and cannot be easily increased without introducing energy losses. An

optimal design can be made by following the rules of Moser et al. [63].

An AMB can achieve levitation in both the radial and axial direction by using electromagnets in which current runs through coils made of conducting material. But a complex control system is needed to create stable levitation and the control system is not able to handle fast events. The system is also costly and larger than the other concepts.

A superconducting magnetic bearing can bypass Earnshaw's theorem by using field quenching. This term is used when a superconductor is cooled to its supercooled state in a magnetic field. The magnetic field is then stored in the superconductor and this causes a stabilising effect in axial and radial direction. The two main disadvantages are that the conductor has to be continuously cooled down to at least 130 K. And the quenching effect slowly deteriorates.

The electrodynamic bearing is the first bearing that can bypass Earnshaw's theorem using Eddy currents induced forces. The principle of the EB is explained in more detail in Section. 4.9.2. The main advantages are a almost negligible friction, simple design, vibration free and high performance. The disadvantage of the EB is that lifting forces are only generated when the rotor is spinning at high rpm and additional bearings are needed when the system is not spinning at a high rate.

Trade-Off Conclusion
After doing a trade-off between different bearing designs and a discussion with a expert in the field of magnetic bearings, T.C. van den Dool and S. Kuiper at Nederlandse Organisatie voor Toegepast Natuurwetenschappelijk Onderzoek, TNO, a conclusion was made that a magnetic bearing is the best choice to reduce the vibrations. PMBs where not a stable option and AMBs would be too large and complex to put in a CubeSat. EBs is the most promising concept if a design can be made to support the shaft when the system is rotating below 5000 rpm. In the next subsection a detailed description is given about the working of the EB and afterwards a implementation design is shown.

4.9.2 Electrodynamic Bearing

The electrodynamic bearing is a new magnetic bearing design developed by Magnetal. It is a simple passive bearing and according to ESA it has a high potential for use in space. The bearing is only offered in one size, the outer diameter is 42 mm, The inner diameter is 15 mm and the width is 17 mm. The components of the bearing can be seen in Figure 4.40. The bearing consists of at least two magnets which generate the magnetic flux that restrains movement in the axial direction. A iron washer is placed between the magnets to concentrate the magnetic flux and the end plates are used to avoid leakage of the magnetic flux. A conducting copper ring is attached to the rotor. In this rotor a magnetic field will be generated that provide radial stiffness. According to Lenz's law a current will be generated in a conducting material when there is a change in the magnetic flux. This can be achieved by moving or rotating a magnet over the conducting material. The generated current is called a Eddy current. This will result in a opposite magnetic field that can be seen as a virtual magnet that radially stabilises the rotor. This can be seen in Figure 4.41. Mind that here a outer bearing (rotor outside the magnet) is shown instead of an inner bearing but the principle stays the same. The minimal rounds per minute, rpm, that need to be achieved so that the repositioning forces can be induces correctly is 5000 rpm. [64]. To have some safety range and to counteract drag of the wheel during the mission lifetime the wheel will be spinning at 7000 rpm.

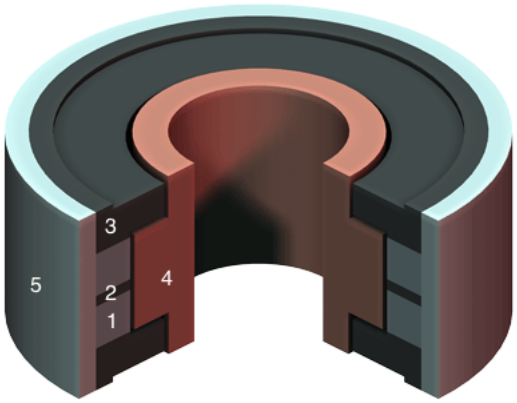

Figure 4.40: Electrodynamic bearing overview; 1 = Magnet, 2 = Iron pole, 3 = End plate, 4 = Conducting rotor, 5 = Housing[34]

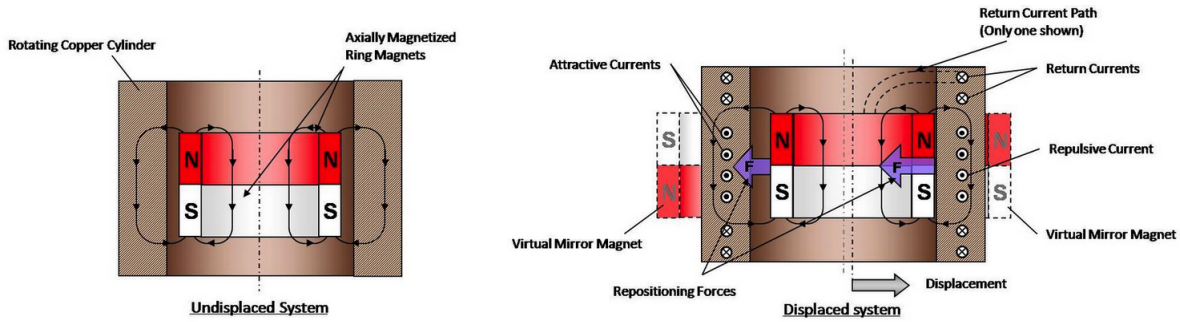

Figure 4.41: Radial stability principle using Eddy currents[34]

Now that the principle behind the EB is known, an analysis is done on the forces acting in the bearing. After detaching the ball bearing as described in the next subsection the satellite consist of two components, the wheel and others, which are not physically connected anymore. The displacement of the shaft in the bearing then becomes a function of the disturbance forces acting on the two components. As mentioned in Section 3.2 the aerodynamic disturbance is by far the highest disturbance in the flight direction and others can be neglected in calculating the forces working in the EB. The relative force working on the bearing is the difference between the aerodynamic drag off the two components. Which is highest at the lowest orbit, at 230 km the wheels drag is 130 mN and the CubeSat's drag is 11 mN. The relative force working in one bearing is than 119 mN. This relative force is shown in Figure 4.42 as F and can be divided in a restoring force, F_R, which is in the same direction as the displacement $\triangle r$ and a tangential force, F_T. θ, The force angle defines which force is larger and is defined in Equation 4.33 where R is the resistance, ω is the rotational speed and L the inductance. θ is plotted versus rotational speed (rpm) in Figure 4.43. For a rpm of 7000 the force angle is 78°. This implies that the displacement of the rotor is almost perpendicular to the applied load on the bearing.

[34] `http://http://www.magnetal.com/products/products.htm` [cited 9 June 2015]

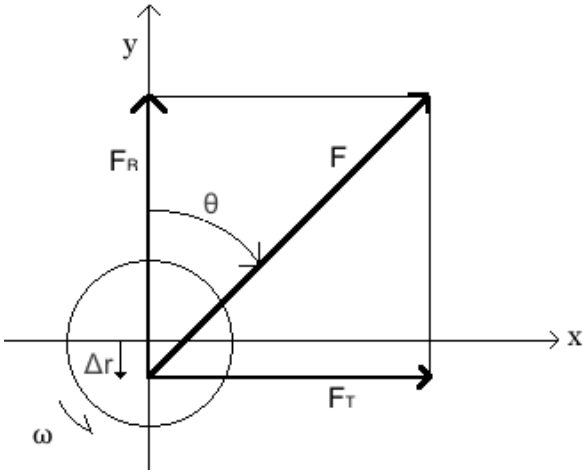

Figure 4.42: Forces working in a electrodynamic bearing

$$\theta = arctan\frac{R}{\omega L} \tag{4.33}$$

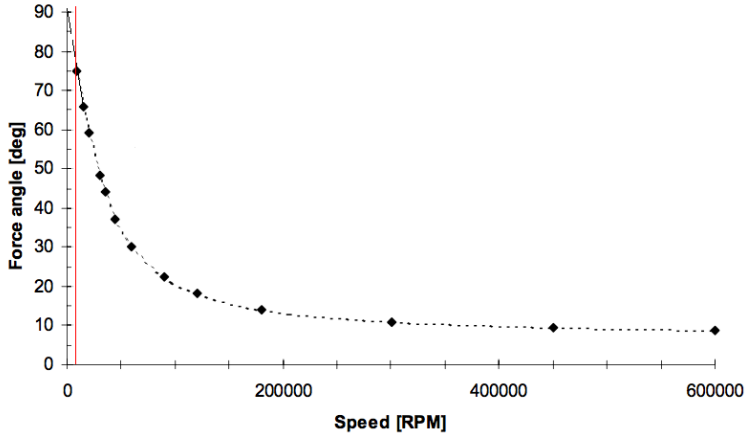

Figure 4.43: Force Angle vs. Rotational Speed [64]

The stiffness of a EB can be specified by three different stiffnesses. The in-plane stiffness, K, is responsible of the load bearing capability. The rotor dynamic stiffness, k, is responsible for the natural frequencies of the bearing. The cross coupling stiffness, K_c, plays a role in the stability. The stiffnesses are expressed in Equations 4.34 to 4.36 [64]. These are plotted versus rotational speed in Figure 4.44. For 7000 rpm one can see that K & k_c are 7 N/mm and k is 1 N/mm. From Equation 4.34, one can calculate that the maximum deflection of the rotor is equal to 0.0017 mm, which is lower than the actual gap of 0.5 mm between the rotor and stator.

The friction of the EB, also known as the brake torque, is dependent on the displacement, when the displacement is zero there will be no losses. The brake torque is also dependent on the restoring force and the dependence is shown in Equation 4.37. The brake torque will change from a minimum of $6 \cdot 10^{-5}$ Nmm at 350 km to $2 \cdot 10^{-4}$ Nmm at 230 km. As this friction is a order of magnitude lower than the aerodynamic disturbances as calculated in Section 3.2.2, this can be counteracted by the ADCS system. The friction decay is of exponential order and can be assumed to have a average value of $1 \cdot 10^{-4}$ Nmm. The time to decelerate the wheel from 7000 rpm to 5000 rpm is equal to the change in angular momentum divided by the average torque. Which is shown in Equation 4.38 and is equal to 223 days. This is longer than the mission life of 200 days.

$$K = -\frac{dF}{d \triangle r} \tag{4.34}$$

$$k = -\frac{dF_R}{d\triangle r} = -\frac{dF}{d\triangle r} cos\ \theta = K\ cos\ \theta \tag{4.35}$$

$$k_c = -\frac{dF_T}{d\triangle r} = -\frac{dF}{d\triangle r} sin\ \theta = K\ sin\ \theta \tag{4.36}$$

$$M_z = \triangle r \cdot F_r = \triangle r \cdot F\ sin\ \theta \tag{4.37}$$

$$\triangle L/\tau = \frac{I(\omega_2 - \omega_1)}{\tau} \tag{4.38}$$

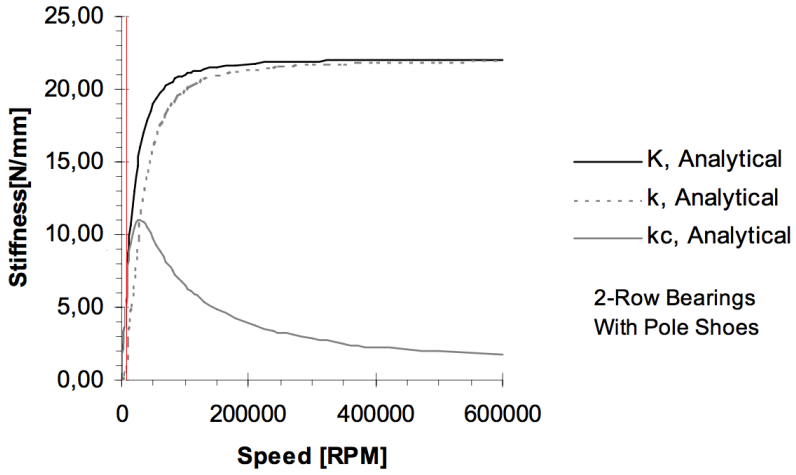

Figure 4.44: Electrodynamic bearing stiffnesses: K = in plane stiffness, k = rotordynamic stiffness, k_c = cross coupling stiffness [64]

There are also three damping coefficients: the in-plane damping, C, the rotordynamic damping, c and the cross coupling damping, c_c. The definitions are given in Equations 4.39 to 4.41 respectively [64]. and the coefficients are plotted versus rotational speed in Figure 4.45. From this figure one can see that the damping coefficient C and c are equal to 7.5 Ns/mm and $c_c = 2.2\ Ns/mm$.

$$C = \frac{K}{\omega} \tag{4.39}$$

$$c = \frac{K}{\omega} sin\ \theta \tag{4.40}$$

$$c_c = \frac{K}{\omega} cos\ \theta \tag{4.41}$$

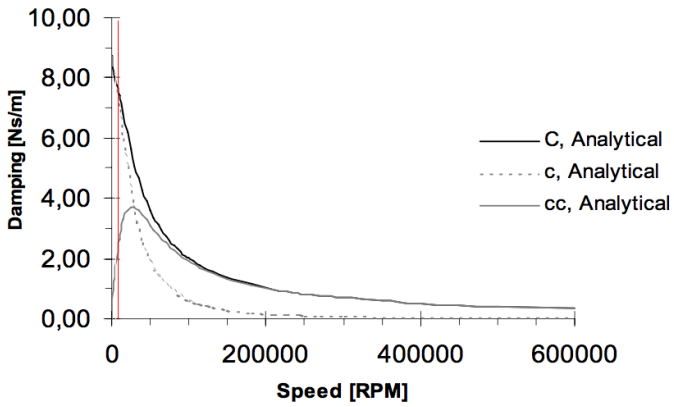

Figure 4.45: Electrodynamic bearing damping coefficients: C = in plane damping, c = rotordynamic damping, c_c = cross coupling damping [64]

Rotordynamics
The natural frequency of a rotating wheel has at least two modes. The first vibrational mode of the magnetic bearing is related to in plane movement and assuming a rigid shaft and two identical bearings the first critical speed ω_1 is given in Equation 4.42 and is equal to 70 rad/s. This mode is also called the cylindrical mode because of the volume the motion encloses. The second mode is related to a conical vibration and is dependent on the mass moment of inertia [65]. The higher the mass moment of inertia, the lower the critical speed. A specific formula cannot be given because of the complexity of this calculation. The momentum wheel spins at a rate of $7000 \cdot 2 \cdot \pi/60 = 733\ rad/s$ which is not close to the first mode.

$$\omega_1 = \sqrt{\frac{2k}{m}} \tag{4.42}$$

Equations of Motion
Now that the stiffnesses and vibrations are known, the equations of motion, EoM, for the rotor can be set up and are given in Equation 4.43 [64]. The disturbance forces are neglected because they will not influence the eigen frequencies of the system. Substituting Equations 4.35, 4.36, 4.40 and 4.41 into the EoM will reduce the EoM to Equation 4.44.

$$\begin{aligned} m\ddot{x} &= -kx - c\dot{x} - k_c y + c_c \dot{y} + F_{dx}(t) \\ m\ddot{y} &= k_c x - c_c \dot{x} - ky - c\dot{y} + F_{dy}(t) \end{aligned} \tag{4.43}$$

$$\begin{aligned} m\ddot{x} &= (-K\ cos(\theta))x + (-\frac{K}{\omega}\ sin(\theta))\dot{x} + (-K\ sin(\theta))y + (\frac{K}{\omega}\ cos(\theta))\dot{y} \\ m\ddot{y} &= (K\ sin(\theta))x + (-\frac{K}{\omega}\ cos(\theta))\dot{x} + (-K\ cos(\theta))y + (-\frac{K}{\omega}\ sin(\theta))\dot{y} \end{aligned} \tag{4.44}$$

Introducing the new variable z as given in Equation 4.45 the EoM can be written in vector notation which is done in Equation 4.46. This equations is of the form as shown in Equation 4.47. Multiplying Equation 4.47 by M^{-1} gives Equation 4.48.

$$\boldsymbol{z} = \begin{bmatrix} x \\ y \end{bmatrix}, \qquad \dot{\boldsymbol{z}} = \begin{bmatrix} \dot{x} \\ \dot{y} \end{bmatrix}, \qquad \ddot{\boldsymbol{z}} = \begin{bmatrix} \ddot{x} \\ \ddot{y} \end{bmatrix} \tag{4.45}$$

$$\begin{bmatrix} m & 0 \\ 0 & m \end{bmatrix} \ddot{\boldsymbol{z}} = \begin{bmatrix} -Kcos(\theta) & -Ksin(\theta) \\ Ksin(\theta) & -Kcos(\theta) \end{bmatrix} \boldsymbol{z} + \begin{bmatrix} -\frac{K}{\omega}sin(\theta) & \frac{K}{\omega}cos(\theta) \\ -\frac{K}{\omega}cos(\theta) & -\frac{K}{\omega}sin(\theta) \end{bmatrix} \dot{\boldsymbol{z}} \tag{4.46}$$

$$M\ddot{\boldsymbol{z}} + C\dot{\boldsymbol{z}} + K\boldsymbol{z} = \boldsymbol{0} \tag{4.47}$$

$$\ddot{\boldsymbol{z}} + M^{-1}C\dot{\boldsymbol{z}} + M^{-1}K\boldsymbol{z} = \boldsymbol{0} \tag{4.48}$$

Natural Frequencies
For a damped system of the above form the undamped natural frequency, ω_n and the modal damping ratio, ζ can be calculated by rewriting the equation in state space form. First the vectors are defined as $\boldsymbol{q_1} = \boldsymbol{z}$ and $\boldsymbol{q_2} = \dot{\boldsymbol{z}}$. Then differentiating these two vectors gives Equation 4.49.

$$\begin{aligned} \dot{\boldsymbol{q}}_{\boldsymbol{1}} &= \dot{\boldsymbol{z}} = \boldsymbol{q_2} \\ \dot{\boldsymbol{q}}_{\boldsymbol{2}} &= \ddot{\boldsymbol{z}} = -M^{-1}K\boldsymbol{z} - M^{-1}C\dot{\boldsymbol{z}} \end{aligned} \tag{4.49}$$

By substituting $\boldsymbol{z} = \boldsymbol{q_1}$ and $\dot{\boldsymbol{z}} = \boldsymbol{q_1}$ in Equation 4.49. The equation can be rewritten into state space form and is given in Equation 4.50.

$$\boldsymbol{q} = \begin{bmatrix} \dot{\boldsymbol{q}}_{\boldsymbol{1}} \\ \dot{\boldsymbol{q}}_{\boldsymbol{2}} \end{bmatrix} = \begin{bmatrix} 0 & I \\ -M^{-1}K & -M^{-1}C \end{bmatrix} \begin{bmatrix} \boldsymbol{q_1} \\ \boldsymbol{q_2} \end{bmatrix} = A\boldsymbol{q} \tag{4.50}$$

Now that the state matrix, A, is known it is not a complicated task to find the eigenvalues, λ, using $Matlab$. The eigenvectors and eigenvalues are found using the command $[V, D] = eig(A)$. The eigenvalues are complex but the natural frequency, ω_n, and modal damping ratio, ζ are found by using Equation 4.51 and 4.52 [66].

$$\omega_i = \sqrt{Re(\lambda_i)^2 + Im(\lambda_i)^2} \tag{4.51}$$

$$\zeta_i = \frac{Re(\lambda_i)}{\sqrt{Re(\lambda_i)^2 + Im(\lambda_i)^2}} \tag{4.52}$$

The damped natural frequencies are calculated and the undamped natural frequency can be found by replacing the C matrix with a zero matrix. The natural frequencies and damping ratios are given in Table 4.38.

Table 4.38: Natural frequencies and damping ratio of the EB system

$\boldsymbol{\omega_n}$ $[\boldsymbol{Hz}]$	$\boldsymbol{\omega_d}$ $[\boldsymbol{Hz}]$	$\boldsymbol{\zeta}$
33.9	26.5	0.64
33.9	26.5	0.64
33.9	26.2	-0.62
33.9	26.2	-0.62

The eigenfrequencies of the bearing can be seen as a forcing function on the satellite and they should not be the same or a multiple of the eigenfrequencies of the satellite. The eigenfrequencies in Table 4.38 are compared with the eigenfrequencies calculated by the Finite Element Method, FEM, given in Table 5.6 and 5.7. The eigenfrequencies of the bearing are not a multiple of the satellite and no additions have to be added to the satellite.

4.9.3 Bearing Integration

Now that the characteristics of the EB are known, a design has to be made for the implementation of the EB. Since the EB does not support the rotor when the wheel is not spinning additional traditional bearings are needed to provide support during initialisation of the spin and also during launch and detumbling. A system should be designed that can switch between the ball bearing and the EB when the wheel is spinning at 7000 rpm. A trade-off has been made between an active actuator and a passive method based on springs. Although both methods are challenging solutions the passive method is the best solution because the bearing system can be made smaller and no power systems are needed.

A cross section of the complete bearing system can be seen in Figure 4.46. In Figure 4.46-B and 4.46-C, two additional cross sections are shown which are indicated in Figure 4.46-A. The system consist of a hollow shaft through which power and data lines are drawn (not shown) that connect the bus with the payload. Onto the shaft the conducting rotor of the EB is placed. The magnetic part of the EB is fitted in the housing. Two ball bearings are placed on linear guides to ensure a pure translational motion. To the outer housing of the ball bearing, compressed springs are attached which will slide the bearings from the shaft when the block masses are moved away from its original position as shown. The shaft is not completely round but has a little protrusion so that the bearing does not have to be

a tied fix and can be pushed off by the springs. The block masses are also connected to linear guides and springs which will compress when the wheel is accelerated. In Figure 4.47 the configuration of the bearing when spinning at 7000 rpm can be seen. The required stiffness of the block mass springs is calculated by setting the radial velocity, v_r, to zero in Equation 4.53 and rewrite the equation for k, which is done in Equation 4.54. The radial distance r should be 18 mm for free movement of the bearing. r_0 is initial radial distance of the block which is 14 mm. The mass of the block, m, is equal to 11 $gram$ when using stainless steel. From this it follows that the total spring stiffness should be 3344 N/mm and using 8 springs for every block as drawn in Figure 4.46 would give a spring stiffness of $418N/mm$.

$$v_r = \sqrt{(\omega^2 - \frac{k}{m})(r^2 - r_0^2) + \frac{2k}{m} r_0(r - r_0)} \tag{4.53}$$

$$k = \frac{-mr_0^2\omega^2 + mr\omega^2}{(r_0 - r)^2} \tag{4.54}$$

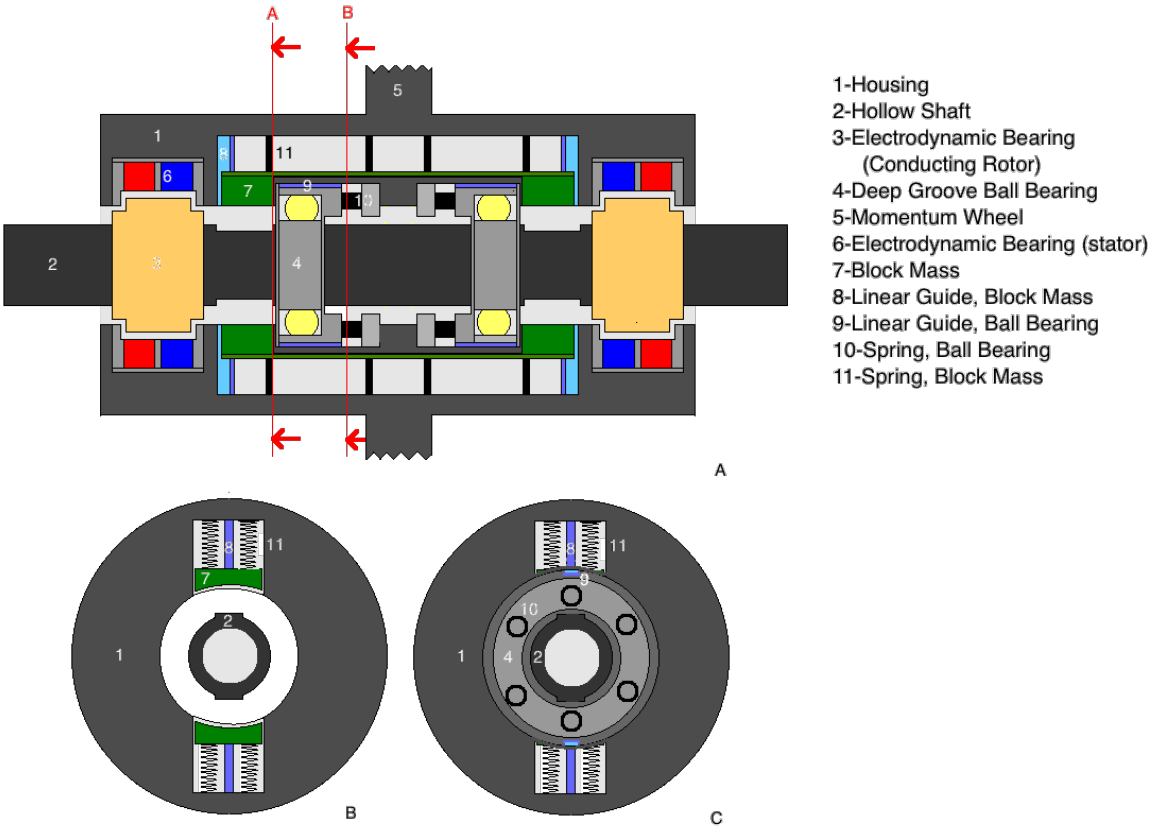

Figure 4.46: A) Cross section of bearing system. B) cross section A, block spring. C) cross section B, ball bearing.

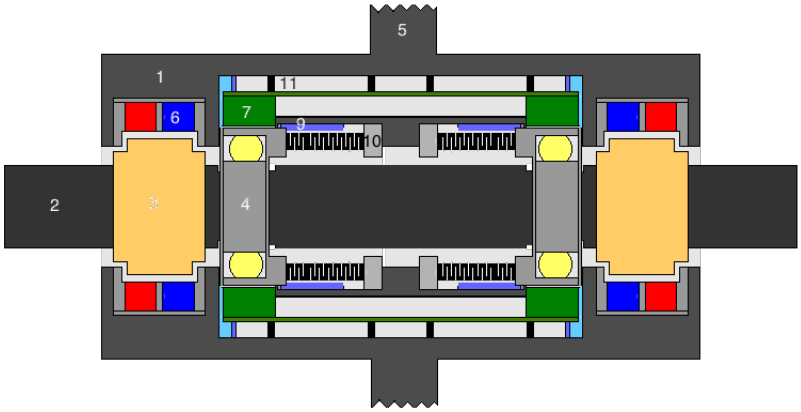

Figure 4.47: Cross section of the bearing system spinning at 7000 rpm

Conclusion
The EB design has important benefits above using traditional ball bearings. Firstly, the friction is almost zero and the disturbances in both the wheel and CubeSats are damped out in the bearing.

For future projects that are related to this bearing design, some recommendations can be made. Firstly, EB will be available in different sizes in the near future and these can considerably reduce the size of the bearing system. Secondly the brake torque can be significantly reduced by placing additional passive magnetic bearing that introduces an offset of the rotor that is as large as the average offset introduced by the disturbances. Third, damper can be placed on the satellite to reduce the vibrations induced by the EB. Lastly, the springs can be replaced by a homogeneous elastic material that will increase the reliability of the system.

4.10 Dampers

Due to the rotational motion of the momentum wheel of the dual-spin CubeSat, nutation is induced. In order to get rid of the nutation, it has to be damped out. Different dampers can be used, but liquid dampers have been used before and are proven successful [67].

The dampers work in the following manner: the fluid has a viscosity and a surface tension such that it damps out certain nutation frequencies under the circumstances that it is free to flow. The dimensions of the damper and the temperature of the liquid determine the efficiency of the damper and the nutation frequency which will be damped out. The damper consists of a long tube containing the liquid and two end-pots in order to give the liquid some space to flow. Figure 4.48 shows the layout of such a damper.

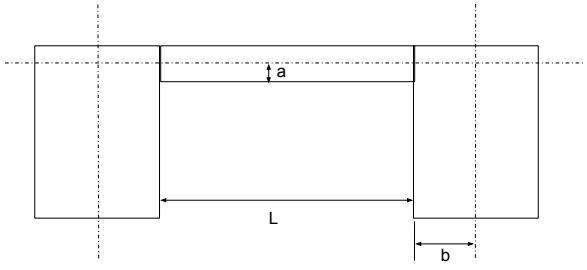

Figure 4.48: Design of a Liquid Damper

In this picture, L is the distance between the two end-pots, a is the radius of the tube containing the liquid and b is the radius of the end-pot.

Based on a program written by Dr. ir. J.M. Kuiper, the dampers are sized as can be seen in Table 4.39.

a	1.5 mm
b	2.5 mm
L	20.0 mm
R_o	28.9 mm

Table 4.39: Damper Sizing

In this table, R_o is the distance from the tube to the centre of the momentum wheel. a, b and L are chosen such that the damper fits in the momentum wheel. The distance R_o is chosen in order to have an optimal design. When the damper is placed farther away from the centre, on the one hand it becomes more efficient because the damping force works over a longer arm. However, on the other hand, the centrifugal forces in the damper get higher, so the liquid has a lower ability to move freely through the tank and the end-pot.

The program calculates the spin rate using Equation 4.55.

$$\omega_0 = \frac{a}{b} \cdot \omega \cdot \sqrt{\frac{2R_o}{L}} \tag{4.55}$$

In this equation, ω_0 is the spin rate of the momentum wheel. The damping strength is plotted against the nutation frequency over the spin rate in Figure 4.49.

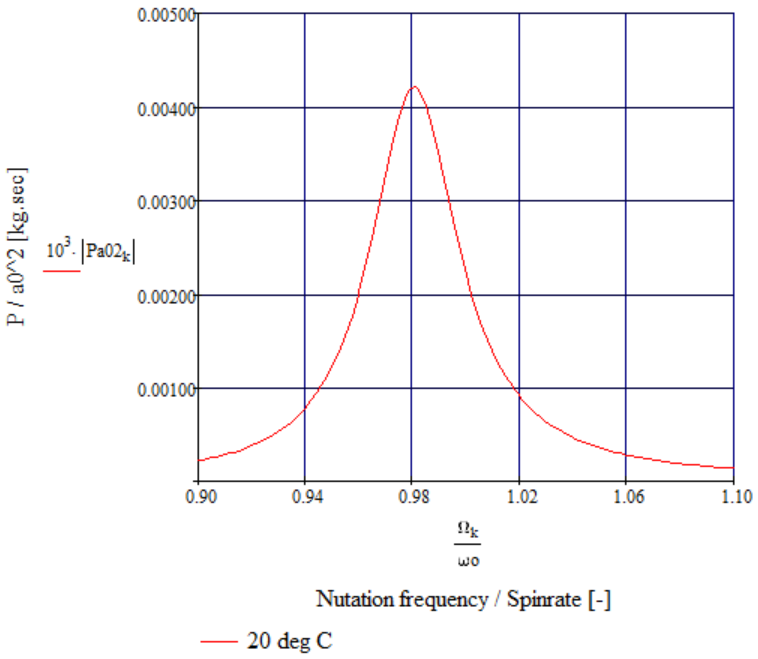

Figure 4.49: Plot of the damping force versus the Nutation frequency over the spin rate

As can be seen, there is only one peak in this graph, so only the nutation is damped. As a recommendation, other dampers could be used in order to also damp the eigenfrequencies of the bearing. The exponential damping time constant τ is 29.7 *minutes* according to Equation 4.56, which means that 99% of the nutation will be damped out within one orbit.

$$\tau = \frac{Iz}{R_o^2 \cdot \Omega_{1200}} \cdot (2 \cdot |Pa02_{1200}|)^{-1} \tag{4.56}$$

The full equations can be found in the program made by Dr. ir. J.M. Kuiper.

Chapter 5

Post-Design

This chapter is devoted to the mission's post-design. It consists out of eight chapters. Firstly, a Budget Analysis is been presented. Secondly, the Cost Analysis and Estimation is elaborated on. In the third section the Reliability, Availability, Maintainability and Safety, RAMS, is explained. The fourth and fifth chapter are devoted to the Sensitivity Analysis and Project Design & Development Logic respectively. Sixthly, the project Gantt Chart is presented. In the final two sections Verification & Validation and the recommendations are explained.

5.1 Budget Analysis

After the final design was elaborated, the budgets needs to be analysed. To ensure that the final design will stay within the intended target budget, a contingency was introduced for each main budget. The contingency matrix can be seen in Table 5.1.

Table 5.1: Contingency allocation for each project phase

	Contingency [%]			
	Mass	**Volume**	**Cost**	**Power**
Draft Phase	20	15	20	15
Conceptual Phase	15	10	15	10
End of DSE	5	5	10	5

After the design phase of this project is finished, the final budgets and performance parameters should be analysed to ensure that the contingency ensures that further development will still meet the target values assigned to that satellite. For this purpose, four different values were analysed for each design phase. These values are the specified, the target, the current and the actual value. The specified value represents the maximum value possible for each design phase and therefore includes the contingency for each phase. The target value represent the assigned value without contingency. The current value is the value of the design at that moment including contingency and the actual value represents the value of the design without contingency.

Firstly, the mass is going to be analysed. At an early stage the design mass was lower than the assigned value. However, the mass drastically increased after the encountered drag was correctly calculated and the propulsion system needed to increase the required propellant to increase the mission life. After this, it was realised that this design is not feasible with heavy propellant and therefore, the payload design was improved to increase the orbital altitude. This, in turn, resulted in a design without propulsion used for orbital maintenance. However, the design mass of the payload also increased. After some further improvements of the whole design, the actual and the current value are both below the target value which results in a promising starting point for further development. The mass analysis can be seen in Figure 5.1.

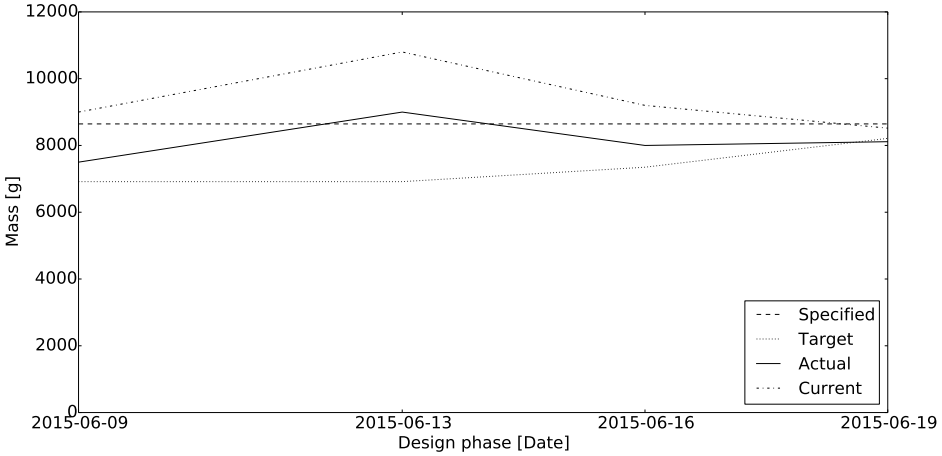

Figure 5.1: Budget analysis for the mass of the satellite

The estimated volume turned out to be smaller at the beginning since the payload design was significantly different. After it was decided that a different payload is going to be used, the volume also increased. However, it was increases over the targeted value. After some further improvements, the actual and current volume can be considered to be below the specified and target volume. This again, is promising for further development. The volume analysis can be seen in Figure 5.2.

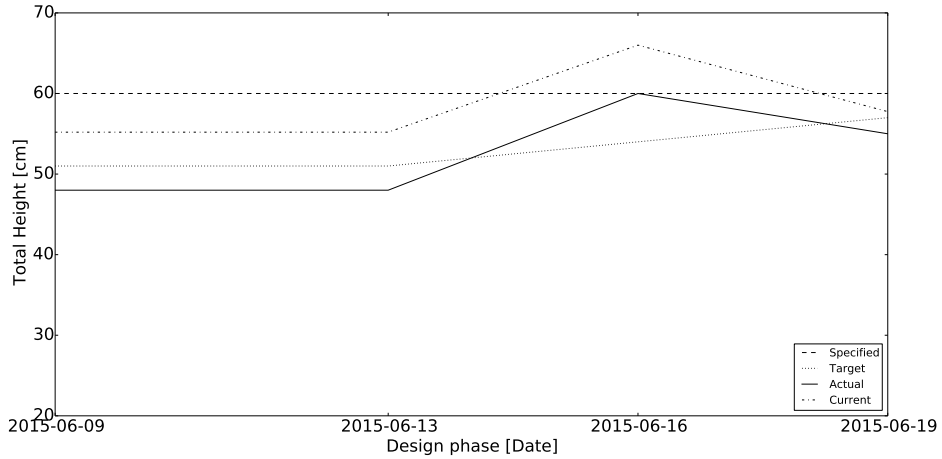

Figure 5.2: Budget analysis for the volume of the satellite; 10x10xTotalHeight *cm*

The cost budget of the whole satellite was expected to be low in the beginning of the design phase. However, as the number of design iterations grew, an increase in propellant mass due to the momentum wheel propulsion system, increased the cost significantly. Here, it is important to notice that the camera design was still assumed to be below € 100,000. The cost analysis can be seen in Figure 5.3. This time, only the actual cost are within the threshold of the specified value. Therefore, further improvement in development should be taken into account. However, as it is analysed in Section 5.2, the total unit cost is below € 500,000. Therefore, a further improvement can be neglected at this stage since, for this analysis, € 400,000 was taken as a specified value.

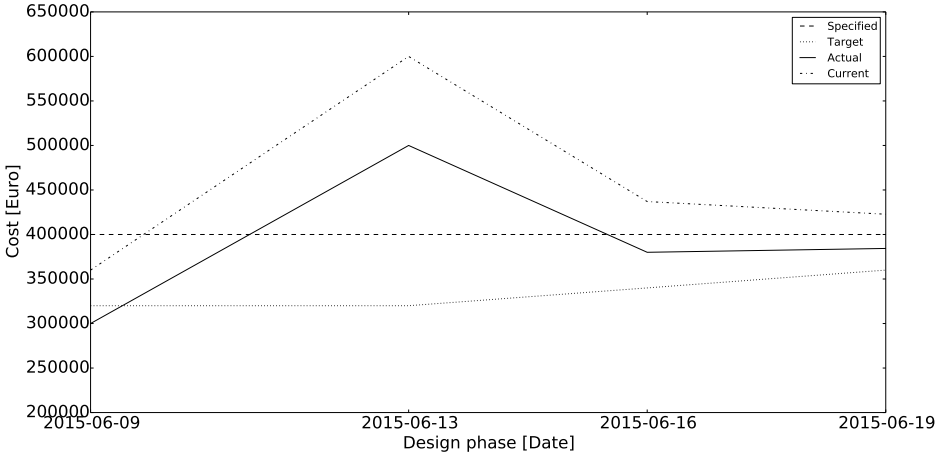

Figure 5.3: Budget analysis for the cost of the satellite

The last budget which was analysed is the power. Here, it is important to notice that not the total power consumption was used since it highly varies over time. Instead, the peak power allowed for the satellite was analysed. The specified value was selected to be 21 W after a first estimation. At the beginning the value is below the limit but with the change in propulsion, the peak power changes drastically and is at this stage considerable. After the propulsion was dropped for orbital maintenance, the peak power decreased again but the power consumption of the payload was doubled. In a final stage, the power consumption of the ADCS needed to be increase to still meet all requirements which resulted in a small increase in the peak power consumption. Finally, both current and actual peak power consumption is below the specified and target peak power consumption and therefore creates a good base for further development. The peak power analysis can be seen in Figure 5.4.

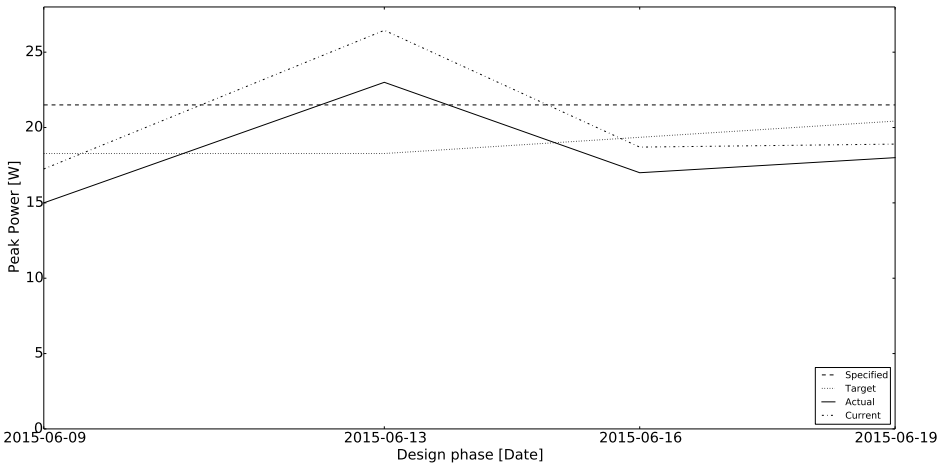

Figure 5.4: Budget analysis for the power of the satellite

5.2 Cost Analysis and Estimation

The main goal of this design project was to create a competitive design which will meet the market needs as described in Section 2.1. Therefore, it is important to provide a realistic cost estimation for further investments. This section will provide this analysis and will calculate the final price of a single unit of one SHAPE. satellite. For this analysis, it is assumed that multiple units of this satellite will be produced since it is designed to operate in a constellation. It is considered that a total number of 100 units will be sold which is comparable with other constellations from other companies like Planet Labs[1]. In general, it is possible to divide all existing costs into two main categories: non-recurring and recurring costs. Non-recurring costs are ones which needs to be invested to be able to start the production of the satellite and recurring cost are ones which needs to be invested to be able to produce a single unit. Therefore, this division will be used in this analysis. A summary of all recurring and

[1]Presentation by: C. Boshuizen, *The Planet Labs Earth-Imaging Constellation*, 8th International Workshop on Satellite Constellations and Formation Flying, 8 June 2015

non-recurring costs can be seen in the Cost Breakdown Structure given in Figure 5.5 and will be further elaborated in Section 5.2.1 and 5.2.2.

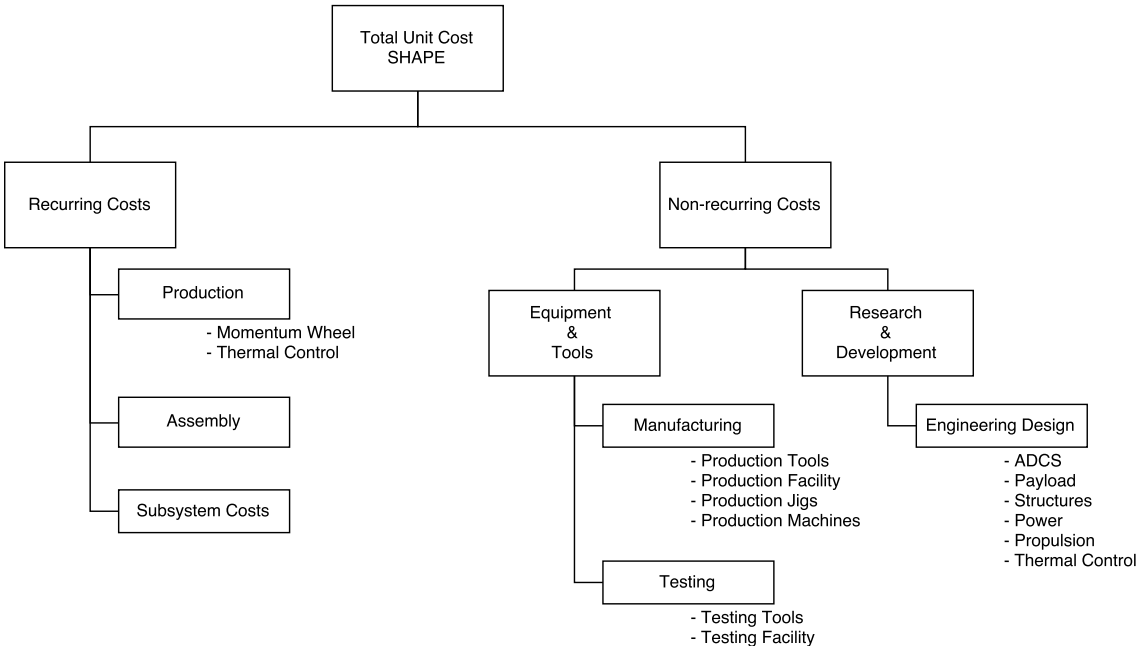

Figure 5.5: The Cost Breakdown Structure for SHAPE.

5.2.1 Non-Recurring Cost

As already described, non-recurring costs are investments which needs to be done to start the production of SHAPE. Therefore, all these cost will be added up and then will be divided over all produced units. This cost consists out of further research and development cost as well as tool and production facility costs.

Research and Development
The design of this satellite is a very promising design and therefore further research and development should be done to optimise the whole design. Since the development process at this stage is rather limited, it should therefore be continued. In the scope of this design synthesis a total of $2,808$ *hours* were used to develop the design up to this stage if nine engineers working eight hours a day. If it is now assumed that the development is 10% finished, a total development time of $28,080$ *hours* needed can be assumed. If a hourly cost of € 75.00 is assumed including facility costs, a total research and development cost can be approximated to be € $2,106,000$.

Equipment and Tools
Every unit needs to be manufactured, assembled and tested. To be able to execute this task, additional tools and equipment are required. This mainly consist out of manufacturing tools, like machines, as well as assembly tools like screwdrivers, manufacturing jigs and similar tools. Since every unit needs to be extensively tested, additional tools are required for this as well. The production and testing of the satellite needs special facilities which either needs to be built or rented. These costs are also taken into account here. For this satellite design, a total tool and equipment costs of € $500,000$ are assumed.

5.2.2 Recurring Cost

As previously described, recurring costs are costs needed to produce every single satellite. This mainly consists out of the different system costs, the manufacturing costs, the assembly costs and the testing costs.

System Part Cost
Every subsystem in this satellite design consists mainly out of already existing components which need to be purchased and in a later stage assembled. Only the momentum wheel needs to be manufactured separately. A summary of all subsystem costs can be seen in Table 5.2

Table 5.2: The total costs of each subsystem

Subsystem	**Costs [€]**
Payload	100,000
ADCS	85,000
Structures	20,000
Bearing	10,000
TT&C	30,000
C&D	10,000
Propulsion	60,000
Power	64,300
Cabling	1,000
Thermal Control	4,025
Total	384,325

From this table it can be concluded that the total part costs is € 384,325. It is important to notice that the material costs for the momentum wheel are included in the costs of the structures subsystem.

Manufacturing
For this design, only the momentum wheel and the thermal subsystem needs to manufactured. The momentum wheel is considered to be produced in five days with eight hours working time each day. This results in 40 *hours* production time of the momentum wheel. If € 50 is assumed per hour of active production, a total production cost for the momentum wheel can be concluded to be € 2,000. The thermal subsystem mainly needs to be attached to the structure of the satellite. Here again, five total working days are assumed to fulfil this manufacturing process. Since this work requires a high precision as well as special trained personal, a total hour cost of € 65 is assumed which result in a total manufacturing cost of € 2,600 for the thermal subsystem. Resulting form this calculations a total manufacturing cost of € 4,600 can be concluded.

Assembly
After all parts of the satellite are purchased or manufactured, the satellite needs to be assembled before it can be soled. The total cost to assemble the satellite is mainly driven by the time spent during assembly. This amount of hours changes drastically over time since an effect of learning occurs with an increase of produced units. This shortens the time spend to assemble the satellite drastically [68]. This effect can be calculated by using the learning curve for production applications. This curve can be calculated using Equation 5.1.

$$t_a = \frac{t_f \cdot n_a^{\log(x)}}{n_a} \tag{5.1}$$

In this equation t_a is the average time needed to assemble one unit, t_f is the time needed to assemble the first unit, which in this case, is the prototype, n_a is the number of units assembled and x is the learning factor. For this satellite it was decided that the first assembling time is considered to be 80 days and the learning factor is considered to be 2.1 which is a good estimate for aerospace application [68]. The learning curve for assembling a total unit ranging from one to 100 units can be seen in Figure 5.6.

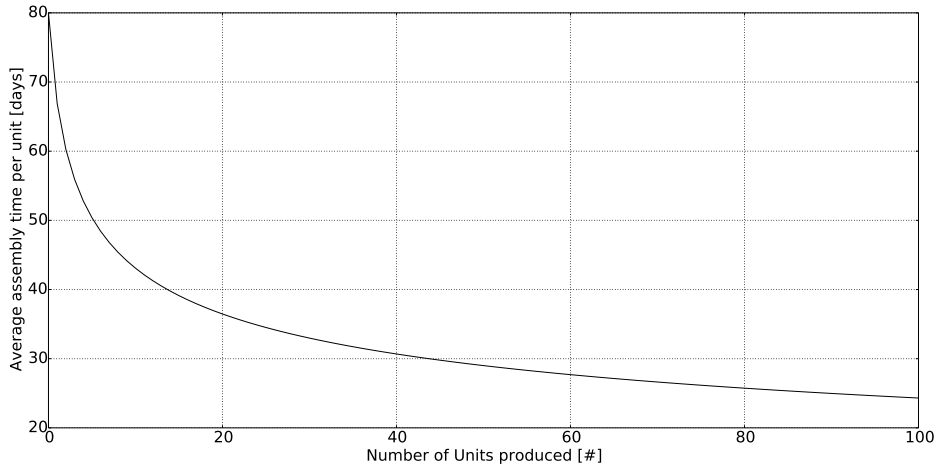

Figure 5.6: The assembly time related to the amount of produced units

If eight hour working day is considered with an assembling cost of 60.00 €/h, a total assembling cost varying from € $38400 - 11,700.54$ can be assumed as an average for the satellite assembling.

Testing
In a final step of the production of one unit, each satellite needs to be tested before it can be launched and operated in its mission. Therefore, it was decided that a total amount of 30 days is required to fully test the whole satellite and to perform small modifications. If a € 60 per hour cost is taken for this procedure, a total testing cost for each satellite of € $18,000$ can be concluded [69].

5.2.3 Final Cost Analysis

Finally, the total unit cost should be calculated. Since the unit cost mainly depends on the amount of unit produced, a cost analysis should be done for a production of $1 - 100$ units. This analysis can be seen in Figure 5.7.

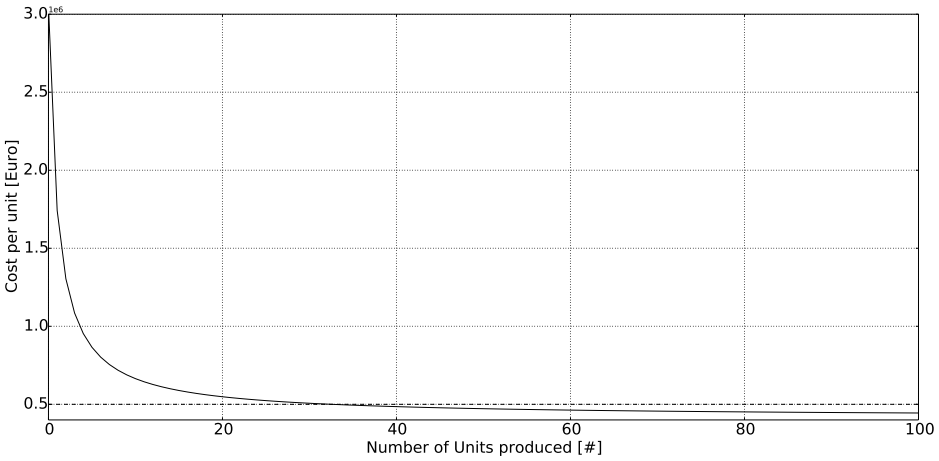

Figure 5.7: The average unit cost related to the amount of units produced

In this figure it can be easily seen that if only a single unit is produced, a average unit cost of around € $300,0000$ can be concluded. If more units are produced, the average unit costs drastically reduce. It can also be observed that at least 34 units should be produced and sold to reach an average unit cost lower than € $500,000$. If it is now assumed that a total number of 100 units is produced, the average unit costs can be concluded as can be seen in Table 5.3.

Table 5.3: Average unit cost per unit if 100 units are produced

Cost factor	Cost [€]
Non-recurring Cost:	-
Research and Development	2,106,000.00
Equipment and Tools	500,000.00
Total non-recurring cost per unit	26,060.00
Recurring Cost:	-
System part costs	384,325.00
Manufacturing	4,600.00
Assembly	11,700.54
Testing	18,000.00
Total recurring cost per unit	418,625.54
Total unit cost	444,685.54

From this analysis it can be concluded the the final unit cost per satellite is € 444685.54 if 100 satellites are produced. It can be concluded from this that the total unit cost is below € 500,000 as it was required.

5.3 RAMS

This section will reflect on reliability, availability, maintainability and the safety of this CubeSat by looking at similar satellites. The CubeSat does not need to be maintained so that part of the RAMS will not be presented within this report.

5.3.1 Reliability

Most of the CubeSats have been launched into a Low Earth Orbit or higher. However, for this mission, the satellite will be in Very Low Earth Orbit, where a complex airflow is present. Therefore, it is hard to predict the reliability of the satellite in such a new environment for the CubeSats [22].

However, it is possible to consider the reliability of each subsystem as an Equation 5.2, where λ is the failure rate and t is the operating time.

$$R = e^{-\lambda t} \tag{5.2}$$

Furthermore, it should be noted that not every subsystem is equal in importance. The ADCS and the payload are the most crucial aspects towards the mission goal since the CubeSat can not operate when only half of these subsystems can be used. Therefore, the reliability of these components should be ensured before the customer can be reassured.

Redundancy
Redundancy is the use of extra components to decrease the risk of the mission failing if one component fails. This is a simple task to accomplish with a CubeSat since components are cheap and small. Redundancy can be applied to the ADCS by using extra sensors or actuators, so that a redundant one is always available in case of failure. Also to the solar panels, a redundancy can be applied in order to provide enough power for the whole lifetime of the CubeSat, accounting for degradation of the solar panels.

For the payload, redundancy will be hard to accomplish, since the camera uses three unit cubes. Hence, it is impossible to add an extra camera.

Redundancy should be applied to the other subsystems too, however the above mentioned are the most crucial.

Testing
As mentioned in Section 2.4, each subsystem, including the structure, will undergo a variety of tests. These are done to ensure reliability of the products that were bought. With the final test, the Vehicle System Test, the CubeSat will be checked for failure one last time. All these tests do ensure that the

satellite will be reliable enough for the mission.

Reliability-Related Design Analysis
This section considers a variety of analysis approaches that are commonly performed on spacecraft, that could apply for the CubeSat [22].

- **Sneak Circuit Analysis** is an analysis which searches for unwanted and unexpected current flows
- **Worst Case Analysis** check whether system will continue if all subsystems are at their worst performance
- **Thermal Analysis** analyses the temperature at different points of the CubeSat since failure rates are a function of temperature
- **Electromagnetic Interference Analysis** checks for electromagnetic interference throughout the satellite

5.3.2 Availability

Since the announcement of the qb50 project in 2014[2], the availability of CubeSat components has increased rapidly. ISIS' CubeSatShop is an example of a webshop with commercially available CubeSat components. A lot of them have been used for this CubeSat. Other developers of CubeSat instruments and subsystems are universities all over the world. The TU Delft itself has already developed 3D-printed reaction wheels [70].

5.3.3 Safety

When thinking about safety, there are two crucial aspects to consider. The first, is to contemplate the safety of the civilians in the neighbourhood of the re-entry location, and the second, to examine the safety of satellite and crew in space. In this mission, the satellite is designed with an end-of-life solution. The CubeSat is given the order to burn up in space during a slow reentry, using the high aerodynamic drag present at this low altitude. This effect is further increased by using the drag-mode as described in Section 1.1.

Furthermore, most manned missions, for example the ISS, tend to be in Low Earth Orbit or higher. This applies to most satellites too. Hence, it can be assumed that this CubeSat that will orbit with an altitude between 230 and 350 km will not affect any space missions or satellites.

5.4 Sensitivity Analysis

This section investigates the sensitivity of the different design solutions for changes in design parameters. It is used to test the robustness of design options for changes in the parameters. The question to be answered in the sensitivity analysis is: "if the design parameters differ from expectations, what is the effect on the whole system and which parameters are causing the largest deviations?". The system engineers are the ones that need to take all these induced subsystem-changes into account, so especially for them, the Sensitivity Analysis is a valuable tool.

5.4.1 Design Parameters

Design parameters are the input for the sensitivity analysis. The difficulty for this sensitivity analysis is that the design parameters are dependent on each other. So if the mass for one subsystem changes, the mass of other subsystems, which are also design parameters, will also change. Examples of design parameters are the following:

- Mass of every subsystem
- Power of every subsystem
- Size of every subsystem
- Cost of every subsystem
- Environmental factors

For the analysis, only the direct influence of one subsystem to another will be measured. If the dependencies are accounted for, the sensitivity analysis would not be linear, so not useful in general.

[2] `https://www.qb50.eu/index.php/schedule` [cited 8 June 2015]

5.4.2 Process

For usual satellites, the changes in mass, power and size induce a snowball-effect. When the mass of a subsystem increases, the structure needs to take it into account. It might need to be designed stronger in order to be able to withstand the higher loads during different mission phases. When the weight is increased due to the higher subsystem weight and the increased structure weight, the ADCS needs to be bigger, because bigger moments should be compensated for. Also, the mass distribution and the moment of inertia might change, so the ADCS also has to account for that. When the ADCS is bigger, it will also consume more power in order to power bigger actuators. In order to produce more power, the solar panels need to be designed bigger thus heavier. Also the battery might be designed bigger. The change in mass again influences the structure and so the ADCS.

For CubeSats however, the process is a little bit different. The size of the structure is always defined in units, U, which are $10x10x10cm$. The standard for the weight of one U is 1.33 kg, with the centre of gravity in the centre of the structure [3]. For CubeSats, the structure is therefore less sensitive to changes, because it has a lot of requirements it needs to fulfil for the launch. In general, it will be a bit over-designed since changes for the structure are unwanted.

5.4.3 Output

The output of a sensitivity analysis is the likelihood of subsystems to change. At first the general parameters are described, to conclude this section with some specific important direct influences. When the mass of a subsystem changes, the mass distribution changes, but that is not allowed to happen. Therefore the mass of the payload needs to be adjusted and the precise locations of the subsystems need to be reconsidered in order to have the centre of gravity aligned with the geometric centre and to have the same MMOI as the cube with the camera. Because the accuracy of the centre of gravity and the MMOI should be as high as possible, a change in mass of a subsystem can have a very high influence on the design, dependent on the location of a subsystem and the magnitude of the change. The placing of subsystems in combination with changing the added weight to the camera can accommodate for the change up to a certain extent. This is necessary for a design in order to be feasible.

When the power usage of a subsystem changes, the amount of solar panel area needs to change and also the size of the battery. There is room left in order to increase the size of the battery. However, changing the amount of solar panel area has such an influence on the MMOI of the satellite that, unless absolutely no other solution is possible, the amount of solar panel area rather should not be changed since the structure also needs to compensate for this change.

If the size of a subsystem changes, either the mass changes, or the mass distribution. Therefore changing the size of a subsystem has the same influence as changing the mass. Since the satellite can compensate for that up to a certain extent, the design is still feasible.

The satellite is at this moment budgeted at € 444,685.54, although the upper margin is at € 500,000. This margin is big enough in order to change even the payload. Therefore, the design is not only feasible because of the margin in the costs, but it is also possible to have the CubeSat as a platform for other payloads, imaging in different spectra.

One of the most important environmental factors is the solar activity. The solar activity is dependent on the launch date. In 2017, the solar activity is low. This means that the satellite can last 200 *days* in orbit without propulsion. If the solar activity however would be high like in the past few years, the satellite would only survive for ± 60 days. Since no mission time is required, this is not a big problem. The reason the satellite can stay longer in orbit is not only because of the solar pressure, but also because the atmosphere reacts heavily on the solar activity. The density increases with solar activity, and so do the disturbances with the density. Fortunately, the ADCS is designed for the worst case scenario. Therefore it should be able to meet the pointing accuracy requirement **S08-MC-ADC-04** in any case.

The following subsystems are a little bit more critical for the design, since they use a lot of the mass, power, volume or cost budget. Therefore, the effect of the possibility of a change for this subsystem is described more into detail. The systems with the highest budgets are listed as input on the first column. The subsystems that are influenced the most by the snowball effect are listed as outputs

on the top row. The sensitivity is given a value between ± for indifferent, and + + + for heavily influenced. The / is used when the input subsystem is the same as the output, because a sensitivity analysis is very difficult to perform when all input variables are directly dependent on themselves.

	Structure Mass	**ADCS Mass**
Payload Mass	±	++
Power Mass	++	+++
ADCS Mass	±	/
Bus Structure Mass	/	+

Table 5.4: Sensitivity Table

Note that for the structural mass, the weight of the structure for the solar panels is included and plays a major role on the influences and dependencies. If the solar panels need to be bigger, the structural mass increases because of that. The mass of the bus structure in general does not change so much as stated before.

The reasoning for the assigned weights is the following:
The payload in general has a lot of the mass budget assigned to according to for instance SMAD [3] and the reader written by B. Zandbergen [28]. However, since the structure is a bit over-designed, the influence on it is minor. The ADCS however has to cope with the change of mass, and is therefore considerably influenced. Also because the reason for the change in payload mass may change the stability or accuracy requirements.

The mass of the power subsystem consists of the solar panels and the battery. When the size of the solar panels change, the weight and dimension of the structure change. Because also the form of the structure changes, the change of the MMOI is even bigger than only for changes in weight, so the influence on the ADCS system is very big.

The mass of the ADCS system does not influence the mass of the structure directly, because the structure is not sensitive to change and the total weight will most likely not change.

When the bus structure mass changes, it will have an effect on the ADCS. The centre of gravity will not change so much with respect to the centroid, because the structure will be mostly symmetric, but the moments will change.

There are more dependent subsystems, however their budgets in comparison to the total are so small that it is not necessary to list them here.

5.5 Project Design & Development Logic

After the detailed design the project has still a long way to go. The steps to be taken are explained in this section and are summarised in Figure 5.8. The main phases are; final design, manufacturing and assembly, integration and verification, preparing for launch, deployment and verification, mission and lastly the management task are mentioned.

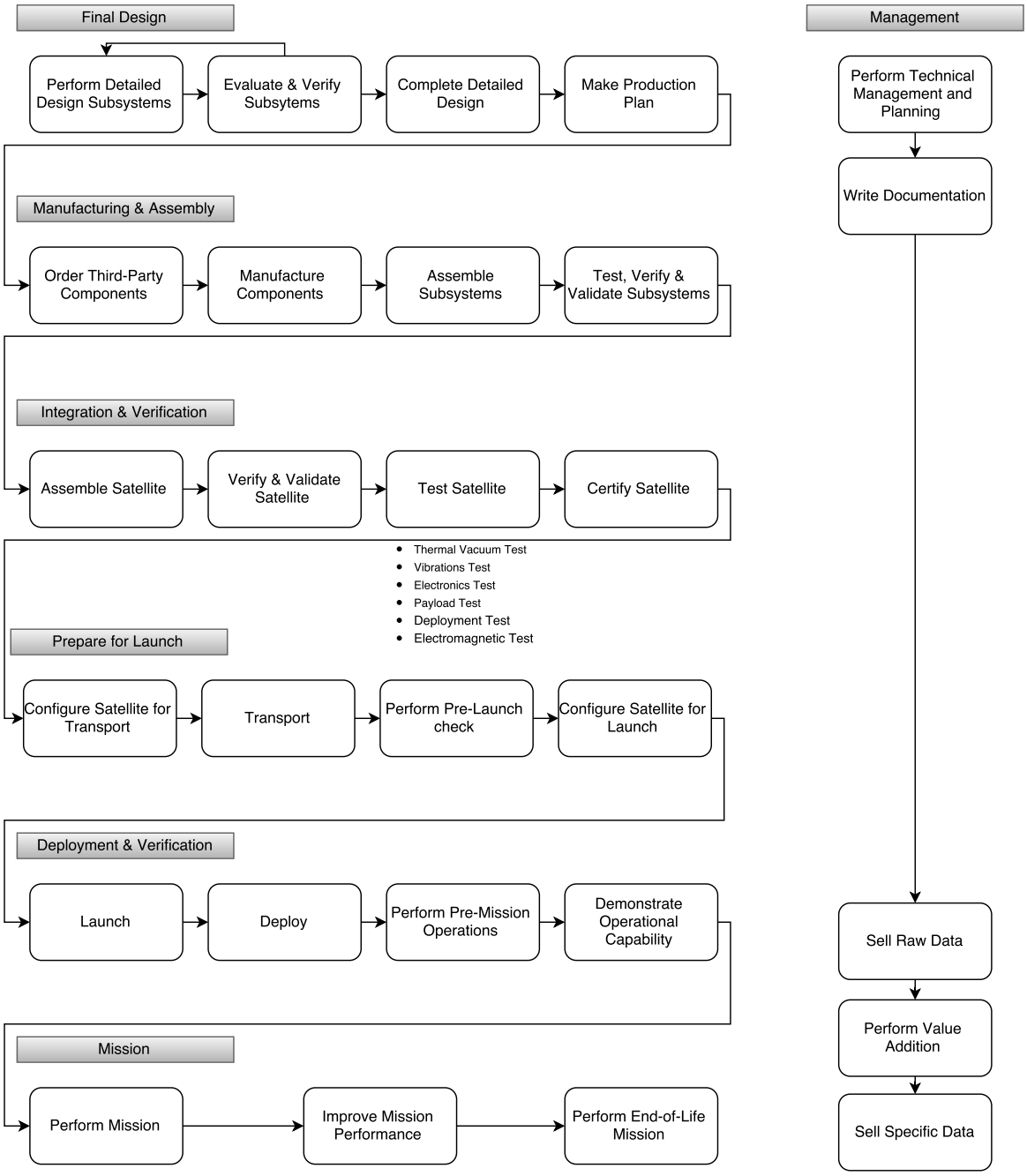

Figure 5.8: Post-DSE Activities

After the detailed design as presented in this report, more iterations can be made to improve the subsystem design. The models have to be verified and if the verification is not satisfactory another look has to be taken on the design. When all the subsystems are done the design can be fixed and a production plan can be set up.

The third party subsystems, components, raw material, tools and machinery have to be ordered first. Than the components can be manufactured and the subsystems can be put together. The subsystems are tested and validated for their specific purpose. After all test are completed positive the subsystems are ready to be put together.

The satellite is assembled and the complete CubeSat is validated and the following test are performed: thermal vacuum test, vibrations test, computing and electrical test, payload test, deployment of the mechanism test and finally a electromagnetic test. When all the test are completed satisfactory the CubeSat is certified and ready to transport. Otherwise the faulty subsystems have to be improved to meet the requirements.

Know that the satellite is completed it has to be configured for transport so that it will not malfunction on site. The CubeSat is transported to Baikonur Cosmodrome in Kazakhstan and on site a pre-launch check is performed. The Cubesat is configured for launch and placed in a launch pod. Now the International Space Company Kosmotras will take over and place the pod in the launcher.

When all conditions are good the rocket will be launched and the CubeSat will be deployed. Pre-mission operations such as starting up the subsystems, detumbling and initialisation of the wheel spin are performed and are checked if the satellite is capable to operate.

Now the mission begins and sell-able data will be sent down to earth. The data is checked and when it is possible to improve the quality of the images or the orbit commands will be sent back to the CubeSat. When the satellite reaches a altitude of 230 km the CubeSat will be put in drag mode and de-orbit within a day.

For the whole time span of the mission the management team will perform the breakdown and planning of the project. Every decision has to be supported with arguments and has to be documented. Continuously the company is looking for customers and the customer can choose to buy raw data or when they are looking for specific data an analysis is performed by the company and the data is sold with a additional value.

5.6 Project Gantt Chart

A planning is made for the post-DSE phase and a gantt chart is shown on the next page. The most important dates are the critical design review on 07-08-2015 Where the design is fixed, The test readiness review on 02-11-2015 where the integration is completed. After successful validation the system acceptance review is planned on 02-12-2015. know the satellite has to be prepared for launch and the flight readiness review is on 01-01-2016. It is important To notice is that the launch date is not set by the launch company yet. The launch will take place in the first half year of 2016. In the current planning the launch is set on the latest possible date of 01-07-2016. After deployment the last critical point is the start of the mission which is now planned for 16-08-2016 and be continued till de-orbit on 23-05-2017.

ID	Task Mode	Task Name	Duration	Start	Finish	Predecessors	Resource Names
1		**Final Design**	**26 days**	**Mon 6-7-15**	**Mon 10-8-15**		
2		Perform Detail Design Subsystems	10 days	Mon 6-7-15	Fri 17-7-15		
3		Evaluate & Verify Subsystems	5 days	Mon 20-7-15	Fri 24-7-15	2	
4		Complete Subsystems	5 days	Mon 27-7-15	Fri 31-7-15	3	
5		Make Production Plan	5 days	Mon 3-8-15	Fri 7-8-15	4	
6		Critical Design Review	0 days	Fri 7-8-15	Fri 7-8-15	5	
7		Order Third Party Components	1 day	Mon 10-8-15	Mon 10-8-15	6	
8		**Manufactoring & Assembly**	**50 days**	**Tue 11-8-15**	**Mon 19-10-15**	**7**	
9		Manufactor Components	20 days	Tue 11-8-15	Mon 7-9-15	7	
10		Assemble Subsystem	20 days	Tue 8-9-15	Mon 5-10-15	9	
11		Test, Verify & Validate Subsystems	10 days	Tue 6-10-15	Mon 19-10-15	10	
12		**Integration and Verification**	**32 days**	**Tue 20-10-15**	**Wed 2-12-15**		
13		Assemble Satellite	10 days	Tue 20-10-15	Mon 2-11-15	11	
14		Test Readiness Review	0 days	Mon 2-11-15	Mon 2-11-15	13	
15		Verify & Validate Satellite	10 days	Tue 3-11-15	Mon 16-11-15	14	
16		Thermal Vacuum Test	2 days	Tue 17-11-15	Wed 18-11-15	15	
17		Vibrations Test	2 days	Thu 19-11-15	Fri 20-11-15	16	
18		Electronics Test	2 days	Mon 23-11-15	Tue 24-11-15	17	
19		Payload Test	2 days	Wed 25-11-15	Thu 26-11-15	18	
20		Deployment Test	2 days	Fri 27-11-15	Mon 30-11-15	19	
21		Electromagnetic Test	2 days	Tue 1-12-15	Wed 2-12-15	20	
22		System Acceptance Review	0 days	Wed 2-12-15	Wed 2-12-15	21	
23		**Launch Preparations**	**152 days**	**Thu 3-12-15**	**Fri 1-7-16**		
24		Configure Satellite for Transport	1 day	Thu 3-12-15	Thu 3-12-15	22	
25		Transport	3 days	Fri 4-12-15	Tue 8-12-15	24	
26		Pre Launch Check	1 day	Wed 9-12-15	Wed 9-12-15	25	
27		Configure Satellite for Launch	1 day	Thu 10-12-15	Thu 10-12-15	26	
28		Flight Readiness Review	0 days	Fri 1-1-16	Fri 1-1-16	27	
29		Launch in H1 2016	131 days	Fri 1-1-16	Fri 1-7-16	28	
30		**Deployment and verification**	**31 days?**	**Fri 1-7-16**	**Mon 15-8-16**		
31		Launch (latest date)	0 days	Fri 1-7-16	Fri 1-7-16	29	
32		Deploy	1 day?	Mon 4-7-16	Mon 4-7-16	31	
33		Perform Premission Operations	30 days	Tue 5-7-16	Mon 15-8-16	32	
34		Demonstrate Operationel Capability	30 days?	Tue 5-7-16	Mon 15-8-16	32	
35		**Mission**	**201 days?**	**Mon 15-8-16**	**Tue 23-5-17**	**34**	
36		Perform Mission	200 days	Tue 16-8-16	Mon 22-5-17	34	
37		Operationel Readiness Review	0 days	Mon 15-8-16	Mon 15-8-16		
38		Decommisioning Review	1 day?	Tue 23-5-17	Tue 23-5-17	36	
39		Perform End of Life	1 day	Tue 23-5-17	Tue 23-5-17	36	

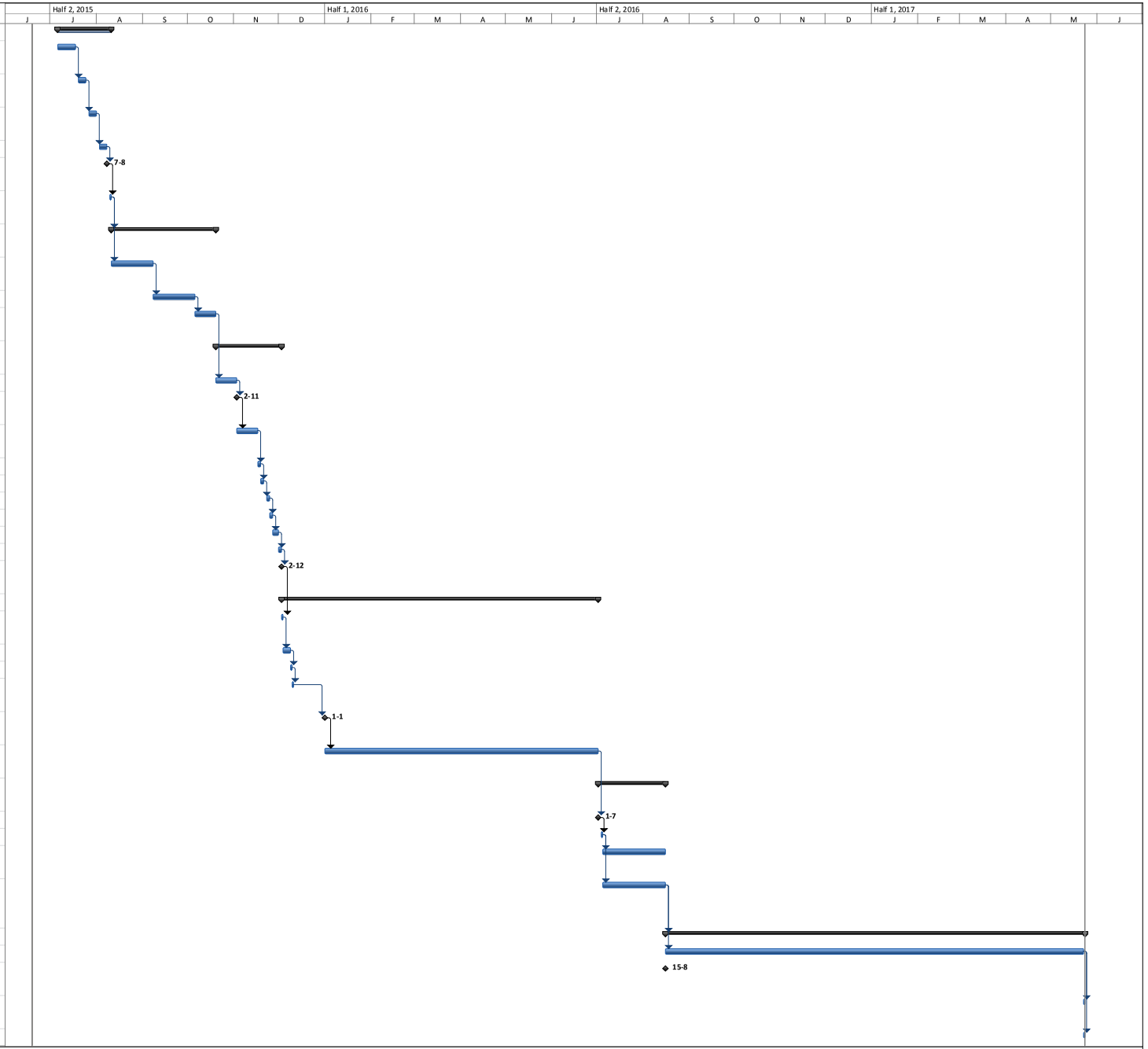

Project: Project1
Date: Fri 19-6-15

Task | Split | Milestone | Summary | Project Summary | External Tasks | External Milestone | Inactive Task | Inactive Milestone | Inactive Summary | Manual Task | Duration-only | Manual Summary Rollup | Manual Summary | Start-only | Finish-only | Deadline | Progress

5.7 Verification and Validation

This section is dedicated to the verification of the different mission tasks performed. Verification is an important factor when considering the accuracy of a specific model. In order to determine the accuracy, the model must be compared to either similar test data, or tested internally to check for errors by the means of unit testing or system testing. After the verification is finished, the program can be validated. Validation is the process of comparing any model or theory with data from experiments and real life data.

5.7.1 Brief Explanation of the Model

For this project, a simulation is made in order to be able to approximate the drag and lift that a satellite will experience at VLEO, where free molecular flow dominates. This flow is hard to predict, therefore a complex model is needed. To verify whether the model is accurate, it will be compared with the thesis from Dr. ir. E.N. Doornbos [25]. Throughout this thesis, a large number of equations to predict the flow is presented.

The simulation consists of three main parts. The first part is an orbital simulator, which calculates the ground track of the satellite. The simulator is able to model and calculate the orbit using an initial position, vector and velocity as shown in Figure 5.9. These are calculated beforehand using Kepler's equations and have been checked using the values from SMAD [3]. If the initial velocity is higher or lower than the required circular velocity for a given altitude, the altitude of the satellite will increase or decrease respectively. Throughout the simulation, the orbit is visualised using a rotating 3D Earth globe which can be seen in Figure 5.10. The satellite is represented as the large dot. Finally, the ground track is plotted on the Earth map, which is represented by Figure 5.11.

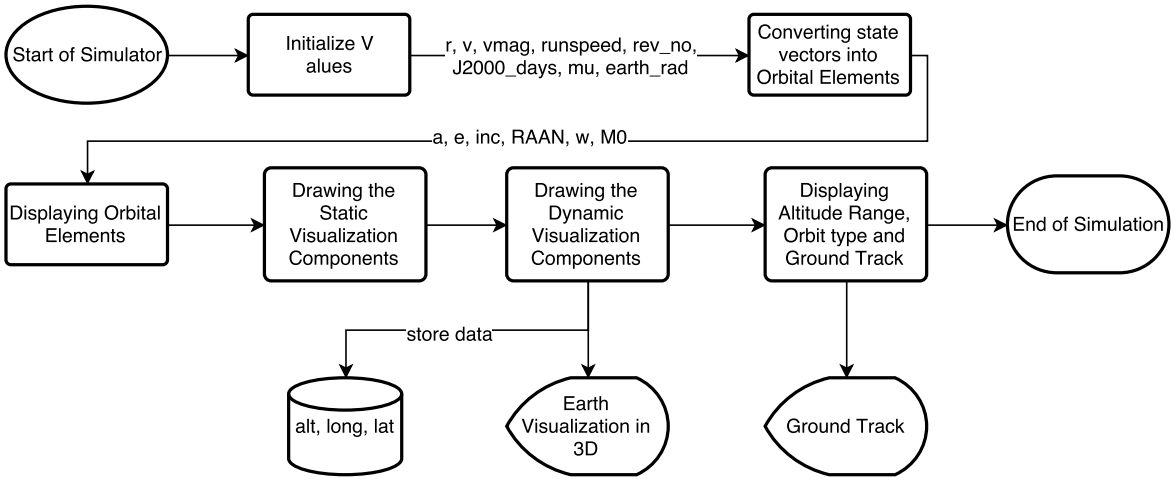

Figure 5.9: Software flowchart of Orbital Simulator

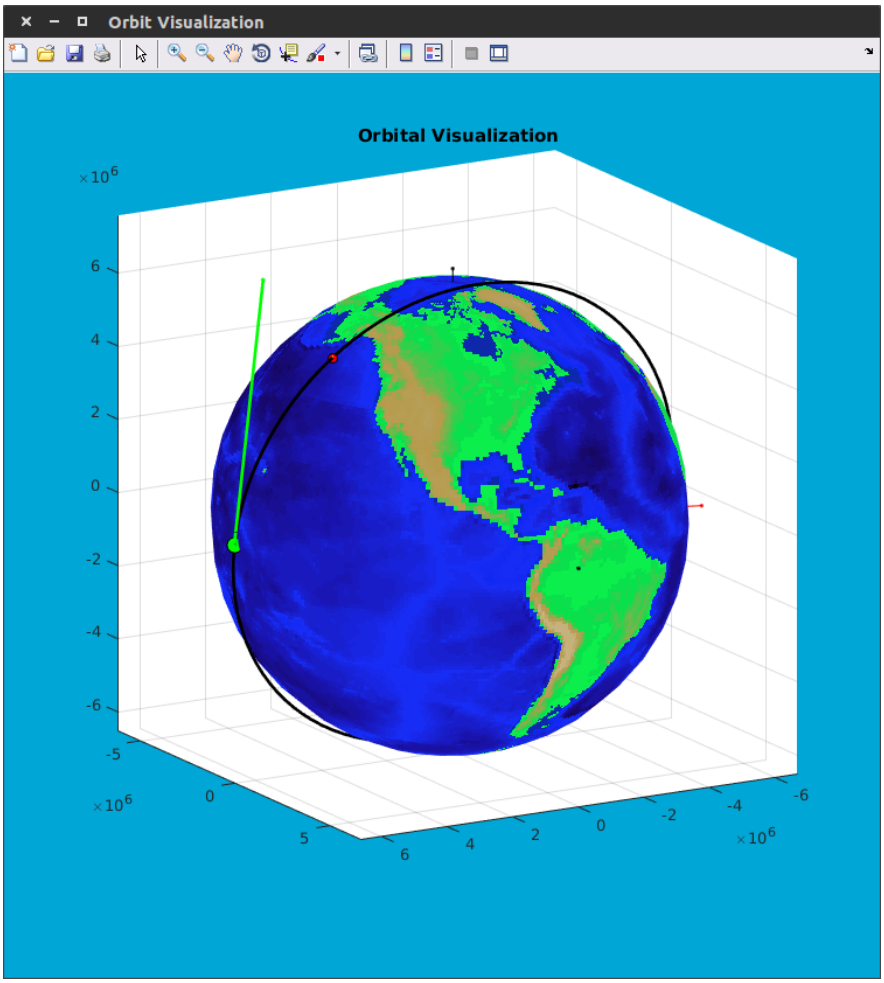

Figure 5.10: Orbital Simulator with 3D visualization

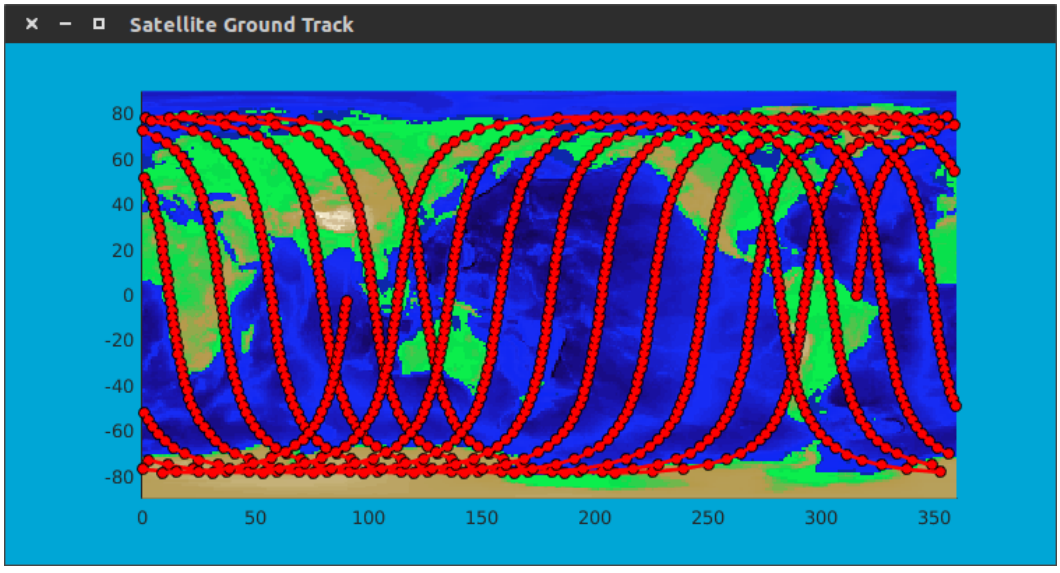

Figure 5.11: Ground track plotted on Earth map

The second part models the thermosphere at a desired altitude, longitude and latitude. The outputs of this function are the ambient temperature, the exospheric temperature and the densities for each molecule. This is showen by Figure 5.9. This model is a built-in MATLAB function (atmosnrlmsise00) so it is presumed that Mathworks[3] has verified and validated this. This is the same model that has

[3] `http://nl.mathworks.com/help/aerotbx/ug/atmosnrlmsise00.html` [cited 23 June 2015]

been used in reference [25]. The results of the atmospheric simulator are also verified by hand and validated with the results with the thesis from Dr. ir. E.N. Doornbos [25].

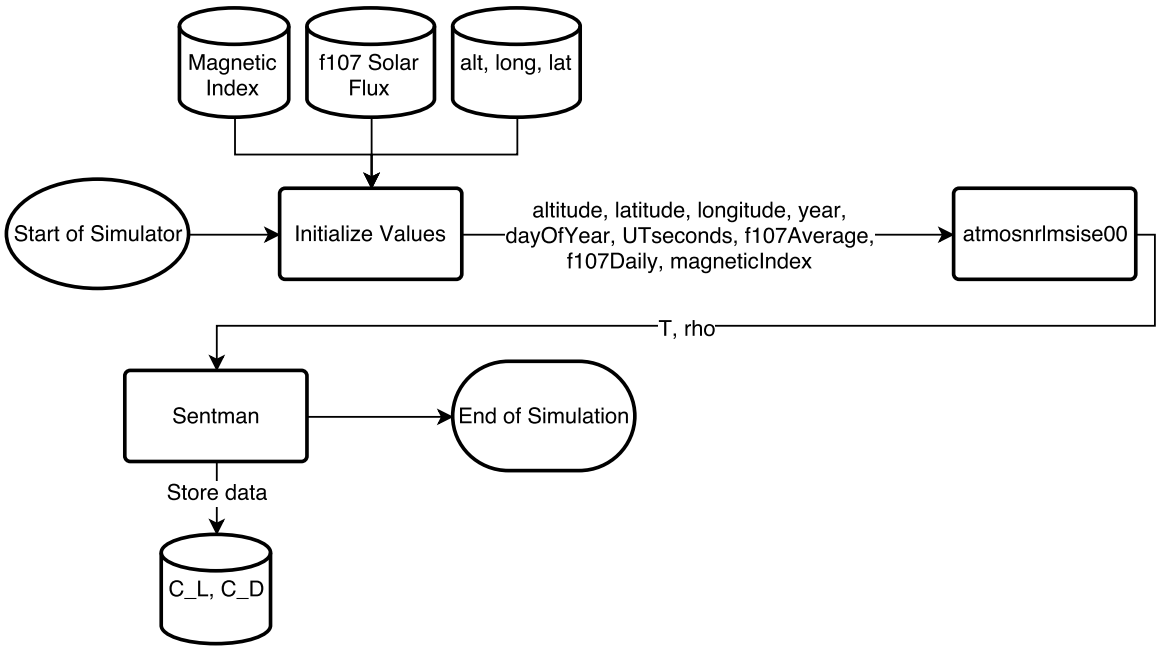

Figure 5.12: Software flowchart of Thermospheric Simulator

The third part of the simulation contains the computation of the lift and drag coefficient of the satellite represented by (C_L) and (C_D), respectively. This is verified by simulating a flat plate of one square metre. In this case, the computations can also be done by hand in order to verify the model in a short and consistent way. In Section 5.7.3, the verification process is explained extensively. Modelling a single square metre plate, shown in Figure 5.13, has also been done in [25]. Meaning it is, in this case, a good validation of the code.

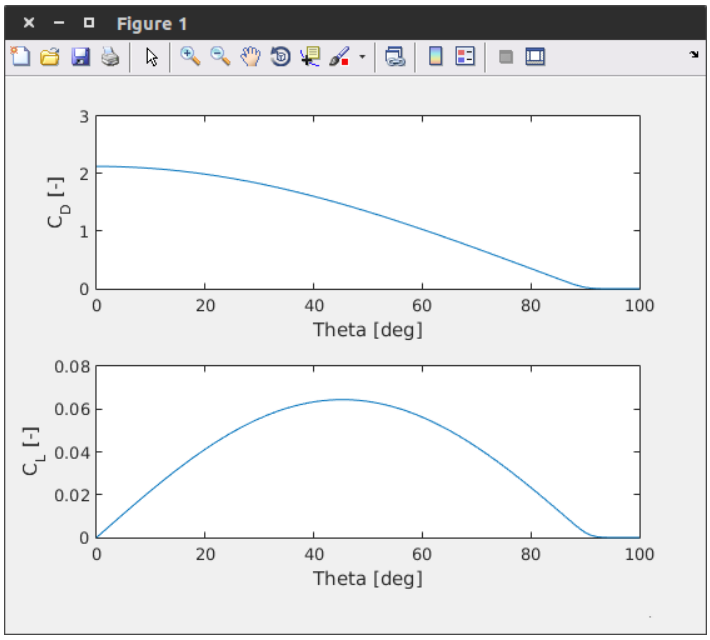

Figure 5.13: Lift and Drag coefficients vs. pitch angle θ

5.7.2 Verification of the Atmosphere model

As stated before, the atmospheric model is produced via a built-in MATLAB function, of which the inputs to that function are listed below.

- Altitude
- Latitude
- Longitude
- Year
- Day of the Year
- Seconds in a day in universal time (UT)
- The f107 average value over 81 days
- The f107 per day
- The Magnetic Index

From this list, most entries are self explanatory and are related to location and time. The f107 is the solar activity measured by The National Oceanic and Atmospheric Administration from[4]. This data gives the solar activity per day in slots of three hours. The average value is calculated around the day of interest, taken 40 days before and 40 days after. This is the only calculation that is performed by hand in this step of the model.

5.7.3 Verification of the C_L and C_D Model

The road from temperature to C_L and C_D, will be discussed in this section. The analytical equations presented in this section are used to calculate the lift and drag of a plate at a certain angle. If the satellite is divided into a number of panels, of which have their own angles, the forces and moments on the satellite can be calculated. If these calculations are integrated in time (and space) the disturbance on the satellite can be computed. From the disturbances, one could find the response time and the strength of the ADCS system. Secondly, the total drag can be computed and therefore, a life time can be estimated. From the market analysis, required revisit times can be estimated and a minimum life time can be set in order to ensure that the system remains profitable. In addition, the satellite can be equipped with thrusters to elongate the life time.

The verification procedure for the model will be unit testing; which involves calculating each step by hand and comparing the results with the numbers from the model. This way, discrepancies can be fixed while checking the equations. The process of calculating the lift and drag coefficient from the ambient temperature is as follows. Firstly, the thermal velocity needs to be calculated using Equation 5.3.

$$c_{mp} = \sqrt{2\frac{k}{m}T} \tag{5.3}$$

In this equation, k is the Boltzmann constant, m is the molecular mass and T is the atmospheric temperature. Once the thermal velocity is known, the molecular speed ratio can be computed using Equation 5.4.

$$S = \frac{v_r}{c_{mp}} \tag{5.4}$$

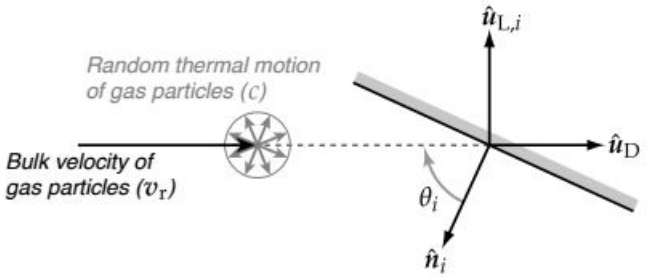

Figure 5.14: Definition of the velocity components and unit vectors used in aerodynamic calculations for a flat panel [25]

From Figure 5.14, it can clearly be seen how the lift and drag is defined for a flat panel in a 'free stream'. From the relative velocity vector, the drag and lift vectors can be defined. As stated in

[4] `ftp://ftp.swpc.noaa.gov/pub/indices/` [cited 23 June 2015]

Equations 5.5 and 5.6 and can be seen in Figure 5.14, the lift is perpendicular to the free stream and the drag is parallel to the free stream.

$$\hat{u}_D = \frac{v_r}{\|v_r\|} \tag{5.5}$$

$$\hat{u}_L = -\frac{(\hat{u}_D \times \hat{n}) \times \hat{u}_D}{\|(\hat{u}_D \times \hat{n}) \times \hat{u}_D\|} \tag{5.6}$$

Since Sentman's equations, which are depicted by Equations 5.15 and 5.16, use the angle between the normal vector and the drag vector which need to be determined. This can either be done by taking the inner product or playing around with sines and cosines. The inner product is a more reliable and solid approach and is expressed by Equations 5.7 and 5.8.

$$\gamma = cos(\theta) = -\hat{u_D} \cdot \hat{n} \tag{5.7}$$

$$l = -\hat{u}_L \cdot \hat{n} \tag{5.8}$$

Sentman's equation is dependent on coefficients based on molecular speed ratio, of which the relations are given by Equations 5.9, 5.10, 5.11 and 5.12. There is also an error function in Sentman's equation which is given by 5.13.

$$G = \frac{1}{2S^2} \tag{5.9}$$

$$P = \frac{1}{S} exp\left(\gamma^2 S^2\right) \tag{5.10}$$

$$Q = 1 + G \tag{5.11}$$

$$Z = 1 + erf(\gamma S) \tag{5.12}$$

$$erf(x) = \frac{2}{\sqrt{\pi}} \int_0^x exp\left(-y^2\right)\, dy \tag{5.13}$$

Equation 5.14 is the speed ratio of the re-emitted v_{re} particles and that of the incoming particles v_{inc} and is called the koppenwallner equation. The α in this equation represents the energy transferred from the particle to the body and is called the thermal accommodation coefficient.

$$\frac{v_{re}}{v_{inc}} = \sqrt{\frac{1}{2}\left[1 + \alpha\left(\frac{4RT_w}{v_{inc}^2} - 1\right)\right]} \tag{5.14}$$

Sentman's equations are given in 5.15 and 5.16. These equations use all the variables mentioned above. There is also an area ratio which relates the area of interest to a reference area. Usually this is the total area of the satellite.

$$C_D = \left[\frac{P}{\sqrt{\pi}} + \gamma Q Z + \frac{\gamma}{2}\frac{v_{re}}{v_{inc}}(\gamma\sqrt{\pi}Z + P)\right]\frac{A}{A_{ref}} \tag{5.15}$$

$$C_L = \left[lGZ + \frac{l}{2}\frac{v_{re}}{v_{inc}}(\gamma\sqrt{\pi}Z + P)\right]\frac{A}{A_{ref}} \tag{5.16}$$

To conclude, this is the method used to calculate the lift and drag at a certain point in space and time for a fixed CubeSat layout. The hand-calculated values and those using MATLAB can be found in Table 5.5. The same values are used as in [25]: $A_{ref} = 1\ m^2$, $T_w = 300\ K$, $\alpha = 1$, $T = 1000\ K$, $m = 16$(atomic oxygen) and $v_r = 7600\ m/s$.

Table 5.5: Drag and Lift coefficient for a flat plate at an angle of 45°

	MATLAB	**Numerical Calculation**	**Error**
C_D	1.0950	1.0952	0.1%
C_L	0.0718	0.0719	1.2%

Now that the program, which can calculate the lift and drag coefficient of a square plate with different angles of attack, has been verified, the modelling of the geometry of the satellite can begin. In the

next subsection, a step by step explanation of the program is given starting with a brief explanation of how the satellite is reconstructed with panels.

Secondly, the whole method described earlier will be used to calculate the lift coefficient and drag coefficient per panel. Thirdly, the lift and drag will be computed per panel and these will be summed to a total lift and drag force on the satellite in a specific orientation. Since the drag mode of the satellite can be used for end of life, the satellite needs to burn up in the atmosphere as soon as possible.

The *fill3* function is a MATLAB function that is able to construct flat-shaded and gouraud-shaded polygons[5]. This is used to create a visualisation of the satellite layout in MATLAB, which can be seen in Figure 5.15. The wheel is constructed using the same method.

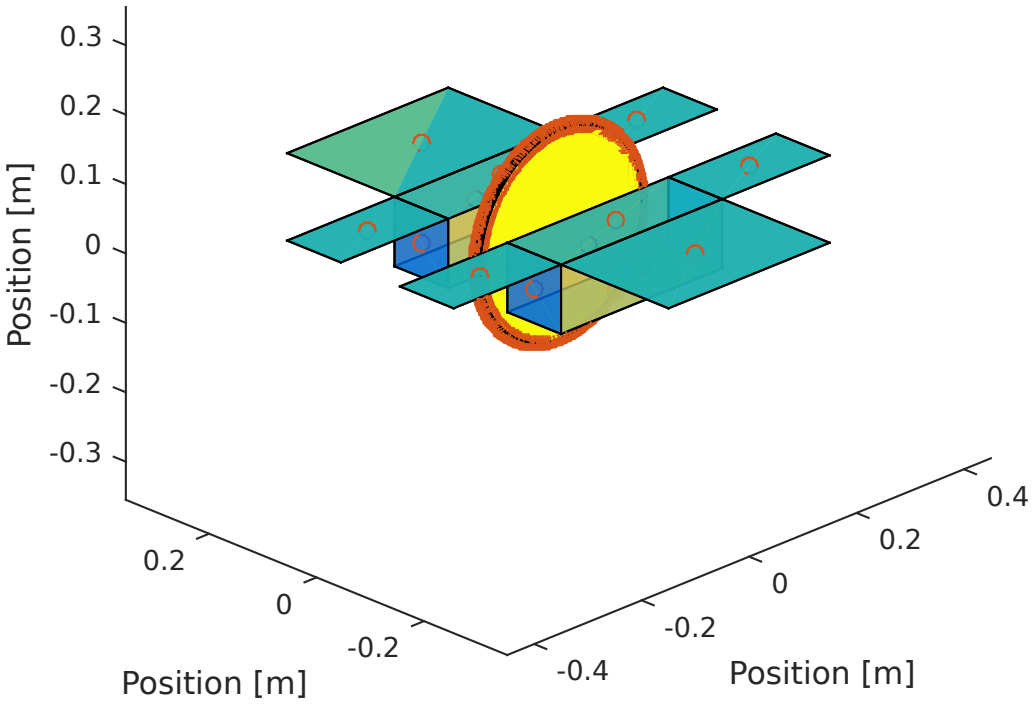

Figure 5.15: Panel method visualised with MATLAB

5.7.4 Verification of Dynamic Loads

In this subsection the dynamic loads that were calculated in 4.8 are verified. These values were compared to values computed through a FEM analysis. The FEM analysis having more degrees of freedom has many more eigenvalues and therefore natural frequencies. The modes computed from the FEM analysis are different from the analytical solution. From the FEM analysis, the 1st, 3rd and 4th mode correspond to the lateral case analysis. These values are compare in Table 5.6.

Table 5.6: Natural Frequency verification for lateral mode

Modes	Natural Frequency (Hz) - Analytical Solution	Natural Frequency (Hz) - FEM Analysis	Error
1	1651.8	894.427	45.85%
2	2423.2	939.355	61.24%
3	3068.8	1235.783	59.73%

[5] `http://nl.mathworks.com/help/matlab/ref/fill3.html` [cited 23 June 2015]

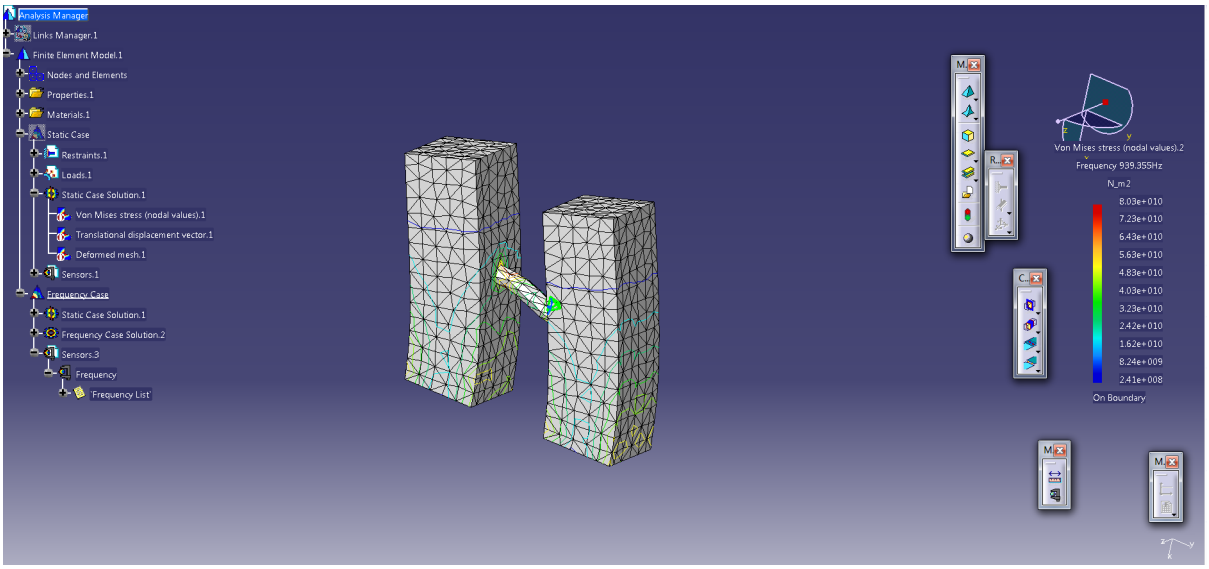

Figure 5.16: Frequency case of the basic skeleton of the satellite structure

As expected the values differ considerably since the analytical model used a much simpler structure. When a full model is taken account, the natural frequencies are seen to be lower than the analytical solution. This is due to the fact that in the FEM analysis, the satellite is modelled as a 3D element. With one more dimension, comes all failures that could occur in that dimension. When does additional structural constraints are added to the analytical structure, which is in 2D, the overall structure will tend to fail at lower frequencies.

The same is done for the longitudinal case. In the FEM analysis, the modes corresponding to the longitudinal motion are the 10^{th} and 11^{th}. For this case, for a total of 12 modes analysed inside the FEM analysis , only two correspond to the longitudinal mode in Table 5.7.

Table 5.7: Natural Frequency verification for longitudinal mode

Modes	Natural Frequency (Hz) - Analytical Solution	Natural Frequency (Hz) - FEM Analysis	Error
1	2957	4281.059	30.93%
2	6073.1	4311.715	29.00%
3	6073.1	-	-

Comparing both values, again discrepancies are present. However, it can be observed that both the analytical and numerical values are higher than their lateral counterparts. In Figure 5.16, a overview of the FEM analysis can be observed

5.7.5 Justification of Subsystem Designs

In this section a short justification of the equated values in different sections is provided.

ADCS
For the ADCS, the only calculations that were made, involved the reaction wheels. For this, the values from the disturbances were used, in combination with a few equations, to find out how much torque needs to be countered. The equations mentioned were taken from the SMAD book and therefore these are validated and verified. However, the results that were received from these equations cannot be validated.

TT&C
The calculations performed in Section 4.2.2 are based on the specifications of the payload. It is assumed that the payload will only produce image data when it is not in eclipse, which is for about 55 *minutes*. In this imaging period 24194 *km* of a total circumference of 40030 *km* of the Earth is covered. With a 4 *m* spatial resolution at 350 *km* altitude, number of Cross-Track-Pixel, CTP, of 4000 pixels, from Table 3.2, and a pixel depth of 12 *bits*, this will result in Equations 5.17, 5.18 and 5.19:

$$TotalPixels = \frac{[CoveredDistance]}{[SpatialResolution]} \cdot [CTP] = \frac{24194 \cdot 10^3}{4} \cdot 4000 \approx 2.4 \cdot 10^{10} \quad (5.17)$$

$$TotalBits = [TotalPixels] \cdot [PixelDepth] = 2.4 \cdot 10^{10} \cdot 12 \approx 2.9 \cdot 10^{11}\ bits \quad (5.18)$$

$$TotalBytes = \frac{[TotalBits]}{8} = \frac{2.9 \cdot 10^{11}}{8} \approx 3.6 \cdot 10^{10}\ bytes \approx 33.8\ GiB \quad (5.19)$$

Bear in mind that:

$$\begin{aligned} 1\ KiB &= 1024\ Bytes \\ 1\ MiB &= 1024^2\ Bytes \\ 1\ GiB &= 1024^3\ Bytes \end{aligned}$$

The contact time to a ground station of 9.4 *minutes* was calculated with the help of a web application called Satellite Orbit Data Calculator[6]. To calculate the required data rate the following Equation 5.20 was used:

$$DataRate = \frac{[TotalBytes]}{[ContactTime]} \quad (5.20)$$

For the calculation of the amount of data that can be sent in one pass, Equation 5.21 was used:

$$OnePassData = [DataRate] \cdot [ContactTime] \quad (5.21)$$

C&DH
The calculations performed in Section 4.3 in the storage part, are mainly based on the same amount of data as was calculated in Equations 5.17, 5.18 and 5.19. It is then divided by the compression ratio and times the orbits per day, to result in the data per day.

Propulsion
The propulsion unit consist of two thrusters on the main momentum wheel. The values that are found in Section 4.4 correspond to the ones that are mentioned in [46]. These are summarised in Table 5.8.

	Mass Flow $[mg/s]$	**Thrust** $[mN]$	**Specific Impulse** $[s]$
Propulsion calculations	0.2-0.1	1.1-0.5	62
values found in reference [46]	1.7-0.3	1.7-0.3	95

Table 5.8: Comparison between a CFD model in [46] and the calculated values in Section 4.4

First off the mass flow is at the low side that is possibly because of the temperature that is 50 degrees lower in the calculations done compared to the Computational Fluid Dynamics, CFD, model of the paper [46]. The same holds for the thrust and the specific impulse. A model should be built to size the thrusters better but that was out of the scope of the DSE project.

Power
The power analysis performed during the design process is mainly based on the incident angle performance variation of the solar cells. To justify these computations, these were compared with other computation tools. The used model also relates the incoming solar radiation to the incident angle. The maximal incoming solar radiation in this tool is considered to be 20 $[W/m^2]$ of which a summary of the comparison can be seen in Table 5.9.

Incident Angle	**Computation** $[W/m^2]$	**Comparison Model** $[W/m^2]$[7]	**Error**
0°	20.0000	20.0000	0.00%
30°	17.3145	17.3205	0.04%
60°	9.9840	10.0000	0.16%
90°	0.0000	0.0000	0.00%

Table 5.9: Comparison computation and real data for the power subsystem

[6] `http://www.csgnetwork.com/satorbdatacalc.html` [cited 10 June 2015]

If both models are compared, it can be concluded that the error of the created model in the scope of this project has a maximal error of 0.16 %. Therefore, the error can be negligible at this stage of the project.

Thermal Control
In this subsection, some comments for the justification of the thermal modelling are given. The one-node and multi-node thermal modelling use the values in Tables 4.26 and 4.28 as inputs for Equation 4.23. The satellite's temperature fluctuations were calculated with a Matlab-based code which was configured with a step size of 1 s. In total, 70 orbits or $382,200$ s were modelled as this was the average time at which all panels attained a constantly cyclical temperature. Although peak temperatures for the critical scenarios were confirmed analytically, the verification was limited due to the calculation effort.

Another verification aspect to be considered is the degree of accuracy of the values from the above-mentioned tables. In particular, the values in Table 4.28 need to be carefully dealt with. The technical sheets for the various coatings and paints explicitly state that the $\alpha\&\epsilon$ coefficients have a $\pm 0.02 - 0.04$ variation from the specified value. As briefly discussed in the multi-node modelling, a panel's temperature can significantly be influenced by the exactness of the absorptivity and emissivity coefficients.

Lastly, the mass, volume and cost budgets resulted in specific figures that should be seen as rough estimates only. Particularly, the mass and volume figures were based on the assumption that the thickness of the coatings was exact up to a micro-metric scales. This assumption is practical for design but rather simplistic, for the application of such coatings depends on factors outside the designer's influence like production techniques and personnel expertise at the time of applying the coating.

Bearing
The calculation of the natural frequencies and the damping ratio are checked by using the matrices of a know example in the vibrations book of Ingman. [66]

5.8 Recommendations

During the design process, different experts were consulted, and different recommendations were done by them in order to increase the quality of this report. However, since the design of a CubeSat itself is already time-consuming, these recommendations will be passed on.

The first recommendation came from Jasper Bouwmeester from the TU Delft department of Space Engineering. The idea is to make a simulation about the self-inductance of electric currents through the wires in the spacecraft. In order to have possible magnetometers as accurate as possible, an idea is to place them at different distances from the satellites core, for instance on the deployable solar panels or a dedicated boom. When the magnitude of the Earth's magnetic field is measured, the difference in magnitude can be an offset caused by the satellite itself, and these results are a way of verifying the simulation performed earlier. This simulation can later be used in order to filter this disturbance out.

The second recommendation came from Johan Leijten from Lens R&D. The idea is to place sun-sensors in a so called MAD-configuration in order to increase their accuracy. This configuration implies putting the sun-sensors in an angle of 45° with respect to each other so so the incidence angle of the Sun is measured twice at different angles.

The third recommendation came from Eelco Doornbos, also from the TU Delft. In order to increase the possibilities of our atmospheric density programme, for instance calculating the drag for concave angles, a Monte-Carlo simulation is needed. This way it is possible to simulate a vast amount of particles with random motions and simulate the reaction of the particles on the surface. When a particle bounces from one surface to another, it is possible to model this.

The last recommendation came from Hans Kuiper. In order to increase the order of accuracy even more, another solution is needed than just increasing the size of the ADCS. Because we use a mirror in order to be able to change the pointing direction of the camera, it would be possible to design the

[7] `http://pveducation.org/pvcdrom/properties-of-sunlight/solar-radiation-on-tilted-surface` [cited 12 June 2015]

mirror such that it is possible to adjust the pointing direction during the mission just by tenths of degrees, such that a higher pointing accuracy can be obtained.

Conclusion

The exercise of designing a cube satellite platform was introduced to the group at the beginning of the Design Synthesis Exercise. Since then, many design choices were made that led to the final design. This report introduced these choices and the consequences that these had on the design.

The final design makes use of a momentum wheel placed in between two conventional 3-unit cube satellites. This was chosen since the momentum wheel provides stabilisation in two axes. However, the wheel must have a high angular velocity. To do this, the propulsion subsystem is used to increase the velocity of the momentum wheel by using a resistojet provided by the TU Delft. In order to decrease the vibrations induced by the high rotation velocity of the momentum wheel, magnetic bearings seemed to be a suitable solution. The nutation vibrations are also damped, however this is done using liquid dampers in the wheel. Another benefit from the magnetic bearings is that the frictional force is very low. Since spinning up the momentum wheel requires power and no cables can go through the magnetic dampers, an additional battery inside the wheel is needed, which also acts as extra mass in order to increase the stabilising properties of the wheel. Moreover, the power subsystem also needs to provide electricity to the main bus, meaning 25 solar cells are required for the CubeSat. The main reason of this large power consumption comes from the ADCS and TT&C. Since the TT&C has to transmit and receive data, which is done by using two bands. Namely, the X-band for imaging data transfer and the UHF band for the attitude information. For the ADCS, the big number of sensors and actuators also require a power consumption of 11.1 W during the de-tumbling phase.

For the payload, an off axis Ritchey-Chretien Telescope is designed. This allows a resolution of 4 m to be achieved at an altitude of 350 km. This was needed, since the orbit was chosen to be a sun synchronous orbit at 350 km, allowing an imaging lifetime of roughly 200 days to be achieved. Furthermore, all of the subsystems, most of which are already mentioned, will need to be placed in a main bus. For this mission, the structure material chosen is aluminium due to its strong characteristics in space.

Therefore, to conclude, an innovative, out of the box idea is revealed with its main goal to tackle the disturbances that are presented by the thermosphere at an altitude of 350 km. The platform aims to do this with the use of a momentum wheel, using the conservation of momentum law.

Bibliography

[1] J. H. Kuiper, "AE3-200 Project Description: VLEO CubeSat designs for Earth Observation," 2015.

[2] D. Gilmore, *Thermal Control Handbook*. The Aerospace Coorporation, 2002.

[3] J. R. Wertz, D. F. Everett, and J. J. Puschell, *Space Mission Engineering: The New SMAD*. Hawthorne, CA: Microcosm Press, 1st. ed., 2011.

[4] J.-F. Castet and J. H. Saleh, "Satellite and satellite subsystems reliability: Statistical data analysis and modeling," *Reliability Engineering & System Safety*, vol. 94, no. 11, pp. 1718–1728, 2009.

[5] E. Buchen and D. DePasquale, "2014 Nano/Microsatellite Market Assessment," *SpaceWorks Enterprises, Inc., Atlanta, GA, February*, 2014.

[6] NSR llc, "Global satellite-based earth observation, 4th edition," 2012.

[7] A. Shao, E. A. Koltz, and J. R. Wertz, "Performance Based Cost Modeling: Quantifying the Cost Reduction Potential of Small Observation Satellties," in *AIAA Reinventing Space Conference, AIAA-RS-2013-1003, Los Angeles, CA, Oct*, pp. 14–17, 2013.

[8] Bouwmeester, J., "DNX-TUD-BU-0018 (5.3) Delfi-n3Xt Mass Budget.xls," [last updated 22 January 2012].

[9] de Jong, J., "DNX-TUD-BU-0303 (2.5) Delfi-n3Xt Volume Budget, Appendix Calculation.xls," [last updated 31 July 2012].

[10] Bouwmeester, J., "DNX-TUD-BU-0017 (7.08) Delfi-n3Xt Power Budget.xlsx," [last updated 07 December 2012].

[11] I. Burton, "Report on Reports: Our Common Future: The World Commission on Environment and Development," *Environment: Science and Policy for Sustainable Development*, vol. 29, no. 5, pp. 25–29, 1987.

[12] S. Kilston, "Capabilities of new Remote Sensing Satellites to support Sustainable Development," *International Archives of Photogrammetry and Remote Sensing*, vol. 32, pp. 183–190, 1998.

[13] D. Gibbon, M. Paul, P. Jolley, V. Zakirov, G. Haag, I. Coxhill, M. Sweeting, and R. Eloirdi, "Energetic Green Propulsion for Small Spacecraft," *AIAA Paper*, vol. 3247, pp. 8–11, 2001.

[14] K. Anflo, T.-A. Grönland, G. Bergman, M. Johansson, and R. Nedar, "Towards Green propulsion for Spacecraft with ADN-based Monopropellants," in *38 th AIAA Joint Propulsion Conference, AIAA Paper*, vol. 3847, p. 2002, 2002.

[15] N. Leach, "3D Printing in Space," *Architectural Design*, vol. 84, no. 6, pp. 108–113, 2014.

[16] S. Kaplan and B. J. Garrick, "On the quantitative definition of risk," *Risk analysis*, vol. 1, no. 1, pp. 11–27, 1981.

[17] A. Kalman and A. Reif, "MISC – A Novel Approach to Low-Cost Imaging Satellites," in *SSC08-X-3*, 2007.

[18] M. van de Bos, R. Bijster, and et al., "Advanced Nano Telescope - A cornerstone solution in Earth observation," tech. rep., Delft University of Technology, 2011.

[19] D. Dolkens, "Off-Axis Modified Ritchey-Chretien Telescope - Design Description," 2015.

[20] AWAIBA Lda., "DRAGSTER LINESCAN SENSOR - Short data sheet," 2015.

[21] H. Klinkrad and B. Fritsche, "Orbit and attitude perturbations due to aerodynamics and radiation pressure," in *ESA Workshop on Space Weather, ESTEC, Noordwijk, Netherlands*, 1998.

[22] W. J. Larson and J. R. Wertz, *Space Mission Analysis and Design*. Hawthorne, CA: Microcosm Press, 3rd. ed., 1999.

[23] R. Noomen, "AE2230-I, lecture hours 19+20," March 2014.

[24] Australian Government Bureau of Meteorology, "Satellite Orbital Decay Calculations." Article.

[25] E. Doornbos, *Thermospheric density and wind determination from satellite dynamics*. Springer Science & Business Media, 2012.

[26] ZARM, "Magnetic Torquers for Micro-Satellites." http://www.zarm-technik.de/downloadfiles/ZARMTechnikAG_CubeSatTorquers_web2010.pdf, 2010.

[27] Steyn, W. H., "Tailored ADCS bundles for Nanosatellites." http://www.isispace.nl/brochures/CubeADCS_Ext_Brochure.pdf, 2015.

[28] B. T. C. Zandbergen, "Aerospace Design & Systems Engineering Elements I Part: Spacecraft (bus) Design and Sizing," 2011.

[29] SSBV, "Cubesat Sun Sensor." http://www.ssbv.com/resources/Datasheets/SSBV_CubeSat_Sun_Sensor_Datasheet_1h-.pdf, [cited 10 June 2015].

[30] SSBV, "Fine Sun Sensor." http://www.ssbv.com/resources/Datasheets/SSBV_Fine_Sun_Sensor_Datasheet_1d-.pdf, [cited 10 June 2015].

[31] SSBV, "Earth Horizon Sensor." https://docs.google.com/viewer?url=http://www.ssbv.com/resources/Datasheets/SSBV_Earth_Horizon_Sensor_Datasheet_1d-.pdf&embedded=true, [cited 10 June 2015].

[32] Maryland Aerospace, "MAI-SES." http://d6110363.ozt807.onezerotech.com/wp-content/uploads/2014/07/MAI-SES-Specification1.pdf, [cited 10 June 2015].

[33] SSBV, "GPS Receiver." http://www.ssbv.com/resources/Datasheets/SSBV_GPS-Receiver_Datasheet_1d-.pdf, [cited 10 June 2015].

[34] Analog Devices, "ADXRS649 Data Sheet." http://www.analog.com/media/en/technical-documentation/data-sheets/ADXRS649.pdf, [cited 12 June 2015].

[35] SSBV, "Reaction Wheel." http://www.ssbv.com/resources/Datasheets/SSBV_Reaction_Wheel_Datasheet_1c-.pdf, [cited 11 June 2015].

[36] Maryland Aerospace, "MAI-100." http://d6110363.ozt807.onezerotech.com/wp-content/uploads/2014/04/MAI101_Specifications.pdf, [cited 11 June 2015].

[37] Maryland Aerospace, "MAI-400." http://d6110363.ozt807.onezerotech.com/wp-content/uploads/2014/06/MAI_Single_Axis_Assembly_Brochure.pdf, [cited 11 June 2015].

[38] SSBV, "CubeSat Magnetorquer Rod." http://www.ssbv.com/resources/Datasheets/SSBV_CubeSat_Magentorquer_Rod_Datasheet_1c-.pdf, [cited 11 June 2015].

[39] E. Peragin, H. Diez, F. Darnon, D. Belot, J. Millerioux, J. Issler, T. Dehaene, Y. Richard, G. Guillois, F. Sépot, *et al.*, "X Band downlink for CubeSat," 2012.

[40] ISIS, "ISIS VHF downlink / UHF uplink Full Duplex Transceiver." http://www.isispace.nl/brochures/ISIS_TRXUV_Transceiver_Brochure_v.12.5.pdf, [cited 16 June 2015].

[41] Antenna Development Corporation, "Microstrip Patch Antennas." http://www.antdevco.com/ADC-0509251107%20R6%20Patch%20data%20sheet_non-ITAR.pdf, [cited 19 June 2015].

[42] ISIS, "Deployable Antenna System for CubeSats." http://www.isispace.nl/brochures/ISIS_AntS_Brochure_v.7.11.pdf.

[43] ISIS, "ISIS On Board Computer." http://www.isispace.nl/brochures/ISIS_ISIS%20OBC_Brochure_v.15.6.pdf, [cited 18 June 2015].

[44] S. De Jong, G. T. Aalbers, and J. Bouwmeester, "Improved command and data handling system for the delfi-n3xt nanosatellite," in *59th International Astronautical Congress: IAC 2008, 29 September-3 October 2008, Glasgow, Scotland*, 2008.

[45] F. La Torre, *Gas flow in miniaturized nozzles for micro-thrusters.* PhD thesis, TU Delft, Delft University of Technology, 2011.

[46] I. Krusharev, R. Poyck, B. T. C. Zandbergen, A. Cervone, and Q. Bellini, "CubeSat Micro-Propulsion Systems For Extending The Capabilities Of Academic Projects," *Impulse [Ns]*, vol. 34, pp. 0–8.

[47] B. T. C. Zandbergen, "Micropropulsion Systems for Cubesats," *Delft University of Technology, Delft*, 2013.

[48] A. Cervone, "AE2230-II, lecture hour 12," February 2015.

[49] T. V. Mathew, B. T. C. Zandbergen, M. Mihailovic, J. F. Creemer, and P. M. Sarro, "A Silicon-Based Mems Resistojet for Propelling CubeSats,"

[50] ASCO, "2 and 3-way Customizable Solenoid Valve."

[51] Kuhnke, "Miniature Valves: Manual, Mechanical, Pneumatic and Electrical Valves."

[52] Bouwmeester, J and Guo, J, "Survey of worldwide pico- and nanosatellite missions, distributions and subsystem technology," *Acta Astronautica*, vol. 67, pp. 854–862, 2010.

[53] S. R. Messenger, G. P. Summers, E. Burke, R. J. Walters, and M. Xapsos, "Modeling solar cell degradation in space: A comparison of the NRL displacement damage dose and the JPL equivalent fluence approaches†," *Progress in Photovoltaics: Research and Applications*, vol. 9, no. 2, pp. 103–121, 2001.

[54] R. Burt, "Distributed electrical power system in cubesat applications," 2011.

[55] D. Erb, S. Rawashdeh, and J. Lumpp Jr, "Evaluation of solar array peak power tracking technologies for cubesats," 2011.

[56] D. Giancoli, *Physics for Scientists & Engineers, Vol. 1 and Vol. 2 and Masteringphysics with E-Book Student Access Kit for Physics for Scientists and Engineers.* Pearson Education, 2011.

[57] GomSpace, "NanoPower P110 Series - Solar Panels Datasheet." `http://gomspace.com/documents/GS-DS-P110-1.0.pdf`, [cited 19 June 2015].

[58] GomSpace, "NanoPower Flexible Battery Pack - BPx series - V2.0." `http://gomspace.com/documents/gs-ds-nanopower-bpx.pdf`, [cited 19 June 2015].

[59] GomSpace, "NanoPower BP series datasheet - QuadBat BP4 V2.0." `http://gomspace.com/documents/gs-ds-bp4.pdf`, [cited 19 June 2015].

[60] GomSpace, "NanoPower P-series Datasheet - P31u / P31us V9.0." `http://gomspace.com/documents/gs-ds-nanopower-p31u-9.0.pdf`, [cited 19 June 2015].

[61] P. Fortescue, G. Swinerd, and J. Stark, *Spacecraft Systems Engineering.* John Wiley & Sons, 2011.

[62] Pijnenburg, J and te Voert, MJA and de Vreugd, J and Vosteen, A and van Werkhoven, W and Mekking, J and Nijland, BAH, "Ultra-stable isostatic bonded optical mount design for harsh environments," in *SPIE Astronomical Telescopes+ Instrumentation*, pp. 845027–845027, International Society for Optics and Photonics, 2012.

[63] R. Moser, J. Sandtner, and H. Bleurer, "Optimization of Repulsive Passive Magnetic Bearings," *Transactions on Magnetics*, 2006.

[64] T. A. Lembke, "Design and Analysis of a Novel Low Loss Homopolar Electrodynamic Bearing," 2005.

[65] B. Murphy, J. Kitzmiller, R. Zowarka, H. T, and W. A, "Rotordynamics Design and Test Results for a Model Scale Cumpolsator Rotor,"

[66] D. J. Inman, "Engineering Vibrations."

[67] H. Kuiper and E. Bongers, "Flight nutation validation of the cos-b and equator-s spacecraft," in *Advances in Aerospace Guidance, Navigation and Control*, pp. 721–740, Springer, 2013.

[68] J. Sinke, "AE3211-II, 11 Organization of the production process."

[69] J. Sinke, "AE3211-II, Quality system in Aerospace industry 9.1."

[70] E. Dekens, G. Brouwer, J. Bouwmeester, and J. Kuiper, "Development of a Nano-Satellite Reaction Wheel System with Commercial Off-The-Shelf Motors." 7th ESA Roundtable on Micro & Nano Technologies for Space Applications, 14 September 2010, ESTEC, Noordwijk, The Netherlands, September 2010.

Appendix A

Technical Drawings

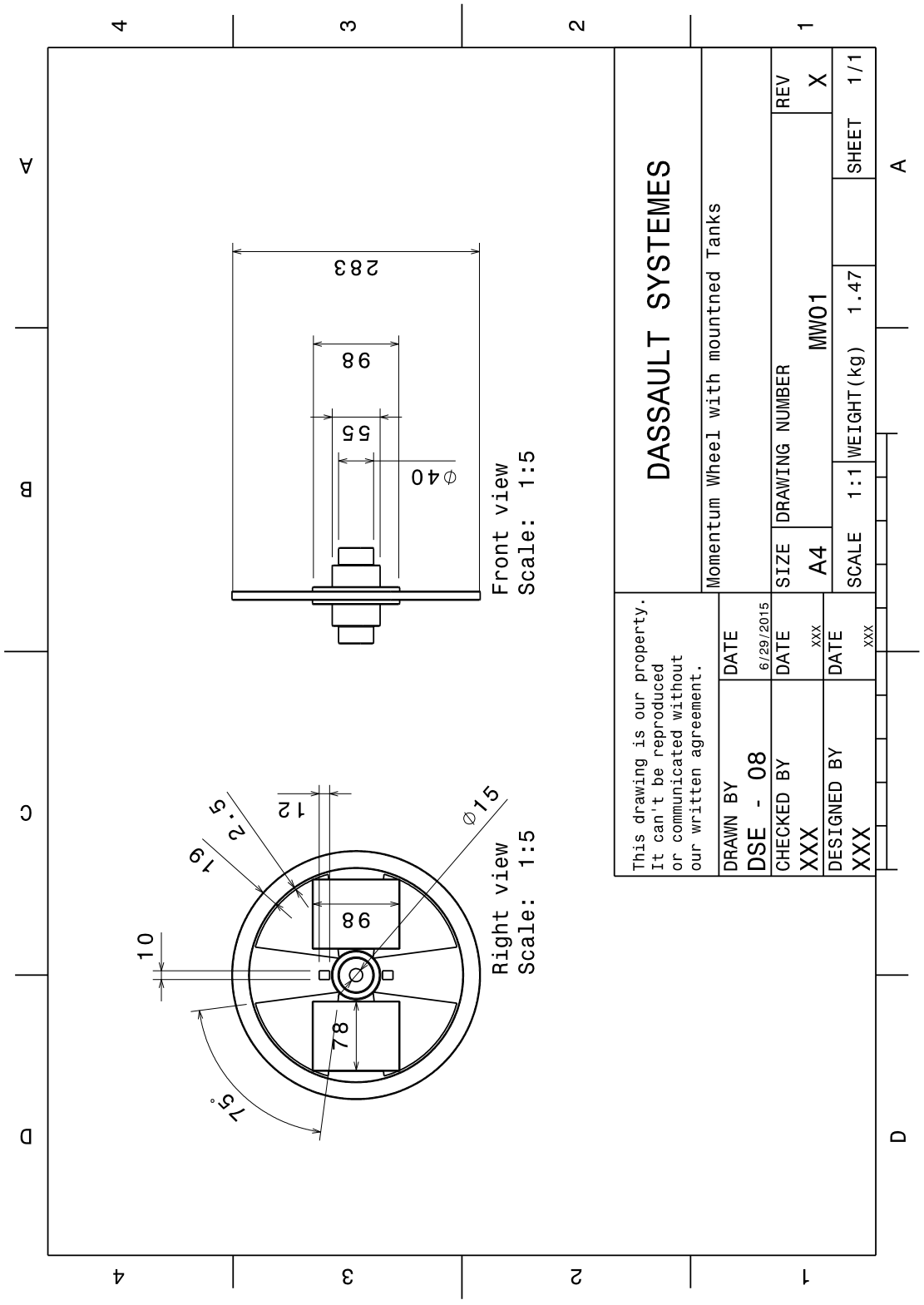

Figure A.1: Technical Drawing of the Momentum Wheel

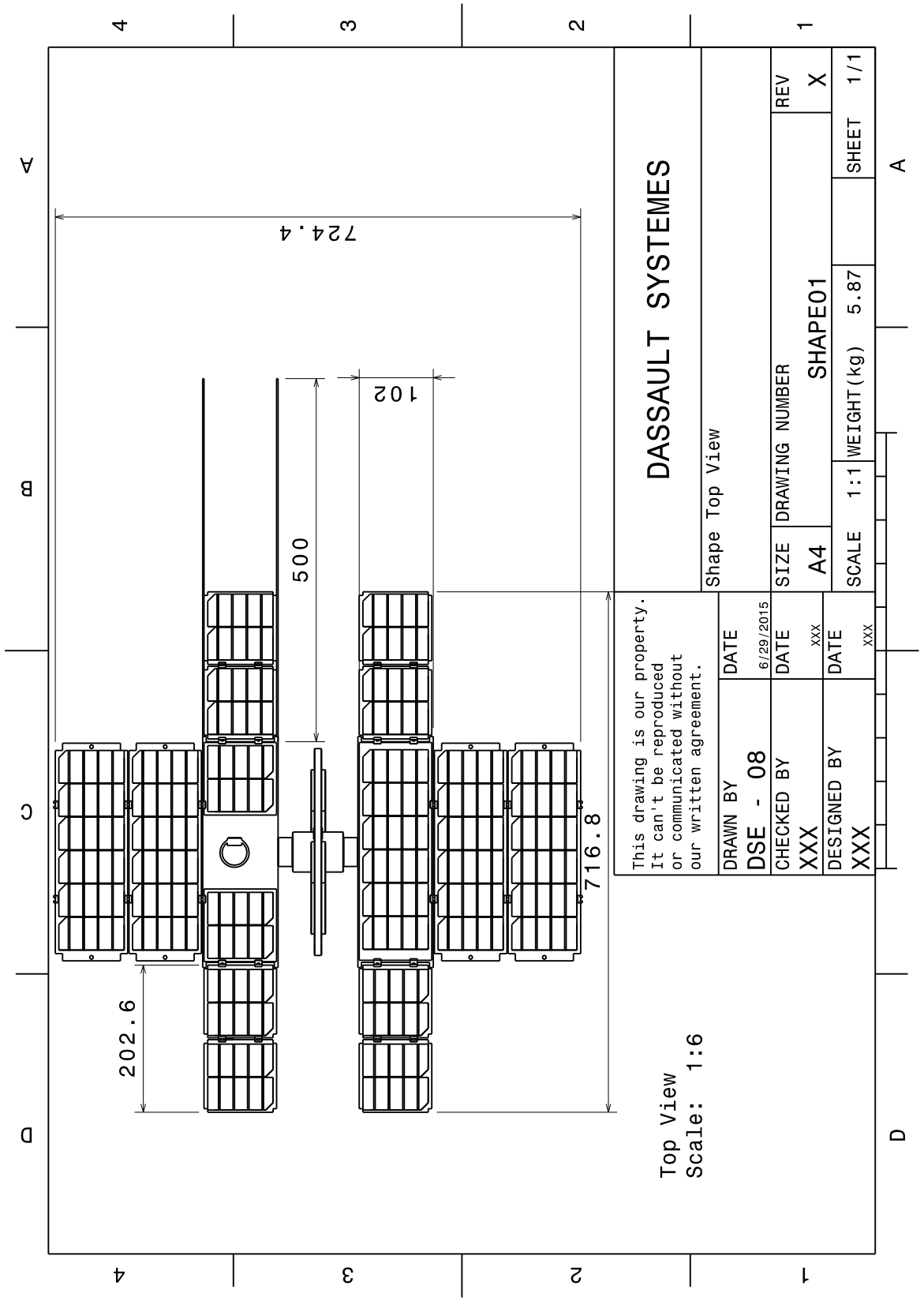

Figure A.2: Top view of the satellite design

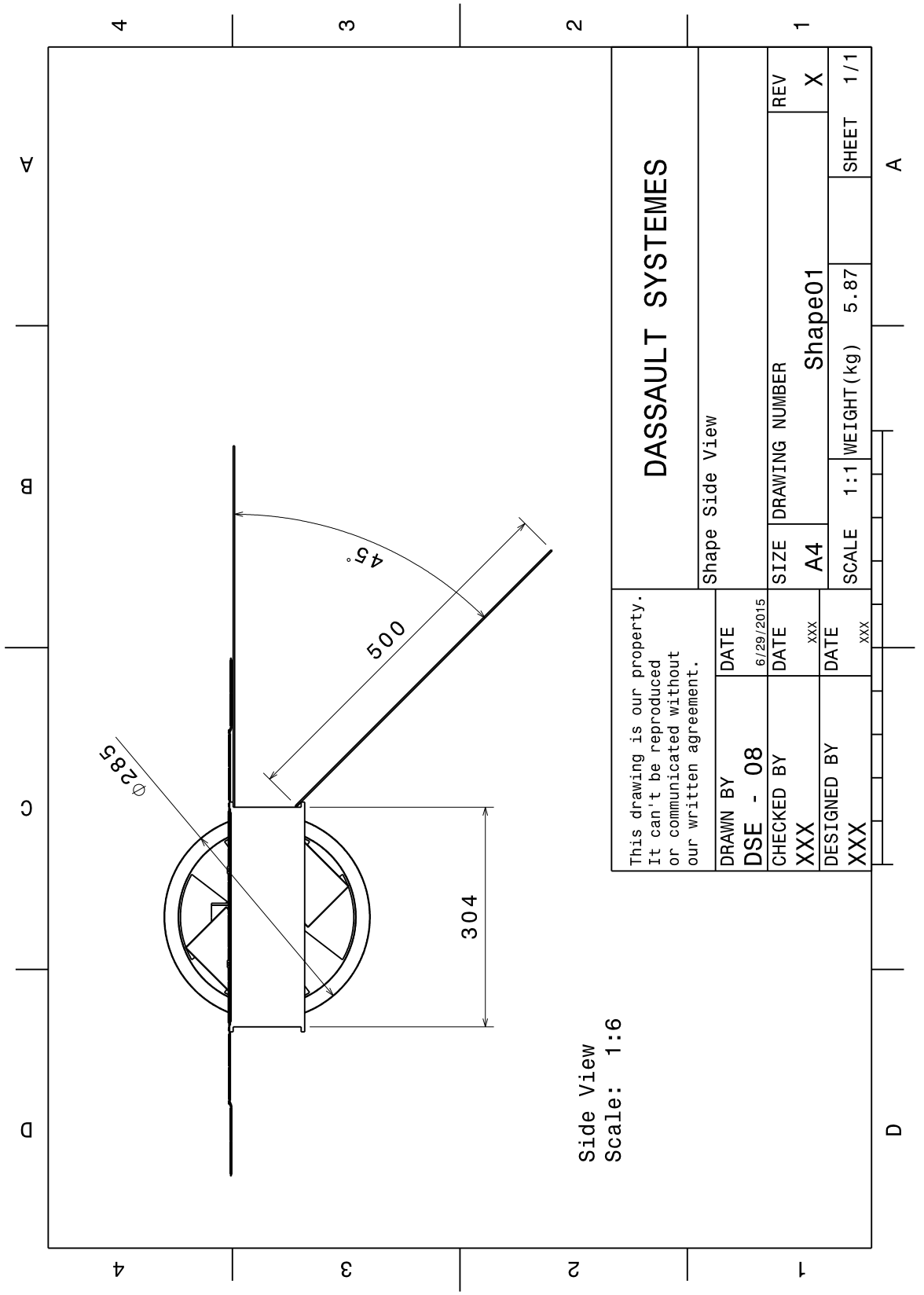

Figure A.3: Side view of the satellite design